Development of a new generation of fiber sensors for structural health monitoring in composites in real-time

Yumna Qureshi

▶ **To cite this version:**

Yumna Qureshi. Development of a new generation of fiber sensors for structural health monitoring in composites in real-time. Materials and structures in mechanics [physics.class-ph]. ENSTA Bretagne - École nationale supérieure de techniques avancées Bretagne, 2020. English. NNT : 2020ENTA0012 . tel-03405241

HAL Id: tel-03405241

https://theses.hal.science/tel-03405241

Submitted on 27 Oct 2021

HAL is a multi-disciplinary open access archive for the deposit and dissemination of scientific research documents, whether they are published or not. The documents may come from teaching and research institutions in France or abroad, or from public or private research centers.

L'archive ouverte pluridisciplinaire **HAL**, est destinée au dépôt et à la diffusion de documents scientifiques de niveau recherche, publiés ou non, émanant des établissements d'enseignement et de recherche français ou étrangers, des laboratoires publics ou privés.

THESE DE DOCTORAT DE

L'ECOLE NATIONALE SUPERIEURE

DE TECHNIQUES AVANCEES BRETAGNE

ECOLE DOCTORALE N° 602
Sciences pour l'Ingénieur
Spécialité : *Mécanique des solides, des Matériaux, des Structures et des Surfaces*

Par **Yumna QURESHI**

Development of new generation fiber sensors for structural health monitoring of composites in real-time

Thèse présentée et soutenue à Brest le 10 juillet 2020
Unité de recherche : Institut de Recherche Dupuy de Lôme – UMR CNRS 6027

Rapporteurs avant soutenance :

Daniel COUTELLIER	Professeur, Université Polytechnique Hauts de France, Valencienne.
Fouad ERCHIQUI	Professeur, Université, Rouyn-Noranda, Canada.

Composition du Jury :

Président :	**Francisco CHINESTA**	Professeur, Arts et Metiers Paris
Examinateurs :	**Mohamed BENBOUZID**	Professeur, Université Européenne de Bretagne
	Daniel COUTELLIER	Professeur, Université Polytechnique Hauts de France
	Fouad ERCHIQUI	Professeur, Université, Rouyn-Noranda, Canada.
	Fodil MERAGHNI	Professeur, ENSAM, METZ
	Daniela PLACHA	Professeur, VŠB–Technical University of Ostrava, République tchèque
Dir. de thèse :	**Mostapha TARFAOUI**	Professeur, ENSTA Bretagne, Brest
Co-dir. de these :	**Khalid LAFDI**	Professeur, Northumbria University/ University of Dayton**.**

ACKNOWLEDGMENT

First and above all, I thank Allah Almighty for His grace, mercy, and help in every step because without Him it wouldn't have been possible to complete this work successfully. After His grace, I hereby acknowledge the valuable support and guidance of my supervisors, Pr. Mostapha TARFAOUI from ENSTA Bretagne and Pr. Khalid LAFDI from Northumbria University / University of Dayton. I would like to pay my heartiest respect because without their support, guidance, trust, and assistance this work would not be presented in this form. Specifically, constant encouragement, insights, thoughtful guidance, timely advice of Pr. Tarfaoui helped me in completing my ambition and face greater challenges. His inquiries always encouraged me for higher quality and his advice guide me through hard times and finish tasks within time.

I would like to say thanks to all my colleagues and friends Hamza BEN YAHIA, Sabrine KHAMMASSI, Manel CHIHI, and Imane BELOUFA without whom it would not have been possible to complete my PhD living alone in France with a child. It is their support, love, and help that made it possible to complete my degree while having and raising a child by myself while living in France.

I would also like to pay my deepest regards to ENSTA Bretagne institute for accepting me for this great opportunity and providing me with a platform to conduct my research and covert my dream into reality. In continuity, I would like to thank the technical staff and lab engineers especially Frederic MONTEL for assisting me through all my experimental procedures and working as a team to overcome any hurdles that could halt my research.

I would also like to acknowledge the patience and support of my husband Sarosh JAMSHED, who could not come with me but still allow me to fulfill my dream and believed in me. He instead of being demanding and frustrating, he understood my determination and let me fulfill my ambition even though, it meant he could not see his child for three years or even miss her birth. My parents and family, especially my father Muhammad Arif QURESHI deserve equal credit for being my support, my ground pillar throughout my life. He is the person who supported me throughout my whole student life and in my career. He dreamed this goal with me and being a PhD doctorate is equally his achievement as it is mine.

Last but not the least, my daughter Imrana Qureshi JAMSHED who was my support system, my motivation, my inspiration, and my backbone during my studies. She provided the required balance in my life during my stay in France for my studies by her positivity, innocence, intelligence, and maturity. She was the only family I had who was physically present to

emotionally support and motivate me to fulfill my goal. Even at the age of 2 years she understood her mother's situation and showed maturity and behaved responsibly. I can proudly say that my daughter is my pride who helped her mother in achieving her biggest goal in her life.

ABSTRACT

Composites have substituted traditional materials in almost every engineering and structural application because of their extraordinary performance but still, they are not exempt from limitations and problems. Despite being a multiphase material, their mechanism of damage initiation and propagation leading to failure are well established and the problem is that these damages or failures are not visible always. So, even when the overall structure is still intact, it is essential to study their performance during operational conditions in real-time to avoid any catastrophic incident. Thus, in-situ structural health monitoring was developed in which structural data can be collected and analyzed in real-time to identify the presence of damage. The study conducted in this research is within the framework of development affective and robust sensor system which can monitor not only the deformation in composite structures in real-time but also can detect damage initiation and damage propagation under different loading conditions. In this study, three different sensor systems are developed using smart functional materials to study their effectiveness in monitoring deformation in composites in different directions and positions under different quasi-static loadings. An additional goal of this research was to study the detection behavior of each sensor system and demonstrate whether they can identify the type of deformation besides their detection in real-time. The results established that each sensor system exhibited good potential as a flexible strain sensor for in-situ monitoring of composites and their arrangement can provide detection over a large section and unapproachable locations. The comparison of their results assisted in the selection of better sensor systems which is then utilized to detect damage and final fracture in composites during overall mechanical behavior under quasi-static and dynamic loadings. This study provides a comprehensive understanding regarding the detection behavior of different sensor systems under different operational loads and also shows that the position and direction of the sensor within the sample plays a vital role in it. Based on this detailed comparison, the selected sensor system does not only monitor the deformation in real-time but also, detect damage initiation, identify the type of damage, quantifies them, and also sense damage propagation under both quasi-static and dynamic loadings. Moreover, numerical models are developed to verify the detection behavior of this sensor system to verify the experimental results. Numerical results not only validated the experimental mechanical behavior of the composite sample but also confirmed the detection signal of the sensor placed in different positions and directions within the composite sample. This research study has resulted in several publications in rank A

journals (8 articles), 1 chapter in a book, 1 publication in SPIE digital library, and 5 oral presentations in different conferences, Annex I.

TABLE OF CONTENTS

INTRODUCTION 1

Motivation 1

Objective and scope 2

Thesis outline 3

References 5

CHAPTER 1 : LITERATURE SURVEY 9

Nomenclature 10

1.1. Introduction 11

1.2. Non-Materials approach and In-situ SHM 13

1.2.1. Infrared (IR) Thermography 13

1.2.2. Digital Image Correlation (DIC) 15

1.2.3. Laser Doppler vibrometer method (LDV) 16

1.3. Smart materials and In-situ SHM 17

1.3.1. Shape Memory Alloys (SMA) 18

1.3.2. Carbon nanotubes (CNTs) 19

1.3.3. Graphene nanoplatelets (GNPs) 21

1.3.4. Metallic nanoparticles 22

1.4. Applications of advance In-situ SHM in the detection of specific modes of failures in Composites 23

1.4.1. Axial, Flexural and Compression Strain failure 23

1.4.2. Shear, interlaminar cracking and delamination 28

1.4.3. Vibration, Fatigue and Impact failure 30

1.4.4. Environmental effects 32

1.4.5. Self-healing and Smart Repair 34

1.5. Computational modeling and In-situ SHM 37

1.6. Summary of real-time SHM methods 39

1.7. Conclusion 40
References 42
CHAPTER 2 : DIFFERENT SENSORS AND THEIR ELECTRO-THERMO-MECHANICAL BEHAVIOR IN REAL-TIME 68
2.1. Introduction 69
2.2. Fabrication process 71
2.2.1. Sensor I: Nylon/Ag fiber sensor 71
2.2.2. Sensor II: Conductive membrane (CM) 74
2.2.3. Sensor III: PAN Carbon Fiber (CF) 75
2.3. Experimental Procedure 76
2.3.1. Standalone sensor under mechanical loading 76
2.3.2. Standalone sensor under thermal loading 77
2.4. Results and discussions 79
2.4.1. Electromechanical Behavior of Each Sensor System 79
2.4.2. Electrothermal Behavior of Each Sensor System 90
2.5. Comparison of three sensor systems 98
2.6. Conclusions 101
References 104
CHAPTER 3 : REAL-TIME MONITORING OF STRAIN DEFORMATION IN COMPOSITES UNDER QUASI-STATIC LOADINGS 112
3.1. Introduction 113
3.2. Fabrication Procedure 114
3.3. Experimental Procedure 115
3.4. Results and discussions 117
3.4.1. Strain monitoring in composites during cyclic tensile loading 117
3.4.2. Strain monitoring in composites during cyclic flexural loading 128
3.5. Comparison of real-time strain monitoring behavior of all three sensor systems 143
3.6. Conclusion 146

References 150

CHAPTER 4 : REAL-TIME MONITORING OF FRACTURE IN COMPOSITE SPECIMENS UNDER DIFFERENT LOADINGS USING NYLON/AG FIBER SENSOR 155

4.1. Introduction 156

4.2. Fabrication Process 157

4.2.1. Sample preparation for tensile test 157

4.2.2. Sample preparation for the three-point bend test 158

4.2.3. Fabrication Procedure for the dynamic test 160

4.3. Experimental Procedure 160

4.3.1. Experimental procedure for tensile test 160

4.3.2. Experimental procedure for three-point bent test 162

4.3.3. Experimental procedure for dynamic test 163

4.4. Results and Discussion 165

4.4.1. Real-time monitoring of composite sample under tensile load 165

4.4.2. Real-time monitoring of composite sample under flexural load. 171

4.4.3. Real-time monitoring of composite sample under dynamic load 176

4.5. Conclusion 186

References 189

CHAPTER 5 : FINITE ELEMENT MODELING AND NUMERICAL INVESTIGATION 193

5.1. Introduction 194

5.2. Section I: Standalone Sensor-Nylon/Ag fiber sensor 196

5.2.1. 3D modeling of Nylon/Ag standalone sensor 196

5.2.2. FE analysis and verification of experimental results 198

5.3. Section II: Sensor embedded within composite under quasi-static loadings -star specimen 205

5.3.1. 3D Model of Star specimen embedded with a sensor 205

5.3.2. FE analysis and verification of experimental results during cyclic tensile loading 208
5.3.3. FE analysis and verification of experimental results during cyclic flexural loading 213
5.4. Section III: Sensor embedded within composite under dynamic impact 220
5.4.1. 3D Model of composite plate specimen embedded with a sensor 220
5.4.2. FE analysis and verification of experimental results during dynamic impact 223
5.5. Conclusion 226
References 228
CHAPTER 6 : CONCLUSIONS & PROSPECTIVES 230
Conclusions 230
Perspectives 233
Annex I: PUBLICATIONS 234

LIST OF FIGURES

Figure 0-1: Flow chart of Research study 3

Figure 1-1: Structural Health Monitoring and Human Nervous System [17]..... 11

Figure 1-2: In-situ monitoring of civil structure using IR thermography (a) Plastered wall having some cracks (b) Infrared image showing cracks and the associated regions (c) Phase image using pulsed phase thermography technique showing single stones by lighter areas and joint stones as darker regions. The phase image confirms the positions of the cracks mainly between the bricks and inside the joints. 14

Figure 1-3: Full-field strain distribution recorded by DIC around the repaired area in yy direction at 40, 80, 120, 140, 150, and 170 (failure) kN [76]. 16

Figure 1-4: A tracking laser scanning vibrometer setup is shown which has been used for measuring the vibration of a map of points on the surface of naval propeller working in water during a complete circular motion [1]. 17

Figure 1-5: (a) Shape Memory Effect and (b) Shape Memory Process [111]. 19

Figure 1-6: Resistive heating of a through-crack in a nanocomposite [2]. 20

Figure 1-7: Smart sensing Graphene sheet for GFRP Composites [161]. 21

Figure 1-8: CNTs based Piezoresistive Strain Sensors in Aircraft Application [182] (a) Experimental setup and specimen characteristics for tensile and flexural tests. (b) Tensile stress and Resistance change response w.r.t. time. 24

Figure 1-9: Investigated strain measurement and damage detection of concrete structures using CNTs experimentally for uncontrolled damage on the sixteen-contact reinforced beam: (a) measured load for each displacement-controlled loading cases; (b) change in resistance for selected sections as a function of the loading cases; and (c) test specimen showing the damage forming in sections 1 and 15, [187]..... 26

Figure 1-10: Use of graphene strain sensor for SHM to measure the strain-induced and damage accumulation in polymer composites (a) schematic of experimental arrangement (b) SEM and Optical images of tensioned polymer composites (a. Unloaded, b. 4% strained, c. 4.5% strained,

d. Fractured) (c) Curve of the residual strength and damage accumulation factor (d) The optical images of the fractured specimens under uniaxial tension [192]. 27

Figure 1-11: Experimental study of strain sensor with 3D functionalized GNPs in polymer composites (a) Piezoresistive and mechanical behaviors under quasi-static tensile loading. (b) Piezoresistive behavior of the f-GnP/epoxy composites as a function of time during incremental cyclic loading [165]. 27

Figure 1-12: Experimental study to detect interlaminar failure in composite (a) Experimental setup (b) Relative resistance change recorded during crack propagation in mode I testing [201]. 29

Figure 1-13: Study of CNTs based on a biomimetic nanocomposite strain sensor (a) MWCNT/Epoxy based fabrication of neuron with spray (b) Piezoresistive characteristics of the strain sensor (c) Dynamic characteristics of the Strain sensor response [208]. 31

Figure 1-14: Experimental study of strain sensor with 3D functionalized graphene nanoplatelets in polymer composites. Piezoresistive behavior of the f-GnP/epoxy composites as a function of time during incremental cyclic loading [165]. 32

Figure 1-15: Damage detection by Piezoelectric Sensors. (a) Crack detection on Steel Truss Bridge [238] (b) Transverse Crack Detection in Beams [239] (c) Damage detection in Aluminum Plate [240] (d) Piezoelectric Repair Patches in delaminated Beam [233] (e) Damage detection in Pipes 35

Figure 1-16: Experimental study of SMAs in concrete structures using a three-point bend test [232]. 36

Figure 1-17: Use SMA bars to study the base isolation for highway bridges (a) Theoretical model (b) Energy vs. histories due to Kobe earthquake with SMA system in bridge (c) Acceleration response with SMA and NZ isolation system to 0.6 g scaled Kobe earthquake [244]. 37

Figure 2-1: Fabrication process of the Nylon/Ag fiber sensor 72

Figure 2-2: SEM Characterization of the Nylon/Ag fiber sensor 73

Figure 2-3: SEM images of CM sensor. (a) CM sensor (b) magnified image on the surface of the CM sensor to demonstrate the network of CNTs (c) SEM at lower magnification on the edge of the membrane (d) magnified SEM image on the edge of the single layer of membrane to show the network of CNTs in forms of threads of a fabric. 74

Figure 2-4: SEM images of the CF sensor. (a) PAN carbon fibers (b) SEM of unidirectional filaments of Carbon aligned together (b) magnified image to show the single fiber of carbon. 75

Figure 2-5: Preparation of each sensor system fiber for the experimental procedure. Electrodes were attached at both end and paper support was used. 77

Figure 2-6: Experimental setup to test the sensitivity of the designed sensor systems. 77

Figure 2-7: Experimental arrangement to examine the electrical behavior of all three designed sensors under thermal loading. 79

Figure 2-8: Mechanical behavior of the Nylon/Ag conductive fiber. 81

Figure 2-9: SEM characterization of the fractured specimen. (a)-(c) show fractured fibers in each specimen with similar morphologies. (d) shows a single fractured filament of the coated yarn at 30 μm zoom presenting both ductile fracture and pull-out of the coating during large deformation. 83

Figure 2-10: Experimental calculation of the sensitivity of the Nylon/Ag Fiber sensor 84

Figure 2-11: The electromechanical response of each Nylon/Ag fiber sensor specimen 84

Figure 2-12: Mechanical performance of CM sensor. 85

Figure 2-13: Experimental behavior and calculation of the strain sensitivity of the CM membrane sensor. 86

Figure 2-14: Overall electromechanical response of CM sensor specimens. 87

Figure 2-15: Mechanical performance of CF sensor. 88

Figure 2-16: Experimental behavior and calculation of the strain sensitivity of the CF membrane sensor 89

Figure 2-17: Overall electromechanical response of CF sensor. 90

Figure 2-18: Electrical behavior of Nylon/Ag conductive fiber during thermal loading to detect thermal change. 92

Figure 2-19: Calculation of empirical relations to describe the nonlinear change in resistance with respect to temperature. 93

Figure 2-20: Electrical behavior of CM during thermal loading to detect thermal change. ... 94

Figure 2-21: Calculation of empirical relations to describe the nonlinear change in resistance with respect to temperature. 95

Figure 2-22: Electrical behavior of CM during thermal loading to detect thermal change. ... 96

Figure 2-23: Calculation of empirical relations to describe the nonlinear change in resistance with respect to temperature. 97

Figure 2-24: Comparison of different properties of all three sensor systems. 101

Figure 3-1: Star Specimen with (a) An example of a composite sample embedded with a sensor system of Nylon/Ag fiber sensors which were visible in each leg. (b) Geometric parameters of the star samples. (c)-(d) Geometrical illustration of the placement of sensor systems in their individual sample i.e. in individual leg and through-thickness (section view) correspondingly. 115

Figure 3-2: Experimental arrangement to examine the real-time strain monitoring response of each sensor system in composites. 117

Figure 3-3: Deformation mechanism of the specimen during the applied tensile strain..... 118

Figure 3-4: Placement of the composite sample between the fixture of the tensile machine 119

Figure 3-5: Mechanical performance of the composite star sample. 119

Figure 3-6: Real-time strain monitoring by Nylon/Ag fiber sensor in the composite star specimen during cyclic tensile loading 121

Figure 3-7: Real-time strain monitoring by Nylon/Ag fiber sensor during cyclic tensile strain. In test-1, sensor A was along the loading axis, sensor B at 45, sensor C at 90° and sensor D in

-45° while in test-3 the specimen was placed transversely with respect to the specimen 1 and sensor C was along the loading axis, sensor D at 45, sensor A at 90° and sensor B in -45°. 122

Figure 3-8: Sensitivity of the Nylon/Ag fiber sensor with respect to the loading axis 122

Figure 3-9: Real-time tensile strain monitoring in the composite by CM sensor and verification of the reproducibility of the test 124

Figure 3-10: Comparison of real-time strain monitoring of composite star specimen by CM sensor during test 1 (when sensor A is placed in loading direction) and test 3 (when sensor C is placed in loading direction). 125

Figure 3-11: Effect of position and direction on the sensitivity of the CM sensor with respect to the applied load. 125

Figure 3-12: Real-time tensile strain monitoring in the composite specimen by CF sensor and verification of the test reproducibility. 127

Figure 3-13: Comparison of real-time strain monitoring of composite star specimen by CF sensor during test 1 (when sensor A is placed in loading direction) and test 3 (when sensor C is placed in loading direction). 128

Figure 3-14: Effect of position and direction on the sensitivity of the CF sensor with respect to the applied load. 128

Figure 3-15: Deformation behavior of star specimen during a three-point bend test. 129

Figure 3-16: Position of the composite star samples between the three rollers for flexural bending (a) Sample placement in test 1 and 2 and (b) Sample placement in test 3. 130

Figure 3-17: Mechanical behavior of all three star-samples during flexural deflection. 131

Figure 3-18: In-situ flexural strain monitoring in composite star sample by Nylon/Ag fiber sensor and validation of electrical response of each fiber sensor..... 132

Figure 3-19: In-situ flexural strain monitoring by Nylon/Ag fiber sensor and study of strain sensitivity of each fiber sensor with respect to its position. In test-1, sensor A was on the bottom position with respect to the loading axis, while in test-2 the specimen was rotated with respect

to the roller axis and placed in such a manner that sensor A was on the top position with respect to the loading axis. 133

Figure 3-20: Effect of position and direction on the sensitivity of the Nylon/Ag fiber sensor with respect to the loading axis and position through-thickness. 135

Figure 3-21: Real-time strain monitoring in composite star specimen during cycle flexural bending using CM sensor 138

Figure 3-22: Comparison of real-time strain monitoring in composite star specimen during cycle flexural bending during test 1 (when sensor A is placed in top position according to the loading axis) and test 3 (when sensor A is placed in bottom position according to the loading axis). 139

Figure 3-23: Effect of position and direction on the sensitivity of the CM sensor with respect to the loading axis and position through-thickness. 139

Figure 3-24: Real-time strain monitoring in composite star specimen during cycle flexural bending using CF sensor. 142

Figure 3-25: Comparison of real-time strain monitoring behavior of CF sensor in composite star specimen during cycle flexural bending during test 1 (when sensor A is placed in top position according to the loading axis) and test 3 (when sensor A is placed in bottom position according to the loading axis). 143

Figure 3-26: Effect of position and direction on the sensitivity of the CF sensor with respect to the loading axis and position through-thickness. 143

Figure 3-27: Comparison of real-time detection behavior of all three sensor systems in each position in their respective composite sample during tensile loading. 145

Figure 3-28: Comparison of real-time detection behavior of all three sensor systems in each position in their respective composite sample during flexural loading. 146

Figure 4-1: (a) Example of a standard composite specimen embedded with Nylon/Ag fiber sensors after the fabrication process. (b) Geometric characteristics of the specimen and schematic representation of the position of Nylon/Ag fiber sensor in 0° and 90° direction. . 158

Figure 4-2: Schematic representation of the position of the Nylon/Ag fiber sensor in each composite specimen. 159

Figure 4-3: Fabrication process of composite specimens with incorporation of Nylon/Ag fiber sensor..... 159

Figure 4-4: Example of a composite specimen after the fabrication process. The specimen became transparent after the curing process and fiber sensor is visible..... 159

Figure 4-5: (a)-(c) Composite sample preparation process with integration of Nylon/Ag fiber sensors (d)-(e) Geometric parameters of the samples and illustration of the placement of Nylon/Ag fiber sensor in each position correspondingly..... 161

Figure 4-6: Experimental setup to test the overall real-time damage detection of the Nylon/Ag fiber sensor in the standard composite specimen. Electrical connections are highlighted with green arrows. 162

Figure 4-7: Experimental setup to test the real-time damage detection of the Nylon/Ag fiber sensor in the composite specimen under a three-point bend test. 163

Figure 4-8: Experimental setup to examine the in-situ strain monitoring behavior of the Nylon/Ag fiber sensor within the composite under dynamic impact..... 164

Figure 4-9: Experimental boundary conditions and position of impact..... 165

Figure 4-10: (a) Deformation behavior of star specimen during tensile loading. (b) Schematic representation of Sample 1 with no initial defect and Sample 2 with initial defect..... 166

Figure 4-11: Experimental stress-strain behavior of standard composite specimen with and without initial defect..... 167

Figure 4-12: SEM characterization of the fractured composite specimen integrated with Nylon/Ag fiber sensor. (a) Random orientation of fibers in the epoxy matrix. It also showed the placement of a Nylon/Ag fiber sensor (after fracture) from both the top and cross-sectional views. (b) Fracture of the Nylon/Ag fiber sensor after the failure of the composite specimen at 100 µm and 786x zoom (c) Single fractured filament of the coated yarn at 30 µm and 2850x zoom. 168

Figure 4-13: Real-time strain monitoring and damage detection by Ny/Ag fiber sensor in standard composite, specimen 1. 170

Figure 4-14: Real-time strain monitoring and damage detection by Ny/Ag fiber sensor in standard composite, specimen 2. 170

Figure 4-15: Comparison of the experimental flexural stress-strain behavior of all specimens. 172

Figure 4-16: Fracture of composite samples subjected to flexural deflection during a three-point bend test. 173

Figure 4-17: Real-time monitoring and damage detection by Nylon/Ag fiber sensor in specimen 2. 175

Figure 4-18: Real-time monitoring and damage detection by Nylon/Ag fiber sensor in specimen 3. 175

Figure 4-19: Real-time monitoring and damage detection by Nylon/Ag fiber sensor in specimen 4 176

Figure 4-20: Comparison of experimental behavior of the first two tests which were without any visible macro damage. 177

Figure 4-21: Mechanical behavior of fractured composite sample and repeatability of mechanical results. Test 1 was performed on the sample integrated with fiber sensors and test 2 and test 3 were performed on sample without fiber sensors. 177

Figure 4-22: Real-time high-speed photographs of dynamic impact test performed at v=6.5 m/s on the composite sample. 178

Figure 4-23: Mechanical behavior of all three sets of tests performed at an impact velocity of 2.5 m/s, 3 m/s, and 6.5 m/s respectively. 179

Figure 4-24: SEM characterization of a fractured sample. (a) three plies of the composite specimen with randomly oriented chopped fibers (b) higher magnification to show the presence of a crack (c)-(d) show the positions where Nylon/Ag fibers were placed. These two images were taken at two different coordinates (e) demonstrate two Nylon/Ag fiber sensors placed

perpendicular to each other and within different plies (f) shows Nylon /Ag fiber sensor at higher magnification. 180

Figure 4-25: In-situ monitoring in the composite sample by Nylon/Ag fiber sensor subjected to dynamic impact at velocity 2.5m/s. 181

Figure 4-26: (a) In-situ monitoring in the composite sample by Nylon/Ag fiber sensor subjected to dynamic impact at velocity 3 m/s. (b) Calculation of empirical relations to describe the nonlinear change in resistance with respect to time. 183

Figure 4-27: In-situ monitoring in the composite sample by Nylon/Ag fiber sensor subjected to dynamic impact at velocity 6.5 m/s. 186

Figure 5-1: 3D model and finite element modeling of the Nylon/Ag fiber sensor. 197

Figure 5-2: Discretization of the model of Ag coated monofilament of Nylon/Ag fiber sensor for numerical simulation. 198

Figure 5-3: Numerical verification of experimental mechanical behavior of Ag coated untwisted nylon yarn 200

Figure 5-4: FE analysis of the electromechanical response of Ag coated monofilament. 201

Figure 5-5: 3D discrete model (a) before failure and (b) after failure. 201

Figure 5-6: Numerical verification of experimental mechanical behavior of Ag coated untwisted nylon yarn using monofilament geometry 203

Figure 5-7: (a) Numerical verification of experimental mechanical behavior of Nylon/Ag fiber sensor (twisted yarn). (b) FE analysis of the electromechanical response of Nylon/Ag fiber sensor (twisted yarn). 204

Figure 5-8: 3D discrete model of after failure of Nylon/Ag fiber sensor monofilament 205

Figure 5-9: 3D model of star specimen embedded with a sensor at different positions and directions. 206

Figure 5-10: Mesh configuration with localized refinement. 207

Figure 5-11: An example of surface interaction between the plies of the composite. 207

Figure 5-12: Mechanical behavior and loading direction of star specimen during numerical investigation. 208

Figure 5-13: Electrical and mechanical boundary conditions applied to the 3D model of sensor embedded within the composite star specimen. 208

Figure 5-14: Maximum Von Mises stress contour during the tensile loading of star specimen. 209

Figure 5-15: Verification of Experimental mechanical behavior of Star specimen during tensile loading 210

Figure 5-16: Electrical behavior of the 3D model. The change in electrical behavior was visible in each sensor with variation with respect to the deformation in their directions. However, it can be seen that electrical behavior was negligible in the composite star specimen because of their poor conductance. 211

Figure 5-17: Real-time signal of all four sensors with respect to their position and their correlation with the cyclic tensile strain deformation of composite star specimen in numerical (N) investigation. 212

Figure 5-18: Correlation between experimental (E) and numerical (N) results of real-time strain monitoring of strain deformation in composite star specimen subjected to cyclic tensile loading in all four positions i.e. sensor A in 0°, sensor B in 45°, sensor C in 90° and sensor D in -45°. 212

Figure 5-19: Comparison of the maximum value of change in resistance of the first cycle between experimental and numerical results. 213

Figure 5-20: Electrical and mechanical boundary conditions applied on the 3D model of sensor embedded with in composite star specimen 214

Figure 5-21: Mesh configuration with local refinement for specimen subjected to flexural bending. 215

Figure 5-22: Maximum Von Mises stress contour during flexural loading of star specimen. 216

Figure 5-23: Verification of Experimental mechanical behavior of Star specimen during flexural loading. 217

Figure 5-24: Position of sensor embedded within it during the numerical investigation under flexural loading. 218

Figure 5-25: Electrical behavior of the 3D model during flexural loading. The change in electrical behavior was visible in each sensor with variation with respect to the deformation in their directions. However, it can be seen that electrical behavior was negligible in the composite star specimen because of their poor conductance. 218

Figure 5-26: Real-time signal of all four sensors with respect to their position and their correlation with the cyclic flexural strain deformation of composite star specimen in numerical (N) investigation. 219

Figure 5-27: Correlation between experimental (E) and numerical (N) results of real-time strain monitoring of strain deformation in composite star specimen subjected to cyclic flexural loading in all four positions i.e. sensor A in 0°, sensor B in 45°, sensor C in 90° and sensor D in -45° with respect to the roller axis. 219

Figure 5-28: Comparison of the maximum value of change in resistance of the first cycle between experimental and numerical results. 220

Figure 5-29: (a)-(b) Geometric parameters of the 3D model of composite plate embedded with Nylon/Ag fiber sensor in each position correspondingly. 221

Figure 5-30: Impactor geometry used in dynamic impact numerical simulation. 222

Figure 5-31: 3D model of whole assembly setup for dynamic impact 222

Figure 5-32: Mesh configuration of the whole assembly. 223

Figure 5-33: Boundary conditions applied to the 3D model assembly for dynamic impact simulation of composite plate embedded with Nylon/Ag fiber sensors. 223

Figure 5-34: Maximum Von Mises stress contour during a dynamic impact at v=2.5 m/s .. 224

Figure 5-35: Verification of experimental mechanical behavior of composite plate during a dynamic impact. 225

Figure 5-36: Conversion of change in resistance of real-time signal of the sensor in L2 position recorded during the experimental (E) test of dynamic impact and converted signal into strain deformation rate. Comparison of this experimental (E) strain deformation rate with the numerical (N) signal all four sensors with respect to their position and their correlation with the cyclic flexural strain deformation of composite star specimen in numerical (N) investigation. 225

Figure 5-37: Real-time deformation monitoring in a composite plate subjected to dynamic impact during elastic deformation in the numerical investigation. 226

LIST OF Tables

Table 2-1: Physical Properties of the PAN Carbon Fibers 75

Table 2-2: Mechanical characteristics of the Nylon/Ag conductive fiber specimens subjected to tensile loading 81

Table 2-3: Mechanical properties of CM sensor under tensile loading 86

Table 2-4: Mechanical properties of CF sensor under tensile loading 88

Table 4-1: Mechanical characteristics of the composite specimens subjected to flexural loading 172

Table 5-1: Experimental elastic, plastic and failure data of nylon and pure Ag-thin film 199

Table 5-2: Experimental mechanical and electrical behavior of star composite specimen and Nylon/Ag fiber sensor 206

INTRODUCTION

Motivation

Composites have substituted traditional materials in almost every engineering and structural application because of their extraordinary mechanical strength, low density, structural durability, resistance to environmental factors, and cost-effectiveness, however, even they have limitations and are prone to damage [1]–[4]. So, it is essential to examine and monitor their behavior during working conditions such as extreme loading situations or environmental surroundings such as moisture, creep, thermal degradation, etc. to avoid their sudden failure [5–7]. Structural health monitoring (SHM) is a well-known technique widely used to study and monitor the performance of the composites and other materials in working conditions to ensure safe and reliable structures [8]. These monitoring systems and sensors were established progressively over time from non-destructive methods to in-situ monitoring of materials [9–12]. In-situ monitoring systems had been frequently designed for detecting various types of failures in structural components such as deformation, thermal distribution, fiber cracking, corrosion, debonding/delamination, intralaminar cracking, etc. to ensure their durable service life [13–18]. Non-destructive techniques (NDT) such as ultrasonic detection, X-rays etc. can detect local damage however they often require disassembly of the structure for inspection and they aren't able to detect damage in instantaneously. Acoustic emission is often used for real-time monitoring of the failure in structures but, interpretation of the data is a complex process and mostly qualitative. So, it's important to discover novel methods for monitoring the deformation of the structure in real-time and structural health monitoring (SHM) is a renowned and extensively used system to study the behavior of the structure in real-time to guarantee their reliability and safety [8], [19]–[22]. Currently used SHM techniques include fiber optic sensors, piezoelectric or piezoresistive sensors, strain gauges and accelerometers to monitor the mechanical deformation, vibrations, or other parameters of the structure during the operation [11], [23]–[32]. However, most of these techniques can detect damage near its location therefore they must be placed near the critical zones on the structure. To counter this, sensors network systems had also been used to triangulate the location of the damage using lamb wave propagation, but the cost, size, and weight of such a system limit their use in addition to their complex data analyzing and processing [33].

So, it is important to develop an efficient multi-mode strain monitoring and damage detection system which could monitor the mechanical behavior of composite structures under different

loading conditions to avoid any catastrophic event. Moreover, through an understanding of detection behavior different sensor systems are essential to comprehend the deformation and damage mechanism of composites.

Objective and scope

The key objective of this study is to develop an efficient, robust, and elaborated detection system for real-time monitoring of different deformation/damage mechanisms in composites under different loading conditions. This includes the development of different sensor systems and comparing their detection behavior in different conditions and finding an appropriate real-time multi-mode strain monitoring and damage detection systems for composites. Following are the objectives of this research study:

i. Develop three different sensor systems using multi-functional materials and study their electromechanical and electrothermal performance in real-time. These three sensor systems include:
    a. **Sensor I**: Nylon/Ag fiber sensor fabricated by coating nylon yarn with a silver (Ag) nanoparticles using electroless plating.
    b. **Sensor II**: Conductive membrane (CM) consisting of a pure network of CNTs deposited in form of flexible thin-film using chemical vapor deposition
    c. **Sensor III**: Carbon Fiber (CF) sensor consisting of PAF carbon fiber filaments aligned straightly together.
ii. Integration of these sensor systems into composite samples respectively to monitor, identify, and quantify strain deformation in composites in different directions and positions under Quasi-static Loadings.
iii. Identify which sensor system amongst all three shows better detection behavior under all aspects.
iv. Incorporate the selected system in composites to study the damage detection and identification during final fracture under different quasi-static loadings.
v. Incorporate the selected system in composites to study the damage detection, identification, and quantification during dynamic loading.
vi. Development of robust finite element models capable of faithfully reproducing the experimental results of the different test pieces under the different loading cases.
vii. Give recommendations on the choice of sensors.

Thesis outline

To achieve the objectives mentioned above, this thesis is organized as follows:

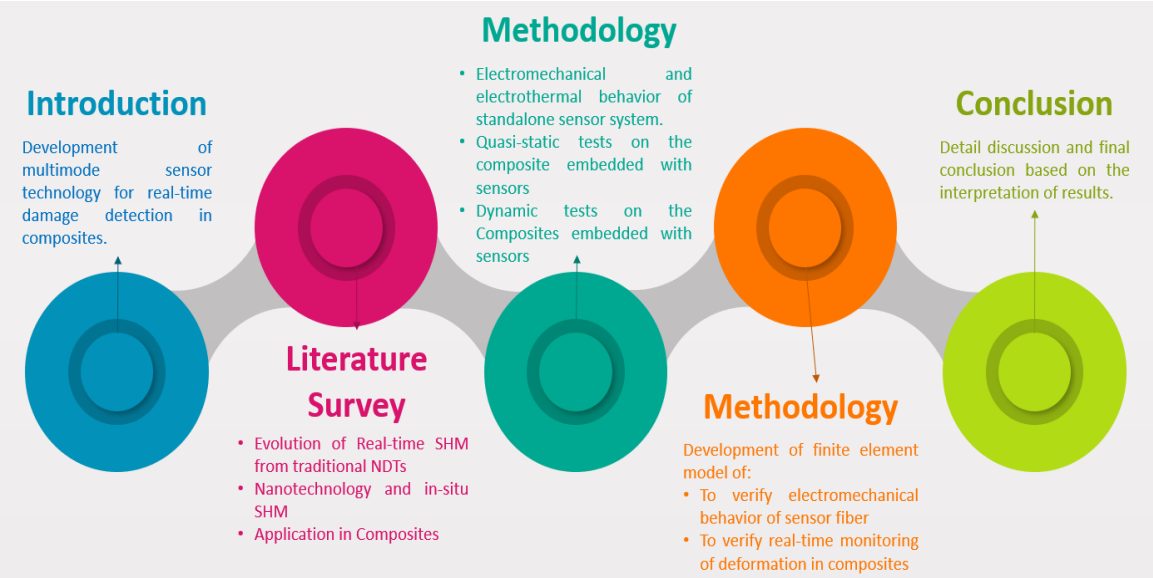

Figure 0-1: Flow chart of Research study

Chapter 1 gives a detailed literature review of structural health monitoring (SHM), its background and evolution form nondestructive testing, different classifications of SHM systems, and how nanotechnology has revolutionized the field of SHM. Furthermore, different SHM techniques were characterized according to their application in composite structures subjected to different loading conditions. Then, a summary of the current numerical and analytical studies about the damage detection by different sensors has been provided.

Chapter 2 gives a detailed description of the 3 different detectors developed as part of this work, i.e. Nylon/Ag conductive fiber, CM sensor, and CF sensor individually as a standalone sensor, as well as the study of their electromechanical and electrothermal behavior. Gauge factor calculations, overall electromechanical behavior, and electrothermal behavior under positive and negative temperature changes with empirical relations have been studied for each sensor system.

Chapter 3 provides an outline of real-time strain monitoring in composite specimens under different cyclic quasi-static mechanical loadings. Each sensor system is placed in individual composite samples at different positions and directions to elaborate strain detection, identification, and quantification. These composite samples are shaped into a star in which each leg represents the direction of the sensor in each case. This chapter also includes the study of

loading direction on the detection signal of sensors for each sensor system. The results are then compared to select the better system for multimode damage detection in composites.

Chapter 4 includes the study of overall damage behavior of composites till final fracture using the selected system under different quasi-static loadings. This chapter provides the study of the detection signal of the sensor during the fracture of standard composite samples to identify different damage modes.

In **Chapter 5**, we are interested in the study of damage detection, identification, and quantification in composite samples under dynamic loading using the selected sensor system. Low-velocity dynamic impact is performed on composite samples integrated with the selected sensors system. This study also showed the detection of damage propagation in composite during dynamic failure.

Chapter 6 provides the development of finite element models with correlation to the experimental results of a standalone sensor, real-time strain monitoring in composite star specimens, and composite plate subjected to dynamic impact.

This thesis is then provided with **general / Overall conclusion** of the research study with future recommendations for this field of research.

References

[1] M. Tarfaoui, M. Nachtane, and A. El Moumen, "Energy dissipation of stitched and unstitched woven composite materials during dynamic compression test," *Compos. Part B Eng.*, vol. 167, pp. 487–496, 2019, doi: https://doi.org/10.1016/j.compositesb.2019.03.023.

[2] O. H. Hassoon, M. Tarfaoui, A. El Moumen, Y. Qureshi, H. Benyahia, and M. Nachtane, "Mechanical performance evaluation of sandwich panels exposed to slamming impacts: Comparison between experimental and SPH results," *Compos. Struct.*, vol. 220, 2019, doi: 10.1016/j.compstruct.2019.04.051.

[3] M. Nachtane, M. Tarfaoui, S. Sassi, A. El Moumen, and D. Saifaoui, "An investigation of hygrothermal aging effects on high strain rate behaviour of adhesively bonded composite joints," *Compos. Part B Eng.*, vol. 172, pp. 111–120, 2019, doi: https://doi.org/10.1016/j.compositesb.2019.05.030.

[4] S. Sassi, M. Tarfaoui, M. Nachtane, and H. Ben Yahia, "Strain rate effects on the dynamic compressive response and the failure behavior of polyester matrix," *Compos. Part B Eng.*, vol. 174, p. 107040, 2019, doi: https://doi.org/10.1016/j.compositesb.2019.107040.

[5] J. W. C. Pang and I. P. Bond, "A hollow fibre reinforced polymer composite encompassing self-healing and enhanced damage visibility," *Compos. Sci. Technol.*, vol. 65, no. 11, pp. 1791–1799, 2005, doi: https://doi.org/10.1016/j.compscitech.2005.03.008.

[6] C. Dry, "Procedures developed for self-repair of polymer matrix composite materials," *Compos. Struct.*, vol. 35, no. 3, pp. 263–269, 1996, doi: https://doi.org/10.1016/0263-8223(96)00033-5.

[7] C. Dry and W. McMillan, "A novel method to detect crack location and volume in opaque and semi-opaque brittle materials," *Smart Mater. Struct.*, vol. 6, no. 1, pp. 35–39, Feb. 1997, doi: 10.1088/0964-1726/6/1/004.

[8] J.-B. Ihn and F.-K. Chang, "Pitch-catch active sensing methods in structural health monitoring for aircraft structures," *Struct. Heal. Monit.*, vol. 7, no. 1, pp. 5–9, 2008.

[9] A. Loayssa, "Optical Fiber Sensors for Structural Health Monitoring," in *New*

Developments in Sensing Technology for Structural Health Monitoring, S. C. Mukhopadhyay, Ed. Berlin, Heidelberg: Springer Berlin Heidelberg, 2011, pp. 335–358.

[10] B. Lin and V. Giurgiutiu, "Modeling and testing of PZT and PVDF piezoelectric wafer active sensors," *Smart Mater. Struct.*, vol. 15, p. 1085, 2006, doi: 10.1088/0964-1726/15/4/022.

[11] A. C. Raghavan and C. Cesnik, "Review of Guided-Wave Structural Health Monitoring," *Shock Vib. Dig.*, vol. 39, pp. 91–114, 2007, doi: 10.1177/0583102406075428.

[12] V. Zilberstein *et al.*, "MWM eddy-current arrays for crack initiation and growth monitoring.," *Int. J. Fatigue.*, vol. 25, no. 9–11, pp. 1147–1155, 2003.

[13] J. P. Lynch, K. H. Law, A. S. Kiremidjian, T. W. Kenny, E. Carryer, and A. Partridge, "The Design of a Wireless Sensing Unit for Structural Health Monitoring," in *3rd International Workshop on Structural Health Monitoring*, 2001.

[14] F.-G. Yuan, *Structural Health Monitoring (SHM) in Aerospace Structures*. Oxford, UK: Elsevier, 2016.

[15] J. E. Michaels, "Detection, localization and characterization of damage in plates with an in situ array of spatially distributed ultrasonic sensors.," *Smart Mater. Struct.*, vol. 17, no. 3, 2008.

[16] X. P. Zhu, P. Rizzo, A. Marzani, and J. Bruck, "Ultrasonic guided waves for nondestructive evaluation/structural health monitoring of trusses.," *Meas. Sci. Technol.*, vol. 21, no. 4, 2010.

[17] S. Sassi, M. Tarfaoui, and H. Ben Yahia., "In-situ heat dissipation monitoring in adhesively bonded composite joints under dynamic compression loading using SHPB," *Compos. Part B Eng.*, vol. 54, pp. 64–76, 2018.

[18] M. Tarfaoui, A. El Moumen, and H. Ben Yahia., "Damage detection versus Heat dissipation in E-Glass/Epoxy laminated composites under dynamic compression at high strain rate.," *Compos. Struct.*, vol. 186, pp. 50–61, 2018.

[19] Y. Qureshi, M. Tarfaoui, K. K. Lafdi, and K. Lafdi, "Development of microscale flexible nylon/Ag strain sensor wire for real-time monitoring and damage detection in composite structures subjected to three-point bend test," *Compos. Sci. Technol.*, vol. 181, 2019, doi:

10.1016/j.compscitech.2019.107693.

[20] Y. Qureshi, M. Tarfaoui, K. K. Lafdi, and K. Lafdi, “Real-time strain monitoring performance of flexible Nylon/Ag conductive fiber,” *Sensors Actuators A Phys.*, vol. 295, pp. 612–622, 2019, doi: https://doi.org/10.1016/j.sna.2019.06.036.

[21] Y. Qureshi, M. Tarfaoui, K. K. Lafdi, and K. Lafdi, “Real-time strain monitoring and damage detection of composites in different directions of the applied load using a microscale flexible Nylon/Ag strain sensor,” *Struct. Heal. Monit.*, vol. 0, no. 0, p. 1475921719869986, doi: 10.1177/1475921719869986.

[22] Y. Qureshi, M. Tarfaoui, K. K. Lafdi, and K. Lafdi, “In-situ Monitoring, Identification and Quantification of Strain Deformation in Composites under Cyclic Flexural Loading using Nylon/Ag Fiber Sensor,” *IEEE Sens. J.*, p. 1, 2020, doi: 10.1109/JSEN.2020.2969329.

[23] C. Bois, P. Herzog, and C. Hochard, “Monitoring a delamination in a laminated composite beam using in-situ measurements and parametric identification,” *J. Sound Vib.*, vol. 299, no. 4, pp. 786–805, 2007, doi: https://doi.org/10.1016/j.jsv.2006.07.026.

[24] G. Park, H. H. Cudney, and D. J. Inman, “An Integrated Health Monitoring Technique Using Structural Impedance Sensors,” *J. Intell. Mater. Syst. Struct.*, vol. 11, no. 6, pp. 448–455, 2000, doi: 10.1106/QXMV-R3GC-VXXG-W3AQ.

[25] V. Giurgiutiu, A. Zagrai, and J. J. Bao, “Piezoelectric Wafer Embedded Active Sensors for Aging Aircraft Structural Health Monitoring,” *Struct. Heal. Monit.*, vol. 1, no. 1, pp. 41–61, 2002, doi: 10.1177/147592170200100104.

[26] C. C. Ciang, J.-R. Lee, and H.-J. Bang, “Structural health monitoring for a wind turbine system: a review of damage detection methods,” *Meas. Sci. Technol.*, vol. 19, no. 12, p. 122001, Oct. 2008, doi: 10.1088/0957-0233/19/12/122001.

[27] T. G. Gerardi, “Health Monitoring Aircraft,” *J. Intell. Mater. Syst. Struct.*, vol. 1, no. 3, pp. 375–385, 1990, doi: 10.1177/1045389X9000100307.

[28] C. R. Farrar and K. Worden, “An introduction to structural health monitoring,” *Philos. Trans. R. Soc. A Math. Phys. Eng. Sci.*, vol. 365, no. 1851, pp. 303–315, 2007, doi: 10.1098/rsta.2006.1928.

[29] J. Leng and A. Asundi, “Structural health monitoring of smart composite materials by

using EFPI and FBG sensors," *Sensors Actuators A Phys.*, vol. 103, no. 3, pp. 330–340, 2003, doi: https://doi.org/10.1016/S0924-4247(02)00429-6.

[30] W. Staszewski, C. Boller, and G. R. Tomlinson, *Health monitoring of aerospace structures: smart sensor technologies and signal processing*. John Wiley & Sons, 2004.

[31] Y. ZOU, L. TONG, and G. P. STEVEN, "Vibration-Based Model-Dependent Damage (Delamination) Identification And Health Monitoring For Composite Structures — A Review," *J. Sound Vib.*, vol. 230, no. 2, pp. 357–378, 2000, doi: https://doi.org/10.1006/jsvi.1999.2624.

[32] S. W. Doebling, C. R. Farrar, M. B. Prime, and D. W. Shevitz, "Damage identification and health monitoring of structural and mechanical systems from changes in their vibration characteristics: A literature review," doi: 10.2172/249299.

[33] J. P. Andrews, A. N. Palazotto, M. P. DeSimio, and S. E. Olson, "Lamb Wave Propagation in Varying Isothermal Environments," *Struct. Heal. Monit.*, vol. 7, no. 3, pp. 265–270, 2008, doi: 10.1177/1475921708090564.

CHAPTER 1 : LITERATURE SURVEY

Vast research had been going on for the past few years to overcome the gap that still hinders real-time failure detection of composites in industrial applications. However, real-time monitoring has been made more applicable to the advancement of smart materials and nanotechnology which emerge as a possible solution for better in-situ monitoring of composite structures. Besides, numerous advance approaches other than nanomaterials are also available nowadays for in-situ SHM of composites such as spectroscopy, microscopy, and imaging. In addition, there is another important aspect on which SHM can be classified which includes a selection of in-situ SHM techniques for specific loading conditions and failure behaviors and it has limited information in the literature. This chapter provides a summary of how smart materials and development in non-material approaches have revolutionized real-time SHM technology. Then, an extensive literature review on the specific applications these advance in-situ SHM techniques to detect and monitor damage in composites under different static/quasi-static/dynamic loading parameters. This is the main objective of this study and will benefit in the selection of in-situ SHM techniques best suitable for the specific damage detection in composites.

Nomenclature

Structural health monitoring	SHM
Destructive testing	DT
Nondestructive testing	NDT
Optical fiber sensors	OFS
Fiber Bragg grating	FBG
Microelectromechanical systems	MEMS
Nuclear magnetic resonance	NME
Carbon nanotubes	CNTs
Graphene nanoplatelets	GNPs
Shape memory alloys	SMA
Single-walled carbon nanotubes	SWCNTs
Multi-walled carbon nanotubes	MWCNTs
Infrared	IR
Digital image correlation	DIC
Laser doppler vibrometer	LDV
Glass fiber reinforced polymers	GFRP
Finite element	FE

1.1. Introduction

Composites have exceptional properties such as high specific strength, specific stiffness, durability, good vibration damping ability and high wear, corrosion, and temperature resistance as compared to traditional materials but still, they are not exempt from limitations and problems [1]–[3]. Despite being a multiphase material, their mechanism of damage initiation and propagation leading to failure are well established such as corrosion, deformation, debonding/delamination, fiber cracking, thermal degradation, intralaminar cracking etc. to ensure save and durable service life of the structures [4]–[9]. The problem is that these damages or failures are not visible always so even when the overall structure is still intact, it is essential to study the strength and load-bearing capabilities of the materials in real-time to avoid any catastrophic incident [10], [11].

SHM tools were initially either destructive (DT) or non-destructive (NDT) based techniques**.** Traditionally, structural monitoring was carried out using DT such as tensile, bend, impact, and hardness test micro & macro examination of the material and NDT such as visual inspection, eddy current, ultrasound, and other wave propagation techniques based on their working principle and mode of damage detection. These methods, however, cannot assess the hidden damage during operation and most of them were validated through a simple plate or beam models and rarely through real-time structural models [12]. Thus, in-situ SHM was developed in which structural data can be collected and analyzed in real-time to identify the presence of damage [13]–[16]. Like the human nervous system, SHM consists of a network of sensors for information gathering, data processing, and decision making [17], Figure 1-1.

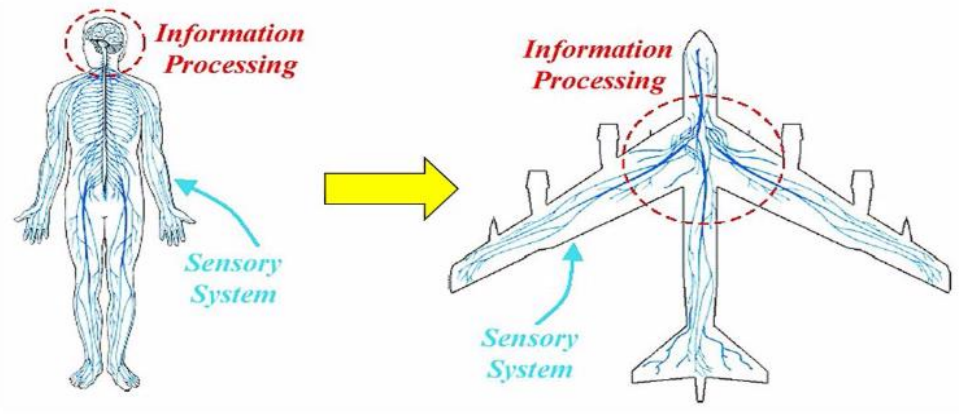

Figure 1-1: Structural Health Monitoring and Human Nervous System [17].

The development of real-time SHM is divided into three basic categories i.e. SHM techniques in the early '90s, Advanced SHM techniques from 1990-2000, and Smart or Active SHM

techniques from 2000 and onwards [18]. In the early '90s, SHM tools included wired technologies and were used only when sensors were physically in contact with the structure [19]. Mostly, impedance-based methods [20]–[23], vibration-based methods [24], data fusion methods [25], [26], and inverse methods were used at that time. The limitations of these SHM techniques included the dependence of sensors on the location, material properties and detection methods applied [19], [27]. Moreover, their installation was complexed, messy, and required a lot of calibration because of numerous wired connections. From 1990-2000, the SHM techniques were improved into wireless technology with self-organizing arrays of sensors which need less calibration. By stimulating fatigue resistance, vibration control, and load-carrying capacity, wireless SHM techniques had numerous applications such as in buildings, tunnels, bridges, and aircraft, however, the main advantage was their implementation on large structures at less cost and time [28], [29]. They consisted of both active and passive sensors with an onboard microprocessor, wireless communication, sensing capability [30]–[32]. These techniques included Optical Fiber Sensors (OFS), Fiber Bragg Grating (FBG), piezoelectric sensors, Microelectromechanical systems (MEMS), Nuclear Magnetic Resonance (NMR) and ultrasonic sensors to monitor damage in concrete, metal and composite structures [33]–[35] . However, these wireless techniques had limitations such as power management issues and reliability of sensors [19]. After 2000, the era of smart or active SHM techniques, also known as the future of SHM technology was started. It consisted of two categories i.e. material or contact approach based on nanotechnology and non-material or non-contact approach such as imaging, spectroscopy etc. Smart SHM was focused to develop a system of real time and continuous inspection, monitoring and damage evaluation with minimum involvement of humans for stable and reliable results [36]. In-situ and real-time SHM has been used frequently now a days for detecting damages such as corrosion, deformation, debonding/delamination, fiber cracking, thermal degradation and intralaminar cracking under static and dynamic loadings to ensure save and durable service life [37]. Shape memory alloys and Smart fluids are also an example of smart sensing technology [38].

Vast research had been going on for the past few years to overcome the gap and limitations that still hinder real-time failure detection of composite structures in industrial applications such as petroleum, bridges, civil structures, offshore structures, military structures, and so on. With the evolution of smart materials and nanotechnology, real-time monitoring has been made more applicable. Numerous advanced approaches other than nanomaterials are also available nowadays for in-situ SHM of composite structures which are categorized as spectroscopy,

microscopy, and imaging. In addition, smart materials such as SMA, CNTs, GNP, and metal nanoparticles are being often used now for real-time and in-situ monitoring of composite structures and are emerging as a possible solution for better in-situ monitoring. However, there is another important aspect on which SHM techniques can be classified and it has limited information in the literature. This classification includes the selection of in-situ SHM techniques based on damage detection techniques for specific loading conditions and failure behaviors. This chapter provides a summary of how the introduction of nanomaterials and development in non-material approaches has revolutionized real-time SHM technology. Then, a detailed review of the specific applications of these advanced in-situ SHM techniques to detect and monitor damage in composites under different static/quasi-static/dynamic loading parameters such as tensile, compression, flexural, shear, fatigue, impact and vibrational loading has been presented. This is the main objective of this study and it will benefit in the selection of in-situ SHM techniques which is best suitable for the specific damage behavior of composite structures. This study is important for better durability, safety, and sustainability of structures.

1.2. Non-Materials approach and In-situ SHM

Numerous advanced approaches are available nowadays for in-situ SHM of composite structures other than nanomaterials which are categorized as spectroscopy, microscopy, and imaging. Infrared (IR) thermography, Digital image correlation (DIC) and Laser Doppler vibrometer (LDV) method are some of the examples we discussed here. These approaches have advanced in methodology and applications rapidly in comparison to other non-material SHM techniques.

1.2.1. Infrared (IR) Thermography

The thermal imaging technique is a surface or subsurface damage detection method in which irregularities are indicated by differences in temperature and thermal diffusivity using IR cameras or sensors [39]. Thermal imaging techniques can be used for both local and global structural monitoring depending on the resolution of the IR camera [40], [41]. This method is categorized into two approaches: active and passive approach. A passive approach is applied generally to the materials that often have a higher temperature than ambient while active is an approach that requires an external stimulus to induce significant thermal contrast [39]. Thermoplastic stress analysis is a type of active approach that was used to study stress distribution of both isotropic and composite materials under cyclic loading even though the stress formulation in composites is more complex [42], [43]. Vibro-thermographic or also

known as sono-thermographic is another example of a thermography technique in which high power ultrasound is used as an external stimulus and can also be used for impact damage monitoring [44]. However, the primary drawbacks of this method lie in the excitation process such as the production of unnecessary heat during operation and excessive friction between the moving contacts and development of new crack while locating the existing damage [45]. Recently, heat generation through pulsed laser and transducers and by halogen lamps were introduced to overcome these drawbacks. IR Thermography had been used for SHM of structures subjected to tensile, impact, and fatigue damage [46]–[51]. IR thermography had been also used during the fatigue test of a wind turbine blade and indicated stress concentration regions & the start of subsurface damage much before any visible failure [42], [52]. IR thermography can monitor evaluation in surface temperature and provide an early indication of the failure zone in composites under both static and dynamic loadings [53]–[58]. Moreover, in the past research, it had been shown that this technique could be used for remote sensing of concrete structures such as roadways, bridges, buildings, airports, ports, and harbors. However, for accurate measurement, additional tools needed because of the presence of reinforcements, restricted accessibility, heterogeneous compositions, and complex geometries[59], [60]. This technique can also be used to monitor the durability of concrete structure by the detection of porosity and initial age hardening of concrete [61], [62]. Many researchers had used this technique to monitor the structural health of ancient buildings in real-time [63]–[65]. An example of using thermography in civil structures i.e. an ancient chapel for real-time damage monitoring is shown in Figure 1-2.

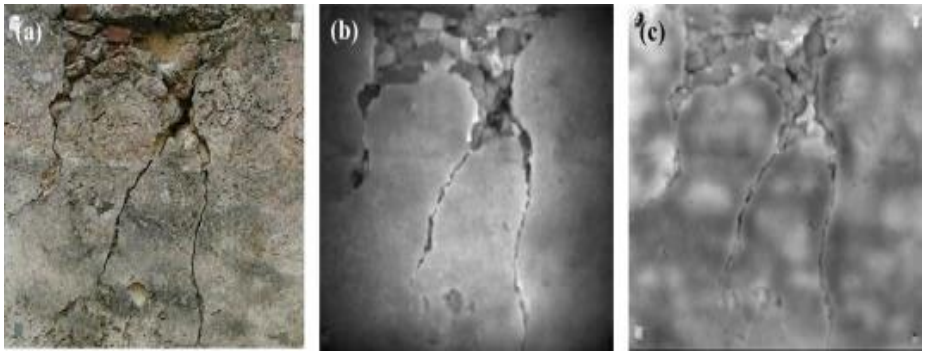

Figure 1-2: In-situ monitoring of civil structure using IR thermography (a) Plastered wall having some cracks (b) Infrared image showing cracks and the associated regions (c) Phase image using pulsed phase thermography technique showing single stones by lighter areas and joint stones as darker regions. The phase image confirms the positions of the cracks mainly between the bricks and inside the joints.

1.2.2. Digital Image Correlation (DIC)

Peters and Ranson first introduced the DIC technique in 1981 by measuring the deformation in the materials using computer-based image acquisition which was further enhanced and merged with a numerical algorithm [66]–[69]. This is an optical technique that can measure the strain and surface displacement in both 2D and 3D in real-time. However, in the case of 3D measurement, a data acquisition system capable of running two cameras simultaneously is required and it is more efficient. This technique can also detect damage initiation on curved surfaces and is not affected by large rigid body displacements. The main principle of this technique is to match the dotted pattern on the specimen before and after loading which can be prepared using white paint of black aerosol [70]. This technique is simple to operate, robust and does not require complicated surface treatments as compared to other experimental procedures such as Moire interferometry and electrical interferometry [71], [72]. However, the quality of the dotted pattern and subset size accuracy of image recording is vital to observe [73], [74]. This technique is becoming more popular than strain gauges and interferometry techniques during the recent years and more articles were published regarding advancement in its methodology and applications [75]. For example, this technique had been used to detect and analyze damage in adhesively repaired composite structures in real-time under quasi-static tensile loading. The DIC images were recorded at every 10-20 kN interval up to 170kN where the specimen started to fail and the interesting strain was in the loading direction i.e. (yy) [76], Figure 1-3.

As discussed previously, the applications of DIC technique in real-time SHM had increased rapidly in recent years ranging from traditional materials to advance composites such as nanoscale in-plane tensile deformation of ultrathin polymeric films, the effect of corrosion on bonding between matrix and reinforcements in concrete structures and measurement of thermal expansion of thin films [77]–[79]. This technique had been used to detect damage from macroscopic to microscopic scale [80]–[82], and from controlled laboratory conditions to extreme environments [83]–[87].

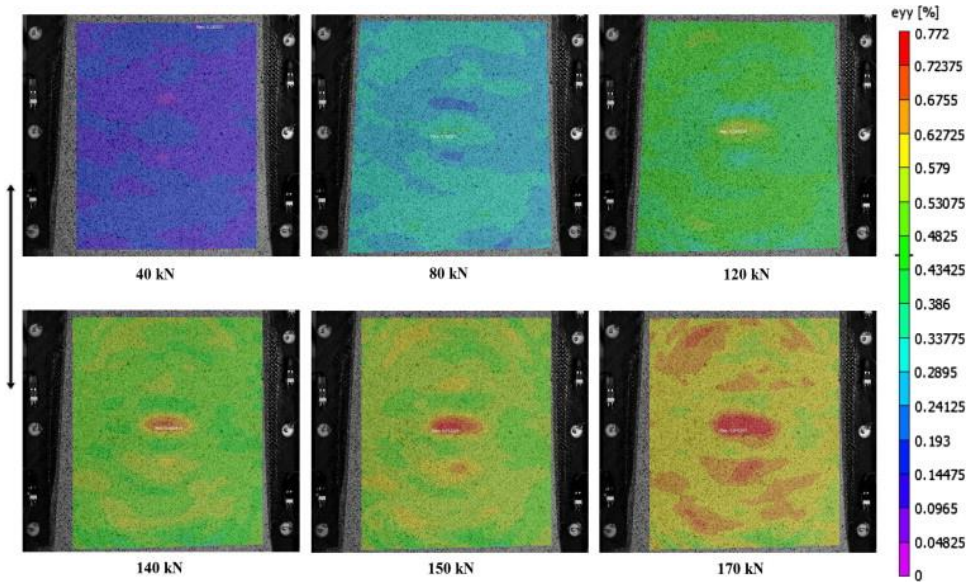

Figure 1-3: Full-field strain distribution recorded by DIC around the repaired area in yy direction at 40, 80, 120, 140, 150, and 170 (failure) kN [76].

1.2.3. Laser Doppler vibrometer method (LDV)

The LDV is also a non-contact model-based damage detection approach which works on the principle of Doppler Effect on the laser beam reflecting from the solid surface [88]. The objective of the Doppler Effect signal was to plot modal frequencies and shapes and any detectable change in these properties of the specimen depicted the presence of damage [89]. This technique has high sensitivity, can operate automatically, provides high resolution of measurement which is difficult to achieve in a conventional measuring approach and measures the response of objects that are inaccessible by traditional methods [90]. Moreover in this technique, different excitation sources can be used such as forced vibration by impact hammer, dynamic shaker, laser pulse, and ambient response [88], [91]–[94]. This method had been used to detect the vibration of a propeller of the boat underwater which showed that this technique can be applied to rotating wind turbines in real-time for damage detection using modal analysis [95]. This technique had been applied to monitor the structural health of wind turbine blades by detecting the change in operational deflection shapes of the blade to locate the damage, Figure 1-4. This was done by recording the operational deflection shapes of the structure before and after the applied load [96]. Fourier transformation was applied to the recorded vibrational response and real amplitudes were plotted at different phase angles. Moreover, with laser pulse excitation, this method is very promising for remote structural monitoring of in-service wind turbines and in extreme situations such as high voltage and temperature. A film can be recorded

and damage evaluation can be done easily. However, this SHM technique is still very expensive to be used at these large scales.

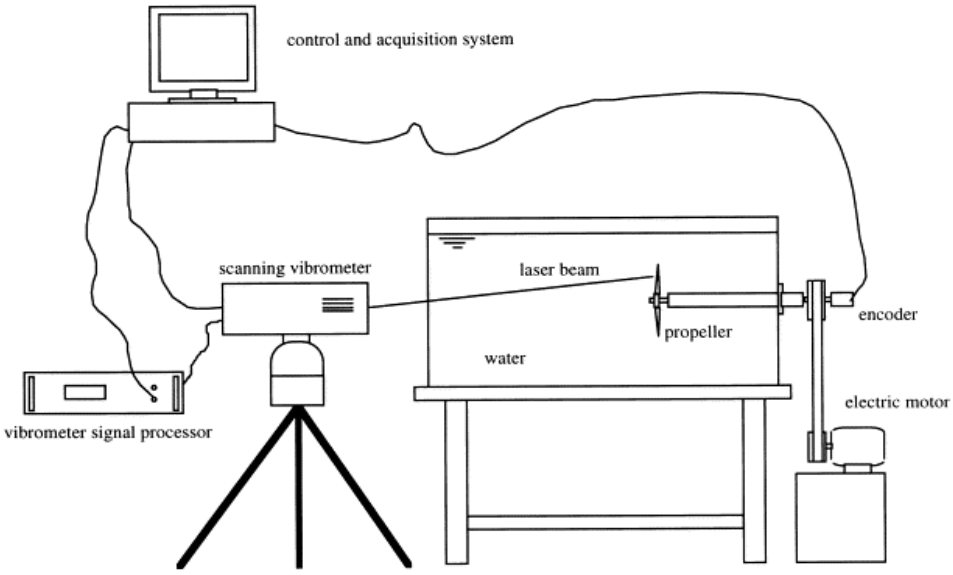

Figure 1-4: A tracking laser scanning vibrometer setup is shown which has been used for measuring the vibration of a map of points on the surface of naval propeller working in water during a complete circular motion [1].

1.3. Smart materials and In-situ SHM

Multifunctional materials for SHM have gained attention for their versatility to sense, actuate, and harvest energy from ambient vibrations [97]. Smart materials, also known as "responsive materials" [98] can respond to the external stimuli like stress, temperature, light, pressure, electric field, moisture, magnetic field, etc. [99], [100] and are a useful tool in diagnosing the damage in materials by changing their properties [101]. These smart materials also referred to as intelligent and active materials can be incorporated into the structures or bonded on the surface. They have structural functionality in addition to the logic control, signal conditioning, and power amplification for the electronic signal [101]–[103]. These smart materials were classified as Piezo-electric materials (mechanical response-dependent), Shape memory alloys, Magnatostrictive materials, Electrorheological materials, and Optical materials. Also, some smart fluids had been developed which can change viscosity over time when applied with a change in the electric or magnetic field [104]. These materials were categorized into two groups based on the input and output responses. One group consisted of materials which upon the application of stimulus generate change in shape or length of the material and the second group consisted of materials which upon the application of stimulus generate change in one of the material properties like electrical conductivity, viscosity, etc. The latter group had wide

applications in mechanical structures especially in designing complex modules and real-time structural health monitoring [105]. SMA, CNTs, GNPs and metal nanoparticles are few examples of nanomaterials used for real-time monitoring of composite structures and will be discussed here.

1.3.1. Shape Memory Alloys (SMA)

SMA is one of the examples of smart materials used for real-time damage detection and self-healing in composite structures. They are mostly metal alloys with unique properties such as complete shape recovery after the application of large strains known as superelasticity or by heating known as shape memory effect, Figure 1-5. Super elasticity [106] of these materials had enabled them to have large deformations (8%) without any residual strain which made the SMAs excellent sensors with a dynamic range 4-5 times more than other strain transducers [107]. Moreover, they presented good deformation behavior and fatigue resistance [108]. Also, these materials provided additional damping effects thus reducing the effect of residual deformation and repair costs after the seismic effects [104], [105], [109]. There are different SMAs based on thermomechanical, thermoelectrical, and thermochemical behaviors under thermal, mechanical, chemical, and electrical conditions. These SMAs, in addition to Ni-Ti and Fe-Mn-Si, also include metal alloys like ferrous SMAs, Cu based SMAs that are widely used in civil structures as metal plates, wires, bars and shells [108]. SMAs like NiTi alloys had been used as macrostrain (8%) sensors based on their simple electric resistive responses and strain relation due to martensitic transformation which are far better than the strain sensors like extensometers, optical fiber gratings etc. [110]. Shape memory polymers formed by incorporating functional nano fillers in polymer matrices, were also emerging as smart multi responsive materials known as shape memory nanocomposites. Shape memory ceramics had been studied by many scientists and researchers in different aspects [108]. These effective characteristics of SMAs has wide applications in the various fields of research such as aerospace and biomedical industries but most importantly civil structures subjected to seismic effect.

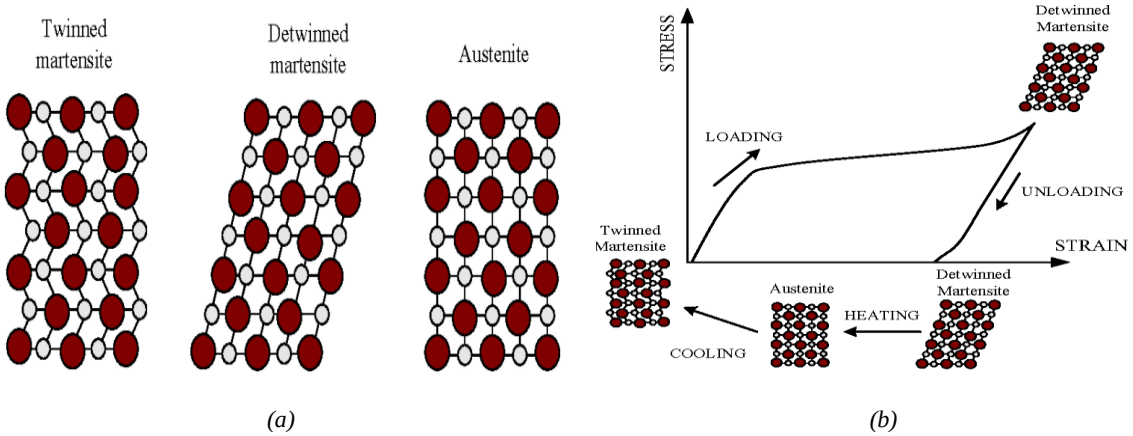

Figure 1-5: (a) Shape Memory Effect and (b) Shape Memory Process [111].

1.3.2. Carbon nanotubes (CNTs)

CNTs are a very promising technique in sensing technology since they offer structural competence and measurable response under applied stresses and strains. They have functional capabilities such as actuation, sensing, and power harvesting even when operating at very low voltage [112]–[116]. Integrating CNTs into polymers results in a whole new range of smart structure applications, advanced sensors and actuators [117]–[125]. For example, CNTs based laminate composites had been used as strain sensors with wireless transmission systems and also as a sensing skin for damage detection [126], [127]. It had been also used to develop hybrid composites with self-sensing properties [128]. Conductive thread created by twisting the CNT forests into a wire had also been used as a sensor to monitor deformation including delamination in composites [129]. There is a wide range of in-situ strain sensors based on multi-walled CNTs which are insensitive to temperature variation [130]. However, problems with the alignment of CNTs with fibers in an epoxy matrix and their dispersion is often difficult so alternative approaches such as radial in-situ growth of CNTs on fiber surface are considered [131]. In addition, the electrical response of the CNTs based sensing film depends on their concentration in the matrix because more concentration leads to more nanotube-to-nanotube junctions thus increasing the conductance but, it is not favorable to increase the concentration beyond the percolation threshold [132]. So, it is vital to evaluate the concentration of CNTs in the sensing film to optimize their sensing performance. Some research studies had also been conducted to develop CNTs based wireless embedded sensors for composite civil structures [133]. CNTs dispersed in the cement matrix not only improve their mechanical properties and develop a smart material for real-time damage detection but also result in an efficient way of crack bridging during initial crack propagation [134], [135]. Recently, the University of Cincinnati studied the potential application of CNTs in large civil structures by developing an artificial

neural system consisting of long films of CNTs as a grid/sensor network attached to the surface of the structure [136]. Furthermore, some researchers had also studied the strain sensing behavior of CNTs based nanoscale sensors using Raman spectroscopy [137] by indirect measurement of the resistance of a nanocomposite but it was very huge to be used in a sensor mechanism. Also, MEMS of these nanoparticles were developed using lithography and aligned SWNTs which can detect small cracks and measure small strains [138]. But, this system required large signal processing because of sensors array to cover large areas for real-time SHM. Recently, a new real-time SHM technique termed as Nano-engineered thermal (NET) sensing had been developed using CNTs and other conductive nanofillers [139]. In this technique, composites having aligned CNTs were heated ohmically through electrical contact and the crack was visualized by thermal imaging, Figure 1-6. Any discontinuity present could affect both thermal and electrical resistance in these structures thus enabling tomographic full-field damage evaluation for in-situ monitoring in structures such as aircrafts, automobiles and wind turbine, among others.

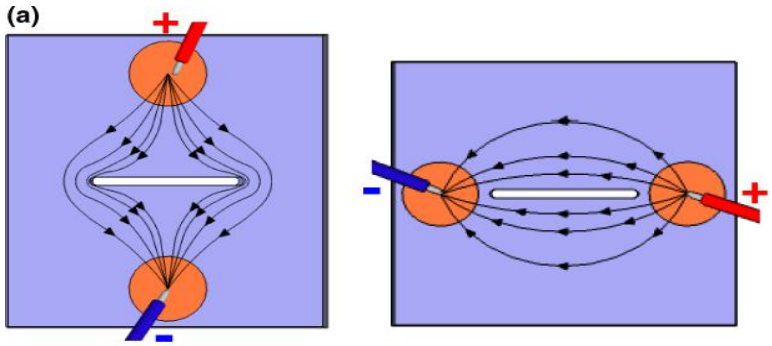

(a) indication of local heating points and electric field line concentrations,

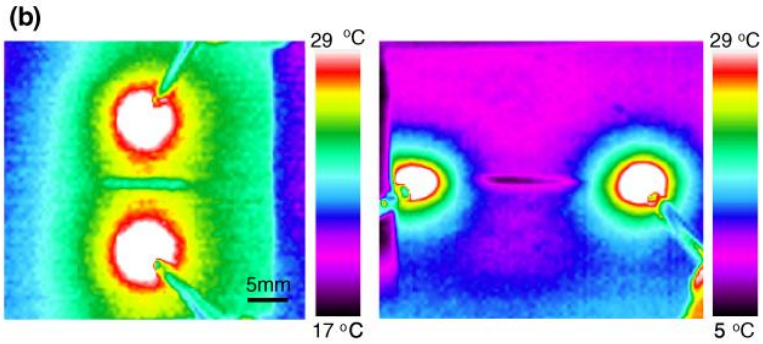

(b) thermographs with power application of < 1 W

Figure 1-6: Resistive heating of a through-crack in a nanocomposite [2].

1.3.3. Graphene nanoplatelets (GNPs)

Since the discovery of graphene and graphene-based materials (G, GO and rGO), they had been extensively used for various structural and real-time SHM applications because of extraordinary properties like ultra-high mobility, good mechanical characteristics, high conductivity and easy processing [140]–[146]. An extensive variety of gas sensors and biosensors had also been produced using graphene materials [147]–[154]. In addition, it had also shown vast potential as chemical sensors due to its high specific surface area [155], sensitivity to variations in the carrier concentration [156], single-molecule adsorption detection [157] and bipolar electric field effect [158]. One of the SHM applications of GNP was as nanofillers in composites for strain sensing [159], [160]. For example, smart sensing nanosheets of graphene were used as a strain sensor in glass fiber composites for SHM [161], Figure 1-7.

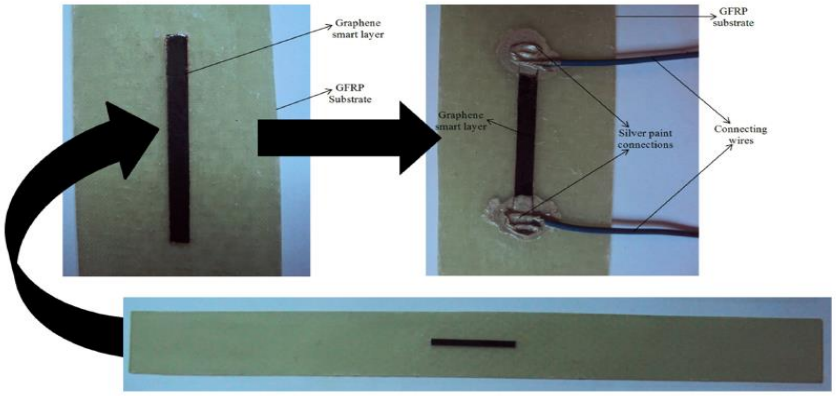

(a) Instrumented specimen

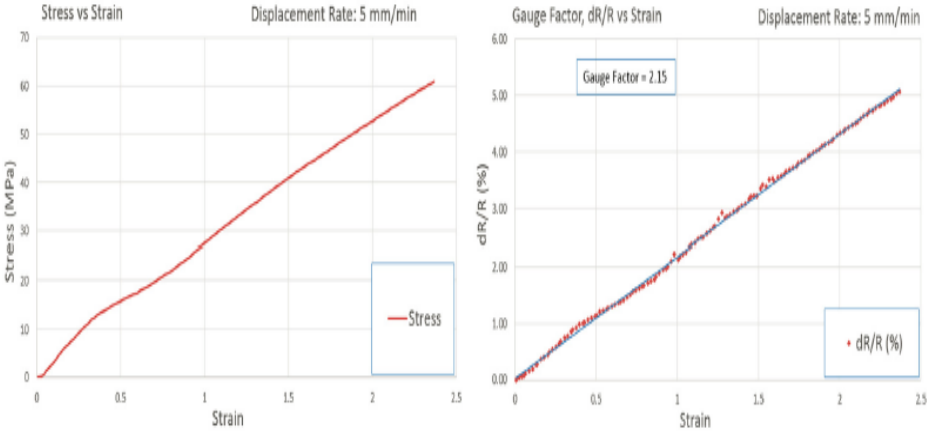

(b) Experimental Stress-Strain behavior and experimental Resistance Ratio -Strain behavior

Figure 1-7: Smart sensing Graphene sheet for GFRP Composites [161].

Moreover, flexible strain sensors for curved concrete structures had also been developed and studied using graphene, microfluidic liquid metal, and stretchable elastomer [162]. Graphene-based strain sensors are capable of differentiating between flexural and tensile strain modes due to different behavior of graphene nanoparticles during the tests [163]. These sensors are more sensitive to strain and temperature than CNTs and can provide additional details on failure and damage accumulation in composites [164]. Sensors with functionalized graphene in the epoxy matrix had also been widely used in the fields of aerospace for real-time SHM of tensile strain [165] and cementitious composites for monitoring mode III anti-plane shear failure [166], [167].

1.3.4. Metallic nanoparticles

Flexible conductive wire sensors are considered to be a very promising solution for in-situ SHM of composite materials. Currently, they had been used in a variety of functional devices especially as smart textiles in biomedical devices such as monitoring heart rate, respiration rate, and human movement [168]–[173]. Flexible electrodes in their sensing applications require high electrical conductivities so choosing a good coating material is vital and for these metallic nanoparticles are preferred over organic materials because electrical resistivity former is 2 times higher than the latter [173]. Metal nanoparticles such as gold, nickel, aluminum, stainless steel, copper, and silver are commonly used as coating materials. However, even though gold has excellent conductivity but it is expensive. Similarly, nickel is hard, brittle, and highly toxic. Stainless steel also contains some amount of nickel and has a problem of corrosion. Copper and aluminum do not have good environmental properties and oxidize rapidly when they are exposed. Amongst all these metal nanoparticles, silver (Ag) has great potential as a coating material on a flexible polymeric substrate because of its excellent conductivity, competitive price, and other mechanical properties [174]. Silver (Ag) had already been used in anti-microbial activity and textile manufacturing and as wearable sensing clothes for medical monitoring and treatments [175]–[178]. Atalay et al. [179] studied the strain sensing application of silver-coated nylon yarn in knitted sensing fabrics and concluded that the knitted fabric with sensing wire showed stability, responsivity, repeatability and low drift in the electrical signal. Moreover, another example of conductive knitted fabric for strain sensing technology was done by Metcalf et al. [180]. Although Ag metal-coated fabric was studied numerous times for antibacterial and medical activities, its application regarding structural health monitoring purposes in composites is still underdeveloped.

1.4. Applications of advance In-situ SHM in the detection of specific modes of failures in Composites

Structures during operation experience different kinds of loads in real-time for example a bridge is subjected to fatigue, vibration, flexural, expansion, and static loads such as self-weight at a time. So, the structure may be subject to different modes of failure in different directions at a time. Numerous research had been conducted over the years to study these failures and how to control them. For this purpose, different researchers had conducted studies to detect, monitor, and control different types of failures according to the application.

In the previous section, different in-situ SHM techniques consisting of non-material approaches and the use of smart materials had been discussed as a possible option for damage sensing in different composites including different stages of failure initiation and damage propagation subjected to different loadings. However, to replace the existing monitoring techniques, improvement of detection sensitivity, and monitoring system reliability, is still a challenge. The majority of the research regarding this field is performed on scale down models or specially designed samples to prove the presented concept. Very few researches have been transferred to realistic composite structures. Therefore, the initial step to bridge this gap must be to apply this knowledge and techniques to standard composite sample tests which are closer to realistic loading conditions.

In this section, we will discuss different categories of static and dynamic failures and the latest research that had been conducted to monitor these defects in real-time using advanced SHM techniques. This study is performed specifically for composite structures due to their vast application horizon.

1.4.1. Axial, Flexural and Compression Strain failure

CNTs were examined as strain sensor skin [181] in composite beam-column and in aircraft structural parts to detect damage under applied stress in both axial and flexural mode [182], Figure 1-8. Strain sensors based on CNTs had also been developed using a facile method of 3D printing to fabricate embedded uniaxial and biaxial strain sensors [183]. Moreover, CNTs base strain sensors have also found to be used for SHM of crack development and crack growth in structures with composite patching under tensile loading [184].

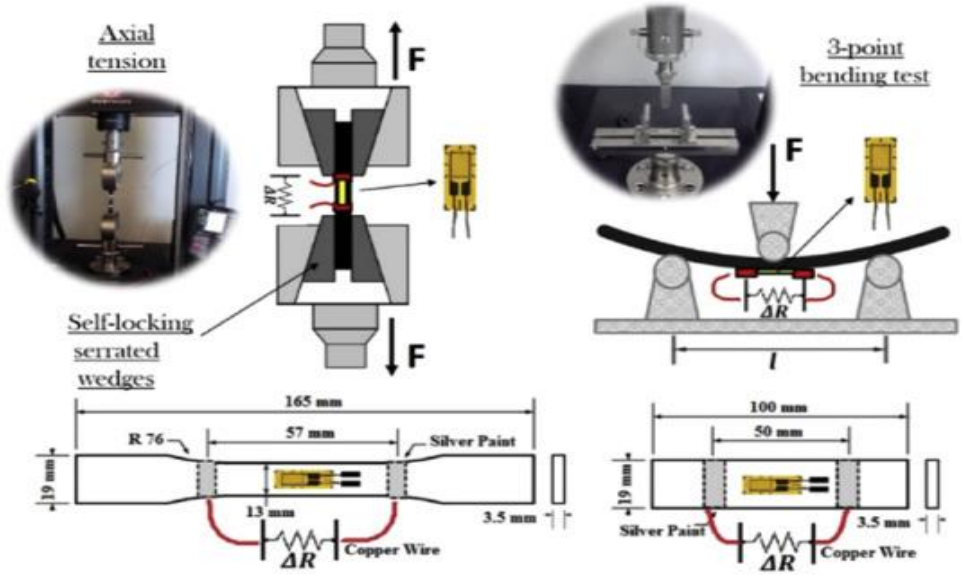

(a)

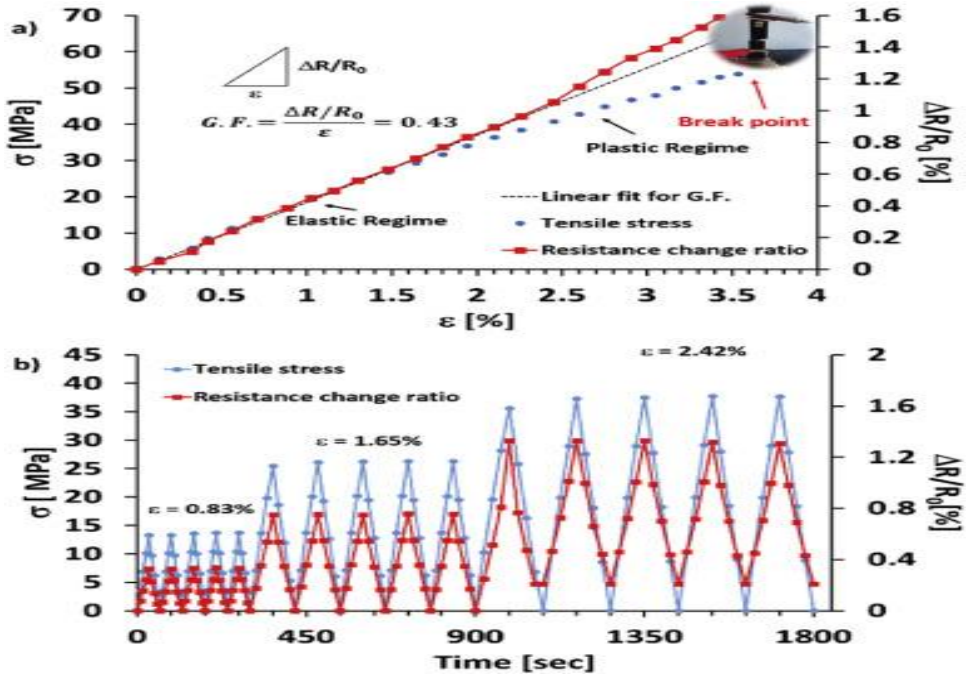

(b)

Figure 1-8: CNTs based Piezoresistive Strain Sensors in Aircraft Application [182] (a) Experimental setup and specimen characteristics for tensile and flexural tests. (b) Tensile stress and Resistance change response w.r.t. time.

Moreover, the CNTs have been also used for the SHM monitoring of structures like concrete as a strain sensor by their effective dispersion within either just the cementitious matrix or cementitious matrix reinforced with steel [185]–[187]. An example is shown in Figure 1-9. CNTs based highly stretchable elastomeric piezoresistive sensors have also been developed and tested un different quasi-static loadings [188]. These large deformation piezoresistive sensors have also potential applications especially in the biomedical field and flexible & wearable devices. Quijano et al. [189] did a similar study and designed flexible strain sensors based on

monofilament composite fibers of CNTs for SHM. CNTs based sensor films have also been developed and experimentally tested under tensile and compressive stresses and showed that strain in multi-direction and multi-location can be detected under axial tensile loading [190]. Similarly, Luo et al. [140] developed a 1D fiber strain sensor for SHM and evaluated the sensors in fiberglass prepreg laminate for multipurpose and multi-directional sensing by embedding fiber sensors at different orientations and locations. The sensor not only provided the stress-strain behavior of laminate in different deformation modes like tension, compression, bending, and failure but also provided the strain data during the curing process.

Similarly like CNTs, sensors based on graphene nanoparticles (GNPs) have also been studied to real-time SHM applications of different structures subjected to quasi-static loadings. Rehman et al. [191] studied the application of GNPs in concrete-based structures under a compressive load and demonstrated that the overall electrical behavior of the structure was decreased by increasing the compressive load especially from 10-70 % of the applied load. Jan et al. [160] prepared a smart sensing layer by dispersing graphene nanosheets in thermoplastic polymer for SHM of glass fiber composites. The results showed excellent strain sensing in the composite specimens due to its piezoresistive behavior.

Graphene-based strain sensor had been developed for SHM of polymer-based composites to measure the strain-induced and damage accumulation in composites by measuring the piezoresistive behavior of the coated fiber with reduced graphene oxide modified epoxy [192]. The electrical response of these sensors showed linear behavior during elastic and nonlinear behavior with an irregular stepped increment during plastic deformation [192], Figure 1-10. Similarly, a strain sensor with 3D functionalized graphene nanoplatelets was developed and used for SHM in polymer composites under tensile loading. This sensor sowed linear variation in low deformation and nonlinear in high deformation [165], Figure 1-11. This nonlinear behavior is correlated with the initiation and propagation of micro-cracks and defects [193]. Moreover, Moriche et al. [163] produced GNPs based SHM nanocomposites and these nanocomposite sensors showed unique capability to differentiate between flexural and tensile strain modes. Similarly, Liu et al. [194] investigated the use of GNPs to prepare cement-based strain sensors and studied their piezoresistive responses in vertical, horizontal, and inclined direction under compression loading. After that, they embedded the sensors in a beam subjected to four-point bending and detected uniaxial compression, uniaxial tension, and combined shear and compression. Moreover, they studied the strain sensing properties of cement-based

composites by incorporating carbon black and showed that a linear relationship exists between the change in resistance and compressive strain even if it is in small fractions [195].

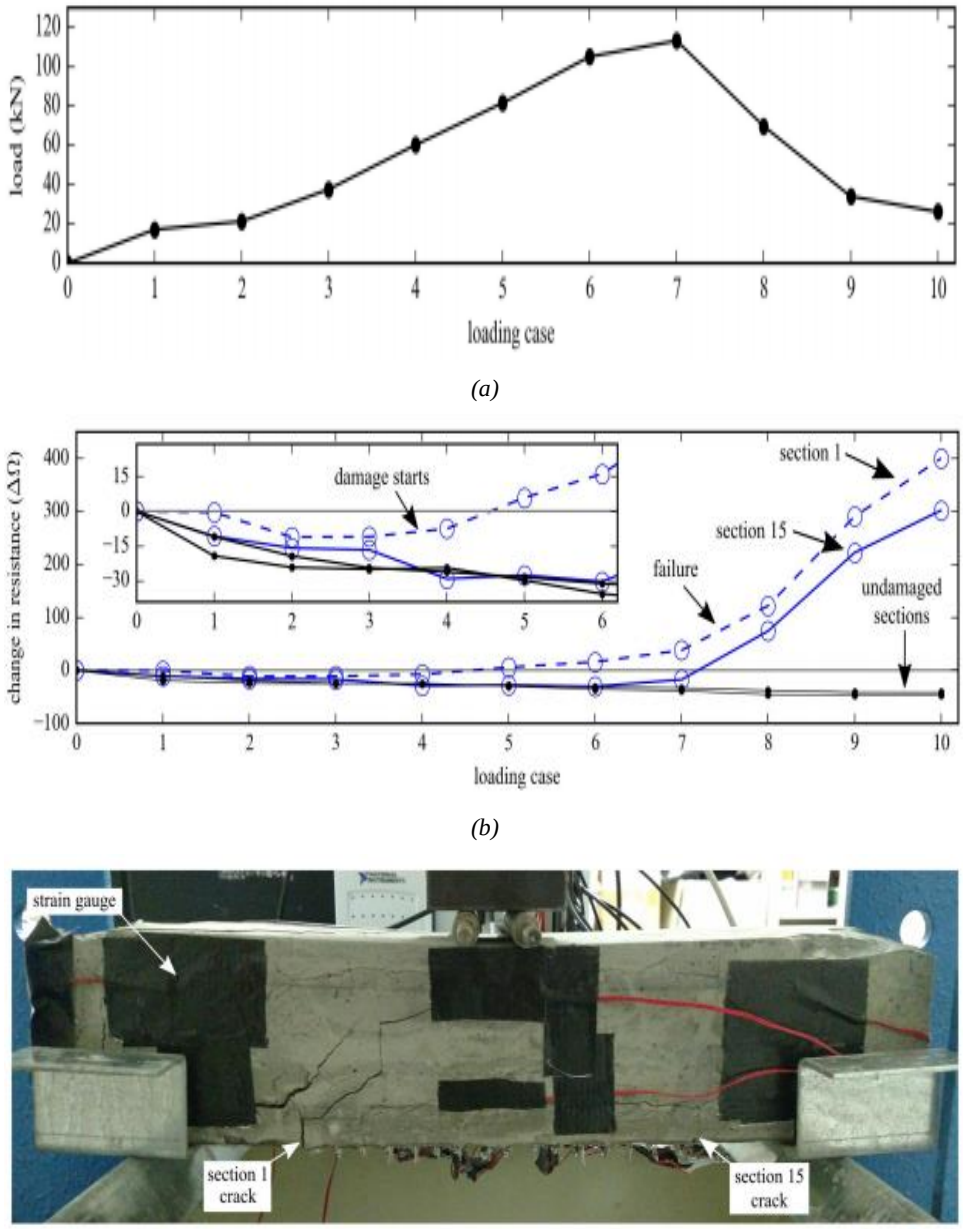

Figure 1-9: Investigated strain measurement and damage detection of concrete structures using CNTs experimentally for uncontrolled damage on the sixteen-contact reinforced beam: (a) measured load for each displacement-controlled loading cases; (b) change in resistance for selected sections as a function of the loading cases; and (c) test specimen showing the damage forming in sections 1 and 15, [187].

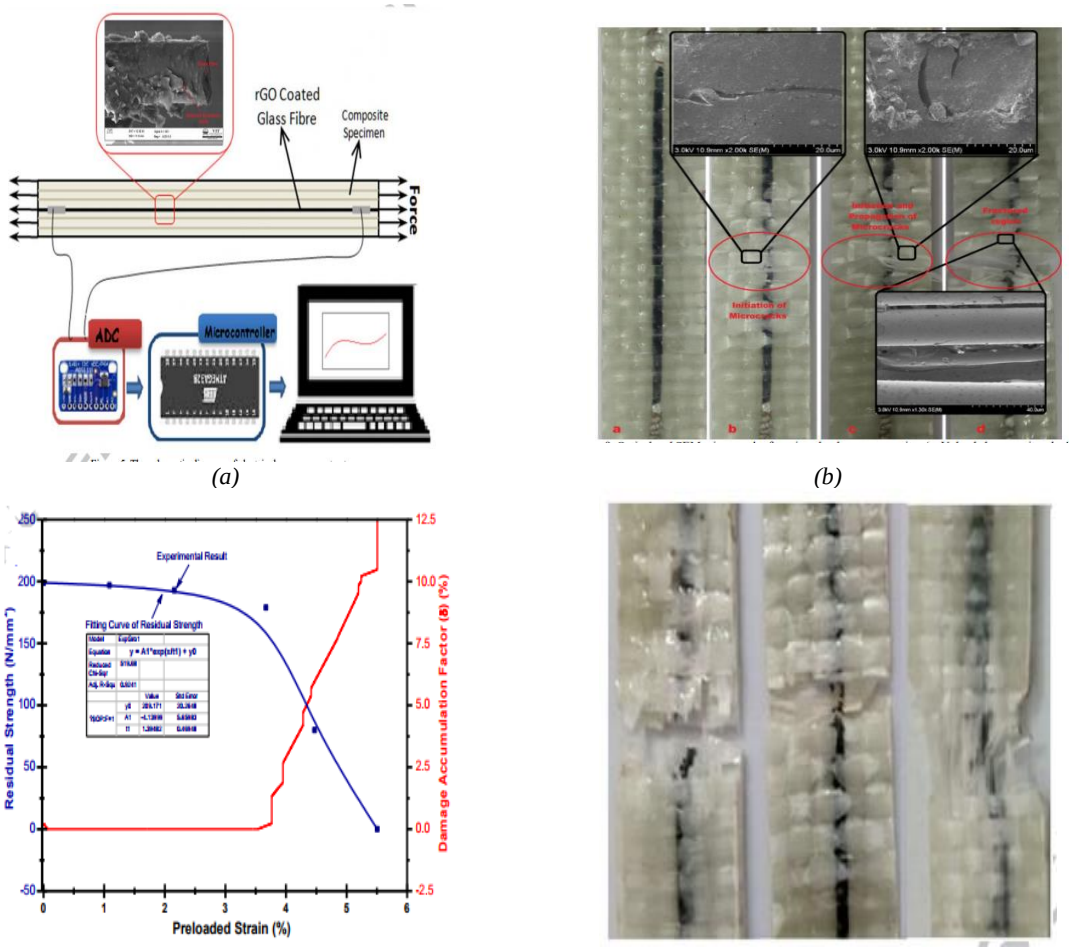

(a) *(b)*

(c) *(d)*

Figure 1-10: Use of graphene strain sensor for SHM to measure the strain-induced and damage accumulation in polymer composites (a) schematic of experimental arrangement (b) SEM and Optical images of tensioned polymer composites (a. Unloaded, b. 4% strained, c. 4.5% strained, d. Fractured) (c) Curve of the residual strength and damage accumulation factor (d) The optical images of the fractured specimens under uniaxial tension [192].

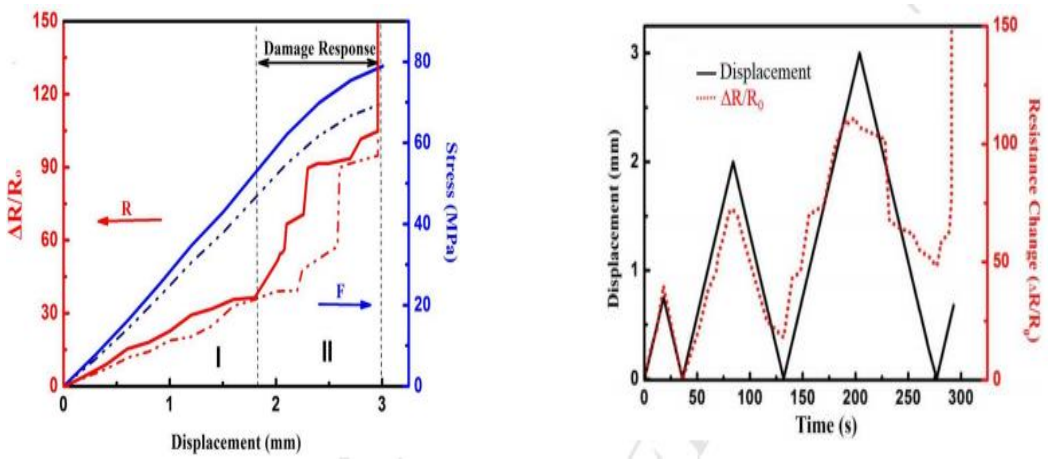

(a) *(b)*

Figure 1-11: Experimental study of strain sensor with 3D functionalized GNPs in polymer composites (a) Piezoresistive and mechanical behaviors under quasi-static tensile loading. (b) Piezoresistive behavior of the f-GnP/epoxy composites as a function of time during incremental cyclic loading [165].

In addition to material approaches, non-material approaches have also been used to study the mechanical behavior of composites in real-time. For example, the DIC method can capture strain singularity regions on the surface of the composite laminate caused by buckling during compression [196]. Likewise, Fiber Bragg Grating (FBG) has been used to studied the real-time monitoring of stiffened composite panels under compression loading using FBG [197]. FBG monitored the structural integrity of the structure by comparing the real-time monitoring of reference, impacted, and fatigued panels under compression loading. The tests clearly showed that the presence of damage affects the buckling of the panel.

1.4.2. Shear, interlaminar cracking and delamination

In addition to tensile and flexural bending, shear and interlaminar failure play a vital role in defining the strength and performance of the composite structures. So it is essential to have SHM systems with the ability to monitor these types of failures in real-time to ensure safe and durable structures. Huang and Chang [198] studied the effect of the use of superelastic SMA bars and tubes as a dowel and studied the double shear connections at different displacements and compared it with mild steel dowels. Although mild steel dowel presented high strength, the SMA dowel connections showed good self-centring behavior and reduced the residual deformation to a large scale after excessive distortion. SMAs hybrid yarn had also been designed and studied as a textile-based actuator in fiber-reinforced polymers [199]. In this hybrid yarn, SMA material act as core and glass & polypropylene staple fibers as cover to ensure maximum SMA movement in the composite through current-induced stimulation.

Also, strain sensors of CNTs have been developed for monitoring delamination and interlaminar defect in composites[130] [200]. For example, CNTs have been used in composites as reinforcement for better interfacial bonding and act as a piezoresistive strain sensor simultaneously [136]. In a short beam of GF/CNT hybrid composites, it was found that through-thickness resistivity was not changed during the study of interlaminar shear failure [141]. However, Zhang et al. [142] detected interlaminar shear damage by monitoring through-thickness resistance, as the signals changed with increasing load simultaneously which ensures detection of early-stage matrix damage. Plasma functionalized carbon nanostructures (CNS) had been developed and incorporated in the interlaminar region of a composite specimen which didn’t only improve the interlaminar properties of the structure but also enabled damage monitoring because of change in electrical resistance with the introduction of crack [201], Figure 1-12.

A 2D laser-based damage illumination method had also been used to monitor and distinguish the crack and delamination of the GFRP specimen in real-time which is useful for automatic digital damage examination [202]. In addition, functionalized graphene epoxy sheets had also been fabricated and inserted in prepreg as a leaf in the carbon epoxy composites [203]. When they were co-cured together not only the mode I fracture energy was increased by 140% but the change in electrical resistance of graphene epoxy leaf helped in monitoring the health of the structure.

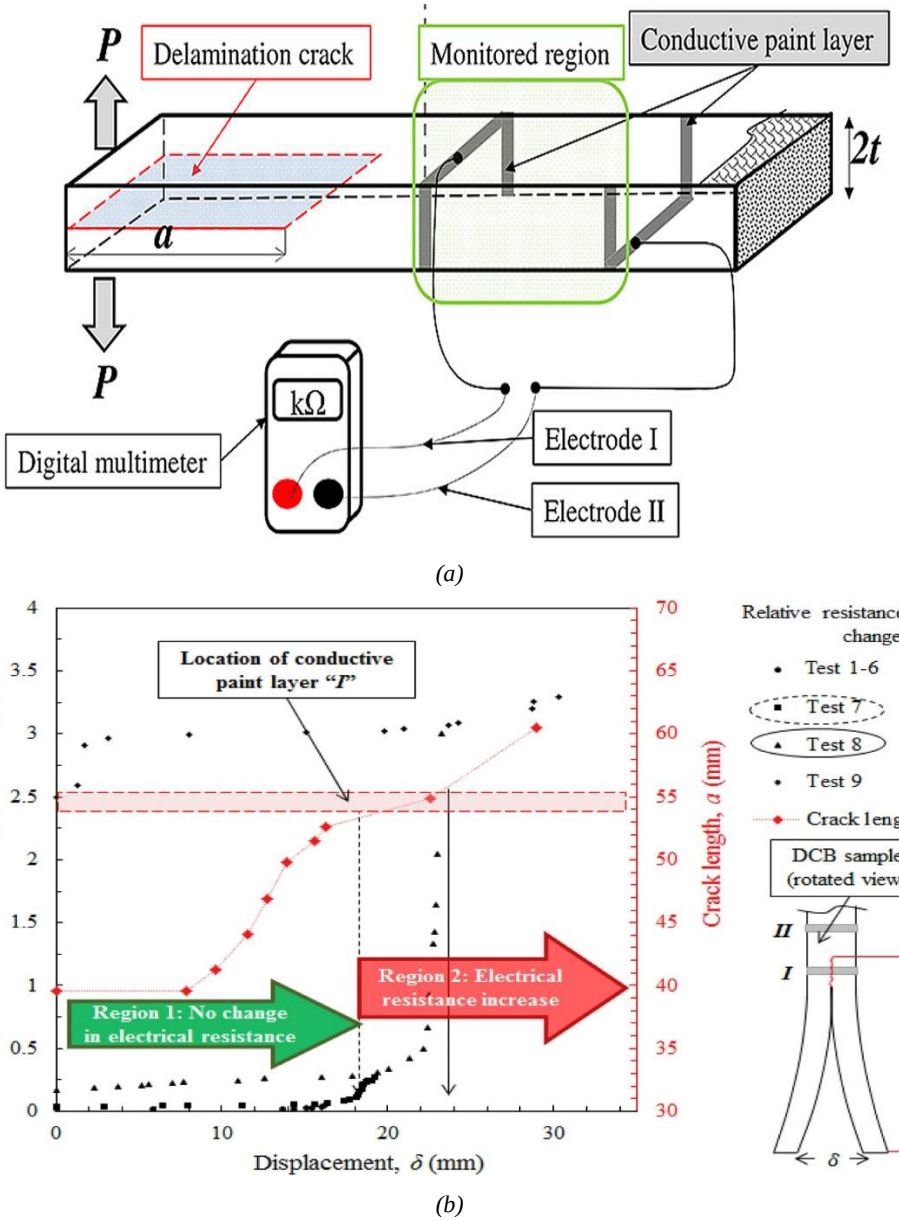

Figure 1-12: Experimental study to detect interlaminar failure in composite (a) Experimental setup (b) Relative resistance change recorded during crack propagation in mode I testing [201].

1.4.3. Vibration, Fatigue and Impact failure

These failures are undoubtedly the most common modes of failures and are extremely complex and often hidden until there is a complete failure. Vibrational, impact, and fatigue cracks are most frequently studied because they are strongly affected by localized properties of the material such as the scratches or welding defects, grain structure of the material, undesired inclusions, etc. Different in-situ SHM techniques had been utilized to detect and study the behavior of such failures to avoid sudden incidents.

NiTi shape memory alloys had been used in developing numerous active, passive and hybrid vibration isolation and absorption devices [204]. These smart materials were also used as passive energy dissipaters and actuators materials [205] such as SMA rubber bearings for controlling building vibrations [206]. Also, Senf et al. [207] studied the characteristics of adaptive composites and their components regarding the integration of SMA wires with high sensitivity for seismic design purposes.

Choi *et al.* [208] developed a biomimetic nanocomposite strain sensor, a neuron for SHM, and detection vibrational failure of a composite cantilever, Figure 1-13. CNT sensors had been used for SHM of crack development and growth in aluminum structures using composite patching under cyclic loading [184]. Moreover, CNTs network had been used as a sensor in advanced fiber composites during cyclic loading [209]. The strain and the electrical resistance relation showed considerable hysteresis because of the formation and opening and closing of crack during loading. Thin-film strain sensors using single-walled CNTs were tested experimentally on partial steel frame under cyclic loading using four-point bending [181]. These thin films can measure a high strain rate (more than 3000 μm/s) with high sensitivity and linearity. Isaac-Medina *et al.* [210] studied the in-situ SHM of impact failure in composites subjected to low-velocity impact using a network of CNTs dispersed in the specimen. They conducted impact test on two types of specimens and spatial electronic resistance was not only able to detect damage progression but also showed that the specimen with multi-walled CNTs (MWCNTs) on fibers were more sensitive to the delamination and interfacial damage than the specimens having MWCNTs only dispersed in the matrix.

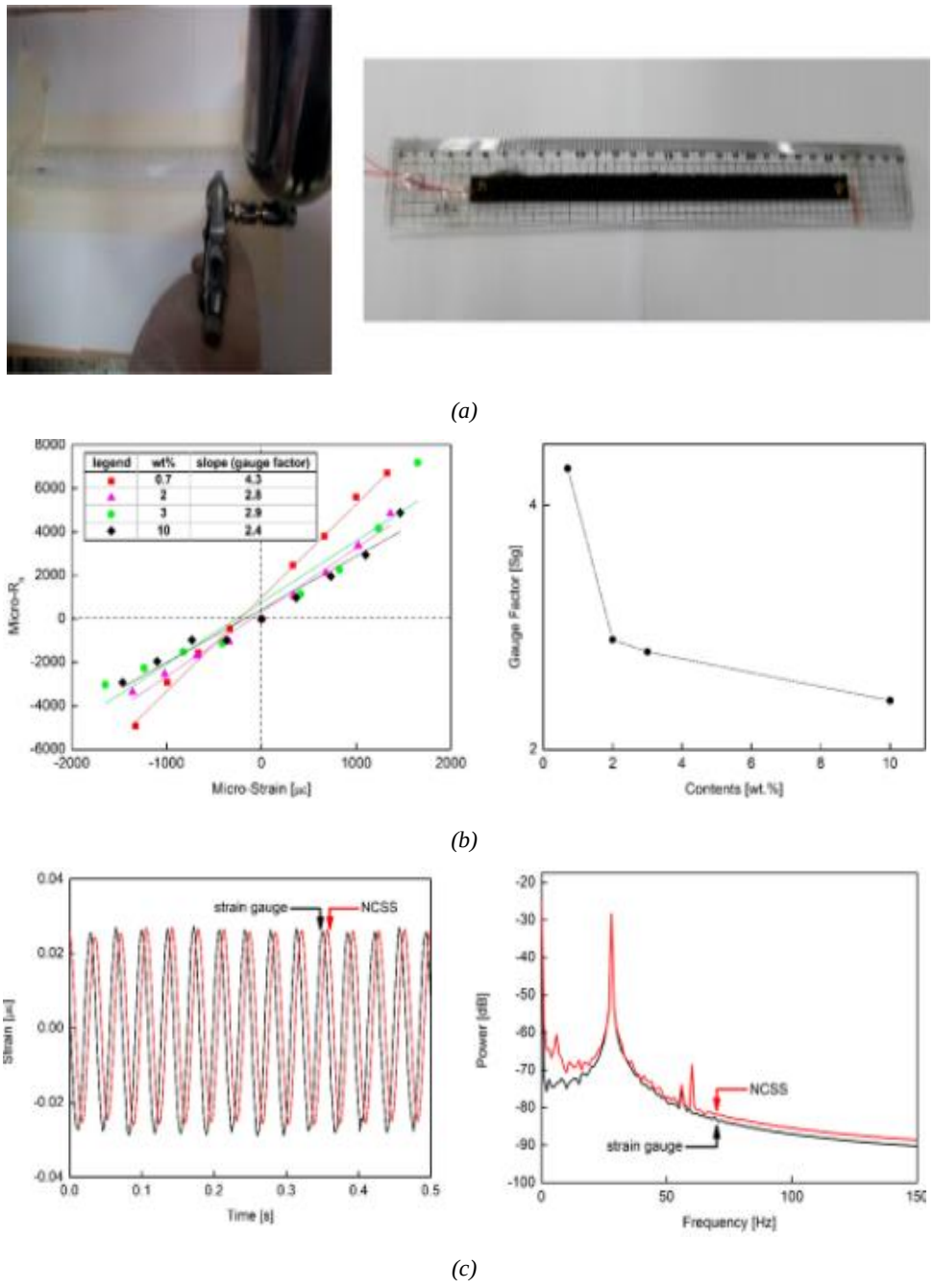

Figure 1-13: Study of CNTs based on a biomimetic nanocomposite strain sensor (a) MWCNT/Epoxy based fabrication of neuron with spray (b) Piezoresistive characteristics of the strain sensor (c) Dynamic characteristics of the Strain sensor response [208].

Similar to CNTs, sensors based on graphene were also developed to monitor the behavior of composites subjected to cyclic loadings and showed linear variation in low deformation and nonlinear in high deformation [165], [211], Figure 1-14.

Fargione et al. [212] studied the thermal energy release and rise in temperature during fatigue testing and showed that fatigue curves can be detected rapidly by this technique. Rosa and

Risitano used a similar procedure to determine the fatigue limit of the materials by examining the temperature change of the external surface [213]. Moreover, infrared thermography could also be used for fatigue induced damage by early detection of intrinsic dissipation of energy and to rapidly evaluate the fatigue strength of the material [49]. IR thermography was also used to study glass/epoxy laminate under bending fatigue by examining the heat dissipation during the test by investigating the change in surface temperature [214]. This thermal change was resulted because of the thermal energy dissipation during the test and fall in temperature after the sudden stopping of fatigue loading.

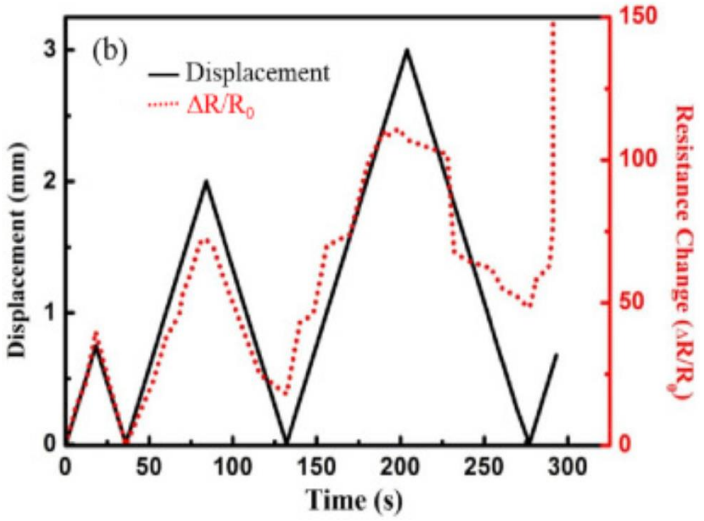

Figure 1-14: Experimental study of strain sensor with 3D functionalized graphene nanoplatelets in polymer composites. Piezoresistive behavior of the f-GnP/epoxy composites as a function of time during incremental cyclic loading [165].

IR thermography had also been used for in-situ SHM of GFRP composites subjected to impact loading and results showed that it is suitable for material characterization [215]. After the specimen was subjected to impact energy below 7J, a quick decrease in temperature followed by rapid recovery to room temperature was observed i.e. material exhibited only elastic response. In contrast, when impact energy above 7J was applied hotspots were observed which indicated the presence of damage initiation regions. Also, it was observed that the heat generation regions and damage initiation regions were the same.

1.4.4. Environmental effects

In composites, many environmental effects are also responsible for degrading their mechanical response during operational conditions. So, it is important to consider the development of in-

situ SHM techniques for monitoring the environmental effects such as corrosion, thermal effect, and in some cases moisture absorption, humidity, and chemical effects. Recent developments in the application of real-time monitoring in the detection of these environmental effects in composite structures will be briefly discussed here.

Infrared (IR) thermography had been used to monitor the corrosion defects hidden in the steel used as reinforcements in concrete structures because corrosion defects cause a change in surface temperature which can be used for their characterization and rate of rising in temperature increased with the degree of corrosion [216], [217]. Moreover, piezoceramic patches had also been used to monitor chloride-induced corrosion in reinforced concrete structure by observing the breakdown of the passive film formed in a highly alkaline environment [218]. CNTs had also been studied as a novel SHM technique to detect a wide range of damages including thermal degradation by monitoring a large area of the specimen in multi-direction [219].

Graphene-based nanosensors [220] demonstrated the use of SHM of concrete structures by monitoring the relative humidity and porosity because it could help to provide useful knowledge of drying shrinkage and intrinsic permeability measurements. Moreover, graphene oxide (GO) film has been used as an optical humidity sensor using a dip-coating technique by showing a linear optical shift with a change in humidity level [221]. This development opened doors for in-situ monitoring in different applications such as civil structures. The graphene-based thin-film had also been studied for moisture adsorption monitoring because of their effective response to change in water gradients [222]. Later Li *et al.* [223] developed a humidity switch yarn sensor based on CNTs and water-swellable polyvinyl alcohol (PVA) which show the change in resistance with an increase in relative humidity for real-time monitoring applications. Starkova *et al.* [224] studied the change in electrical resistance of CNTs nanocomposites to monitor the hydrothermal aging effect. The specimens with different pre-history environmental exposure were studied under tensile loading and specimen with fewer CNTs showed a more nonlinear increase in their resistance because of epoxy swelling and the dominant role of the tunnelling effect.

Moreover, nanocomposite sensors were developed to monitor and studied acid penetration detection in composites over time [225]. The sensors developed using CNTs showed high sensitivity whereas sensors developed from polyaniline showed more adequate tracking of acid penetration.

1.4.5. Self-healing and Smart Repair

Piezoelectric repair patches are used for SHM because their interaction and strength can be adjusted to work with environmental changes and they have less stress concentration on the damaged component. These smart patches have multiple functions like self-structural health monitoring, self-healing, and self-vibration control. The repair piezoelectric materials were first used in damaged steel structures [226]–[228] then to repair concrete beams [229] and fractured [230] and damaged structure with moving masses [231]. For the first time, Song et al. [232] studied the piezoelectric smart patches with shape memory alloy in which piezoelectric material was used to detect the cracks and their severity while shape memory cables were used to heal the damage in the structure. These patches were also used for in-situ SHM and repairment of the delamination of beams [233], the notched beam under static [234] and dynamic loading [235] and notched column under compression. Some of these aplications are illustrated in Figure 1-15. A new approach to repair GFRP composites by using ultraviolet (UV) cured resin had been presented in literature in which damaged part is repaired by by exposing it to UV light [236]. The repair process was examined by subjecting the composite specimens injected with UV resin to a double cantilever beam test. Ahmed et al. [237] presented a novel approach in which CNTs based sensing layer was integrated in the adhesive bond between steel and composite structure. This didn't only monitor the crack developed in the primary substrate and bond integrity but also act as a repair patch when studied under fatigue test. These patches were developed by coating aramid fibers with CNTs and they increased the fatigue life of the specimen by 380-500%.

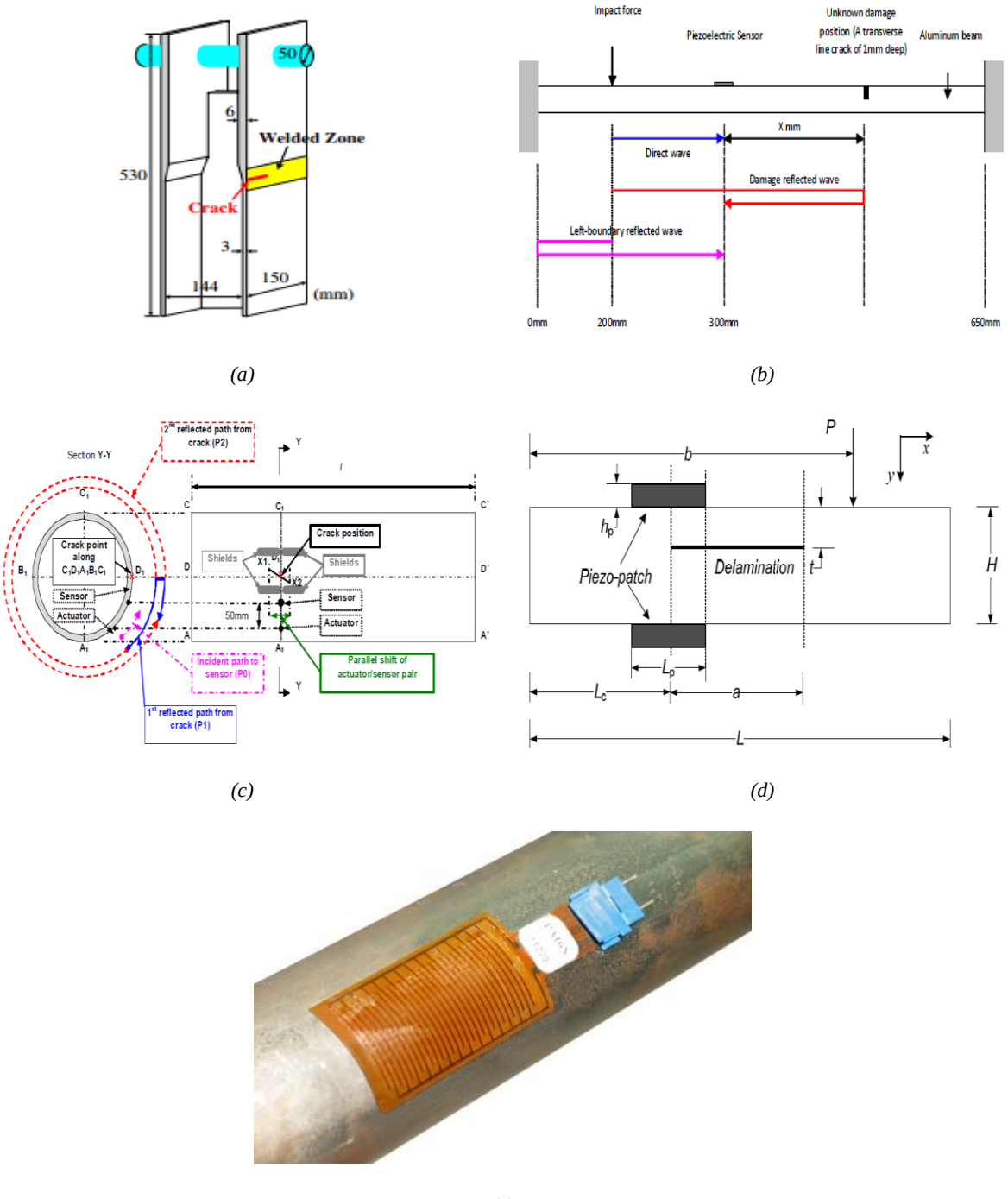

(e)

Figure 1-15: Damage detection by Piezoelectric Sensors. (a) Crack detection on Steel Truss Bridge [238] (b) Transverse Crack Detection in Beams [239] (c) Damage detection in Aluminum Plate [240] (d) Piezoelectric Repair Patches in delaminated Beam [233] (e) Damage detection in Pipes

Shape memory polymers and their composites have large applications such as morphing structure, smart textiles and fabrics, foams, deployable structures, and self-healing composite systems [241]. SMAs are used in self SHM, rehabilitation, and vibration damping of flexural damage in concrete structures using two smart materials i.e. SMAs and piezoceramics [232], Figure 1-16. They are also used in the detection of strain deflection and healing in concrete

beams [242], monitor and repair of loosened bolts in bolted joints [243], and detection and damping of vibrations in highway bridges [244], Figure 1-17. Shape memory alloy particles are used to local and repair structural damage in the root rib of an aircraft wing[245]. These smart materials are also used as wire actuators for detection and suppression of mode I and mode II interlaminar crack in composites under static and cyclic loading [246], detection of deflection, and repairing of the beam by smart fiber metal laminate [247]. Zhu et al. [248] presented a novel technique of self-pressurized healing system for composite structures in which polypropylene (PP) tubes filled with the mixture of foaming agent and healing agent were placed between the plies. At the time of healing, the internal pressure is greatly increased because of the foaming agent and the healing agent will flow smoothly soon after breakage. More details about the recent research regarding self-healing polymeric composites can be found in [249].

(a) Crack formation during loading

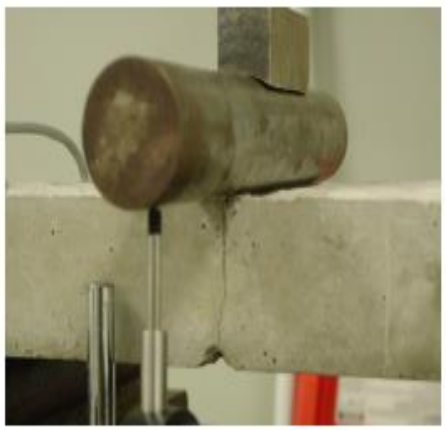

(b) Closing of crack after healing

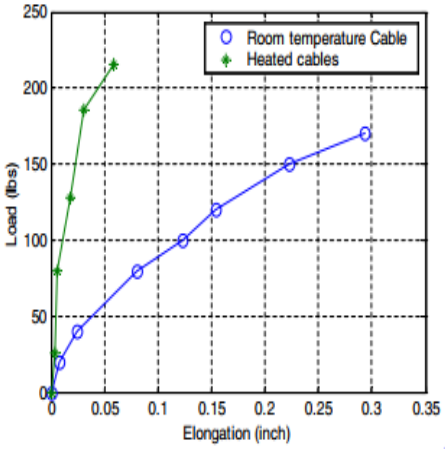

(c) Load-Elongation curve of SMA Cables

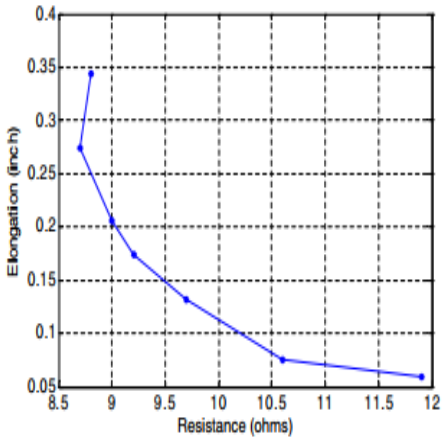

(d) Elongation-Resistance curve of SMA cables reinforced in concrete beam

Figure 1-16: Experimental study of SMAs in concrete structures using a three-point bend test [232].

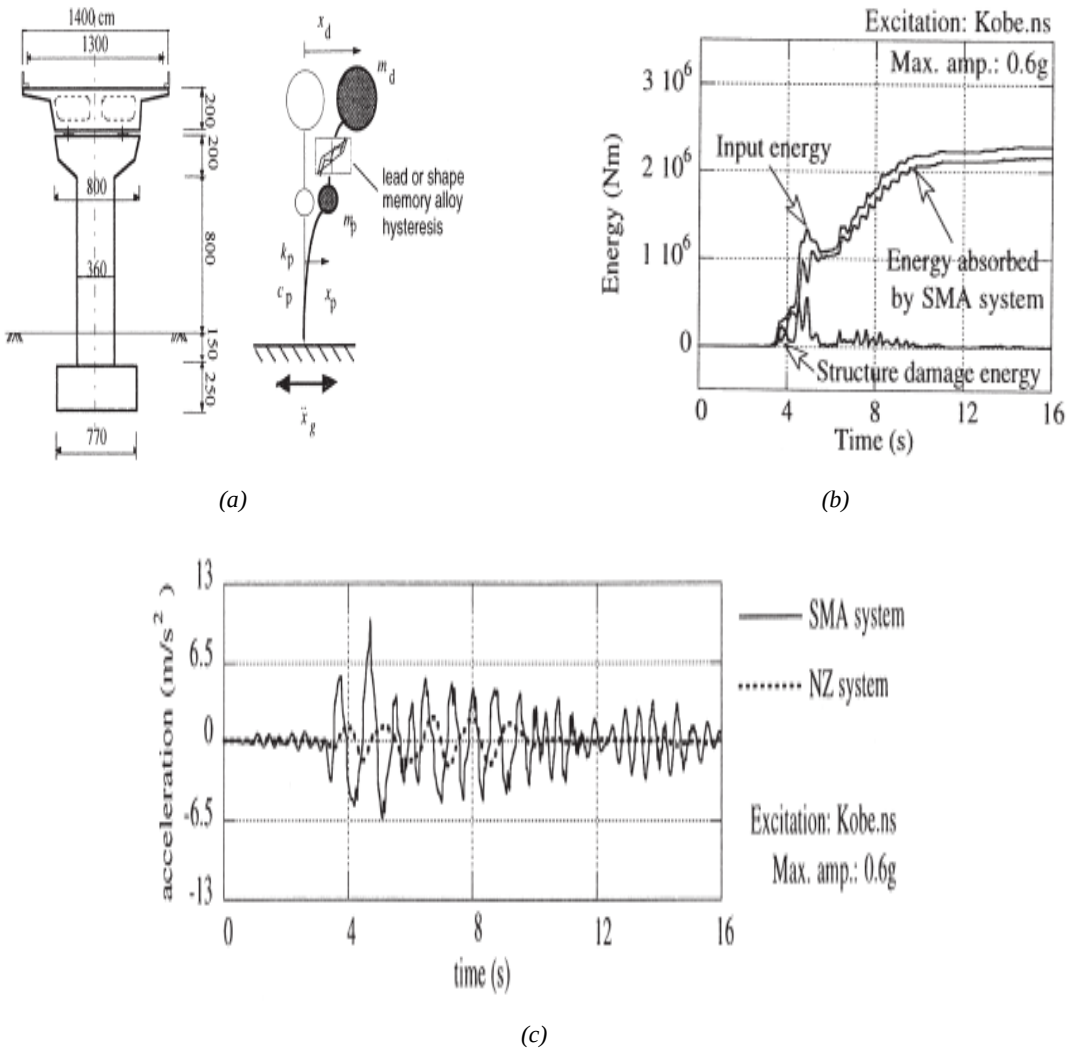

(a) *(b)*

(c)

Figure 1-17: Use SMA bars to study the base isolation for highway bridges (a) Theoretical model (b) Energy vs. histories due to Kobe earthquake with SMA system in bridge (c) Acceleration response with SMA and NZ isolation system to 0.6 g scaled Kobe earthquake [244].

1.5. Computational modeling and In-situ SHM

In addition to experimental investigation, numerical and analytical approaches had also been used to model the real-time behavior of different sensing techniques. They include advanced in-situ SHM techniques such as Piezo-electric sensors, ultrasonic transducers to in-situ SHM with nanomaterials. However, the FE modeling of SHM with nanotechnology is still under development. In this section, recent advancements and applications of FE modeling in real-time monitoring will be briefly discussed with examples specifically related to in-situ SHM with nanomaterials.

Numerous analytical approaches were developed in the past to study the electromechanical response of nanomaterials reinforced adhesives and composites [250], [251]. Research

conducted by Anand *et al.* [251] to develop a mathematical approach based on Bruggeman's effective medium theory is an example. This approach considered the nonlinear electro-mechanical behavior of nanocomposites thin film because of the relatively large strains in the polymer matrix. Similarly, Shindo *et al.* [250] established an analytical model to predict the change in the resistance of CNTs reinforced nanocomposites because of crack propagation. This was done by assuming the current follow through two parallel paths formed because of the percolation phenomena of CNTs in the matrix and the resistance was affected when there was a hindrance in the path due to the presence of crack or damage.

Besides this, various numerical models were also established in recent years to overcome restrictions of analytical approaches [252], [253]. Park *et al.* [252] established a simplified numerical approach in which change in resistance of CNTs was studied by subjecting the nanocomposites to tensile loading. However, they assumed that the tunneling effect of CNTs influenced the overall electrical response only when the specimen was subjected to high strain values. Furthermore, Li *et al.* [253] developed a more advanced model of real-time damage sensing in composites incorporated with CNTs and showed that change in the electrical conductivity of the specimen is because of the damage initiation occurring in cross-ply when subjected to tensile loading. More advanced models to study the electromechanical behavior of CNTs based nanocomposites were also developed later which can be found in [254], [255]. However, the interaction between the CNTs and between CNTs and matrix at nanoscale still had very little information in finite element modeling because of the complexity and numerous other variables to consider so electromechanical coupling mechanism between CNTs and the composite materials remained imprecise [253]. In a recently published article, Meguid and Alian [256] developed a multi-scaled coupled electromechanical numerical model by treating the electrical and mechanical response in a sequential manner of two steps to study the piezoresistive behavior of CNTs-reinforced composites under tension, compression, and shear loads. They verified their experimental results using this model approach. These numerical approaches were more focused on electromechanical response of nanocomposites developed by inserting the smart nanoparticles in the parent structure but no or very limited research had been conducted in developing finite element modeling in which real-time sensor wires or thin films created by nanomaterials such as CNTs, graphene or metal nanoparticles is attached or inserted in the structure and to correlate the electromechanical response of the sensor with the mechanical behavior of the specimen. This area is still to be discovered.

1.6. Summary of real-time SHM methods

The current study has provided a discussion of the use of different real-time SHM techniques for damage sensing in various composite structures. These techniques were characterized in two approaches i.e. non-material approaches and smart materials. In general, these real-time SHM approaches are further subdivided in embedded sensors such as fiber Bragg, nanocomposite sensors and surface-mounted sensors such as IR camera, DIC etc. in industries, surface-mounted sensors are more preferred in short-term especially in civil structures because of their simplicity and most importantly preservation of structural integrity. However, regarding the application viewpoint, SHM techniques based on smart materials are still in the experimental phase and have to go through a long validation period of tests before it can be applied in realistic structures.

However, surface mounted approaches have their limitations such as an increase in weight of the structure, degradation in extreme environmental conditions, etc. Besides, these techniques are more effective in detecting surface damage than internal damage in composite structures. On the other hand, despite being uncertified, embedded sensor systems consisting of smart materials can be integrated into composite structures without the requirement of additional equipment and increasing the weight of the structure.

The use of smart materials and sensing systems for real-time damage detection of structures is a long-term objective of industries. Therefore, the industrial sector preferred embedded sensor technologies and the use of smart materials over surface mounted techniques or techniques like IR images or DIC in the long-term to avoid additional cost and equipment. Though, it must be assured that the embedded system would not affect the structural integrity and performance of the structure with no or minimum requirement of additional components, and provide reliable sensing information with the ability of multi-mode damage detection. Evident from the current comparison presented in this study, smart materials have the advantage of lightweight, easy integration, and multi-mode detection in a composite. However, in the current situation, even these techniques have some limitations and drawbacks such as isolation of conductive nanoparticles from naturally conductive composites, to form a detection network over large sections of the structure, molecular interaction when inserted within the composites, and its effect on their detection signal. The first two concerns can be solved based on the knowledge from previous SHM techniques, however, regarding the third issue, innovative manufacturing techniques of smart sensors such as spray coating, growth of nanoparticles on the surface of the

fiber, electrophoresis, or electroless plating can provide an interesting alternative for affective real-time damage sensing.

Study of real-time SHM of composite structures using smart materials is still underdeveloped or in an early stage however, it has already been showing promising solutions for potential real-time SHM of composites. These intelligent materials techniques currently require the assistant of NDT techniques established in the detection of damage in real-time before it reaches maturity. For example, the use of CNTs based sensors to detect a multimode failure in composites under different loading conditions would require the assistance of acoustic emission to distinguish different modes of failure and their validation, however, in the future, use of nanomaterials for self-sensing and damage detection in composites has great potential.

1.7. Conclusion

It is essential to improve the reliability of composites' use in structural applications and, for this reason, continuous advancement and selection of appropriate real-time damage detection techniques are essential. Numerous researchers are working to develop more effective sensing technology which will not affect the properties of the parent structure but will only improve them. So, in the past decades, structural health monitoring has been developed from non-destructive testing to real-time monitoring and in some cases self-repairing and self-healing of the structures. Each technique had its pros and cons and is suitable for the detection of certain modes of failure. However, the chief advancement in in-situ structural health monitoring is based on the evolution of smart materials and nanotechnology. The use of smart materials in damage detection and failure analysis in different composite structures has been studied extensively over recent years. Smart materials such as nanoparticles such as carbon nanotubes, conductive metal particles, graphene, and shape memory alloys, have revolutionized the real-time structural health monitoring. They have also open doors for self-healing and In-situ repairing of the structures to avoid failure and make it cost-effective. The main objective of the above literature study was to present that numerous studies have examined the potential of smart sensing and real-time structural health monitoring and their applications in the detection of different failure modes based on promising results.

Moreover, a real-time damage sensing approach consisting of smart materials has extensively studied the use of nanoparticles such as CNTs and graphene However, the use of metal nanoparticles is still underdeveloped. Studies regarding the use of metal nanoparticles such as aluminum, gold, silver, etc. can be found but their use as a multimode sensor in composite

materials has very little or no information. It is important to notice that different manufacturing and dispersion processes can have a significant effect on their feasibility of industrial scale-up. In addition, the manufacturing of sensing technologies consisting of metal nanoparticles could include insertion within fibers, dispersion technique, or coating process and each process has its pros and cons, which might be suitable for a certain application.

It would be interesting to generate results that could confirm smart materials as a potential sensing technology to identify different failure and deformation modes in composites under different loading conditions. However, the industrialization of this knowledge and technology is still a concern. To reduce this gap, repeatable and reliable sensing data and cost-effective manufacturing at an industrial scale are necessary for the progress. Then the implementation of this smart sensing in real-time industrial components for damage detection is required to improve the structural integrity and lifetime estimation of the structural components.

References

[1] A. El Moumen, M. Tarfaoui, K. Lafdi, and H.Benyahia, “Dynamic properties of carbon nanotubes reinforced carbon fibers/epoxy textile composites under low velocity impact,” *Compos. Part B Eng.*, vol. 125, pp. 1–8, 2017.

[2] T. Mostapha, “Experimental Investigation of Dynamic Compression and Damage Kinetics of Glass/Epoxy Laminated Composites under High Strain Rate Compression,” in *Advances in Composite Materials*, B. Attaf, Ed. Rijeka: IntechOpen, 2011.

[3] M. Nachtane, M. Tarfaoui, A. El Moumen, and D. Saifaoui, “Damage prediction of horizontal axis marine current turbines under hydrodynamic, hydrostatic and impacts loads,” *Compos. Struct.*, vol. 170, pp. 146-157., 2017.

[4] O. R. Shah and M. Tarfaoui, “Determination of mode I & II strain energy release rates in composite foam core sandwiches: an experimental study of the composite foam core interfacial fracture resistance.,” *Compos. Part B Eng.*, vol. 111, no. 134–142, 2017.

[5] A. Moumen, M. Tarfaoui, O. Hassoon, K. Lafdi, H. Benyahia, and M. Nachtane, “Experimental study and numerical modelling of low velocity impact on laminated composite reinforced with thin film made of carbon nanotubes,” *Appl Compos Mater*, 2017, doi: 10.1007/s10443-017-9622-8.

[6] Z. K. Awad, T. Aravinthan, Y. Zhug, and F. Gonzalez., “A review of optimization techniques used in the design of fibre composite structures for civil engineering applications.,” *Mater. Des.*, vol. 33, pp. 534–544, 2012.

[7] M. Tarfaoui, A. El Moumen, and K. Lafdi., “Progressive damage modeling in carbon fibers/carbon nanotubes reinforced polymer composites.,” *Compos. Part B Eng.*, vol. 112, no. 185–195, 2017.

[8] J. Arbaoui, M. Tarfaoui, C. Bouery, and A. E. M. Alaoui., “Comparative study of mechanical properties and damage kinetics of two- and three-dimensional woven composites under high-strain rate dynamic compressive loading,” *Int. J. Damage Mech.*, vol. 25, no. 6, pp. 878–899.

[9] J. Arbaoui, M. Tarfaoui, J. Arbaoui, and A. E. M. Alaoui, “Mechanical behavior and damage kinetics of woven E-glass/vinylester laminate composites under high strain rate dynamic compressive loading: Experimental and numerical investigation,” *Int. J. Impact*

Eng., vol. 87, pp. 44–54, 2016.

[10] B. Dawson, “Vibration Condition Monitoring Techniques for Rotating Machinery,” *Shock Vib. Dig.*, vol. 8, no. 3., 1976.

[11] E. P. Carden and P. Fanning, “Vibration Based Condition Monitoring: A Review,” *Struct. Heal. Monit.*, vol. 3, no. 4, pp. 355–377, 2004.

[12] D. Montalvão, N. Maia, and A. E. Ribeiro, “A review of vibration-based structural health monitoring with special emphasis on composite materials,” 2006.

[13] S. W. Doebling, C. R. Farrar, and M. B. Prime, “A Summary Review of Vibration-Based Damage Identification Methods,” *Shock Vib. Dig.*, vol. 30, no. 2, pp. 91–105, 1998.

[14] D. Achenbach and J., *Structural health monitoring ? {What} is the prescription? {Mechanics} {Research} {Communications}, 36(2)*. 137-142, 2009.

[15] G. K. Chan, M. S. Lin, and B. Thambirajah, “Damage Detection of Buildings: Numerical and Experimental Studies,” *J. Struct. Eng.*, vol. 121, no. 8, pp. 1155–1160, Aug. 1995, doi: 10.1061/(ASCE)0733-9445(1995)121:8(1155).

[16] J. Malley and T. Moutos, “Capital Accumulation and Unemployment: A Tale of Two ‘Continents,’” *Scand. J. Econ.*, vol. 103, no. 1, pp. 79–99, 2001, doi: 10.1111/1467-9442.00231.

[17] A. M. Abdel-Basset, *Structural Health Monitoring, History, Applications and Future*. New York: Open Science, 2014.

[18] P. C. Chang, A. Flatau, and S. C. Liu, “Review Paper: Health Monitoring of Civil Infrastructure,” *Struct. Heal. Monit.*, vol. 2, no. 3, pp. 257–267, 2003.

[19] D. R. Dhakal, K. Neupane, C. Thapa, and G. V Ramanjaneyulu, “Different Techniques of Structural Health Monitoring,” *Transp. Res. Part C Emerg. Technol.*, vol. 3, no. 2, pp. 55–66, 2013.

[20] B. Grisso and D. Inman, *Developing an Autonomous On-Orbit Impedance-Based {SHM} for Thermal Protection Systems*. International Workshop on Structural Health Monitoring. Stanford, 2005.

[21] S. PARK, C.-B. YUN, and D. J. INMAN, “Structural health monitoring using electro-mechanical impedance sensors,” *Fatigue Fract. Eng. Mater. Struct.*, vol. 31, no. 8, pp.

714–724, 2008, doi: 10.1111/j.1460-2695.2008.01248.x.

[22] B. L. Grisso, J. Kim, J. R. Farmer, D. S. Ha, and D. J. Inman, “A system -on-board impedance based approach for structural health monitoring,” *Sensors Smart Struct. Technol. Civil, Mech. Aerosp. Syst.*, vol. 65., 2007.

[23] S. Park, S. Ahmad, C.-B. Yun, and Y. Roh, “Multiple Crack Detection of Concrete Structures Using Impedance-based Structural Health Monitoring Techniques,” *Exp. Mech.*, vol. 46, no. 5, pp. 609–618, 2006, doi: 10.1007/s11340-006-8734-0.

[24] C.-P. Fritzen, “Vibration-Based Structural Health Monitoring – Concepts and Applications,” *Key Eng. Mater. - KEY ENG MAT*, vol. 293, 2005, doi: 10.4028/www.scientific.net/KEM.293-294.3.

[25] Z. Xiukuan, G. Haichang, S. Gangbing, M. Y. L., and X. Jinwu, “Structural Health Monitoring with Data Fusion Method,” *Earth and Space 2010*. pp. 2509–2517, 02-May-2020, doi: doi:10.1061/41096(366)234.

[26] O. Basir and X. Yuan, “Engine fault diagnosis based on multi-sensor information fusion using Dempster–Shafer evidence theory,” *Inf. Fusion*, vol. 8, no. 4, pp. 379–386, 2007, doi: https://doi.org/10.1016/j.inffus.2005.07.003.

[27] C. R. Farrar and K. Worden, “An introduction to structural health monitoring,” *Philos. Trans. R. Soc. A Math. Phys. Eng. Sci.*, vol. 365, no. 1851, pp. 303–315, 2007, doi: 10.1098/rsta.2006.1928.

[28] C. R. Farrar, “Historical overview of structural health monitoring,” in *Lecture notes on structural health monitoring using statistical pattern recognition*, Los Alamos, USA.: Los Alamos Dynamics, 2001.

[29] Y. Yang and Y. Hu, “Electromechanical impedance modeling of PZT transducers for health monitoring of cylindrical shell structures,” *Smart Mater. Struct.*, vol. 17, p. 15005, 2007, doi: 10.1088/0964-1726/17/01/015005.

[30] S. Cho, C.-B. Yun, J. P. Lynch, J. Zimmerman A. T., B. F., and T. Nagayama, “Smart Wireless Sensor Technology for Structural Health Monitoring of Civil Structures,” *Steel Struct.*, vol. 8, pp. 267–275, 2008.

[31] A. Oth and M. Picozzi, “Structural Health Monitoring Using Wireless Technologies: An Ambient Vibration Test on the Adolphe Bridge, Luxembourg City,” *Adv. Civ. Eng.*, vol.

2012, 2012, doi: 10.1155/2012/876174.

[32] V. Giurgiutiu, *Structural Health Monitoring with Piezoelectric Wafer Active Sensors*. Boston: Elsevier Academic Press, 2008.

[33] C.-B. Yun and J. Min, "Smart sensing, monitoring, and damage detection for civil infrastructures," *KSCE J. Civ. Eng.*, vol. 15, no. 1, pp. 1–14, 2011, doi: 10.1007/s12205-011-0001-y.

[34] J. P. Lynch, K. H. Law, A. S. Kiremidjian, T. W. Kenny, E. Carryer, and A. Partridge, "The Design of a Wireless Sensing Unit for Structural Health Monitoring," in *3rd International Workshop on Structural Health Monitoring*, 2001.

[35] T. Nagayama, S.-H. Sim, Y. Miyamori, and B. Spencer, "Issues in structural health monitoring employing smart sensors," *Smart Struct. Syst.*, vol. 3, 2007, doi: 10.12989/sss.2007.3.3.299.

[36] F. K. Chang, *Structural health monitoring: a summary report on the first international workshop on structural health monitoring*. 2rd International Workshop on Structural Health Monitoring. Lancaster, 1997.

[37] K. P. Chong, "Health monitoring of civil structures," *J. Intell. Mater. Syst. Struct.*, vol. 9, no. 11, pp. 892–898, 1999.

[38] M. Sun, W. Staszewski, and R. Swamy, "Smart Sensing Technologies for Structural Health Monitoring of Civil Engineering Structures," *Adv. Civ. Eng.*, vol. 2010, 2010, doi: 10.1155/2010/724962.

[39] N. P. Avdelidis, D. P. Almond, C. Ibarra-Castanedo, A. Bendada, S. Kenny, and X. Maldague, *Structural integrity assessment of materials by thermography*. Conf, 2006.

[40] R. Paynter and A. Dutton, "The Use of a Second Harmonic Correlation to Detect Damage in Composite Structures Using Thermoelastic Stress Measurements," *Strain*, vol. 39, pp. 73–78, 2003, doi: 10.1046/j.1475-1305.2003.00056.x.

[41] J. M. Nichols, "Structural health monitoring of offshore structures using ambient excitation," *Appl. Ocean Res.*, vol. 25, no. 3, pp. 101–114, 2003, doi: https://doi.org/10.1016/j.apor.2003.08.003.

[42] A. G. Dutton, *Thermoelastic stress measurement and acoustic emission monitoring in*

wind turbine blade testing {European}{Wind}{Energy}. Conf. {EWEC}. London, 2004.

[43] R. Haj-Ali, B. Wei, S. Johnson, and R. Elhajjar, "Thermoelastic and infrared-thermography methods for surface strains in cracked orthotropic composite materials," *Eng. Fract. Mech.*, vol. 75, pp. 58–75, 2008, doi: 10.1016/j.engfracmech.2007.02.014.

[44] G. Walle, M. Abuhamad, E. Toma, and U. Netzelmann, "Defect indications in sono-thermography in relation to defect location and structure," 2004, doi: 10.21611/qirt.2004.033.

[45] D. W. Wilson and J. A. Charles, "Thermographic detection of adhesive-bond and interlaminar flaws in composites," *Exp. Mech.*, vol. 21, no. 7, pp. 276–280, 1981, doi: 10.1007/BF02327018.

[46] B. Venkataraman, B. Raj, C. K. Mukhopadhyay, and T. Jayakumar, "Correlation of infrared thermographic patterns and acoustic emission signals with tensile deformation and fracture processes," *AIP Conf. Proc.*, vol. 557, no. 1, pp. 1443–1450, 2001, doi: 10.1063/1.1373923.

[47] J. Kumar, S. Baby, and V. Kumar, "Thermographic studies on IMI-834 titanium alloy during tensile loading," *Mater. Sci. Eng. A*, vol. 496, no. 1, pp. 303–307, 2008, doi: https://doi.org/10.1016/j.msea.2008.05.040.

[48] H. Ait-Amokhtar, C. Fressengeas, and S. Boudrahem, "The dynamics of Portevin–Le Chatelier bands in an Al–Mg alloy from infrared thermography," *Mater. Sci. Eng. A*, vol. 488, pp. 540–546, 2008.

[49] M. P. Luong, "Fatigue limit evaluation of metals using an infrared thermographic technique," *Mech. Mater.*, vol. 28, no. 1, pp. 155–163, 1998, doi: https://doi.org/10.1016/S0167-6636(97)00047-1.

[50] M. L. Pastor, X. Balandraud, M. Grédiac, and J. L. Robert, "Applying infrared thermography to study the heating of 2024-T3 aluminium specimens under fatigue loading," *Infrared Phys. Technol.*, vol. 51, no. 6, pp. 505–515, 2008, doi: https://doi.org/10.1016/j.infrared.2008.01.001.

[51] H. Wang, L. Jiang, P. K. Liaw, C. R. Brooks, and D. L. Klarstrom, "Infrared temperature mapping of ULTIMET alloy during high-cycle fatigue tests," *Metall. Mater. Trans. A*, vol. 31, no. 4, pp. 1307–1310, 2000, doi: 10.1007/s11661-000-0126-y.

[52] F. Hahn, C. W. Kensche, R. J. Paynter, A. G. Dutton, C. Kildegaard, and J. Kosgaard, “Design, fatigue test and {NDE} of a sectional wind turbine rotor blade,” *J. Thermoplast. Compos. Mater.*, vol. 15, pp. 267–277, 2002.

[53] C. Meola, G. Carlomagno, A. Squillace, and G. Giorleo, “Non-destructive control of industrial materials by means of lock-in thermography,” *Meas. Sci. Technol.*, vol. 13, p. 1583, 2002, doi: 10.1088/0957-0233/13/10/311.

[54] M. Tarfaoui, A. El Moumen, and H. Ben Yahia., “Damage detection versus Heat dissipation in E-Glass/Epoxy laminated composites under dynamic compression at high strain rate.,” *Compos. Struct.*, vol. 186, pp. 50–61, 2018.

[55] M. Tarfaoui, A. El Moumen, M. Boehle, O. Shah, and K. Lafdi, “Self-heating and deicing epoxy/glass fiber based carbon nanotubes buckypaper composite,” *J. Mater. Sci.*, vol. 54, no. 2, pp. 1351–1362, 2019, doi: 10.1007/s10853-018-2917-9.

[56] S. Sassi, M. Tarfaoui, and H. B. Yahia, “Thermomechanical behavior of adhesively bonded joints under out-of-plane dynamic compression loading at high strain rate,” *J. Compos. Mater.*, vol. 52, no. 30, pp. 4171–4184, 2018, doi: 10.1177/0021998318777048.

[57] S. Sassi, M. Tarfaoui, and H. Ben Yahia., “In-situ heat dissipation monitoring in adhesively bonded composite joints under dynamic compression loading using SHPB,” *Compos. Part B Eng.*, vol. 54, pp. 64–76, 2018.

[58] O. R. Shah and M. Tarfaoui, “Effect of damage progression on the heat generation and final failure of a polyester–glass fiber composite under tension–tension cyclic loading,” *Compos. Part B Eng.*, vol. 62, pp. 121–125, 2014, doi: https://doi.org/10.1016/j.compositesb.2014.02.020.

[59] O. Büyüköztürk, “Imaging of concrete structures,” *NDT E Int.*, vol. 31, no. 4, pp. 233–243, 1998, doi: https://doi.org/10.1016/S0963-8695(98)00012-7.

[60] S. A. Ljungberg, “Infrared techniques in buildings and structures: Operation and maintenance,” *Infrared Methodol. Technol.*, vol. 7, p. 211, 1994.

[61] A. Poblete and M. [Acebes Pascual], “Thermographic measurement of the effect of humidity in mortar porosity,” *Infrared Phys. Technol.*, vol. 49, no. 3, pp. 224–227, 2007, doi: https://doi.org/10.1016/j.infrared.2006.06.009.

[62] M. Azenha, R. Faria, and H. Figueiras, “Thermography as a technique for monitoring early age temperatures of hardening concrete,” *Constr. Build. Mater.*, vol. 25, pp. 4232–4240, 2011.

[63] E. Grinzato, P. Bison, and S. Marinetti, “Monitoring of ancient buildings by the thermal method,” *J. Cult. Herit.*, vol. 3, pp. 21–29, 2002.

[64] N. Avdelidis and A. Moropoulou, “Applications of infrared thermography for the investigation of historic structures,” *J. Cult. Herit.*, vol. 5, pp. 119–127, 2004.

[65] A. Tavukçuoğlu, A. Düzgüneş, E. N. Caner-Saltık, and Ş. Demirci, “Use of IR thermography for the assessment of surface-water drainage problems in a historical building, Ağzıkarahan (Aksaray), Turkey,” *NDT E Int.*, vol. 38, no. 5, pp. 402–410, 2005, doi: https://doi.org/10.1016/j.ndteint.2004.11.003.

[66] W. H. Peters and W. F. Ranson, “Digital Imaging Techniques In Experimental Stress Analysis,” *Opt. Eng.*, vol. 21, no. 3, pp. 427–431, 1982, doi: 10.1117/12.7972925.

[67] T. Chu, W. Ranson, M. Sutton, and W. Peters, “Applications of digital image correlation techniques to experimental mechanics,” *Exp. Mech.*, vol. 25, no. 3, pp. 232–244, 1985.

[68] M. A. Sutton, W. J. Wolters, W. H. Peters, W. F. Ranson, and S. R. McNeill, “Determination of displacements using an improved digital correlation method,” *Image Vis. Comput.*, vol. 1, no. 3, pp. 133–139, 1983, doi: https://doi.org/10.1016/0262-8856(83)90064-1.

[69] W. H. Peters, W. F. Ranson, M. A. Sutton, T. C. Chu, and J. Anderson, “Application Of Digital Correlation Methods To Rigid Body Mechanics,” *Opt. Eng.*, vol. 22, no. 6, pp. 738–742, 1983, doi: 10.1117/12.7973231.

[70] F. Lagattu, M. C. Lafarie-Frenot, T. Q. Lam, and J. Brillaud, “Experimental characterisation of overstress accommodation in notched CFRP composite laminates,” *Compos. Struct.*, vol. 67, no. 3, pp. 347–357, 2005, doi: https://doi.org/10.1016/j.compstruct.2004.01.016.

[71] M. Grédiac, “The use of full-field measurement methods in composite material characterization: interest and limitations,” *Compos. Part A Appl. Sci. Manuf.*, vol. 35, no. 7, pp. 751–761, 2004, doi: https://doi.org/10.1016/j.compositesa.2004.01.019.

[72] Z. Y. Wang, H. Q. Li, J. W. Tong, M. Shen, F. Aymerich, and P. Priolo, “Dual

magnification digital image correlation based strain measurement in CFRP Laminates with open hole," *Compos. Sci. Technol.*, vol. 68, no. 9, pp. 1975–1980, 2008, doi: https://doi.org/10.1016/j.compscitech.2007.04.026.

[73] B. Pan, H. Xie, Z. Wang, K. Qian, and Z. Wang, "Study on subset size selection in digital image correlation for speckle patterns," *Opt. Express*, vol. 16, no. 10, pp. 7037–7048, May 2008, doi: 10.1364/OE.16.007037.

[74] T. Hua, H. Xie, S. Wang, Z. Hu, P. Chen, and Q. Zhang, "Evaluation of the quality of a speckle pattern in the digital image correlation method by mean subset fluctuation," *Opt. Laser Technol.*, vol. 43, no. 1, pp. 9–13, 2011.

[75] Y. Dong and B. Pan, "A Review of Speckle Pattern Fabrication and Assessment for Digital Image Correlation," *Exp. Mech.*, vol. 57, no. 8, 2017.

[76] M. A. Caminero, S. Pavlopoulou, M. Lopez-Pedrosa, B. G. Nicolaisson, C. Pinna, and C. Soutis, "Analysis of adhesively bonded repairs in composites: Damage detection and prognosis," *Compos. Struct.*, vol. 95, pp. 500–517, 2013, doi: https://doi.org/10.1016/j.compstruct.2012.07.028.

[77] X. Li, W. Xu, M. A. Sutton, and M. Mello, "In Situ Nanoscale In-Plane Deformation Studies of Ultrathin Polymeric Films During Tensile Deformation Using Atomic Force Microscopy and Digital Image Correlation Techniques," *IEEE Trans. Nanotechnol.*, vol. 6, no. 1, pp. 4–12, Jan. 2007, doi: 10.1109/TNANO.2006.888527.

[78] A. Ouglova, Y. Berthaud, F. Foct, M. François, F. Ragueneau, and I. Petre-Lazar, "The influence of corrosion on bond properties between concrete and reinforcement in concrete structures," *Mater. Struct.*, vol. 41, no. 5, pp. 969–980, 2008, doi: 10.1617/s11527-007-9298-x.

[79] P. Bing, X. Hui-min, H. Tao, and A. Asundi, "Measurement of coefficient of thermal expansion of films using digital image correlation method," *Polym. Test.*, vol. 28, no. 1, pp. 75–83, 2009, doi: https://doi.org/10.1016/j.polymertesting.2008.11.004.

[80] H. W. Schreier, D. Garcia, and M. A. Sutton, "Advances in light microscope stereo vision," *Exp. Mech.*, vol. 44, no. 3, pp. 278–288, 2004, doi: 10.1007/BF02427894.

[81] S. M. Guo, M. A. Sutton, P. Majumdar, K. M. Reifsnider, L. Yu, and M. Gresil, "Development and application of an experimental system for the study of thin

composites undergoing large deformations in combined bending 0compression loading," *J. Compos. Mater.*, vol. 48, no. 8, 2014.

[82] G. Murasawa, S. Yoneyama, and T. Sakuma, "Nucleation, bifurcation and propagation of local deformation arising in {NiTi} shape memory alloy," *Smart Mater. Struct.*, vol. 16, no. 1, pp. 160–167, Jan. 2007, doi: 10.1088/0964-1726/16/1/020.

[83] B. Grant, B. M., H. J. Stone, P. J. Withers, and M. Preuss, "High-temperature strain field measurement using digital image correlation.," *J. Strain Anal. Eng. Des.*, vol. 44, no. 4, 2009.

[84] B. Pan, D. Wu, and Y. Xia, "High-temperature deformation field measurement by combining transient aerodynamic heating simulation system and reliability-guided digital image correlation," *Opt. Lasers Eng.*, vol. 48, no. 9, pp. 841–848, 2010, doi: https://doi.org/10.1016/j.optlaseng.2010.04.007.

[85] Y. Dong, H. Kakisawa, and Y. Kagawa, "Optical system for microscopic observation and strain measurement at high temperature," *Meas. Sci. Technol.*, vol. 25, no. 2, p. 25002, Dec. 2013, doi: 10.1088/0957-0233/25/2/025002.

[86] J. Banks, L. M. Giovannetti, X. Soubeyran, A. M. Wright, S. R. Turnock, and S. W. Boyd, "Assessment of digital image correlation as a method of obtaining deformations of a structure under fluid load," *J. Fluids Struct.*, vol. 58, 2015.

[87] B. Pan, L. Yu, and D. Wu, "Thermo-mechanical response of superalloy honeycomb sandwich panels subjected to non-steady thermal loading," *Mater. Des.*, vol. 88, pp. 528–536, 2015, doi: https://doi.org/10.1016/j.matdes.2015.09.016.

[88] M. MARTARELLI, G. M. REVEL, and C. SANTOLINI, "AUTOMATED MODAL ANALYSIS BY SCANNING LASER VIBROMETRY: PROBLEMS AND UNCERTAINTIES ASSOCIATED WITH THE SCANNING SYSTEM CALIBRATION," *Mech. Syst. Signal Process.*, vol. 15, no. 3, pp. 581–601, 2001, doi: https://doi.org/10.1006/mssp.2000.1336.

[89] S. S. Kessler, S. M. Spearing, M. J. Atalla, C. E. S. Cesnik, and C. Soutis, "Damage detection in composite materials using frequency response methods," *Compos. Part B Eng.*, vol. 33, no. 1, pp. 87–95, 2002, doi: https://doi.org/10.1016/S1359-8368(01)00050-6.

[90] D. M. Siringoringo and Y. Fujino, “Experimental study of laser Doppler vibrometer and ambient vibration for vibration-based damage detection,” *Eng. Struct.*, vol. 28, no. 13, pp. 1803–1815, 2006, doi: https://doi.org/10.1016/j.engstruct.2006.03.006.

[91] A. Stanbridge, A. Z. Khan, and D. Ewins, “Modal Testing Using Impact Excitation and a Scanning LDV,” *Shock Vib.*, vol. 7, 1998, doi: 10.1155/2000/527389.

[92] A. B. Stanbridge, M. Martarelli, and D. J. Ewins, “Measuring area vibration mode shapes with a continuous-scan LDV,” *Measurement*, vol. 35, no. 2, pp. 181–189, 2004, doi: https://doi.org/10.1016/j.measurement.2003.07.005.

[93] P. Castellini, G. M. Revel, and L. Scalise, “Measurement of vibrational modal parameters using laser pulse excitation techniques,” *Measurement*, vol. 35, no. 2, pp. 163–179, 2004.

[94] A. Bougard and B. Ellis, “Laser Measurement of Building Vibration and Displacement,” *Shock Vib.*, vol. 7, no. 5, pp. 287–289, 2000.

[95] P. Castellini and C. Santolini, “Vibration measurements on blades of a naval propeller rotating in water with tracking laser vibrometer,” *Measurement*, vol. 24, no. 1, pp. 43–54, 1998.

[96] A. Ghoshal, M. J. Sundaresan, M. J. Schulz, and P. F. Pai, “Structural health monitoring techniques for wind turbine blades,” *J. Wind Eng. Ind. Aerodyn.*, vol. 85, no. 3, pp. 309–324, 2000, doi: https://doi.org/10.1016/S0167-6105(99)00132-4.

[97] K. J. Loh, J. H. Kim, and J. P. Lynch, “Self-sensing and power harvesting carbon nanotube-composites based on piezoelectric polymers,” 2002.

[98] V. Badami and B. Ahuja, *Biosmart Materials: Breaking New Ground in Dentistry*. Scientific World Journal, 2014.

[99] F. Ansari, “Structural health monitoring with fiber optic sensors,” *Front. Mech. Eng. China*, vol. 4, no. 2, pp. 103–110, 2009.

[100] L. Savage, “Sensing Trouble: Fiber-Optics in Civil,” *Opt. Photonics News*, vol. 24, p. 26, 2013, doi: 10.1364/OPN.24.3.000026.

[101] E. F. Crawley, “Intelligent structures for aerospace - {A} technology overview and assessment,” *AIAA J.*, vol. 32, no. 8, pp. 1689–1699, 1994.

[102] C. A. Rogers, D. K. Barker, and C. A. Jaeger, “Introduction to smart materials and structures,” *Smart Mater. Struct. Math. Issues,* pp. 17–28, 1988.

[103] C. Rogers and I. Ahmad, “US Army Research Office Workshop on Smart Materials, Structures and Mathematical Issues proceedings,” 2020.

[104] E. Udd, “Fiber optic smart structures,” *Proc. IEEE,* vol. 84, no. 6, pp. 884–894, Jun. 1996, doi: 10.1109/5.503144.

[105] B. Sun, “Smart materials and structures,” in *Lecture at Swiss Federal Institute of Technology Zurich*, 2015.

[106] V. Nováka, P. Šittner, G. N. Dayananda, F. M. Braz-Fernandes, and K. K. Mahesh, “Electric resistance variation of NiTi shape memory alloy wires in thermomechanical tests: Experiments and simulation,” *Mater. Sci. Eng. A*, vol. 481–482, pp. 127–133, 2008, doi: https://doi.org/10.1016/j.msea.2007.02.162.

[107] F. Santos, “Shape-memory alloys as macrostrain sensors,” *Struct. Control Heal. Monit.*, vol. 24, 2016, doi: 10.1002/stc.1860.

[108] L. Janke, C. Czaderski, M. Motavalli, and J. Ruth, “Applications of shape memory alloys in civil engineering structures—Overview, limits and new ideas,” *Mater. Struct.*, vol. 38, pp. 578–592, 2005, doi: 10.1007/BF02479550.

[109] M. Kekana and B. Sun, “Smart materials and structures,” in *The South African Mechanical Engineer*, 48th ed., 1998, pp. 13–17.

[110] F. Casciati and R. Rossi, *Sensor devices exploiting C}-based SMA physical properties*. Third European Workshop Structural Health Monitoring, 2006.

[111] O. Ozbulut, S. Hurlebaus, and R. Desroches, “Seismic Response Control Using Shape Memory Alloys: A Review,” *J. Intell. Mater. Syst. Struct. - J INTEL MAT SYST STRUCT*, vol. 22, pp. 1531–1549, 2011, doi: 10.1177/1045389X11411220.

[112] *Introduction to Nondestructive Testing*. [Online]. Available: https: //asnt.org/MinorSiteSections/AboutASNT/Intro-to-NDT.aspx, 2017.

[113] B. Raj; T. Jayakumar; M. Thavasimuthu, *Practical Non-Destructive Testing*. Oxford: Alpha Science International Ltd., 2008.

[114] R. Parkash, “Non-Destructive Testing Of Composites,” *Composites*, vol. 11, no. 4, pp.

217–224, 1980.

[115] J. T. P. Yao and H. G. Natke, “Damage detection and reliability evaluation of existing structures,” *Struct. Saf.*, vol. 15, no. 1, pp. 3–16, 1994, doi: https://doi.org/10.1016/0167-4730(94)90049-3.

[116] S. Casciati and A. Marzi, “Experimental studies on the fatigue life of shape memory alloy bars.,” *Smart Struct. Syst.*, vol. 6, no. 1, pp. 73–85, 2010.

[117] P. M. Ajayan and O. Zhou, “Applications of carbon nanotubes,” in *Carbon Nanotubes Synthesis, Structure, Properties and Applications*, G. Dresselhaus and P. Avouris, Eds. Berlin: Springer, 2001.

[118] R. H. Baughman, A. A. Sakhidov, and W. A. de Heer, “2002 Carbon nanotubes-the route toward applicatons,” *Science vol. 80*, no. 297, pp. 787–792, 2002.

[119] S. Peng *et al.*, “Carbon nanotube chemical and mechanical sensors,” 2001, pp. 1–8.

[120] S. Ghosh, A. K. Sood, and N. Kumar, “Carbon nanotube flow sensors,” *Science (80-.).*, vol. 299, pp. 1042–1044, 2003.

[121] J. Wood and D. Wagner, “Single-wall carbon nanotubes as molecular pressure sensors,” *Appl. Phys. Lett.*, vol. 76, pp. 2883–2885, 2000, doi: 10.1063/1.126505.

[122] J. Kong *et al.*, “Nanotube Molecular Wires as Chemical Sensors,” *Science (80-.).*, vol. 287, no. 5453, pp. 622–625, 2000, doi: 10.1126/science.287.5453.622.

[123] R. H. Baughman *et al.*, “Carbon Nanotube Actuators,” *Science (80-.).*, vol. 284, no. 5418, pp. 1340–1344, 1999, doi: 10.1126/science.284.5418.1340.

[124] M. Tahhan, V.-T. Truong, G. M. Spinks, and G. G. Wallace, “Carbon nanotube and polyaniline composite actuators{\ast},” *Smart Mater. Struct.*, vol. 12, no. 4, pp. 626–632, Jun. 2003, doi: 10.1088/0964-1726/12/4/313.

[125] E. Smela, “Conjugated Polymer Actuators for Biomedical Applications,” *Adv. Mater.*, vol. 15, no. 6, pp. 481–494, 2003, doi: 10.1002/adma.200390113.

[126] K. J. Loh, J. P. Lynch, and N. A. Kotov, “Inductively coupled nanocomposite wireless strain and {pH} sensors,” *Smart Struct. Syst.*, vol. 4, no. 5, pp. 531–548, 2008.

[127] K. J. Loh, T. C. Hou, J. P. Lynch, and N. A. Kotov, “Nanotube-based sensing skin for crack detection and impact monitoring of structures,” in *Proceedings of the6th*

{International} {Workshop} on {Structural} {Health} {Monitoring}, {Stanford}, {CA}, {USA}, 2007.

[128] L. Boger, C. Viets, M. H. Wichmann, and K. Schulte, *Glass fibre reinforced composites with a carbon nanotube modified epoxy matrix as self sensing material*. Proceedings of the 7th International Workshop on Structural Health Monitoring, 2009.

[129] J. L. Abota, Y. S. Maruthi, S. Vatsavayaa, S. Medikonda, Z. Kiera, and Jayasingheb C., "Schulz," *M. {J}. (2010). {Delamination} Detect. with carbon Nanotub. thread self-sensing Compos. Mater. {Composites}{Science}{Technology}*, vol. 70, no. 7, pp. 1113–1119.

[130] J. L. Abot *et al.*, "Delamination detection with carbon nanotube thread in self-sensing composite materials," *Compos. Sci. Technol.*, vol. 70, no. 7, pp. 1113–1119, 2010, doi: https://doi.org/10.1016/j.compscitech.2010.02.022.

[131] A. Raghavan, S. S. Kessler, C. T. Dunn, D. Barber, S. Wicks, and B. L. Wardle, "Structural health monitoring using carbon nanotube ({CNT}) enhanced composites," in *Proceedings of the 7th International Workshop on Structural Health Monitoring, Stanford, {CA}, {USA}*, 2009.

[132] M. Stadermann *et al.*, "Nanoscale study of conduction through carbon nanotube networks," *Phys. Rev. B*, vol. 69, no. 20, p. 201402, May 2004, doi: 10.1103/PhysRevB.69.201402.

[133] M. Saafi, "Wireless and embedded carbon nanotube networks for damage detection in concrete structures," *Nanotechnology*, vol. 20, no. 39, p. 395502, 2009, doi: 10.1088/0957-4484/20/39/395502.

[134] J. Makar, J. Margeson, and J. Luh, "Carbon nanotube/cement composites - early results and potential applications," in *Proceedings of the 3rd International Conference on Construction Materials: Performance, Innovation and Structural Implications, Vancouver, Canada*, 2005.

[135] F. Azhari and N. Banthia, *Carbon fiber/nanotube cement-based sensors for structural health monitoring*. Proceedings of the 7th International Workshop on Structural Health Monitoring, 2009.

[136] I. Kang, M. J. Schulz, J. H. Kim, V. Shanov, and D. Shi, "A carbon nanotube strain

sensor for structural health monitoring," *Smart Mater. Struct.*, vol. 15, no. 3, pp. 737–748, Apr. 2006, doi: 10.1088/0964-1726/15/3/009.

[137] J. Wood *et al.*, "Carbon nanotubes: From molecular to macroscopic sensors," *Phys. Rev. B*, vol. 62, 2000, doi: 10.1103/PhysRevB.62.7571.

[138] A. N. Watkins, J. L. Ingram, J. D. Jordan, R. A. Wincheski, J. M. Smits, and P. A. Williams, "Single wall carbon nanotube-based structural health monitoring sensing materials," in *NSTI Conf-Nanotech, {NASA} Langley Research Center, {US}*, 2004.

[139] R. G. de Villoria, N. Yamamoto, A. Miravete, and B. L. Wardle, "Multi-physics damage sensing in nano-engineered structural composites," *Nanotechnology*, vol. 22, no. 18, p. 185502, Mar. 2011, doi: 10.1088/0957-4484/22/18/185502.

[140] S. Luo, W. Obitayo, and T. Liu, "SWCNT-thin-film-enabled fiber sensors for lifelong structural health monitoring of polymeric composites - From manufacturing to utilization to failure," *Carbon N. Y.*, vol. 76, pp. 321–329, 2014, doi: https://doi.org/10.1016/j.carbon.2014.04.083.

[141] L. Böger, M. H. G. Wichmann, L. O. Meyer, and K. Schulte, "Load and health monitoring in glass fibre reinforced composites with an electrically conductive nanocomposite epoxy matrix," *Compos. Sci. Technol.*, vol. 68, no. 7, pp. 1886–1894, 2008, doi: https://doi.org/10.1016/j.compscitech.2008.01.001.

[142] H. Zhang, Y. Liu, E. Bilotti, and T. Peijs, "In-Situ Monitoring of Interlaminar Shear Damage in Carbon Fibre Composites," *Adv. Compos. Lett.*, vol. 24, pp. 92–97, 2015, doi: 10.1177/096369351502400405.

[143] P. Avouris and C. Dimitrakopoulos, "Graphene: synthesis and applications," *Mater. Today*, vol. 15, no. 3, 2012.

[144] X. Huang *et al.*, "Graphene-Based Materials: Synthesis, Characterization, Properties, and Applications," *Small*, vol. 7, no. 14, pp. 1876–1902, 2011, doi: 10.1002/smll.201002009.

[145] H. Shen, L. Zhang, M. Liu, and Z. Zhang, "Biomedical Applications of Graphene," *Theranostics*, vol. 2, pp. 283–294, 2012, doi: 10.7150/thno.3642.

[146] W. Choi, I. Lahiri, R. Seelaboyina, and Y. S. Kang, "Synthesis of graphene and its applications: a review," *Crit. Rev. Solid State Mater. Sci.*, vol. 35, no. 1, pp. 52–71, 2010.

[147] K. S. Novoselov *et al.*, “Electric Field Effect in Atomically Thin Carbon Films,” *Science (80-.).*, vol. 306, no. 5696, pp. 666–669, 2004, doi: 10.1126/science.1102896.

[148] S. S. Varghese, S. Lonkar, K. K. Singh, S. Swaminathan, and A. Abdala, “Recent advances in graphene based gas sensors,” *Sensors Actuators B Chem.*, vol. 218, pp. 160–183, 2015, doi: https://doi.org/10.1016/j.snb.2015.04.062.

[149] K. Bonfig, M. Denker, and U. Kuipers, “Das direkte digitale messverfahren als grundlage einfacher und dennoch genauer und storsicherer sensoren,” *Sensor*, vol. 3, 1988.

[150] V. Matko, “Next Generation AT-Cut Quartz Crystal Sensing Devices,” *Sensors (Basel).*, vol. 11, pp. 4474–4482, 2011, doi: 10.3390/s110504474.

[151] V. Matko, “New Quartz Oscillator Switching Method for Nano-Henry Range Inductance Measurements,” *Sensors (Basel).*, vol. 12, pp. 3105–3117, 2012, doi: 10.3390/s120303105.

[152] B. Culshaw, “Optical fiber sensor technologies: {Opportunities} and-perhaps-pitfalls.,” *J. Light. Technol.*, vol. 22, pp. 39–50, 2004.

[153] V. Matko and M. Milanović, “Temperature-compensated capacitance–frequency converter with high resolution,” *Sensors Actuators A Phys.*, vol. 220, pp. 262–269, 2014, doi: https://doi.org/10.1016/j.sna.2014.09.022.

[154] C. Elosua, I. Matias, C. Bariain, and F. Arregui, “Volatile organic compound optical fiber sensors: {A} review.,” *Sensors*, vol. 6, 2006.

[155] A. O. Siefker-Radtke *et al.*, “A phase 2 clinical trial of sequential neoadjuvant chemotherapy with ifosfamide, doxorubicin, and gemcitabine followed by cisplatin, gemcitabine, and ifosfamide in locally advanced urothelial cancer,” *Cancer*, vol. 119, no. 3, pp. 540–547, 2013, doi: 10.1002/cncr.27751.

[156] Z.-S. Wu, W. Ren, L. Gao, B. Liu, C. Jiang, and H.-M. Cheng, “Synthesis of high-quality graphene with a pre-determined number of layers,” *Carbon N. Y.*, vol. 47, no. 2, pp. 493–499, 2009, doi: https://doi.org/10.1016/j.carbon.2008.10.031.

[157] S. Stankovich *et al.*, “Graphene-based composite materials,” *Nature*, vol. 442, no. 7100, pp. 282–286, 2006, doi: 10.1038/nature04969.

[158] S. Stankovich *et al.*, “Synthesis of graphene-based nanosheets via chemical reduction of

exfoliated graphite oxide," *Carbon N. Y.*, vol. 45, no. 7, pp. 1558–1565, 2007, doi: https://doi.org/10.1016/j.carbon.2007.02.034.

[159] V. Eswaraiah, K. Balasubramaniam, and S. Ramaprabhu, "Functionalized graphene reinforced thermoplastic nanocomposites as strain sensors in structural health monitoring," *J. Mater. Chem.*, vol. 21, no. 34, pp. 12626–12628, 2011, doi: 10.1039/C1JM12302E.

[160] I. Balberg, "Tunneling and nonuniversal conductivity in composite materials," *Phys. Rev. Lett.*, vol. 59, 1987.

[161] R. Jan *et al.*, "Liquid exfoliated graphene smart layer for structural health monitoring of composites," *J. Intell. Mater. Syst. Struct.*, vol. 28, no. 12, pp. 1565–1574, 2017, doi: 10.1177/1045389X16672729.

[162] Y. Jiao *et al.*, "Wearable Graphene Sensors With Microfluidic Liquid Metal Wiring for Structural Health Monitoring and Human Body Motion Sensing," *IEEE Sens. J.*, vol. 16, no. 22, pp. 7870–7875, Nov. 2016, doi: 10.1109/JSEN.2016.2608330.

[163] R. Moriche, M. Sánchez, A. Jiménez-Suárez, S. G. Prolongo, and A. Ureña, "Strain monitoring mechanisms of sensors based on the addition of graphene nanoplatelets into an epoxy matrix," *Compos. Sci. Technol.*, vol. 123, pp. 65–70, 2016, doi: https://doi.org/10.1016/j.compscitech.2015.12.002.

[164] B. Hao, Q. Ma, S. Yang, E. Mäder, and P.-C. Ma, "Comparative study on monitoring structural damage in fiber-reinforced polymers using glass fibers with carbon nanotubes and graphene coating," *Compos. Sci. Technol.*, vol. 129, pp. 38–45, 2016, doi: https://doi.org/10.1016/j.compscitech.2016.04.012.

[165] J.-W. Zha, B. Zhang, R. K. Y. Li, and Z.-M. Dang, "High-performance strain sensors based on functionalized graphene nanoplates for damage monitoring," *Compos. Sci. Technol.*, vol. 123, pp. 32–38, 2016, doi: https://doi.org/10.1016/j.compscitech.2015.11.028.

[166] J. Le, S. Pang, and H. Du, "Using graphite nanoplatelet reinforced cementitious composites as a self-sensing material: theory and experiments," in *EMI 2013 Conference*, 2013.

[167] J.-L. Le, H. Du, and S. D. Pang, "Use of 2D Graphene Nanoplatelets (GNP) in cement

composites for structural health evaluation," *Compos. Part B Eng.*, vol. 67, pp. 555–563, 2014, doi: https://doi.org/10.1016/j.compositesb.2014.08.005.

[168] H. Peng *et al.*, "Efficient organic light-emitting diode using semitransparent silver as anode," *Appl. Phys. Lett.*, vol. 87, no. 17, p. 173505, 2005, doi: 10.1063/1.2115076.

[169] R. Paradiso, G. Loriga, and N. Taccini, "A wearable health care system based on knitted integrated sensors," *IEEE Trans. Inf. Technol. Biomed.*, vol. 9, no. 3, pp. 337–344, 2005, doi: 10.1109/TITB.2005.854512.

[170] D. Bowman and B. R. Mattes, "Conductive Fibre Prepared From Ultra-High Molecular Weight Polyaniline for Smart Fabric and Interactive Textile Applications," *Synth. Met.*, vol. 154, no. 1, pp. 29–32, 2005, doi: https://doi.org/10.1016/j.synthmet.2005.07.017.

[171] Y. Qin, X. Wang, and Z. L. Wang, "Microfibre–nanowire hybrid structure for energy scavenging," *Nature*, vol. 451, no. 7180, pp. 809–813, 2008, doi: 10.1038/nature06601.

[172] F. Marchini, "Advanced Applications of Metallized Fibres for Electrostatic Discharge and Radiation Shielding," *J. Coat. Fabr.*, vol. 20, no. 3, pp. 153–166, 1991, doi: 10.1177/152808379102000303.

[173] K. Bertuleit., "Silver Coated Polyamide: A Conductive Fabric," *J. Coat. Fabr.*, vol. 20, no. 3, pp. 211–215, 1991.

[174] R. X. Wang, X. M. Tao, Y. Wang, G. F. Wang, and S. M. Shang., "Microstructures and electrical conductance of silver nanocrystalline thin films on flexible polymer substrates.," *Surf. Coatings Technol.*, vol. 204, no. 8, pp. 1206–1210, 2010.

[175] H. Wang, J. Wang, J. Hong, Q. Wei, W. Gao, and Z. Zhu, "Preparation and characterization of silver nanocomposite textile," *J. Coat. Technol. Res.*, vol. 4, pp. 101–106, 2007, doi: 10.1007/s11998-007-9001-8.

[176] Q. Wei, L. Yu, D. Hou, and Y. Wang, "Comparative studies of functional nanostructures sputtered on polypropylene nonwovens," *e-Polymers*, vol. 7, no. 1, 2007.

[177] N. Perkas, G. Amirian, S. Dubinsky, S. Gazit, and A. Gedanken, "Ultrasound-assisted coating of nylon 6,6 with silver nanoparticles and its antibacterial activity," *J. Appl. Polym. Sci.*, vol. 104, no. 3, pp. 1423–1430, 2007, doi: 10.1002/app.24728.

[178] S.-W. Park, H.-S. Bae, Z. Xing, O. H. Kwon, M. Huh, and I.-K. Kang, "Preparation and

Properties of Silver-Containing Nylon 6 Nanofibers Formed by Electrospinning," *J. Appl. Polym. Sci.*, vol. 112, pp. 2320–2326, 2009, doi: 10.1002/app.29520.

[179] O. Atalay, A. Tuncay, M. D. Husain, and W. R. Kennon, "Comparative study of the weft-knitted strain sensors," *J. Ind. Text.*, vol. 46, no. 5, pp. 1212–1240, 2017, doi: 10.1177/1528083715619948.

[180] C. Metcalf *et al.*, "Fabric-based Strain Sensors for Measuring Movement in Wearable Telemonitoring Applications," *IET Semin. Dig.*, vol. 2009, 2009, doi: 10.1049/ic.2009.0042.

[181] A. R. Burton, J. P. Lynch, M. Kurata, and K. H. Law, "Fully Integrated Carbon Nanotube Composite Thin Film Strain Sensors on Flexible Substrates for Structural Health Monitoring," *Smart Mater. Struct.*, vol. 26, no. 9, 2017.

[182] L. Vertuccio, L. Guadagno, G. Spinelli, P. Lamberti, V. Tucci, and S. Russo, "Piezoresistive properties of resin reinforced with carbon nanotubes for health-monitoring of aircraft primary structures," *Compos. Part B Eng.*, vol. 107, pp. 192–202, 2016, doi: https://doi.org/10.1016/j.compositesb.2016.09.061.

[183] J. F. Christ, C. J. Hohimer, N. Aliheidari, A. Ameli, C. Mo, and P. P tschke, *3D printing of highly elastic strain sensors using polyurethane/multiwall carbon nanotube composites*. SPIE Smart Structures and Materials + Nondestructive Evaluation and Health Monitoring, 2017.

[184] T. Olson, Y. Kwon, D. Hart, D. Loup, and E. Rasmussen, "Carbon Nanotube Based Sensor to Monitor Crack Growth in Cracked Aluminum Structures Underneath Composite Patching," *Appl. Compos. Mater.*, vol. 22, 2014, doi: 10.1007/s10443-014-9417-0.

[185] Z. Metaxa, W. Neri, P. Poulin, and N. Alexopoulos, "Strain monitoring of cement-based materials with embedded polyvinyl alcohol - carbon nanotube (PVA-CNT) fibers," *Frat. ed Integrità Strutt.*, vol. 11, pp. 61–73, 2017, doi: 10.3221/IGF-ESIS.40.06.

[186] L. A. Chia, *Dispersion Effectiveness of Carbon Nanotube Additives in Self-sensing Cementitious Materials for Structural Health Monitoring (Thesis)*. North Dakota State University: {ProQuest} Dissertations Publishing, 2016.

[187] A. Downey, E. Garcia-Macias, A. D'Alessandro, S. Laflamme, R. Castro-Triguero, and

F. Ubertini, *Continuous and embedded solutions for {SHM} of concrete structures using changing electrical potential in self-sensing cement-based composites*. Event: {SPIE} Smart Structures and Materials + Nondestructive Evaluation and Health Monitoring, 2017.

[188] Y. Yan, V. Sencadas, J. Zhang, G. Zu, D. Wei, and Z. Jiang, "Processing, characterisation and electromechanical behaviour of elastomeric multiwall carbon nanotubes-poly (glycerol sebacate) nanocomposites for piezoresistive sensors applications," *Compos. Sci. Technol.*, vol. 142, pp. 163–170, 2017, doi: https://doi.org/10.1016/j.compscitech.2017.02.007.

[189] J. R. Bautista-Quijano, B. PetraP�tschke, H., and G. Heinrich, "Strain sensing, electrical and mechanical properties of polycarbonate/multiwall carbon nanotube monofilament fibers fabricated by melt spinning," *Polymer (Guildf).*, vol. 82, pp. 181–189, 2016.

[190] P. Dharap, Z. Li, S. Nagarajaiah, and E. V Barrera, "Nanotube film based on single-wall carbon nanotubes for strain sensing," *Nanotechnology*, vol. 15, no. 3, pp. 379–382, Jan. 2004, doi: 10.1088/0957-4484/15/3/026.

[191] S. K. U. R. Z. I. M. F. J. M. U. H. K. Ghaedi, "Self-Sensing Carbon Based Cement Composite Material," in *2nd International Conference on Advances in Engineering and Technology (RTET-2017)*, 2017.

[192] R. Balaji and M. Sasikumar, "Graphene based strain and damage prediction system for polymer composites," *Compos. Part A*, vol. 103, pp. 48–59, 2017.

[193] S.-H. Bae, Y. Lee, B. K. Sharma, H.-J. Lee, J.-H. Kim, and J.-H. Ahn, "Graphene-based transparent strain sensor," *Carbon N. Y.*, vol. 51, pp. 236–242, 2013, doi: https://doi.org/10.1016/j.carbon.2012.08.048.

[194] Q. Liu, R. Gao, V. W. Y. Tam, W. Li, and J. Xiao, "Strain monitoring for a bending concrete beam by using piezoresistive cement-based sensors," *Constr. Build. Mater.*, vol. 167, pp. 338–347, 2018, doi: https://doi.org/10.1016/j.conbuildmat.2018.02.048.

[195] H. Li, H. Xiao, and J. Ou, "Effect of compressive strain on electrical resistivity of carbon black-filled cement-based composites," *Cem. Concr. Compos.*, vol. 28, no. 9, pp. 824–828, 2006, doi: https://doi.org/10.1016/j.cemconcomp.2006.05.004.

[196] C. Bataxi, Y. X., W. Z., H., and C. Bil, “Strain Monitoring on Damaged Composite Laminates Using Digital Image Correlation,” *Procedia Eng.*, vol. 99, pp. 353–360, 2015.

[197] R. Ruzek, M. Kadlec, K. I. Tserpes, and E. Karachalios, “Monitoring of compressive behaviour of stiffened composite panels using embedded fibre optic and strain gauge sensors,” *Int. J. Struct. Integr.*, vol. 8, 2017, doi: 10.1108/IJSI-11-2015-0052.

[198] W.-S. Chang and H. Huang, “Seismic resilience timber connection - adoption of shape memory alloy tubes as dowels,” *Struct. Control Heal. Monit.*, vol. 24, 2016, doi: 10.1002/stc.1980.

[199] M. Ashir, L. Hahn, A. Kluge, A. Nocke, and C. Cherif, “Development of innovative adaptive 3{D} {Fiber} {Reinforced} {Plastics} based on {Shape} {Memory} {Alloys},” *Compos. Sci. Technol.*, vol. 126, pp. 43–51, 2016.

[200] H. Liu, K. Liu, A. Mardirossian, D. Heider, and E. Thostenson, “Carbon nanotube-based structural health monitoring for fiber reinforced composite materials,” in *Nondestructive Characterization and Monitoring of Advanced Materials, Aerospace, and Civil Infrastructure, Portland, Oregon, United States*, 2017.

[201] O. G. Kravchenko, D. Pedrazzoli, D. Kovtun, X. Qian, and I. Manas-Zloczower, “Incorporation of plasma-functionalized carbon nanostructures in composite laminates for interlaminar reinforcement and delamination crack monitoring,” *J. Phys. Chem. Solids*, vol. 112, pp. 163–170, 2018, doi: https://doi.org/10.1016/j.jpcs.2017.09.018.

[202] T. J. Adam, F. Nolte, B. Begemann, and P. Horst, “Selective laser illumination method for enhanced damage monitoring of micro cracking and delamination in GFRP laminates,” *Polym. Test.*, vol. 65, pp. 125–133, 2018, doi: https://doi.org/10.1016/j.polymertesting.2017.11.022.

[203] X. Du *et al.*, “Graphene/epoxy interleaves for delamination toughening and monitoring of crack damage in carbon fibre/epoxy composite laminates,” *Compos. Sci. Technol.*, vol. 140, pp. 123–133, 2017, doi: https://doi.org/10.1016/j.compscitech.2016.12.028.

[204] S. Saadat *et al.*, “An overview of vibration and seismic applications of {NiTi} shape memory alloy,” *Smart Mater. Struct.*, vol. 11, no. 2, pp. 218–229, Apr. 2002, doi: 10.1088/0964-1726/11/2/305.

[205] G. Song, N. Ma, and H.-N. Li, “Applications of shape memory alloys in civil structures,”

Eng. Struct., vol. 28, no. 9, pp. 1266–1274, 2006, doi: https://doi.org/10.1016/j.engstruct.2005.12.010.

[206] P. D. Mondal, A. D. Ghosh, and S. Chakraborty, "Control of underground blast induced building vibration by shape-memory-alloy rubber bearing (SMARB)," *Struct. Control Heal. Monit.*, vol. 24, no. 10, p. e1983, 2017, doi: 10.1002/stc.1983.

[207] B. Senf *et al.*, "Sensing and Actuating Functions by Shape Memory Alloy Wires Integrated into Fiber Reinforced Plastics," *Procedia CIRP*, vol. 66, pp. 249–253, 2017, doi: https://doi.org/10.1016/j.procir.2017.03.291.

[208] G. Choi *et al.*, "A spray-on carbon nanotube artificial neuron strain sensor for composite structural health monitoring," *Sensors*, vol. 16, no. 8, p. 1171, 2016.

[209] E. T. Thostenson and T.-W. Chou, "Real-timein situsensing of damage evolution in advanced fiber composites using carbon nanotube networks," *Nanotechnology*, vol. 19, no. 21, p. 215713, Apr. 2008, doi: 10.1088/0957-4484/19/21/215713.

[210] B. K. S. Isaac-Medina, A. Alonzo-García, and F. Avilés, "Electrical self-sensing of impact damage in multiscale hierarchical composites with tailored location of carbon nanotube networks," *Struct. Heal. Monit.*, vol. 18, no. 3, pp. 806–818, 2019, doi: 10.1177/1475921718776198.

[211] S. Sun *et al.*, "Nano graphite platelets-enabled piezoresistive cementitious composites for structural health monitoring," *Constr. Build. Mater.*, vol. 136, pp. 314–328, 2017, doi: https://doi.org/10.1016/j.conbuildmat.2017.01.006.

[212] G. Fargione, A. Geraci, G. Rosa, and A. Risitano, "Rapid determination of the fatigue curve by the thermographic method," *Int. J. Fatigue*, vol. 24, pp. 11–19, 2002.

[213] G. [La Rosa] and A. Risitano, "Thermographic methodology for rapid determination of the fatigue limit of materials and mechanical components," *Int. J. Fatigue*, vol. 22, no. 1, pp. 65–73, 2000, doi: https://doi.org/10.1016/S0142-1123(99)00088-2.

[214] M. Naderi, A. Kahirdeh, and M. M. Khonsari, "Dissipated thermal energy and damage evolution of Glass/Epoxy using infrared thermography and acoustic emission," *Compos. Part B Eng.*, vol. 43, no. 3, pp. 1613–1620, 2012, doi: https://doi.org/10.1016/j.compositesb.2011.08.002.

[215] C. Meola and G. M. Carlomagno, "Impact damage in GFRP: New insights with infrared

thermography," *Compos. Part A Appl. Sci. Manuf.*, vol. 41, no. 12, pp. 1839–1847, 2010, doi: https://doi.org/10.1016/j.compositesa.2010.09.002.

[216] E. Grinzato and V. Vavilov, "Corrosion evaluation by thermal image processing and 3{D} modelling," *Rev. {Generale} {Thermique}*, vol. 37, no. 8, pp. 669–679, 1998.

[217] L. Chung, I. Paik, S. Cho, and Y. Roh, "Infrared Thermographic Technique to Measure Corrosion in Reinforcing Bar," *Key Eng. Mater. - KEY ENG MAT*, vol. 321–323, pp. 821–824, 2006, doi: 10.4028/www.scientific.net/KEM.321-323.821.

[218] V. Talakokula and S. Bhalla, "Reinforcement corrosion assessment capability of surface bonded and embedded piezo sensors for reinforced concrete structures," *J. Intell. Mater. Syst. Struct.*, vol. 26, no. 17, pp. 2304–2313, 2015, doi: 10.1177/1045389X14554133.

[219] J. Sebastian *et al.*, "Health monitoring of structural composites with embedded carbon nanotube coated glass fiber sensors," *Carbon N. Y.*, vol. 66, pp. 191–200, 2014, doi: https://doi.org/10.1016/j.carbon.2013.08.058.

[220] B. Lebental, W. Moujahid, C. S. Lee, J.-L. Maurice, and C. Cojocaru, "Graphene-based resistive humidity sensor for in-situ monitoring of drying shrinkage and intrinsic permeability in concrete," 2012.

[221] H. Chi, Y. J. Liu, F. Wang, and C. He, "Highly Sensitive and Fast Response Colorimetric Humidity Sensors Based on Graphene Oxides Film," *ACS Appl. Mater. Interfaces*, vol. 7, no. 36, 2015.

[222] J. He *et al.*, "Highly Efficient Actuator of Graphene/Polydopamine Uniform Composite Thin Film Driven by Moisture Gradients," *Adv. Mater. Interfaces*, vol. 3, no. 14, p. 1600169, 2016, doi: 10.1002/admi.201600169.

[223] W. Li, F. Xu, L. Sun, W. Liu, and Y. Qiu, "A novel flexible humidity switch material based on multi-walled carbon nanotube/polyvinyl alcohol composite yarn," *Sensors Actuators B Chem.*, vol. 230, pp. 528–535, 2016, doi: https://doi.org/10.1016/j.snb.2016.02.108.

[224] O. Starkova, E. Mannov, K. Schulte, and A. Aniskevich, "Strain-dependent electrical resistance of epoxy/MWCNT composite after hydrothermal aging," *Compos. Sci. Technol.*, vol. 117, pp. 107–113, 2015, doi: https://doi.org/10.1016/j.compscitech.2015.06.004.

[225] C. Liu and K. Lafdi, “Environmental Monitoring of Composite Durability Use Multiple Sensing Technologies,” in *CAMX 2018 – The Composites and Advanced Materials Expo, Dallas, {TX}, {US}*, 2018.

[226] Q. Wang and S. T. Quek, “Enhancing flutter and buckling capacity of column by piezoelectric layers,” *Int. J. Solids Struct.*, vol. 39, pp. 4167–4180, 2002, doi: 10.1016/S0020-7683(02)00334-7.

[227] Q. Wang, G. Y. Zhou, and S. T. Quek, “Repair of Delaminated Beams Subjected to Compressive Force via Piezoelectric Layers,” *Adv. Struct. Eng.*, vol. 8, no. 4, pp. 411–425, 2005, doi: 10.1260/136943305774353142.

[228] N. Wu and Q. Wang, “Repair of vibrating delaminated beam structures using piezoelectric patches,” *Smart Mater. Struct.*, vol. 19, no. 3, p. 35027, Feb. 2010, doi: 10.1088/0964-1726/19/3/035027.

[229] O. Rabinovitch, “Piezoelectric Control of Edge Debonding in Beams Strengthened with Composite Materials: Part I – Analytical Modeling,” *J. Compos. Mater. - J Compos MATER*, vol. 41, pp. 525–546, 2007, doi: 10.1177/0021998306063790.

[230] T. J.-C. Liu, “Crack repair performance of piezoelectric actuator estimated by slope continuity and fracture mechanics,” *Eng. Fract. Mech.*, vol. 75, no. 8, pp. 2566–2574, 2008, doi: https://doi.org/10.1016/j.engfracmech.2007.11.004.

[231] A. Ariaei, S. Ziaei-Rad, and M. Ghayour, “Repair of a cracked Timoshenko beam subjected to a moving mass using piezoelectric patches,” *Int. J. Mech. Sci.*, vol. 52, no. 8, pp. 1074–1091, 2010, doi: https://doi.org/10.1016/j.ijmecsci.2010.04.001.

[232] G. Song, Y. L. Mo, K. Otero, and H. Gu, “Health monitoring and rehabilitation of a concrete structure using intelligent materials,” *Smart Mater. Struct.*, vol. 15, no. 2, pp. 309–314, Jan. 2006, doi: 10.1088/0964-1726/15/2/010.

[233] W. H. Duan, S. T. Quek, and Q. Wang, “Finite element analysis of the piezoelectric-based repair of a delaminated beam,” *Smart Mater. Struct.*, vol. 17, no. 015-017., 2007.

[234] Q. Wang, S. Quek, and K. Liew, “On the repair of a cracked beam with a piezoelectric patch,” *Smart Mater. Struct.*, vol. 11, p. 404, 2002, doi: 10.1088/0964-1726/11/3/311.

[235] Q. Wang, W. H. Duan, and S. T. Quek, “Repair of notched beam under dynamic load using piezoelectric patch,” *Int. J. Mech. Sci.*, vol. 46, no. 10, pp. 1517–1533, 2004, doi:

https://doi.org/10.1016/j.ijmecsci.2004.09.012.

[236] L. Bao, T. Okazawa, A. Xu, and J. Shi, “A simple repair method for {GFRP} delamination using ultraviolet-curable resin,” *Adv. Compos. Mater.*, vol. 27, no. 3, 2017.

[237] S. Ahmed, E. T. Thostenson, T. Schumacher, S. M. Doshi, and J. R. McConnell, “Integration of carbon nanotube sensing skins and carbon fiber composites for monitoring and structural repair of fatigue cracked metal structures,” *Compos. Struct.*, vol. 203, pp. 182–192, 2018.

[238] S. Park, C.-B. Yun, Y. Roh, and J.-J. Lee, “PZT-based active damage detection techniques for steel bridge components,” *Smart Mater. Struct.*, vol. 15, no. 4, pp. 957–966, Jun. 2006, doi: 10.1088/0964-1726/15/4/009.

[239] W. H. Duan, Q. Wang, and S. T. Quek, “Applications of Piezoelectric Materials in Structural Health Monitoring and Repair: Selected Research Examples,” *Materials (Basel).*, vol. 3, pp. 5169–5194, 2010.

[240] P. Tua, S. Quek, and Q. Wang, “Detection of cracks in cylindrical pipes and plates using piezo-actuated Lamb waves,” *Smart Mater. Struct.*, vol. 14, p. 1325, 2005, doi: 10.1088/0964-1726/14/6/025.

[241] J. Leng, X. Lan, Y. Liu, and S. Du, “Shape-memory polymers and their composites: Stimulus methods and applications,” *Prog. Mater. Sci.*, vol. 56, no. 7, pp. 1077–1135, 2011, doi: https://doi.org/10.1016/j.pmatsci.2011.03.001.

[242] Z. Q. Liu, “Study on damage self-monitoring and self-repair of SMA smart concrete beam,” Dissertation for the Doctor Degree, Harbin Institute of Technology, 2006.

[243] J. Park and S. Park, “Intelligent bolt-jointed system integrating piezoelectric sensors with shape memory alloys,” *Smart Struct. Syst.*, vol. 17, pp. 135–147, 2016, doi: 10.12989/sss.2016.17.1.135.

[244] K. Wilde, P. Gardoni, and Y. Fujino, “Base isolation system with shape memory alloy device for elevated highway bridges,” *Eng. Struct.*, vol. 22, no. 3, pp. 222–229, 2000, doi: https://doi.org/10.1016/S0141-0296(98)00097-2.

[245] B. R. Bielefeldt, J. D. Hochhalter, and D. J. Hartl, *Shape Memory Alloy Sensory Particles for Damage Detection: Experiments, Analysis, and Design Studies*. Structural Health Monitoring, 2017.

[246] H. Kimura, Y. Akiniwa, K. Tanaka, H. Tanaka, and Y. Okumura, “Smart structure for suppression of mode I and II crack propagation in CFRP laminates by shape memory alloy TiNi actuator,” *Int. J. Fatigue*, vol. 28, no. 10, pp. 1147–1153, 2006, doi: https://doi.org/10.1016/j.ijfatigue.2006.02.002.

[247] K. S. C. Kuang, S. T. Quek, and W. J. Cantwell, “Active control of a smart composite with shape memory alloy sheet using a plastic optical fiber sensor,” *Sensors Actuators A Phys.*, vol. 201, pp. 182–187, 2013, doi: https://doi.org/10.1016/j.sna.2013.06.024.

[248] Y. Zhu, X. J. Ye, M. Z. Rong, and M. Q. Zhang, “Self-Healing Fiber Composites With a Self-Pressurized Healing System,” in *Polymer-Based Multifunctional Nanocomposites and Their Applications*, K. Song, C. Liu, and J. Z. Guo, Eds. Elsevier, 2019, pp. 137–156.

[249] K. Mphahlele, S. Sinha Ray, and A. Kolesnikov, “Self-Healing Polymeric Composite Material Design, Failure Analysis and Future Outlook: A Review,” *Polymers (Basel).*, vol. 9, p. 535, 2017, doi: 10.3390/polym9100535.

[250] Y. Shindo, Y. Kuronuma, T. Takeda, F. Narita, and S.-Y. Fu, “Electrical resistance change and crack behavior in carbon nanotube/polymer composites under tensile loading,” *Compos. Part B Eng.*, vol. 43, no. 1, pp. 39–43, 2012, doi: https://doi.org/10.1016/j.compositesb.2011.04.028.

[251] S. Anand and M. D. Roy, “Quasi-static and dynamic strain sensing using carbon nanotube/epoxy nanocomposite thin films,” *Smart Mater. Struct.*, vol. 18., 2009.

[252] M. Park, H. Kim, and J. Youngblood, “Strain-dependent electrical resistance of multi-walled carbon nanotube/polymer composite films,” *Nanotechnology*, vol. 19, p. 55705, 2008, doi: 10.1088/0957-4484/19/05/055705.

[253] C. Li and T.-W. Chou, “Modeling of damage sensing in fiber composites using carbon nanotube networks,” *Compos. Sci. Technol.*, vol. 68, no. 15, pp. 3373–3379, 2008, doi: https://doi.org/10.1016/j.compscitech.2008.09.025.

[254] Alamusi, Y. L. Liu, and N. Hu, “Numerical Simulations on Piezoresistivity of CNT/Polymer Based Nanocomposites,” *Comput. Mater. Contin.*, vol. 20, pp. 101–117, 2010.

[255] B. Hu *et al.*, “Multi-scale numerical simulations on piezoresistivity of {CNT}/polymer

nanocomposites," *Nanoscale Res. Lett.*, vol. 7, no. 1, 2012.

[256] A. R. Alian and S. A. Meguid, "Multiscale modeling of the coupled electromechanical behavior of multifunctional nanocomposites," *Compos. Struct.*, vol. 208, pp. 826–835, 2019, doi: https://doi.org/10.1016/j.compstruct.2018.10.066.

CHAPTER 2 : DIFFERENT SENSORS AND THEIR ELECTRO-THERMO-MECHANICAL BEHAVIOR IN REAL-TIME

In this chapter, three sensor systems i.e. sensor I consisting of Nylon/Ag conductive fiber, sensor II consisting of a conductive membrane (CM) of CNTs and sensor III consisting of polyacrylonitrile (PAN) carbon fibers are fabricated respectively. These three sensor systems are then studied individually as standalone sensors to demonstrate their electromechanical by calculating the gauge factor (GF) and electrothermal behavior by using empirical relations. In addition, the overall electromechanical response of each sensor was studied up to fracture to demonstrate the behavior of the sensor when it experiences large strain or any damage which was essential to understand its use in high strain applications. In the next step, each sensor was attached to the electrodes and put in an oven to monitor the change in its electrical behavior during a change in the temperature of its surroundings.

2.1. Introduction

Nowadays, different textiles are used as a substrate material for coating or surface treatment and generated huge interest in the development of smart portable and flexible devices because of their flexibility. This has led to the development of in-situ monitoring and wearable technologies. Textiles with sensing behavior are known as smart textiles and they consist of fabric, mat, or yarn. These smart textiles can be developed by either using conductive polymers or by incorporating conductive\sensing nanomaterials and they can generate response signals to change in any stimulus such as pressure, electrical current, temperature, and force. Moreover, the nature of fabrics or yarn makes them ideal for designing smart wearable devices that can come in direct interaction with human beings and these smart wearable devices are the prime focus of research in the field of military, medicine, aerospace or commercial use [1]–[4]. Smart textiles can be used for a variety of applications however, this area of research is still under development and these smart textiles cannot replace conventional electronics completely at an industrial scale. Moreover, the focus of this chapter is to discuss the use of smart textiles for high strain applications such as in-situ structural health monitoring and medical monitoring.

Flexible conductive wire sensors were considered to be a very promising solution for high strain applications. After integration, they not only perform damage sensing but also act as reinforcement [5]–[8]. These smart textiles, fabrics, and yarns were first developed by using conductive polymers for real-time damage detection in composite structures but they were unstable when exposed to the environment and had low conductivity in comparison to nanoparticles [9]–[13]. Similarly, Coating or inserting conductive nanoparticles such as carbon nanotubes (CNTs), graphene, etc. into the filaments were also considered as a possible solution of real-time strain monitoring [14]. Moreover, metal nanoparticles such as gold, nickel, aluminum, stainless steel, copper, and silver were commonly used as coating materials for in-situ SHM applications [15]–[17]. Amongst all these metal nanoparticles, silver (Ag) showed great potential as a coating material on the flexible polymeric substrate because of its excellent conductivity, competitive price, stability in the air, and other mechanical properties [18]. Silver had already been used in anti-microbial activity and as wearable sensing clothes for medical monitoring and showed better stability, responsivity, repeatability, and low drift in electrical signals in strain sensing applications [19]–[22]. Although the silver (Ag) metal-coated fabric was studied numerous times for antibacterial and medical activities, its application regarding structural health monitoring purposes in composites is still underdeveloped.

Numerous studies had also focused on piezoresistive polymers made by dispersing nanofillers such as carbon nanotubes (CNTs) into the filaments of fibers or in the polymer matrix to increase the overall conductance of the structure were also considered as a possible solution of real-time strain monitoring [14], [23]–[31]. In addition, a conductive polymer in the form of a thin-film, ribbon, a thread, or any other desired shape can be formed using CNTs for sensing applications [26][32]. CNTs have been considered exceptional material since their discovery because of their high aspect ratio, electrical conductivity, and excellent mechanical and thermal properties [33][34]. Fibers consisting of CNTs had been used in SHM of damage in structures due to their excellent mechanical behavior, flexibility and deformation sensitivity [35]–[38]. To have excellent conductivity, CNTs are usually implemented in well-aligned free-standing or a conductive membrane (sheet) of randomly oriented CNTs named as bucky paper [33], [39]–[45]. However, several studies showed that oriented and grown CNTs on a specific substrate required critical control on the fabrication process to ensure better dimension and spacing of CNTs [46]–[48]. Therefore, the fabrication of bucky paper / conductive membrane was inspired by the simplicity of the fabrication process and ease to use especially on a large scale. The conductive membrane is a laminar structure of randomly oriented CNTs held together by the Van Der Waal's forces. This conductive membrane/bucky paper had been utilized to developed chemical sensors, actuators, supercapacitors, flexible fibers, and deicing systems [33], [49]–[53]. However, examination of behavior and change in electrical properties of a pure network of CNTs in the form of a membrane under mechanical and thermal loads in real-time is still underdeveloped or limited.

In addition, carbon fibers (CF) used as a sensor because of their good electrical conductivity is a possible simple, durable, and cost-effective solution for damage monitoring in real-time[54]. CF consists of graphite-based microstructure and loading these fibers could deduce change in electrical behavior because of the change in their mechanical structure thus, depicting piezoresistive behavior [55]. furthermore, the integration of CF in fiber-reinforced composites is quite easy because of the textile processing compatibility [56]–[58]. The electromechanical response of Carbon fibers was first to study by Concor and Owston [59] which showed that resistance of these fibers rises linearly with the applied strain and they also studied their mechanical performance and contact resistance [56]. After these studies, continuous carbon fibers had been in use as self-sensing materials in composites because of simplicity in application, high mechanical performance and less cost [60]–[65]. However, straightness of the filaments in the CF sensor plays a vital role to define the contact resistance and overall performance of the sensor [59], [65], [66].

So, in this chapter, three sensor systems i.e. sensor I consisting of Nylon/Ag conductive fiber, sensor II consisting of a conductive membrane (CM) of CNTs and sensor III consisting of polyacrylonitrile (PAN) carbon fibers are fabricated respectively. These three sensor systems are then studied individually as standalone sensors to demonstrate their electromechanical response by calculating the gauge factor (GF) and electrothermal behavior by using empirical relations. In addition, the overall electromechanical response of each sensor was studied up to fracture to demonstrate the behavior of the sensor when it experiences large strain or any damage which was essential to understand its use in high strain applications. In the next step, each sensor was attached to the electrodes and put in an oven to monitor the change in its electrical behavior during a change in the temperature of its surroundings. These results gave interesting behavior and showed that each sensor did not only detected the strain under mechanical loading but also showed a change in its resistance under thermal loads, which could be useful in detecting a release of thermal energy in a structure because of the presence of micro or macro cracks [67].

2.2. Fabrication process

2.2.1. Sensor I: Nylon/Ag fiber sensor

Nylon yarn behaved well mechanically with good flexibility but was poor in electrical conductance so, it was required to improve the conductivity of the material for strain sensing. There were studies where nanofillers can be inserted inside the fiber but only up to a certain weight percentage because a further increase can result in a decrease in mechanical performance [68]. For this purpose, the silver (Ag) metal nanoparticles were deposited in the form of continuous and uniform coating on the surface of each filament of nylon yarn at the nanoscale using simple and efficient electroless plating process which can be easily done on complex substrates/geometries. In addition, with the coating process, 100% uniform coating was formed without affecting the structural integrity or flexibility of core material. Nylon-6 yarn was cleaned with ethanol to remove any dust particles or surface impurities to ensure good adhesion for the nanoparticles of Ag metal. Then nylon was treated with silver nitrate (AgNO3) and sodium hydroxide (NaOH) at 130 °C for 2 hours. The addition of silver nitrate to the alkali solution led to the formation of a hydrated form of Ag+ as $[Ag(H2O)_4]^+$, which then became silver oxide (Ag_2O) sediment through the reaction of OH^- ions with Ag^+ ions and treatment at 130 °C in a strong alkali solution (NaOH) led to the dissociation of Ag_2O into Ag^+ ions which

bonded to the hydroxyl (−OH) and carboxylate (−COO−) end groups on the fiber surface through an ionic interaction [69]–[71]. After that, reduction process in ammonia (NH3) environment was carried out for 2 hours which produced ethylene by the alkali hydrolysis of polyester fabrics as a reducing agent to reduce the Ag^{+} ions to Ag^{0} element by producing electrons resulting in a transparent clear solution of Ag [69], [70], [72]. Finally, after post-treatment with ammonia, silver nanoparticles were deposited on the surface of nylon. The complete process is demonstrated in Figure 2-1.

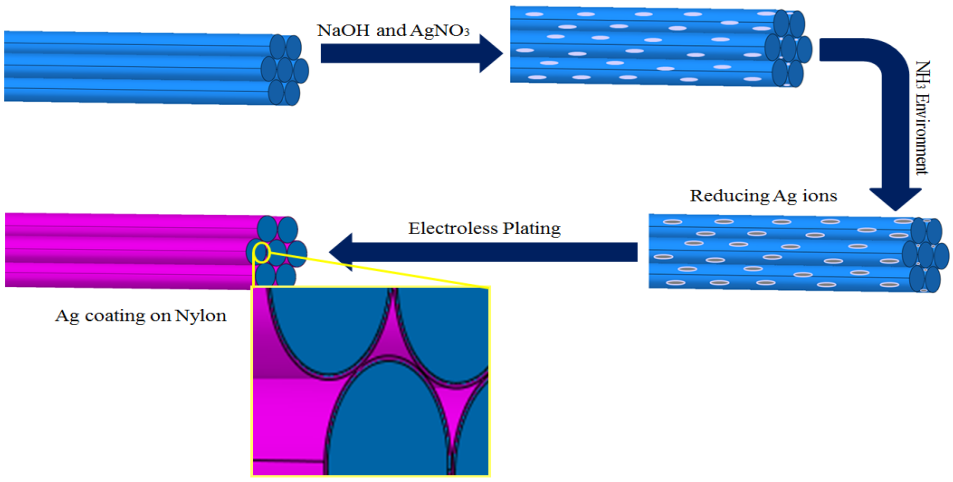

Figure 2-1: Fabrication process of the Nylon/Ag fiber sensor

SEM characterization was performed on Nylon/Ag conductive fibers fabricated with different coating thicknesses of Ag metal film. The SEM images revealed that the Nylon/Ag conductive fiber with 1% or less thickness showed lots of discontinuities and defects in the Ag metal coating layer, Figure 2-2(a)-(d). However, Nylon yarn with approximately 2% of coating thickness showed a uniform and continuous application of Ag-metal nanoparticles on the surface of each filament of the yarn and does not require a higher concentration of the Ag-metal and that is why this thickness of Ag-coating was chosen. This can be seen in SEM characterization which was conducted at three different locations and magnifications on the same specimen to verify the uniform and continuous application of the coating, Figure 2-2(e)-(i). Nylon-6 filaments showed good adhesion bonding because of their surface roughness. These small cavities acted as anchoring points for deposited metallic particles and thus showed better adhesion as compared to polyester and polypropylene polymeric materials [73]. Furthermore, larger magnification of SEM confirmed that the Ag coating was formed by the continuous deposition of Ag nanoparticles on the surface of Nylon-6 yarn and very few filaments exhibited minute gaps (or nanoscale) regardless of which the electrical current flow through the yarn was almost 100% because these minute imperfections were found in very few filaments in

comparison to the whole yarn and their presence did not affect the overall path of current flow, Figure 2-2 (j).

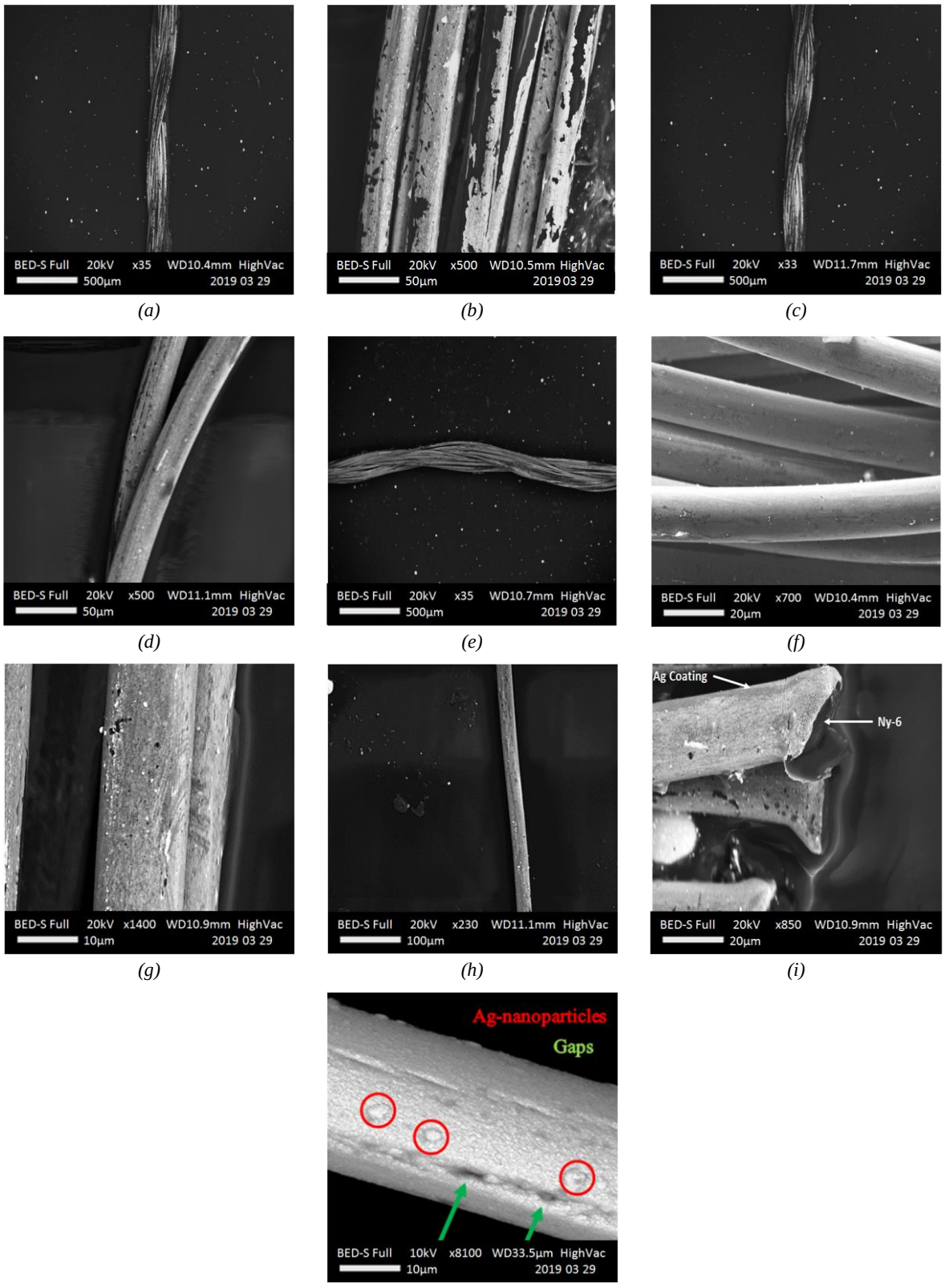

Figure 2-2: SEM Characterization of the Nylon/Ag fiber sensor

2.2.2. Sensor II: Conductive membrane (CM)

Conductive membrane (CM) was fabricated using a chemical vapor deposition (CVD) method by growing CNTs on a quartz crystal. This process consisted of two steps in which the first catalyst was prepared and then CNTs were synthesized. The wafer, cut in specific dimensions, was first heated in an oven at 500 °C for 10 mins and then after cooling down to the room temperature, it was dipped in the catalyst solution consisting of ethanol and Fe-Mo in a mol ratio of 10:1. Afterward, the FE catalyst deposited on the wafer was reduced by placing it in a quartz tube in a tube furnace and heating at 800°C in argon and hydrogen gas. Lastly, in the presence of ethylene gas, the substrate was subjected to a carbon source. This ethylene gas triggered the breakdown of carbon and led to the synthesis and deposition of CNTs on the wafer. After fabrication, the sample was pressed between two parallel plates in successive steps to ensure denser film in the form of a membrane of 120 µm thickness and separate it from the wafer. We managed to produce CNTs with a length of about 200 µm with a diameter of about 10nm. Figure 2-3 demonstrates the SEM characterization of the CM sensor consisting of a dense network of CNTs. It's a laminar structure of randomly oriented CNTs held together by the Van Der Waal's forces.

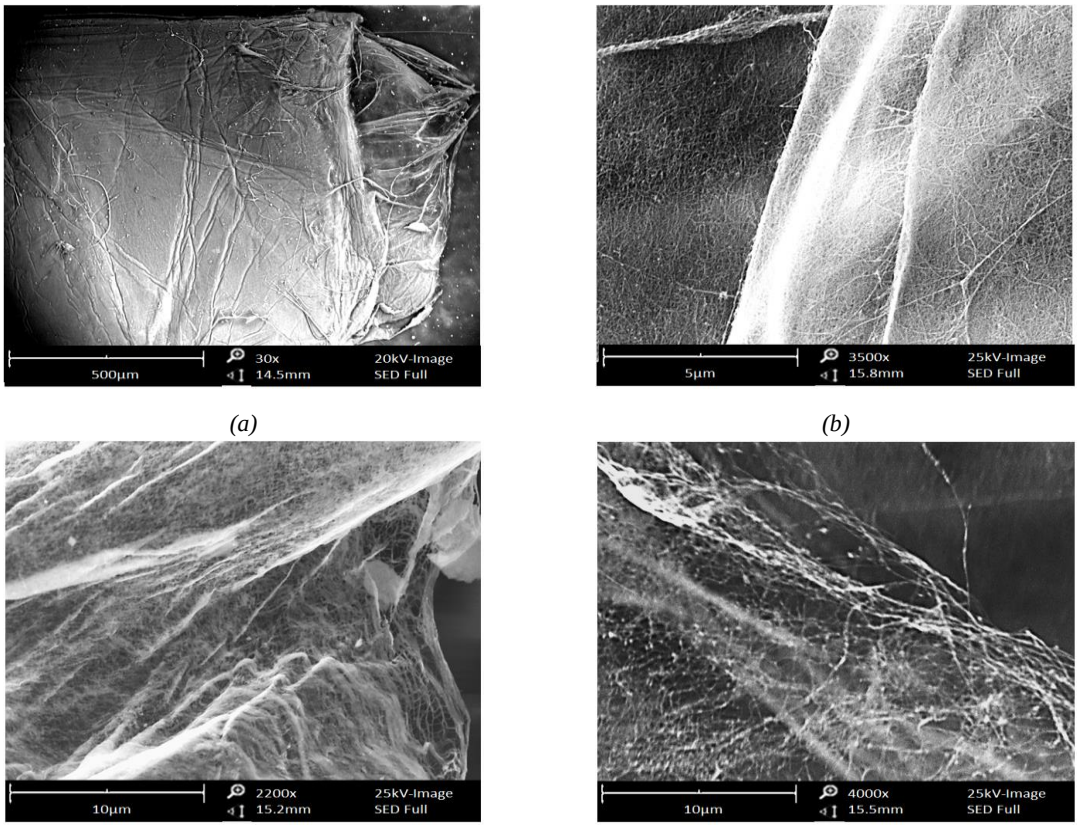

(a) *(b)*

(c) *(d)*

Figure 2-3: SEM images of CM sensor. (a) CM sensor (b) magnified image on the surface of the CM sensor to demonstrate the network of CNTs (c) SEM at lower magnification on the edge of the membrane (d) magnified SEM image on the edge of the single layer of membrane to show the network of CNTs in forms of threads of a fabric.

2.2.3. Sensor III: PAN Carbon Fiber (CF)

Carbon fibers (CF) consisted of unidirectional filaments of carbon produced at low-pressure vacuum from a precursor Polyacrylonitrile (PAN) polymer and this process is described in detail in [81]. PAN carbon fibers were purchased from the Nanomaterials Laboratory of the University of Dayton. First, PAN Fibers are thermally stabilized at 200-300°C at room temperature and then, these fibers were carbonized in an inert environment above 1000°C. Afterwards, the surface of the fibers was etched during surface treatment. Some of the physical properties are mentioned in Table 2-1 for the PAN carbon fibers. SEM characterization was performed to demonstrate the filaments of CF, Figure 2-4.

Table 2-1: Physical Properties of the PAN Carbon Fibers

Density (g/cc)	1.76
Coefficient of thermal expansion (CTE) (µm/m-°C)	-0.6
Thermal Conductivity (W/m-K)	8.50
Electrical Resistance (ohm-cm)	0.00180

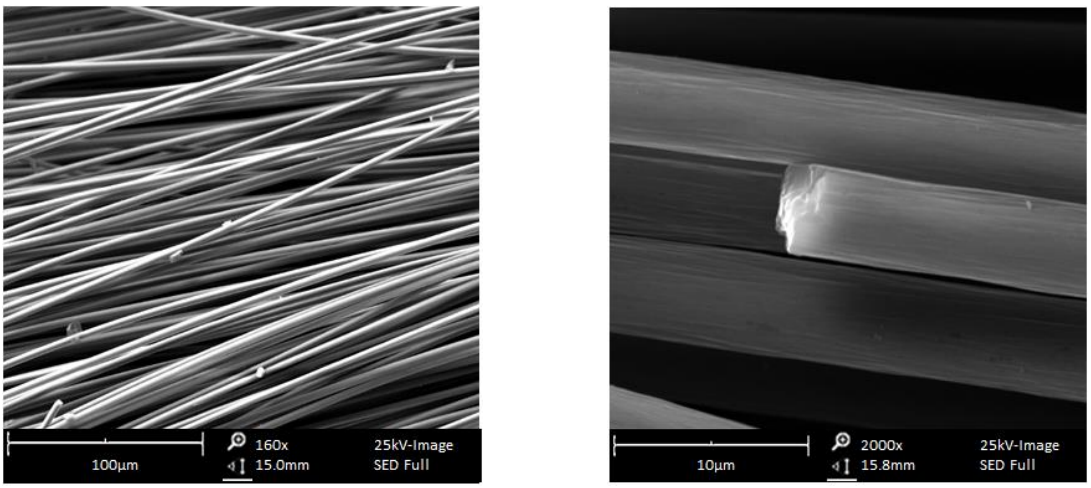

(a) *(b)*

Figure 2-4: SEM images of the CF sensor. (a) PAN carbon fibers (b) SEM of unidirectional filaments of Carbon aligned together (b) magnified image to show the single fiber of carbon.

2.3. Experimental Procedure

2.3.1. Standalone sensor under mechanical loading

All three sensors were tested under mechanical tensile load as a standalone sensor of 72mm in length using the INSTRON-50 apparatus and oscilloscope were used at the same time to calculate the sensitivity of each sensor by calculating its gauge factor. Many experimental challenges were encountered, such as difficulties in gripping the samples inside the fixtures of the machine because of its size, and also it was critical to making sure that the conductive fiber was not in contact with any metallic portion of the machine. All the necessary parts of the machine were insolated by covering with the insulation tape so the electrical response of the conductive fiber could not be affected. It was difficult to place the specimen directly in the machine fixtures so paper support was attached with each sensor in the tensile machine, however; the paper frame was cut before conducting the test so the mechanical response of the sensors could not be affected during the test, Figure 2-5. Besides this, electrode wires were attached at both ends of the specimen to provide a better connection with an oscilloscope by reducing any chance of perturbation in the signal during the test, and then, the sensor was placed within the fixture of the tensile machine, Figure 2-6. One thing should be kept in mind that each sensor was unstrained when attached to the electrodes on the paper support with adhesive tape and there was no slippage between the connections during the test because it was properly fixed between the fixtures of the tensile machine. The tensile test was performed at a low strain rate i.e. 2mm/min. Three successful tensile tests were conducted to determine the reproducibility of results. Each sensor was loaded respectively within the elastic limit and electromechanical response was plotted as the change of resistance concerning the strain. Afterward, each sensor system was applied with maximum strain up to fracture to understand its electromechanical response under high strain application. INSTRON-50 machine and HBM Spider 8 oscilloscope were used at the same time to examine the sensing behavior and the paper frame was used for support similar to the previous test. The tensile test was performed in a quasi-static state at a loading speed of 2mm/min and overall mechanical behavior was obtained during the test along with the resistance profile. Three tests were conducted to see the repeatability of the results and each specimen was fractured from the center.

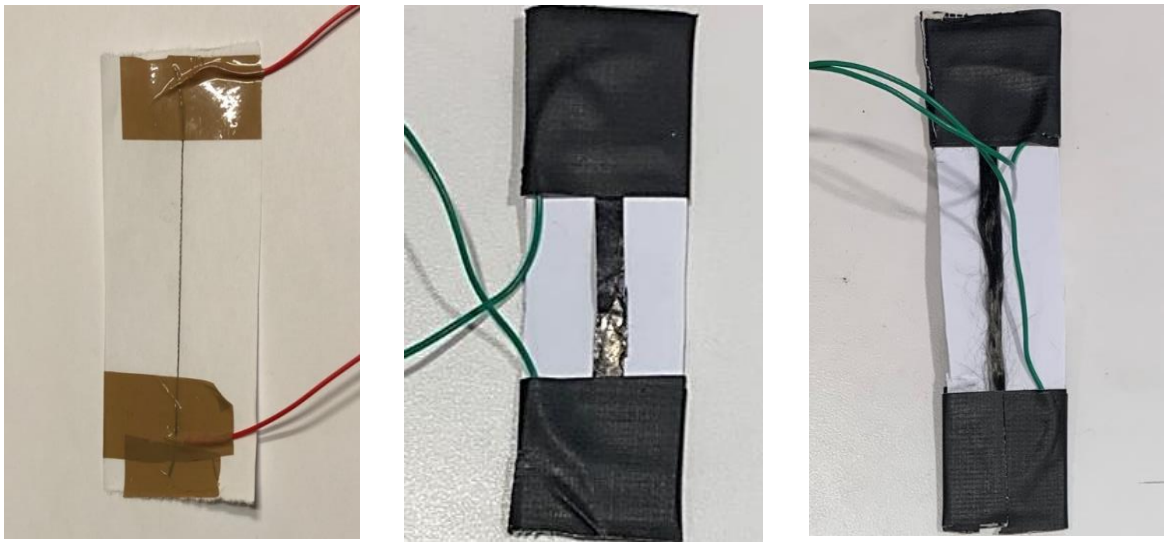

(a) Sensor I: Nylon/Ag fiber sensor

(b) Sensor II: Conductive membrane (CM) sensor

(c) Sensor III: Carbon Fiber (CF) fiber sensor

Figure 2-5: Preparation of each sensor system fiber for the experimental procedure. Electrodes were attached at both end and paper support was used.

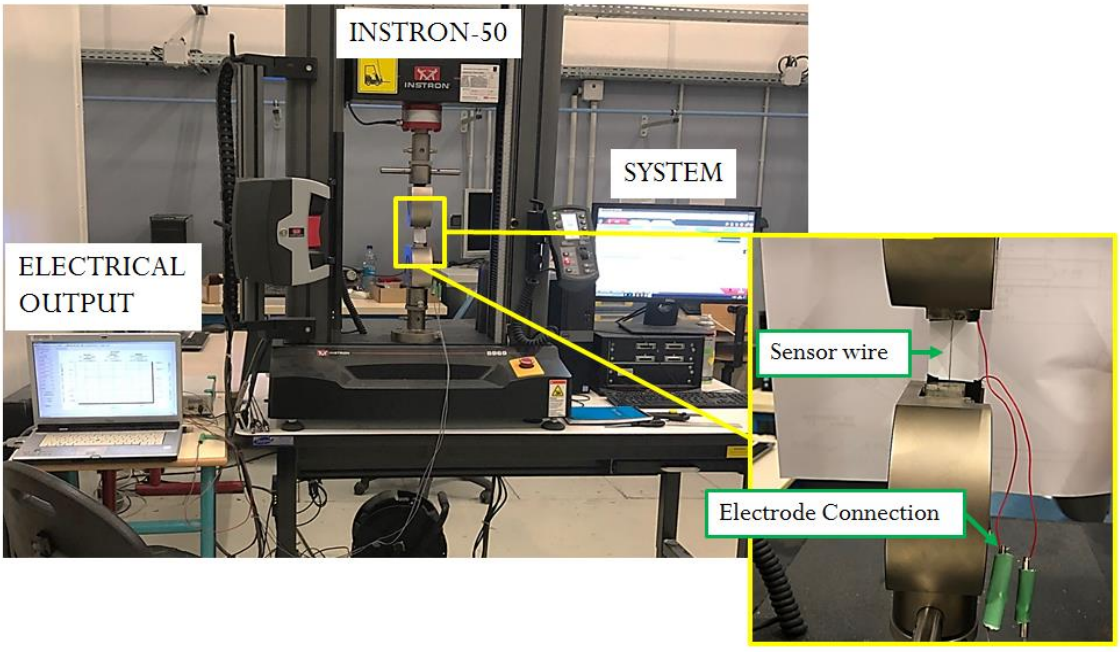

Figure 2-6: Experimental setup to test the sensitivity of the designed sensor systems.

2.3.2. Standalone sensor under thermal loading

All three sensor systems were tested under the thermal load as a standalone sensor of 72 mm in length using the CECASI oven apparatus, Figure 2-7. The CECASI oven system has a data acquisition system in which you can design the entire program of the thermal behavior including, temperature range, each step initial and final limit, and temperature change speed

from one step to another. A paper sheet was used to place all three samples in the machine to support and isolate them from any metallic part of the shelf. The temperature of the machine was controlled using the operating system and the data acquisition system was attached to each sensor using electrodes for real-time monitoring of change in resistance with the change in temperature. A K-type thermocouple was also placed within the CECASI to verify the temperature change within the chamber. Type K thermocouple is used in this experiment. Type K is the most common type of thermocouple. It's inexpensive, accurate, reliable, and has a wide temperature range. The type K is commonly found in nuclear applications because of its relative radiation hardness. The maximum continuous temperature is around 1,100°C. It has a temperature range of -200°C to 1250°C with an error sensitivity of 0.4-0.75%. CECASI was programmed to change the thermal environment while thermocouple and the sensor were attached to the separate data acquisition system (Spider 8 manufactured by HBM) which can simultaneously record the thermal change of the thermocouple and resistance change of the sensor. The thermocouple was attached to one input of the acquisition system and electrodes attached to the sensor were attached to the other input of the acquisition system. Two sets of tests were performed on each sensor system, the first test included increase in temperature up to 38°C starting from the room temperature i.e. 15°C and the second one included decrease in temperature up to -7°C starting from room temperature i.e 15°C. In each test, the temperature was changed by one degree with a rate of 0.2 °C/min, and at each degree, the temperature was kept constant for 10 mins. This step was carried out to understand the change in electrical resistance of the sensor systems in detail with defining the limit of precision.

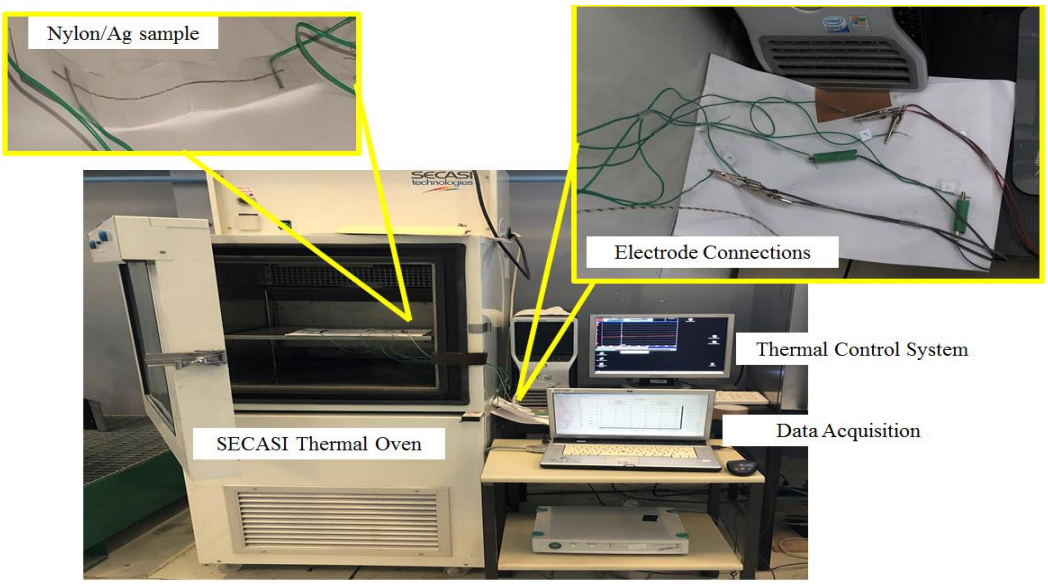

Figure 2-7: Experimental arrangement to examine the electrical behavior of all three designed sensors under thermal loading.

2.4. Results and discussions

2.4.1. Electromechanical Behavior of Each Sensor System

The resistance was changed as the strain was applied to specimens of each sensor system however, a large and sudden increase in resistance was observed as the failure started to initiate and ultimately, the resistance went to a maximum value at final fracture. The sensitivity of the fiber sensor was demonstrated by calculating the gauge factor (G.F). Gauge factor defines the sensitivity of the sensor by comparing the change in resistance of the sensor against the applied strain and equation (2-1) was used to calculate it.

$$\boldsymbol{G.F} = \frac{(\frac{\triangle \boldsymbol{R}}{\boldsymbol{R_o}})}{\boldsymbol{\varepsilon}} \qquad (2\text{-}1)$$

In this equation, $\triangle R/R_o$ is a key component in calculating the gauge factor of any strain sensor and represents the ratio of original or initial resistance of the sensor to the change in resistance to the applied strain ε generated because of the applied uniaxial stress along the strain gauge axis. This change in resistance against the applied strain represents the sensitivity of the strain sensor.

Specimens of each sensor system individually showed good electrical signal response during the mechanical loading of the specimen. The resistance was changing in each case with the

gradual increase of the applied strain and each specimen showed similar overall behavior. The global electrical response of each specimen showed a change of resistance with the increase of strain in the specimen and resistance reached maximum value during the crack propagation and final fracture.

Besides, during plastic strain deformation, each specimen showed a simultaneous persistent increase of resistance. This change in resistance during plastic strain deformation was because of the reason that resistance is directly proportional to the length of the specimen and any change or elongation can increase the electric resistance signal. This phenomenon can be understood by Equations (2-2) - (2-3). Equation (2-3) shows that the instantaneous length of the specimen during elongation will show an instantaneous increase in the resistance of the Nylon/Ag conductive fiber.

$$\alpha = 1/\rho \tag{2-2}$$

$$R = \rho L/A \tag{2-3}$$

Where α is Electrical Conductivity, ρ is Resistivity, L is Length, A is Cross-sectional Area, and R is Resistance

A. Sensor I: Nylon/ Ag Fiber sensor

The Nylon/Ag conductive fiber showed good mechanical response during loading and unloading within the elastic limit but for high strain applications, it was vital to investigate the overall mechanical performance of Nylon/Ag conductive fiber up to fracture to understand its parameters and limits for high strain monitoring. The average Young's modulus and yield strength of all the tested samples were about 4269.27 MPa and 21.727 MPa on average respectively, Figure 2-8 (a). Overall, the mechanical behavior of Nylon/Ag conductive fiber is shown in Fig. 2-8 (b). Moreover, each specimen showed large plastic deformation before damage initiation which indicated the following interpretations:

- First was that even after the application of metal coating the Nylon-6 polymer yarn did not show any compromise of its flexibility. The decided coating thickness was appropriate for flexible uniform coating with minimum chance of any gaps or defects.
- The second was that this large deformation before damage initiation showed that this conductive fiber could be used for high strain application without any compromise on its mechanical performance.

- The third was that the exponential increase in the strength during plastic deformation was because of the geometric parameters of yarn such as the number of filaments or twists in a single yarn.

Furthermore, the damage initiation and damage propagation in the Nylon/Ag conductive fiber indicated that the damage was not sudden but depended on the gradual breakage of each filament in the yarn fiber. In addition, mechanical properties consisting of tensile strength, Young's modulus and fracture strain are given in Table 2-1.

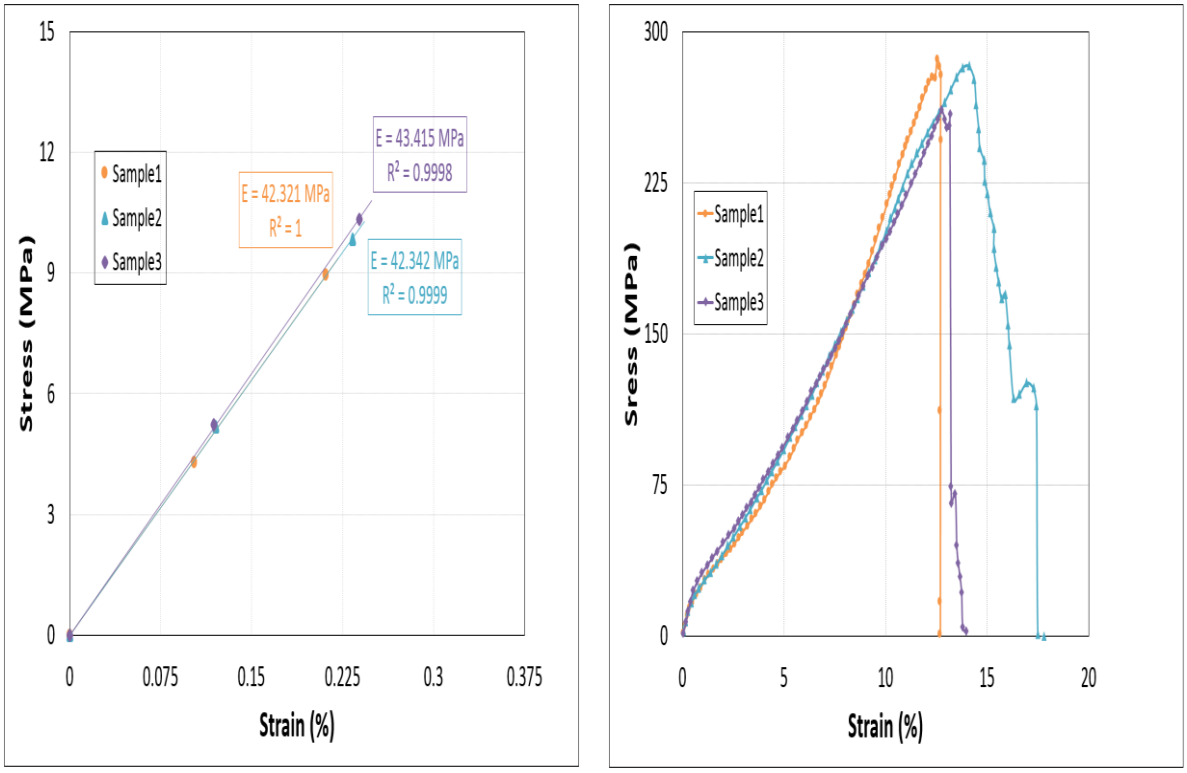

(a) *(b)*

Figure 2-8: Mechanical behavior of the Nylon/Ag conductive fiber.

Table 2-2: Mechanical characteristics of the Nylon/Ag conductive fiber specimens subjected to tensile loading

Properties	**Elastic Modulus**	**Fracture Strain**	**Yield Strength**
Unit	MPa	%	MPa
Sample 1	4232.10	12.69	21.24
Sample2	4234.20	13.21	21.12
Sample3	4341.50	15.71	22.73
Average	4269.27	13.87	21.70

Standard deviation	62.5647	1.6146	0.8969

Fractured specimens of Nylon/Ag conductive fiber were also studied using SEM and two distinct features and morphologies were observed. Almost every filament of the Nylon/Ag conductive fiber showed a clean ductile fracture with both coating and core material, Fig. 2-9 (a)-(b). In addition, some filaments also showed a pullout or flaking off of the coating during the tensile strain. This pullout or flaking off of the coating was because of the strain deformation of the core material during elongation and it was more prominent near the ductile failure of the filaments, Fig. 2-9 (c)-(d). This breaking off of the conductive layer during the strain deformation of the core material resulted in the rise of resistance and it was noticeable during the large plastic deformation or damage initiation and propagation just before the final failure of the Nylon/Ag conductive fiber. This phenomenon was the actual concept behind the real-time strain monitoring performance of the Nylon/Ag conductive fiber.

The resistance was changed gradually as the strain was applied to the fiber sensor. This progressive behavior of the fiber sensor validated the good correlation between the electrical and mechanical responses of the sensor, Figure 2-10 (a). The results were very encouraging and tracking the resistance change of this conductive yarn as a function of increasing load seemed to be correlating very well.

The gauge factor of this flexible fiber sensor was found to be in the range of 21-25 within the elastic limit, Figure 2-10 (b). This showed that the Nylon/Ag fiber sensor had good sensitivity and could be used for real-time damage detection applications.

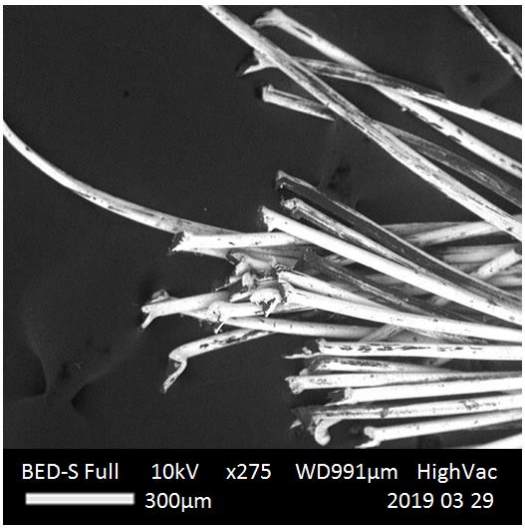

(a)

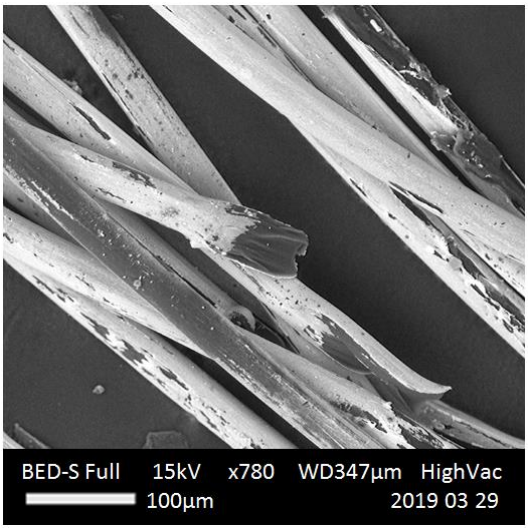

(b)

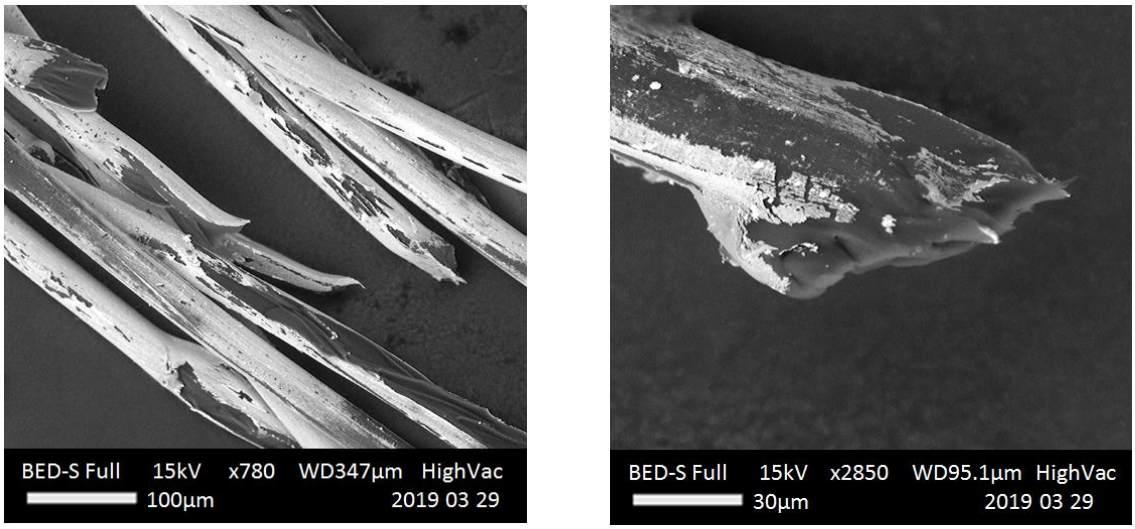

(c) *(d)*

Figure 2-9: SEM characterization of the fractured specimen. (a)-(c) show fractured fibers in each specimen with similar morphologies. (d) shows a single fractured filament of the coated yarn at 30 µm zoom presenting both ductile fracture and pull-out of the coating during large deformation.

In addition, each specimen also showed good electromechanical correlation individually from the elastic region up to the final fracture. The significant correlation of electromechanical response was observed within the plastic strain deformation by all three specimens, Figure 2-11. This showed that the change in resistance became more prominent at high strain deformation and this behavior was observed in each test confirming the reproducibility of the response. Therefore, these results confirmed the ability of Nylon/Ag conductive fiber for real-time monitoring in high strain application.

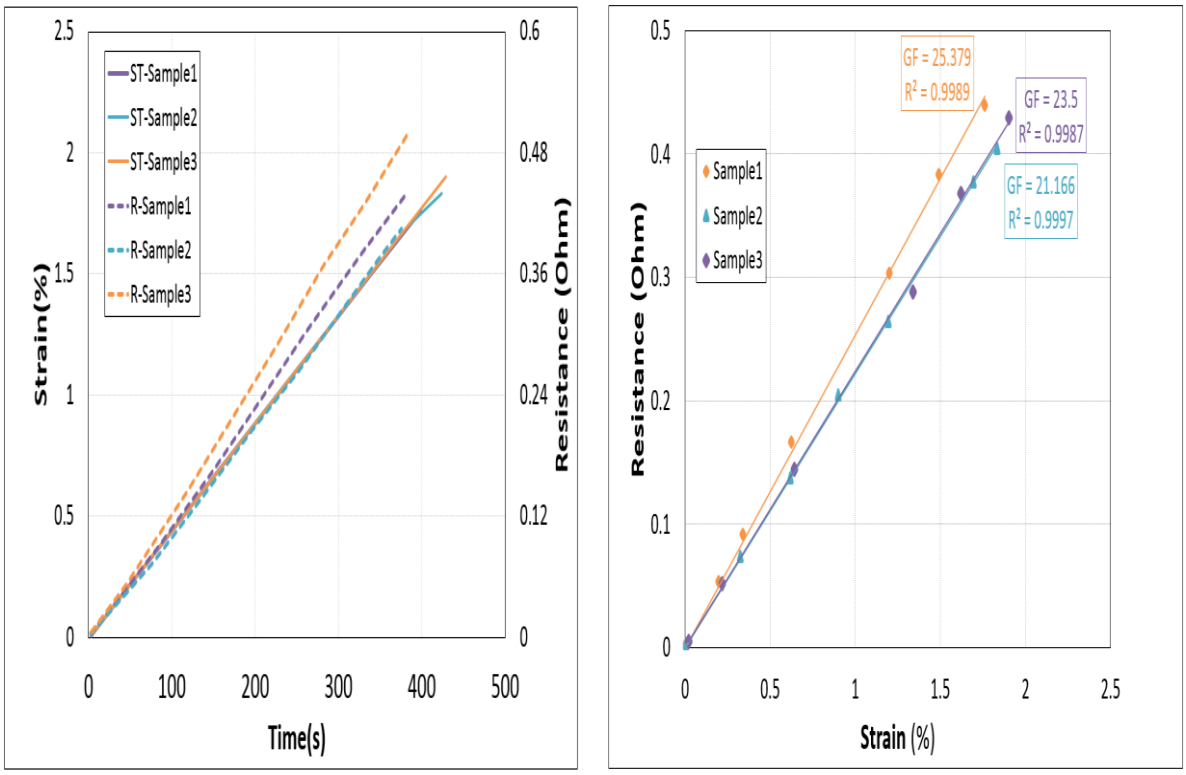

(a) *(b)*

Figure 2-10: Experimental calculation of the sensitivity of the Nylon/Ag Fiber sensor

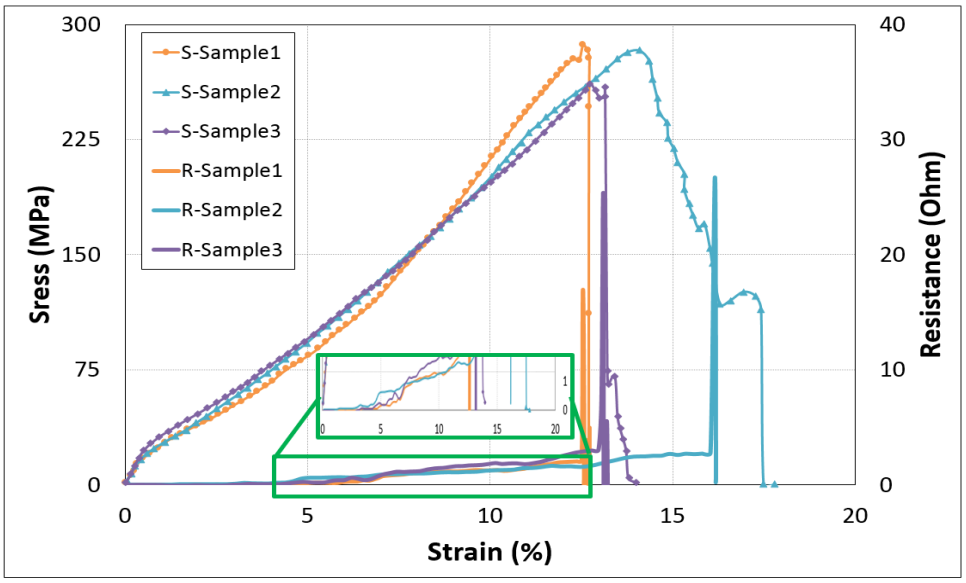

Figure 2-11: The electromechanical response of each Nylon/Ag fiber sensor specimen

B. Sensor II: CM sensor

The CM sensor displayed good mechanical behavior and Young's modulus and yield strength of all the examined CM sensor samples were about 1118.43 MPa and 1.06 MPa on average,

respectively, Figure 2-12 (a). Table 2-2 summarizes the mechanical behavior of CM sensor, consisting of yield's strength, Young's modulus, and fracture strain. In overall mechanical behavior, each sensor sample exhibited nonlinear deformation before final fracture which specified that the membrane was quite flexible and might be applicable in high strain applications without compromising its mechanical performance, Figure 2-12 (b). When the membrane was elongated, the dense network of CNTs in the CM started to overcome the Van der Waals forces between the different layers of CNTs network because of the shear forces between them and it showed nonlinear deformation before the initiation of its breakage. Furthermore, it was observed that after plastic deformation, the damage initiation and propagation were not sudden, and the membrane was fractured gradually.

The resistance of the CM sensor was increased with the applied tensile strain which verified good correlation among its electromechanical response, Figure 2-13 (a). The GF of this flexible CM was calculated to be inside 8-8.25 range within the elastic limit, Figure 2-13 (b). It was confirmed that from these results that the CM sensor had good strain sensitivity range and might be used for instantaneous strain monitoring of structures.

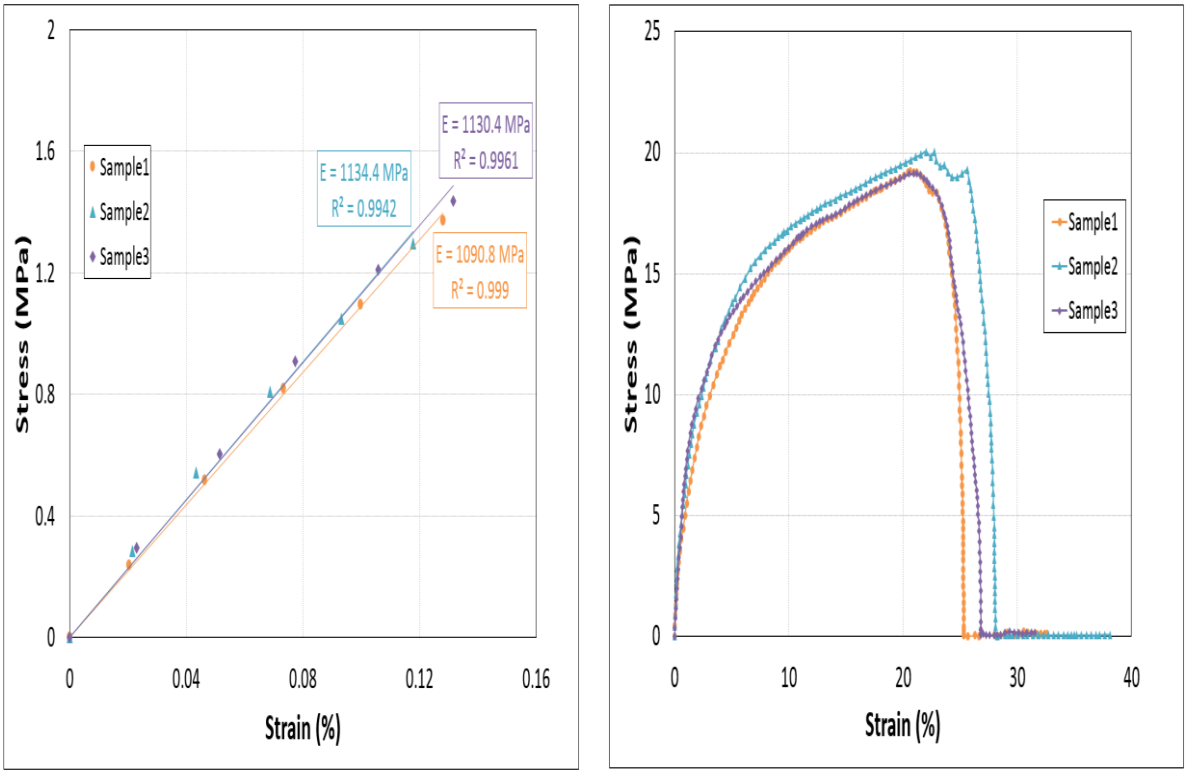

(a) Elastic Modulus

(b)Overall mechanical behavior

Figure 2-12: Mechanical performance of CM sensor.

Table 2-3: Mechanical properties of CM sensor under tensile loading

	Elastic Modulus (MPa)	Fracture Strain (%)	Yield Strength (MPa)
Sample 1	1090.50	25.40	1.60
Sample2	1134.40	28.08	1.58
Sample3	1130.40	26.80	1.63
Average	1118.43	26.76	1.60
Standard deviation	24.2735	1.3419	0.0256

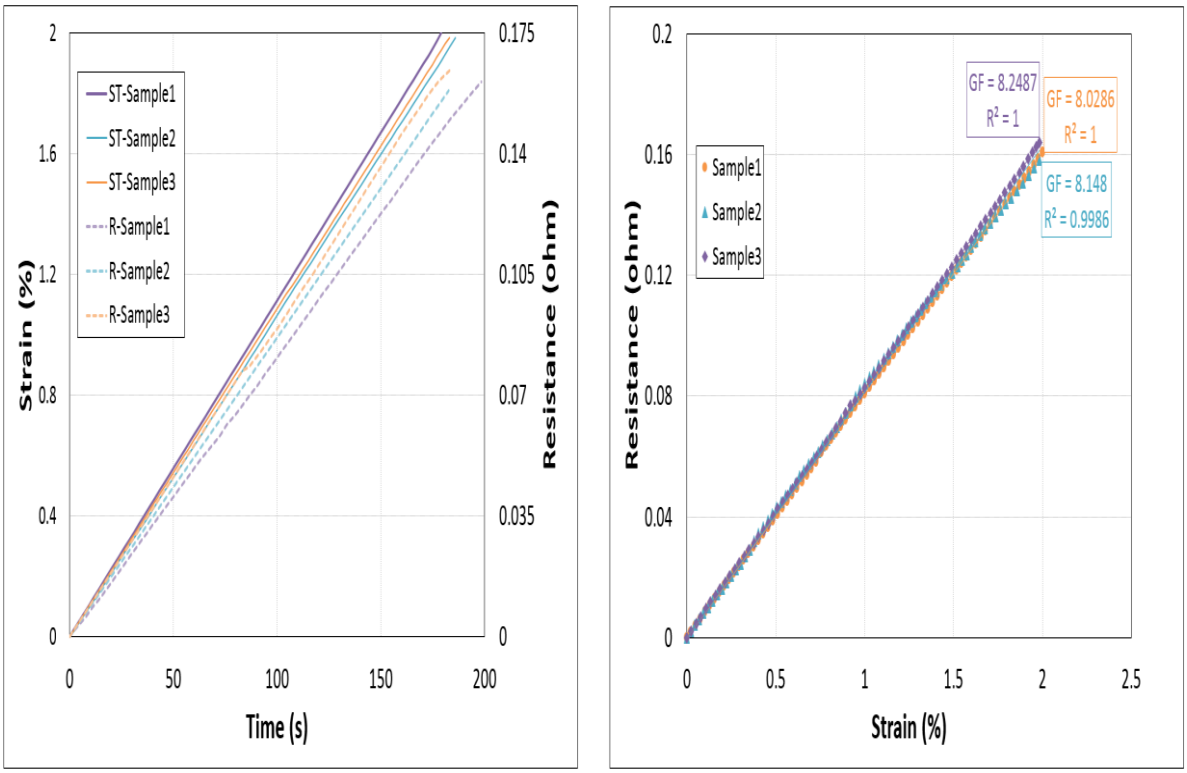

(a) Strain and resistance change

(b) GF calculation

Figure 2-13: Experimental behavior and calculation of the strain sensitivity of the CM membrane sensor.

Each specimen of CM sensor presented good electrical behavior throughout the applied tensile strain, resistance changed gradually, and all samples displayed similar overall performance. The overall behavior of the CM sensor presented that, during elastic-plastic behavior the change in resistance was linear, and when the mechanical behavior of the sensor started to degrade there

was a sudden increase in the resistance which reached maximum value upon fracture of the membrane, Figure 2-14.

In addition, it was observed in all specimens that the increase in resistance became more prominent during large plastic deformation which confirmed its ability to use for real-time strain monitoring application during high strain deformation of structures.

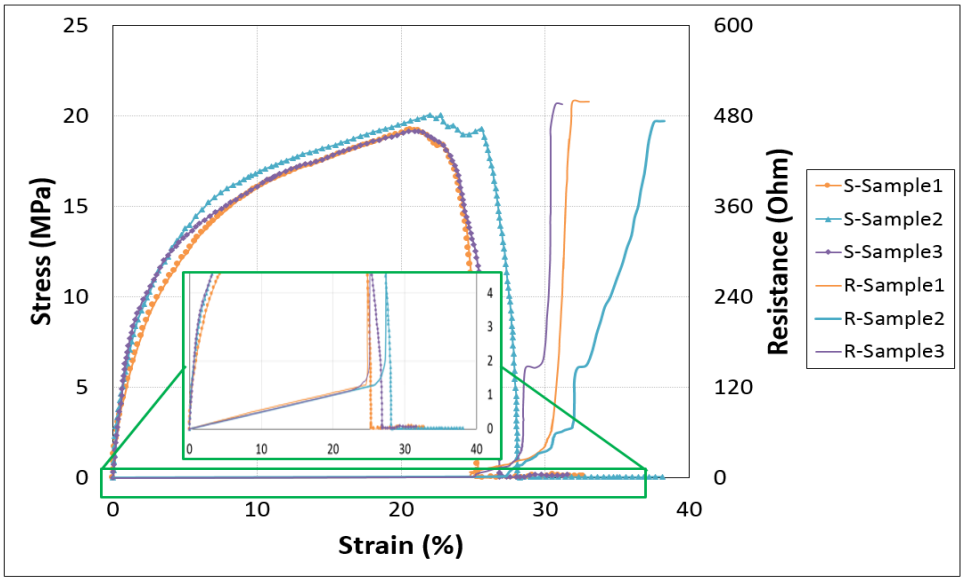

Figure 2-14: Overall electromechanical response of CM sensor specimens.

C. Sensor III: CF sensor

The CF sensor displayed good mechanical behavior and the Young's modulus and yield strength of all the examined CF sensor samples were about 94.53 MPa and 1.73 MPa on average during the standalone test, respectively, Figure 2-15 (a). Table 2-3 summarizes the mechanical behavior of the CF sensor, consisting of yield's strength, Young's modulus, and fracture strain. In overall mechanical behavior each sensor sample exhibited linear elastic deformation before the start of final fracture because of the high stiffness and CF sensor did not show any plastic deformation however, reduction in mechanical behavior was gradual due to the consecutive breakage of the filaments. Even though CF sensor showed high stiffness, but it was quite flexible because carbon filaments were held together loosely together and were combined only in the both ends were electrodes were attached. Therefore, these sensors could be used in high strain applications without compromising their mechanical performance, Figure 2-15 (b).

Furthermore, it was observed that the damage initiation and propagation were not sudden, and the membrane was fractured gradually with the breakage of each filament.

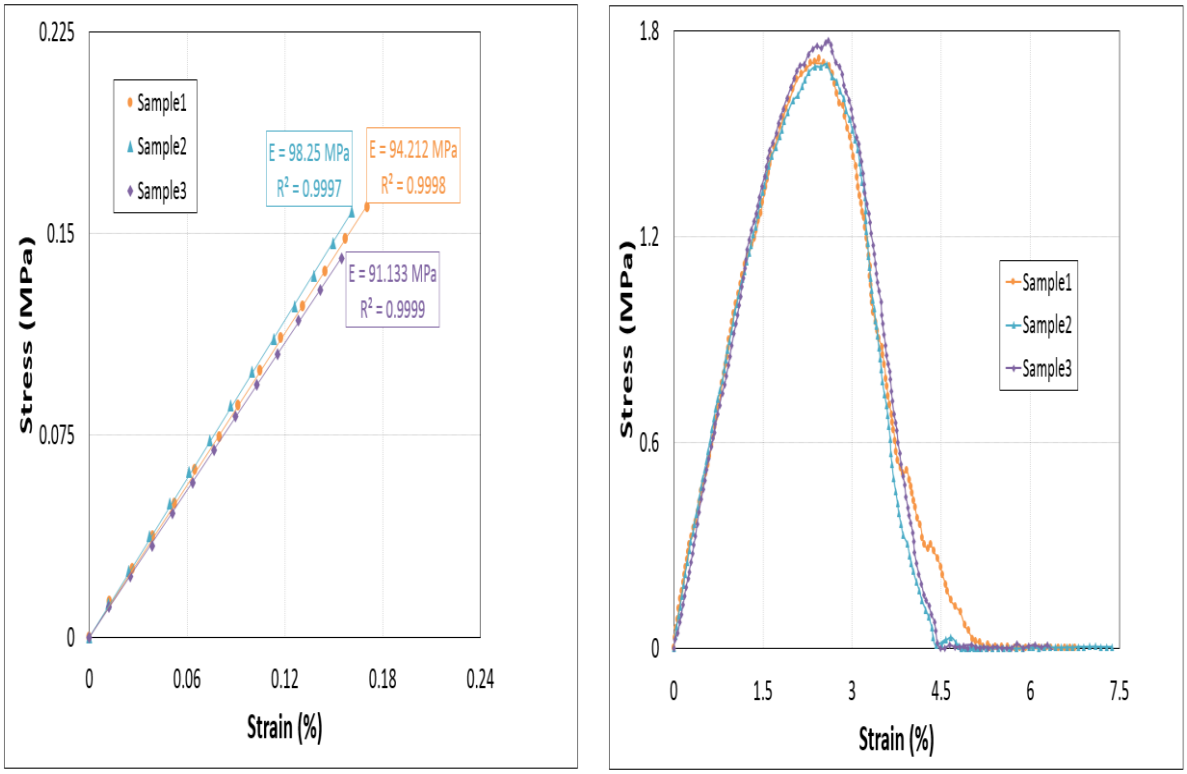

(a) Elastic Modulus (b) Overall mechanical behavior

Figure 2-15: Mechanical performance of CF sensor.

Table 2-4: Mechanical properties of CF sensor under tensile loading

	Elastic Modulus (MPa)	**Fracture Strain (%)**	**Yield Strength (MPa)**
Sample 1	94.212	5.16	1.72
Sample 2	98.247	4.44	1.70
Sample 3	91.133	4.49	1.77
Average	94.53	4.46	1.73
Standard deviation	3.5677	0.0354	0.0360

The resistance of the CF sensor was increased with the applied tensile strain which verified good correlation among its electromechanical response, Figure 2-16 (a). The GF of this sensor was calculated to be inside 10.2-10.8 range within the elastic limit, Figure 2-16 (b). It was

confirmed that from these results the CF sensor had good strain sensitivity range and might be used for instantaneous strain monitoring of structures.

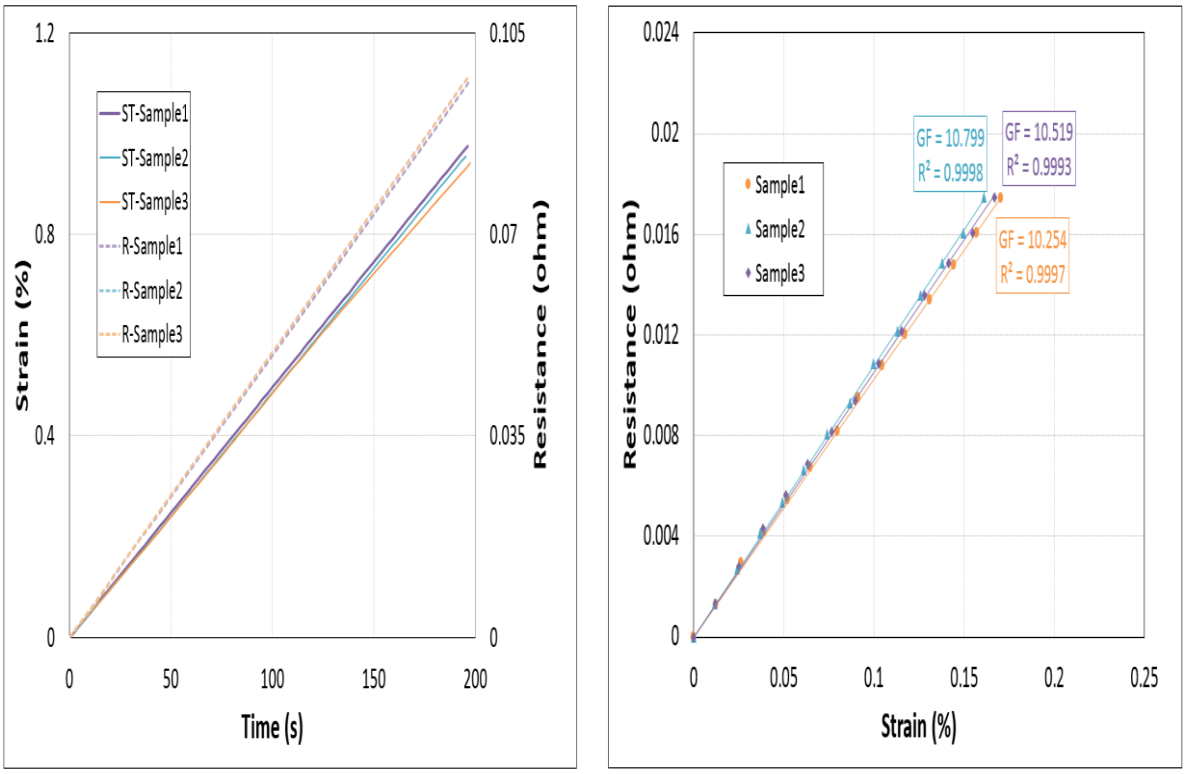

(a) Strain and resistance change

(b) GF calculation

Figure 2-16: Experimental behavior and calculation of the strain sensitivity of the CF membrane sensor

Each specimen of the CF sensor presented good electrical behavior throughout the applied tensile strain, resistance changed gradually, and all samples displayed similar overall performance. The overall behavior of the CF sensor presented that, during elastic behavior the change in resistance was linear, and when the mechanical behavior of the sensor started to degrade there was a sudden increase in the resistance which reached maximum value upon fracture of the membrane, Figure 2-17. In addition, the sudden increase in the resistance of the sensor with the degradation of the mechanical behavior was progressing gradually to the maximum value because the carbon filaments in the sensor were breaking individual with the elongation, and with each breakage, the resistance showed variation. It was observed that when the strength of the CF sensor began to drop after achieving the peak value, its resistance started to increase linearly which confirmed good sensitivity of the sensor to detect damage initiation. All samples showed the same maximum stress and demonstrated the start of damage initiation at almost the same time. The degradation of stress in each sample showed the one by one failure

of their filaments and this evolution or damage was slightly in comparison. This slight difference of failure was also observed in the evolution of respective electrical resistance of each sample and each CF sensor showed saturation of resistance to a maximum value when there were complete fracture and stress reached zero value. This confirmed its ability to use for real-time strain monitoring applications during high strain deformation of structures because the sensor showed good electrical conductance until all the filaments in it were broken.

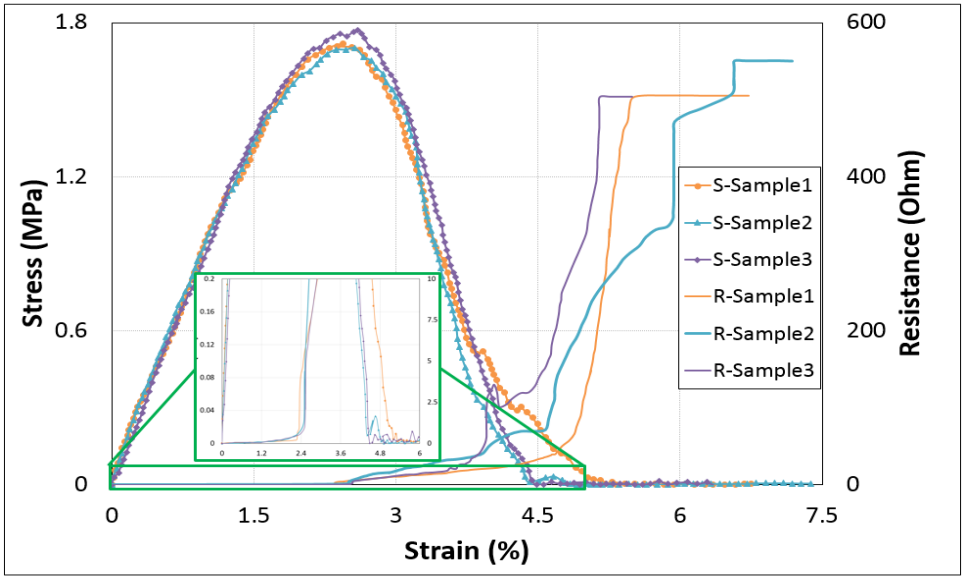

Figure 2-17: Overall electromechanical response of CF sensor.

2.4.2. Electrothermal Behavior of Each Sensor System

A standard two probe test was performed on three different samples between the temperature ranges of -7°C to 38°C in two sets in an oven at atmospheric pressure. Data acquisition (Spider 8 manufactured by HBM) was used to moni/tor the change in resistance of each specimen of all three sensor systems and the thermocouple. A constant current of 4 mA was applied to all three samples which were randomly cut from the manufactured specimen. The applied current was kept low to prevent the self-heating of the samples and effect their electro-thermal behavior. Moreover, As described earlier, the thermal load program was designed to halt the temperature change at each degree for 10 mins and error bars show the mean distribution of these data points at each degree. Overall curve profile showed the effect of temperature on the conductivity of the sensor.

A. Sensor I: Nylon/ Ag Fiber sensor

All three samples showed an increase in resistance with an increase of temperature, Figure 2-18 (a). Moreover, each data point is provided by the error bar demonstrating the behavior of the Nylon/Ag conductive fiber at each temperature change. Overall curve profile showed a nonlinear parabolic increase in the resistance with the increase in temperature. All three samples showed good reproducibility in results in both cases and small error bars ensured the precision of the readings at each change of degree. Generally, it was expected to see an opposite response with the decrease in temperature but, Nylon/Ag conductive fiber also showed a nonlinear parabolic increase in resistance with decreasing the temperature up to 0°C, Figure 2-18 (b). From 0°C to -7°C the resistance was increasing with the decrease in temperature, but the intensity of the change was slightly more than the change in resistance of the sample during a positive change of temperature. Moreover, the resistance change of Nylon/Ag conductive fiber with respect to the change in temperature could be because of the thermal expansion behavior, however, resistance change because of the decrease in temperature could be resulted because of the mismatched two materials i.e. Nylon and Ag coating with different thermal expansion coefficients. Though, it should be kept in mind that the Nylon/Ag conductive fiber detected the change in the surrounding temperature by the change in its electrical behavior which could be used to detect energy release during damage failure which always results in an increase in temperature.

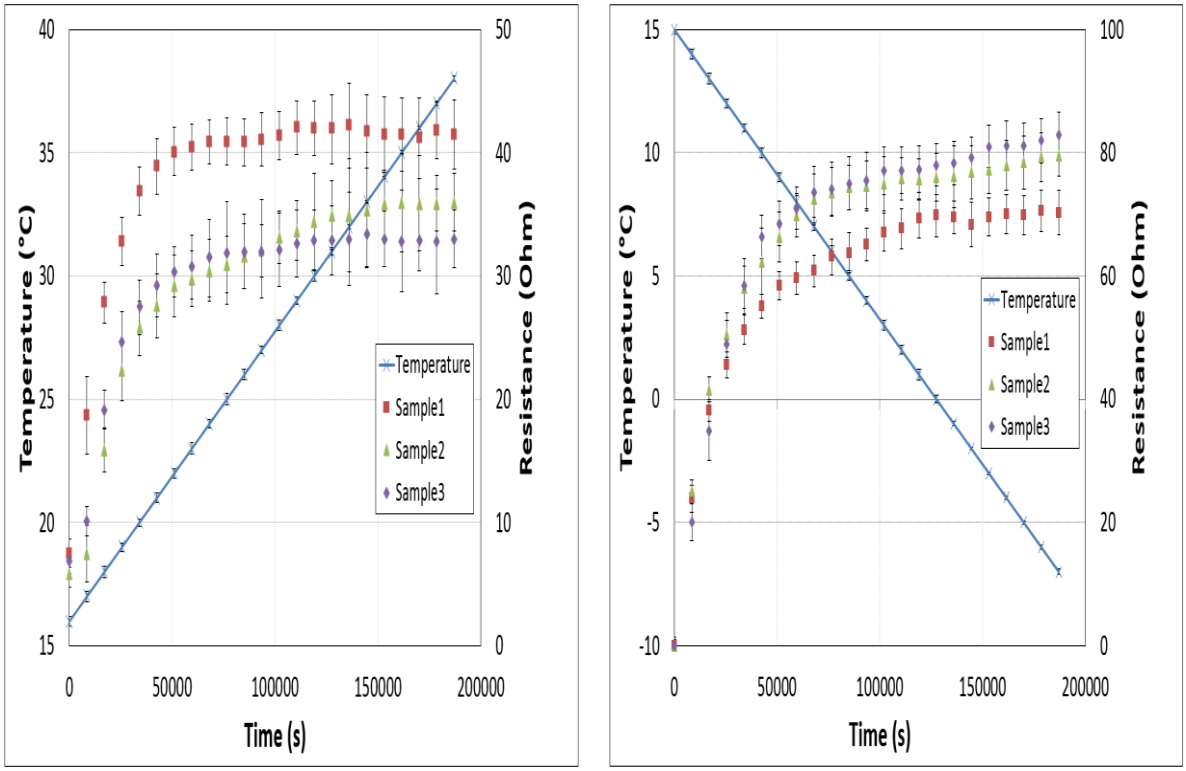

(a) Test performed with an increase in temperature *(b) Test performed with a decrease in temperature*

Figure 2-18: Electrical behavior of Nylon/Ag conductive fiber during thermal loading to detect thermal change.

To further explain the behavior of Nylon/Ag conductive fiber under thermal loading, non-linear equations were found to accurately describe the relation of the change in resistance with the change of temperature. These empirical relations were derived from the average behavior of all three samples which showed a nonlinear change in the resistance (Ohm) with respect to the temperature (°C), Figure 2-19. Two equations were derived, one during the positive change in temperature $R(T_P)$ and one during the negative change in temperature $R(T_N)$. These equations are presented as follow:

$$R(T_P) = 0.0115T^3 - 1.0458T^2 + 31.264T - 271.78 \quad (2\text{-}4)$$

$$R^2 = 0.9788$$

$$R(T_N) = -0.0256T^3 + 0.0588T^2 + 0.5211T + 73.388 \quad (2\text{-}5)$$

$$R^2 = 0.9759$$

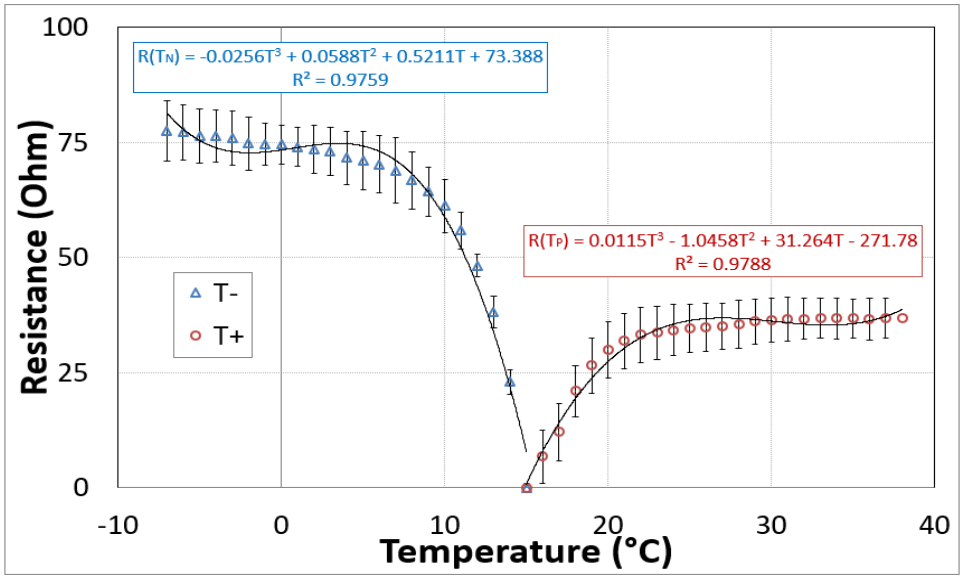

Figure 2-19: Calculation of empirical relations to describe the nonlinear change in resistance with respect to temperature.

Both equations represented similar empirical relations with an accuracy of 98% which further verified the behavior of sensors for the quantification of damage. The relation of resistance with temperature could be generalized as follow:

$$\boldsymbol{R(t) = aT^3 + bT^2 + cT^1 + d} \qquad (2\text{-}6)$$

where *a, b, c, and d* are empirical constants.

B. Sensor II: CM sensor

All three samples showed a negative change in resistance with an increase of temperature while a positive change in resistance with a decrease in resistance, Figure 2-20. Moreover, it can be seen that each data point is provided by the error bar demonstrating the behavior of the CM sensor at each temperature change. Overall curve profile showed the effect of temperature on the conductivity of the sensor. It showed minute stability in the electrical behavior and then there was a linear increase/decrease in the two cases. All three samples showed good reproducibility in results in both cases and small error bars ensured the precision of the readings at each change of degree. Generally, the resistance change of MWCNTs bundles [74]or film [75] with respect to the change in temperature shows non-metallic behavior i.e. decrease with increase in temperature and vice versa while crossover temperature has been documented for bucky paper [76]. Moreover, in the case of SWCNTs a crossover thermal range was observed

35K (-238.15 °C) for a single well-aligned cord to 250 K (-23.15°C) for a twisted rope in the form of a yarn [77]. Therefore, it is difficult to have a consistent scenario for CNTs which also show an increase in resistance with temperature below 0°C [74], [78]. Variable range hopping (VRH) conduction and thermal fluctuation-induced tunneling (FIT) models have been used to explain the nonmetallic electrothermal behavior of systems such as the network of conductive filaments with minute insulating gaps to define random heterogeneous systems [79], [80]. For example, considering the CM sensor as a heterogeneous disordered system, FIT model described that the tunneling barriers exist because of the intertubular contacts between the network of CNTs explaining the electrothermal behavior because on a membrane level the tunneling effect of CNTs become more dominant over the individual conductance of a CNT.

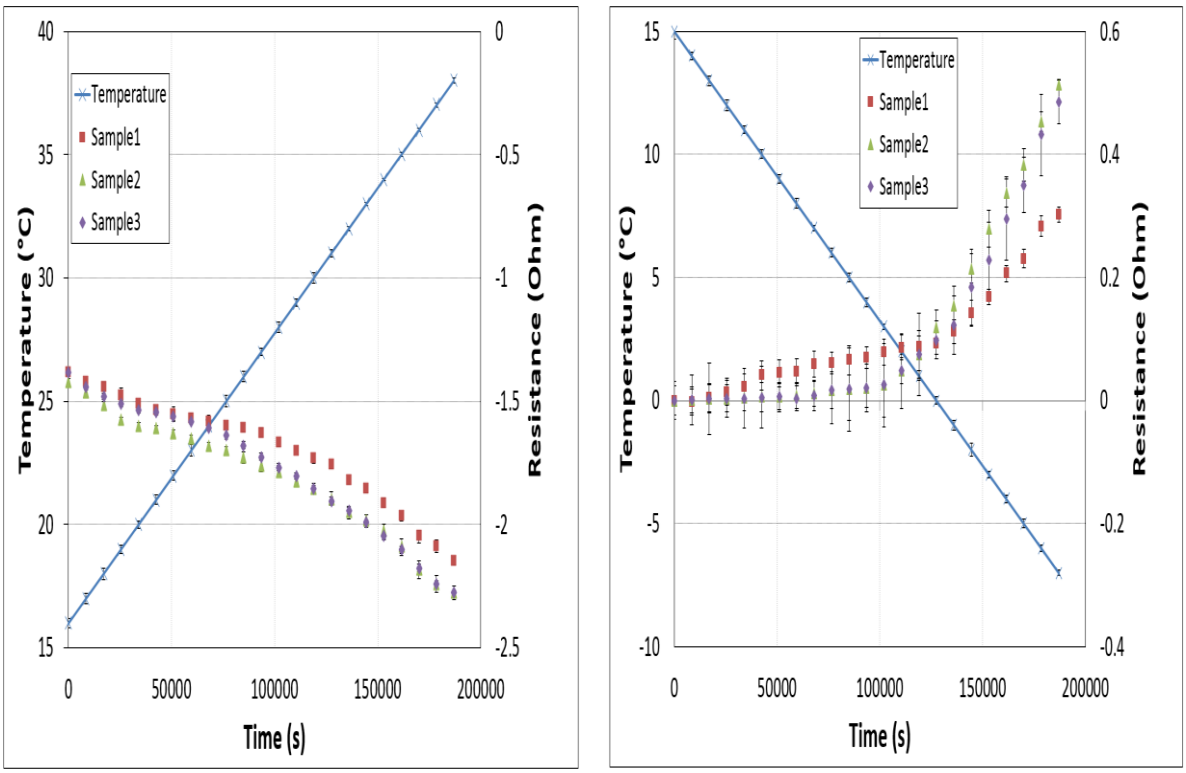

(a) Test performed with an increase in temperature

(b) Test performed with a decrease in temperature

Figure 2-20: Electrical behavior of CM during thermal loading to detect thermal change.

To further explain the behavior of CM sensor under thermal loading, non-linear equations were found to accurately describe the relation of the change in resistance with the change of temperature. These empirical relations were derived from the average behavior of all three samples which showed a nonlinear change in the resistance (Ohm) with respect to the temperature (°C), Figure 2-21. Two equations were derived, one during the positive change in

temperature $R(T_P)$ and one during the negative change in temperature $R(T_N)$. These equations are presented as follow:

$$\boldsymbol{R(T_P) = -7x10^{-5}T^3 + 0.0045T^2 - 0.1204T + 1.0152} \quad (2\text{-}7)$$

$$\mathbf{R^2 = 0.9979}$$

$$\boldsymbol{R(T_N) = -8x10^{-5}T^3 + 0.0025T^2 - 0.0267T + 0.1108} \quad (2\text{-}8)$$

$$\mathbf{R^2 = 0.9966}$$

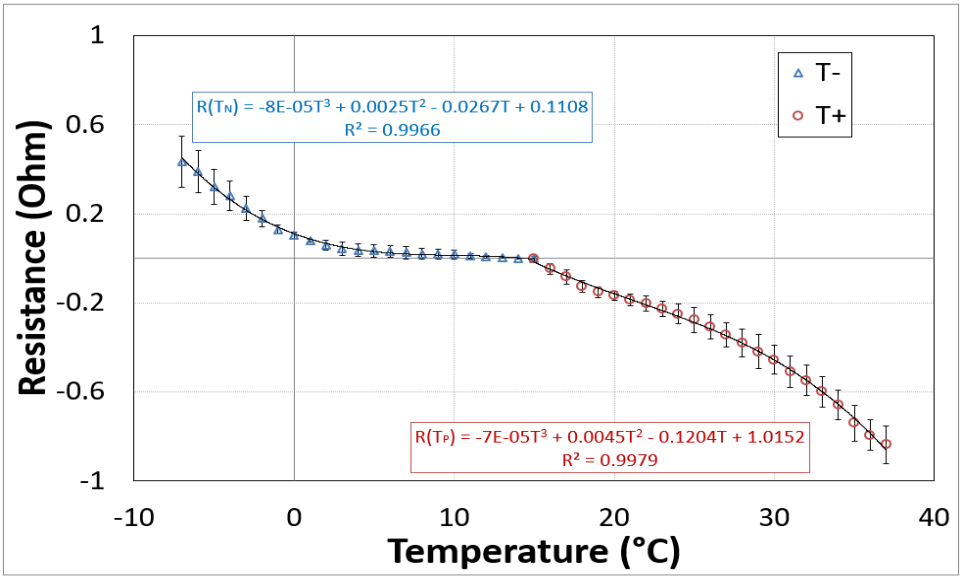

Figure 2-21: Calculation of empirical relations to describe the nonlinear change in resistance with respect to temperature.

Both equations represented similar empirical relations with an accuracy of 99.95% which further verified the behavior of sensors for the quantification of damage. The relation of resistance with time could be generalized as follow:

$$\boldsymbol{R(t) = aT^3 + bT^2 + cT^1 + d} \quad (2\text{-}9)$$

where *a, b, c, and d* are empirical constants.

C. Sensor III: CF sensor

All three samples showed an increase in resistance with an increase of temperature, Figure 2-22. Moreover, each data point is provided by the error bar demonstrating the behavior of the CF sensor at each temperature change. Overall curve profile showed the effect of temperature on the conductivity of the sensor. It showed a nonlinear parabolic increase in the resistance with

the increase in temperature. All three samples showed good reproducibility in results in both cases and small error bars ensured the precision of the readings at each change of degree. Generally, it was expected to see the opposite response with the decrease in temperature but, the CF sensor showed an almost linear increase in resistance with decreasing the temperature up to 0°C, Figure 2-22 (b). From 0°C to -7°C the resistance was increasing with the decrease in temperature, but the slope of the curve was reduced. Moreover, it was observed that there was a minute decrease in the resistance of the CF sensor with a decrease in temperature and it started to increase. This behavior of sensor could be because of the fact the all the filaments of the CF were combined only at the ends where the electrodes were attached and were freely aligned in between which could be the reason behind the unique response during the decrease in temperature. Moreover, the resistance change of CF sensor with respect to the change in temperature could be because of the thermal expansion behavior, however, resistance change because of the decrease in temperature could be resulted in a loose alignment of the filaments in the CF sensor and decrease in electrical contact points during possible compression of the sensor [82]–[85]. Though, it should be kept in mind that the CF sensor detected the change in the surrounding temperature by the change in its electrical behavior which could be used to detect energy release during damage failure which always results in an increase in temperature.

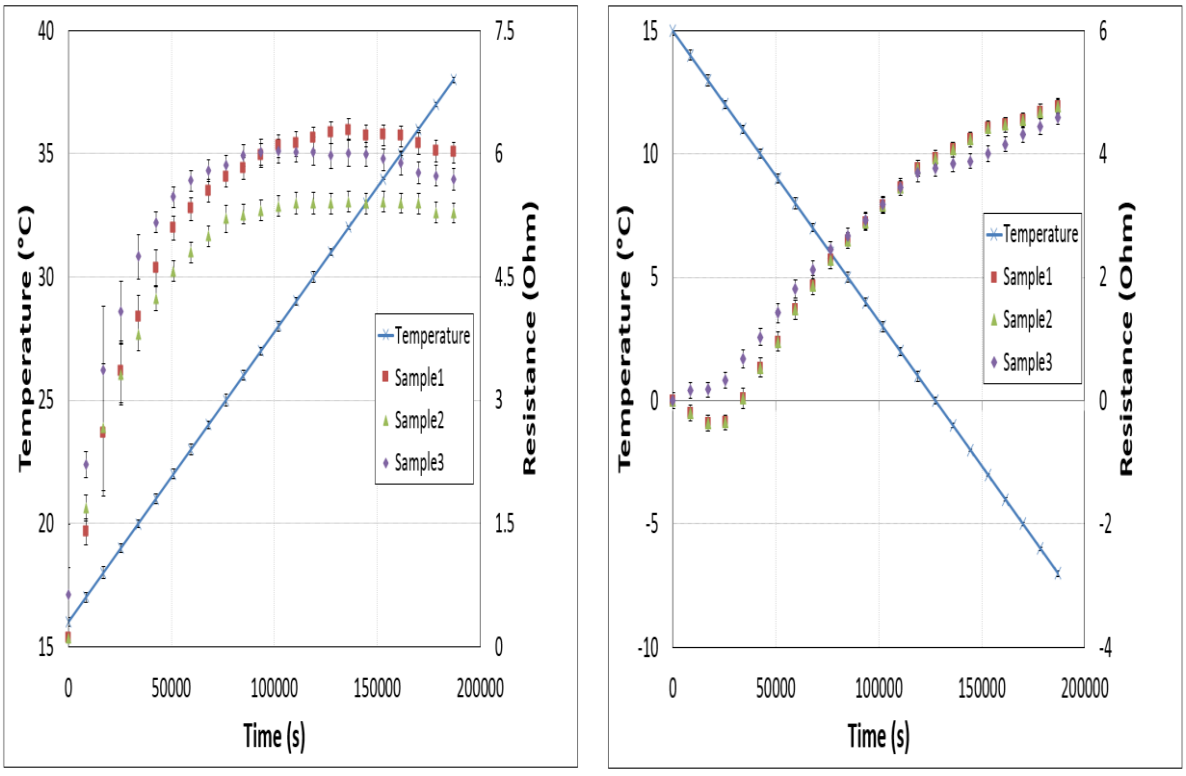

(a) Test performed with an increase in temperature *(b) Test performed with a decrease in temperature*

Figure 2-22: Electrical behavior of CM during thermal loading to detect thermal change.

To further explain the behavior of the CF sensor under thermal loading, non-linear equations were found to accurately describe the relation of the change in resistance with the change of temperature. These empirical relations were derived from the average behavior of all three samples which showed a nonlinear change in the resistance (Ohm) with respect to the temperature (°C), Figure 2-23. Two equations were derived, one during the positive change in temperature $R(T_P)$ and one during the negative change in temperature $R(T_N)$. These equations are presented as follow:

$$\boldsymbol{R(T_P) = \ 0.0014T^3 - \ 0.1378T^2 + \ 4.3424T - 39.225} \qquad \text{(2-10)}$$

$$\boldsymbol{R^2 \ = \ 0.9907}$$

$$\boldsymbol{R(T_N) = \ 0.0008T^3 - 0.0158T^2 \ - 0.2308T + 3.9059} \qquad \text{(2-11)}$$

$$\boldsymbol{R^2 \ = \ 0.9889}$$

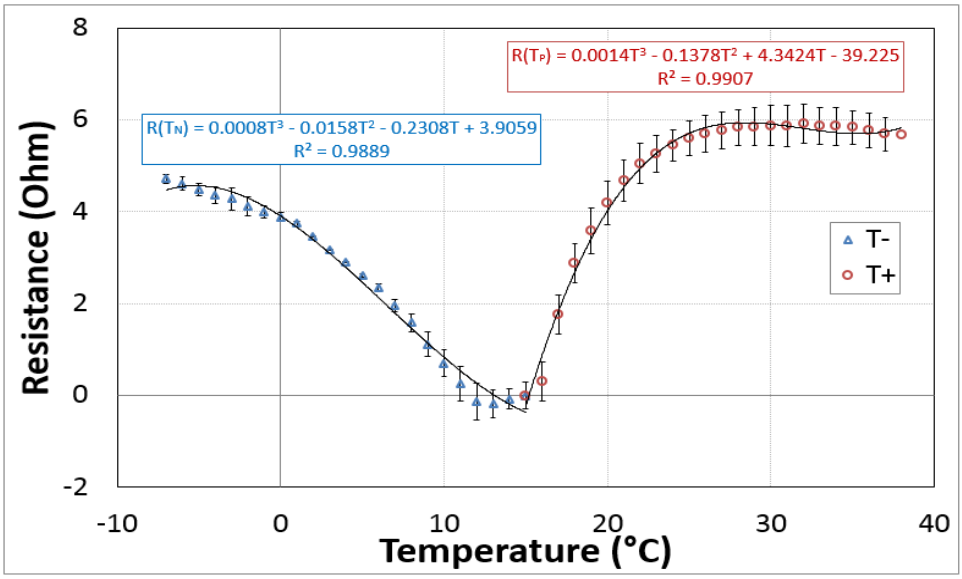

Figure 2-23: Calculation of empirical relations to describe the nonlinear change in resistance with respect to temperature.

Both equations represented similar empirical relations with an accuracy of 98% which further verified the behavior of sensors for the quantification of damage. The relation of resistance with time could be generalized as follow:

$$\boldsymbol{R(t) = \ aT^3 + \ bT^2 + \ cT^1 + \ d} \qquad \text{(2-12)}$$

where *a, b, c, and d* are empirical constants.

The empirical relations representing the electrothermal behavior of each sensor system can be further related to change in length or strain induced in the sample and we can use the following relation:

$$\boldsymbol{GF} = \frac{\boldsymbol{\Delta R/R}}{\boldsymbol{\varepsilon}} \tag{2-13}$$

$$\boldsymbol{R'} = \frac{\boldsymbol{\Delta R}}{\boldsymbol{R}}$$

$$\boldsymbol{\varepsilon} = \boldsymbol{R'} * (\frac{\boldsymbol{1}}{\boldsymbol{GF}}) \tag{2-14}$$

where *GF* is the gauge factor constant of the sensor, *R* is the original resistance of the sensor, and ΔR is the change in the resistance of the sensor with the applied strain ε.

By substituting equation (2-12) in equation (2-14), the change of resistance against temperature can give us a change in strain with respect to temperature.

$$\boldsymbol{\varepsilon(T)} = \boldsymbol{R'(T)} * (\frac{\boldsymbol{1}}{\boldsymbol{GF}}) \tag{2-15}$$

This equation can quantify the damage or strain induced in a structure because of thermal heating or change of environmental conditions. Moreover, it can also be used to monitor the additional damage or strain rate induced in the specimen by the amount of energy released during the deformation or damage process. This can be sued to monitor damage in different structural materials in real-time.

2.5. Comparison of three sensor systems

In this section, the performance of all three sensor systems is compared based on different criteria to understand and select a better system for structural health monitoring of composite structures. Individually, each sensor system showed distinct and interesting performance during both electromechanical and electrothermal behavior however, their comparison will facilitate understanding their performance under different conditions. A comparison of mechanical performance showed that Nylon/Ag fiber sensor showed better stiffness, strength, and deformation behavior as a standalone sensor in comparison with the other two systems, Figure 2-24 (a)-(c). This comparison of mechanical performance is vital to ensure the good structural integrity of the detection system for the ability to use for real-time strain monitoring applications during high strain deformation of structures during quasi-static or dynamic loadings. Nylon/Ag fiber sensor has higher yield strength and young's modulus than the other

two systems because of its twisted yarn structure however, the total strain of the CM sensor was the highest. Even though the CM showed more plastic deformation but its strain sensitivity was the lowest among all three sensor systems which showed that change of resistance with respect to the applied strain was less effective, Figure 2-24 (d). This could be because CM sensor consisted of a dense network of CNTs held together by the Van der Waals forces and even with the larger strain the network of CNTs had good interlinks between them to facilitate the flow of current. Nylon/Ag fiber sensor showed better strain sensitivity among all three sensor systems. Moreover, change of electrical resistance was more sensitive to thermal change during the case of the Nylon/Ag fiber sensor with an increase in resistance during both increase and decrease of resistance, Figure 2-24 (e). CF sensor showed similar behavior as Nylon/Ag fiber sensor however, CM sensor showed an increase in resistance during drop in temperature and a decrease in resistance during the increase in temperature. The comparison of electrothermal behavior showed that CM sensor not only detected the change in environmental temperature as the other two systems but also distinguish the behavior of temperature change.

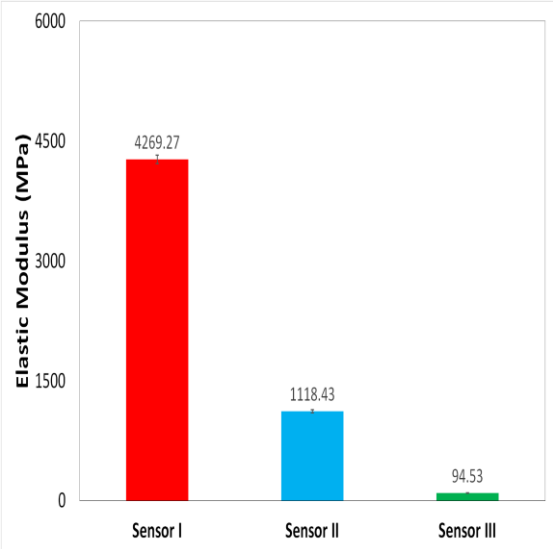

(a) Comparison of Elastic Modulus

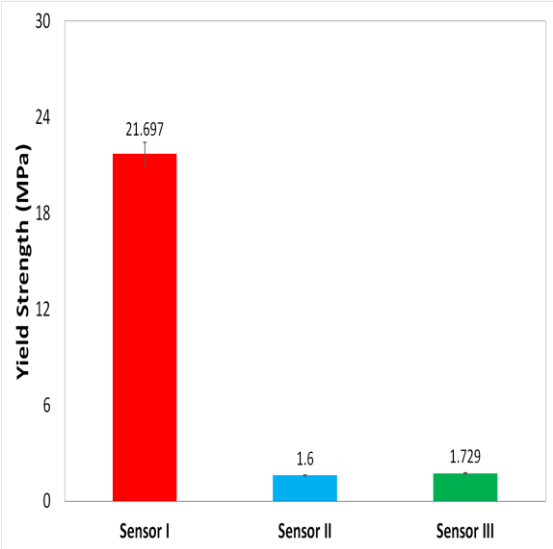

(b) Comparison of Yield Strength

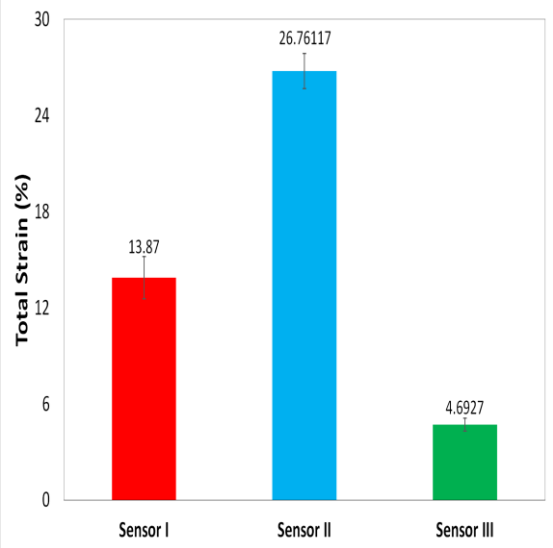

(c) Comparison of Strain

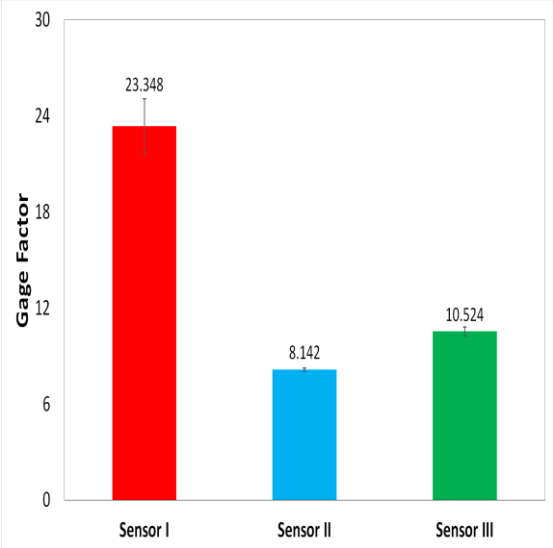

(d) Comparison of GF

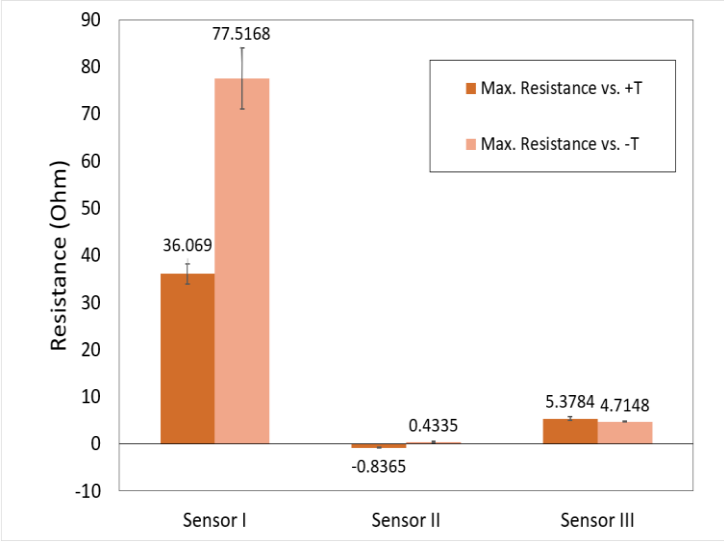

(e) Comparison of resistance change with respect to thermal loading
Figure 2-24: Comparison of different properties of all three sensor systems.

2.6. Conclusions

In this chapter experimental investigation was carried out to develop different sensor systems for application in real-time structural health monitoring of composite structures. These sensor systems included a Nylon/ Ag fiber sensor developed by deposition of Ag nanoparticles on nylon yarn through electroless plating, CM sensor developed using deposition of a dense network of CNTs in form of thin film using chemical vapor deposition and CF sensor consisting of PAN carbon fiber filaments aligned unidirectionally together. All these three sensor systems were studies individually as a standalone sensor under both mechanical and thermal loadings and their performance was studied in detail.

Nylon/Ag conductive fiber was tested experimentally and it showed good sensitivity to applied strain with a gauge factor in the range of 21-25. Then, this conductive polymer fiber was strained up to fracture to understand the overall electromechanical behavior and study its limits under high strain loading. SEM images of the Nylon/Ag conductive fiber also confirmed a uniform and continuous thin film metal coating formed by the deposition of Ag nanoparticles on the surface of each filament of the Nylon-6 yarn which validated the good conductivity response of the sensor. Besides, the thickness of the coating was kept small enough that it does not compromise the weight, cost, and flexibility of the conductive fiber while thick enough to avoid any defects, voids or cracks in it. After the final fracture, it was observed that in addition to the clean ductile failure, pull out or breakage of the coating was observed which gave rise to the resistance of the conductive fiber with the strain deformation of the Nylon-6 yarn and it was more prominent during the damage initiation and damage propagation after the maximum strain deformation. The electro-thermal behavior showed that thermal detection with the change of resistance was because of thermal expansion and results confirmed that sensor in both tests reacted to the applied stimuli and showed a distinct change in their change in resistance because of two different materials with different thermal expansion coefficients thus, not only monitoring the deformation but also detecting the change in temperature in the surrounding at atmospheric pressure.

This CM sensor showed high sensitivity to applied strain in the range of 8-8.25, were more flexible and could be easily integrated within the composite specimens. The electrothermal behavior showed that thermal detection with the change of resistance was because of the

tunneling effect of the heterogeneous network of CNTs. Results confirmed that CM sensors in both tests reacted to the applied stimuli and showed a distinct change in their change in resistance thus, not only monitoring the deformation but also detecting the change in temperature in the surrounding at atmospheric pressure. However, further study is required to understand the precise mechanism responsible for changing the resistance of the sensors to apprehend its response under thermal loading which could be because of the tunneling effect between the network of CNTs thus resulting in an increase of resistance with the decrease in temperature and vice versa. These CM sensors consisting of a pure network of CNTs with high conductance can further advance itself in the real-time sensing applications within composite structures including strain monitoring, thermal degradation, and detection of failure and energy release during dynamic loading. The sensitivity of this sensor can be further tailored and amplified as desired parameters by modifying the deposition of CNTs network and without any significant requirements.

The CF sensor showed a simple, robust, and cost-effective sensor system with high electrical conductance for multimode real-time monitoring under different loadings. This sensor showed high sensitivity to applied strain in the range of 10.2-10.8, were more flexible and could be easily integrated within any structure. The electro-thermal behavior showed that thermal detection with the change of resistance was because of thermal expansion and distance between the electrical connection points of straightly aligned carbon filaments in the CF sensor. Results confirmed that CF sensors in both tests reacted to the applied stimuli and showed a distinct change in their change in resistance thus, not only monitoring the deformation but also detecting the change in temperature in the surrounding at atmospheric pressure. However, further study is required to understand the precise mechanism responsible for changing the resistance of the sensors to apprehend its response under thermal loading. These CF sensors can further advance itself in the real-time sensing applications within composite structures including strain monitoring, thermal degradation, and detection of failure and energy release during dynamic loading. The sensitivity of this sensor can be further tailored and amplified as desired parameters by modifying the number and alignment of carbon filaments and without any significant requirements.

The results were very encouraging and the electromechanical response was reproducible not only in overall behavior but also during plastic strain deformation and fracture for all three sensor systems which showed that they are suitable for high strain applications and real-time

sensing applications within composite structures including strain monitoring, thermal degradation and detection of failure and energy release during dynamic loading.

Moreover, the comparison of these sensor systems showed that Nylon/Ag fiber sensor showed better performance than the other two systems in mechanical and strain sensitivity behaviors. However, CM sensor not only detected the change in environmental temperature but also distinguished it whether it was positive or negative but showing an increase in resistance during temperature drop and decrease in resistance during elevation of temperature. However, this comparative study is based on their individual performance and it is important to study their performance within specimens for the selection of better real-time multimode detection systems for composite structures which will be the discuss in the next chapter.

References

[1] J. Farringdon, “Wearable electronics and clothing from Philips and Levi,” vol. 10, pp. 22–24, 2001.

[2] F. Axisa, P. M. Schmitt, C. Géhin, G. Delhomme, E. McAdams, and A. Dittmar, “Flexible technologies and smart clothing for citizen medicine, home healthcare, and disease prevention,” *IEEE Trans. Inf. Technol. Biomed.*, vol. 9, pp. 325–336, 2005.

[3] “Universal Serial Fabric Bus, US Army Natick Soldier Systems Center.,” 2013.

[4] C. Simon, E. Potter, M. McCabe, and C. Baggerman, “Smart fabrics technology development,” 2010.

[5] B. Christian, “Next generation structural health monitoring and its integration into aircraft design.,” *Int. J. Syst. Sci.*, vol. 31, no. 11, pp. 1333–1349, 2000.

[6] V. K. Varadan and V. Varadan., “Microsensors, microelectromechanical systems (mems), and electronics for smart structures and systems.,” *Smart Mater. Struct.*, vol. 9, no. 6, pp. 953–972, 2000.

[7] N. Trifigny, F. M. Kelly, C. Cochrane, F. Boussu, V. Koncar, and D. Soulat, “PEDOT: PSS-based piezo-resistive sensors applied to reinforcement glass fibres for in situ measurement during the composite material weaving process.,” *Sensors*, vol. 13, no. 8, pp. 10749–10764, 2013.

[8] O. Atalay and W. R. Kennon, “Knitted Strain Sensors: Impact of Design Parameters on Sensing Properties,” in *Sensors*, 2014.

[9] S. Seyedin, J. M. Razal, P. C. Innis, A. Jeiranikhameneh, S. Beirne, and G. G. Wallace, “Knitted strain sensor textiles of highly conductive all-polymeric fibers,” *ACS Appl. Mater. Interfaces*, vol. 7, no. 38, pp. 21150–21158, 2015.

[10] I. Jerkovic, V. Koncar, and A. Grancaric, “New textile sensors for in situ structural health monitoring of textile reinforced thermoplastic composites based on the conductive poly(3,4-ethylenedioxythiophene)-poly(styrenesulfonate) polymer complex,” *Sensors*, vol. 17, no. 10, 2017.

[11] H. Cheng *et al.*, “Textile electrodes woven by carbon nanotube–graphene hybrid fibers for flexible electrochemical capacitors,” *Nanoscale*, vol. 5, no. 8, p. 3428, 2013.

[12] K. Kawano, R. Pacios, D. Poplavskyy, J. Nelson, D. D. C. Bradley, and J. R. Durrant, “Degradation of organic solar cells due to air exposure,” *Sol. Energy Mater. Sol. Cells*, vol. 90, no. 20, pp. 3520–3530, 2006.

[13] H. Liu *et al.*, “Electrically conductive polymer composites for smart flexible strain sensors: a critical review,” *J. Mater. Chem. C*, vol. 6, no. 45, pp. 12121–12141, 2018, doi: 10.1039/C8TC04079F.

[14] S. Nauman, I. Cristian, F. Boussu, and V. Koncar, “Smart Sensors for Industrial Applications. Part V Piezoresistive, Wireless, and Electrical Sensors,” USA,: K. Iniewski, 2013.

[15] T. Kinkeldei, C. Denier, C. Zysset, N. Muenzenrieder, and G. Troester., “2D Thin Film Temperature Sensors Fabricated onto 3D Nylon Yarn Surface for Smart Textile Applications,” *Res. J. Text. Appar.*, vol. 17, no. 2, pp. 16–20, 2013.

[16] J. Xie, H. Long, and M. Miao, “High sensitivity knitted fabric strain sensors.,” *Smart Mater. Struct.*, vol. 25, no. 10, 2016.

[17] D. Ryu, K. J. Loh, R. Ireland, M. Karimzada, F. Yaghmaie, and A. M. Gusman, “In situ reduction of gold nanoparticles in PDMS matrices and applications for large strain sensing. Smart Structures and Systems,” vol. 8, no. 5, pp. 471–486, 2011.

[18] R. X. Wang, X. M. Tao, Y. Wang, G. F. Wang, and S. M. Shang., “Microstructures and electrical conductance of silver nanocrystalline thin films on flexible polymer substrates.,” *Surf. Coatings Technol.*, vol. 204, no. 8, pp. 1206–1210, 2010.

[19] N. Perkas, G. Amirian, S. Dubinsky, S. Gazit, and A. Gedanken, “Ultrasound-assisted coating of nylon 6,6 with silv er nanoparticles and its antibacterial activity,” *J. Appl. Polym. Sci.*, vol. 104, no. 3, 2007.

[20] O. Atalay, A. Tuncay, M. D. Husain, and W. R. Kennon, “Comparative study of the weft-knitted strain sensors,” *J. Ind. Text.*, vol. 46, no. 5, pp. 1212–1240, 2016.

[21] Y. Atwa, N. Maheshwari, and I. A. Goldthorpe., “Silver nanowire coated threads for electrically conductive textiles.,” *J. Mater. Chem. C*, vol. 3, no. 16, pp. 3908–3912, 2015.

[22] S. Zhang *et al.*, “Ultrasensitive and Highly Compressible Piezoresistive Sensor Based on Polyurethane Sponge Coated with a Cracked Cellulose Nanofibril/Silver Nanowire Layer,” *ACS Appl. Mater. Interfaces*, vol. 11, no. 11, pp. 10922–10932, Mar. 2019, doi: 10.1021/acsami.9b00900.

[23] K. S. Karimov, F. A. Khalid, and M. T. S. Chani, “Carbon nanotubes based strain sensors,” *Measurement*, vol. 45, no. 5, pp. 918–921, 2012, doi: https://doi.org/10.1016/j.measurement.2012.02.003.

[24] I. Kang, M. J. Schulz, J. H. Kim, V. Shanov, and D. Shi, “A carbon nanotube strain sensor for structural health monitoring,” *Smart Mater. Struct.*, vol. 15, no. 3, pp. 737–748, Apr. 2006, doi:

10.1088/0964-1726/15/3/009.

[25] E. T. Thostenson and T.-W. Chou, “Real-timein situsensing of damage evolution in advanced fiber composites using carbon nanotube networks,” *Nanotechnology*, vol. 19, no. 21, p. 215713, Apr. 2008, doi: 10.1088/0957-4484/19/21/215713.

[26] R. J. Grow, Q. Wang, J. Cao, D. Wang, and H. Dai, “Piezoresistance of carbon nanotubes on deformable thin-film membranes,” *Appl. Phys. Lett.*, vol. 86, no. 9, p. 93104, 2005, doi: 10.1063/1.1872221.

[27] Alamusi, N. Hu, H. Fukunaga, S. Atobe, Y. Liu, and J. Li., “Piezoresistive strain sensors made from carbon nanotubes based polymer nanocomposites,” *Sensors*, vol. 11, pp. 10691–10723.

[28] P. Dharap, Z. Li, S. Nagarajaiah, and E. V Barrera, “Nanotube film based on single-wall carbon nanotubes for strain sensing,” *Nanotechnology*, vol. 15, no. 3, pp. 379–382, Jan. 2004, doi: 10.1088/0957-4484/15/3/026.

[29] N. Hu, Y. Karube, C. Yan, Z. Masuda, and H. Fukunaga, “Tunneling effect in a polymer/carbon nanotube nanocomposite strain sensor,” *Acta Mater.*, vol. 56, no. 13, pp. 2929–2936, 2008, doi: https://doi.org/10.1016/j.actamat.2008.02.030.

[30] N. Hu, Y. Karube, M. Arai, T. Watanabe, C. Yan, and Y. Li., “Investigation on sensitivity of polymer/carbon nanotube composite strain sensor.,” *Carbon N. Y.*, vol. 48, no. 680–687, 2010.

[31] B. Hu *et al.*, “Performance characterization of {VGCF}/epoxy nanocomposite sensors under static load cycles and in static structural health monitoring,” *Smart Mater. Struct.*, vol. 22, no. 4, p. 45008, Mar. 2013, doi: 10.1088/0964-1726/22/4/045008.

[32] J. L. Abot *et al.*, “Delamination detection with carbon nanotube thread in self-sensing composite materials,” *Compos. Sci. Technol.*, vol. 70, no. 7, pp. 1113–1119, 2010, doi: https://doi.org/10.1016/j.compscitech.2010.02.022.

[33] M. Tarfaoui, A. El Moumen, M. Boehle, O. Shah, and K. Lafdi, “Self-heating and deicing epoxy/glass fiber based carbon nanotubes buckypaper composite,” *J. Mater. Sci.*, vol. 54, no. 2, pp. 1351–1362, 2019, doi: 10.1007/s10853-018-2917-9.

[34] S. Iijima, “Helical microtubules of graphitic carbon,” *Nature*, vol. 354, no. 6348, pp. 56–58, 1991, doi: 10.1038/354056a0.

[35] Z. Wan, J. Guo, and M. Jia., “Damage detection of three-dimensional braided composite materials using carbon nanotube thread,” *Sci. Eng. Compos. Mater.*, vol. 24, no. 2, pp. 213-220., 2015.

[36] S. Wang *et al.*, “Smart wearable kevlar-based safeguarding electronic textile with excellent

sensing performance.," *Soft Matter.*, vol. 13, no. 13, pp. 2483–2491, 2017.

[37] Q. Li *et al.*, "Superhydrophobic Electrically Conductive Paper for Ultrasensitive Strain Sensor with Excellent Anticorrosion and Self-Cleaning Property," *ACS Appl. Mater. Interfaces*, May 2019, doi: 10.1021/acsami.9b03421.

[38] H. Liu *et al.*, "Electrically conductive strain sensing polyurethane nanocomposites with synergistic carbon nanotubes and graphene bifillers," *Nanoscale*, vol. 8, no. 26, pp. 12977–12989, 2016, doi: 10.1039/C6NR02216B.

[39] D. Kim, J.-E. Bourée, and S. Y. Kim, "Calculation of the field enhancement for a nanotube array and its emission properties," *J. Appl. Phys.*, vol. 105, no. 8, p. 84315, 2009, doi: 10.1063/1.3091282.

[40] M. Shahi *et al.*, "Effect of purity, edge length, and growth area on field emission of multi-walled carbon nanotube emitter arrays," *J. Appl. Phys.*, vol. 113, no. 20, p. 204304, 2013, doi: 10.1063/1.4807916.

[41] F. Giubileo *et al.*, "Local probing of the field emission stability of vertically aligned multi-walled carbon nanotubes," *Carbon N. Y.*, vol. 47, no. 4, pp. 1074–1080, 2009, doi: https://doi.org/10.1016/j.carbon.2008.12.035.

[42] A. Di Bartolomeo *et al.*, "A local field emission study of partially aligned carbon-nanotubes by atomic force microscope probe," *Carbon N. Y.*, vol. 45, no. 15, pp. 2957–2971, 2007, doi: https://doi.org/10.1016/j.carbon.2007.09.049.

[43] H. Liu, Y. Shi, B. Chen, X. Li, Y. Ding, and B. Lu, "Effect of patterned and aligned carbon nanotubes on field emission properties," *Vacuum*, vol. 86, no. 7, pp. 933–937, 2012, doi: https://doi.org/10.1016/j.vacuum.2011.07.047.

[44] F. Giubileo *et al.*, "Field emission properties of as-grown multiwalled carbon nanotube films," *Carbon N. Y.*, vol. 50, no. 1, pp. 163–169, 2012, doi: https://doi.org/10.1016/j.carbon.2011.08.015.

[45] Y. Chen *et al.*, "Emitter spacing effects on field emission properties of laser-treated single-walled carbon nanotube buckypapers," *Nanotechnology*, vol. 21, no. 49, p. 495702, Nov. 2010, doi: 10.1088/0957-4484/21/49/495702.

[46] P. Rai, D. R. Mohapatra, K. S. Hazra, D. S. Misra, and S. P. Tiwari, "Nanotip formation on a carbon nanotube pillar array for field emission application," *Appl. Phys. Lett.*, vol. 93, no. 13, p. 131921, 2008, doi: 10.1063/1.2996283.

[47] T.-W. Weng, Y.-H. Lai, and K.-Y. Lee, "Area effect of patterned carbon nanotube bundle on

field electron emission characteristics," *Appl. Surf. Sci.*, vol. 254, no. 23, pp. 7755–7758, 2008, doi: https://doi.org/10.1016/j.apsusc.2008.02.020.

[48] R. Seelaboyina, S. Boddepalli, K. Noh, M. Jeon, and W. Choi, "Enhanced field emission from aligned multistage carbon nanotube emitter arrays," *Nanotechnology*, vol. 19, no. 6, p. 65605, Jan. 2008, doi: 10.1088/0957-4484/19/6/065605.

[49] S. Roy *et al.*, "Enhanced Field Emission and Improved Supercapacitor Obtained from Plasma-Modified Bucky Paper," *Small*, vol. 7, no. 5, pp. 688–693, 2011, doi: 10.1002/smll.201002330.

[50] M. Kaempgen, C. K. Chan, J. Ma, Y. Cui, and G. Gruner, "Printable Thin Film Supercapacitors Using Single-Walled Carbon Nanotubes," *Nano Lett.*, vol. 9, no. 5, pp. 1872–1876, May 2009, doi: 10.1021/nl8038579.

[51] A. Bonanni, M. J. Esplandiu, and M. del Valle, "Impedimetric genosensors employing COOH-modified carbon nanotube screen-printed electrodes," *Biosens. Bioelectron.*, vol. 24, no. 9, pp. 2885–2891, 2009, doi: https://doi.org/10.1016/j.bios.2009.02.023.

[52] N. Behabtu, M. J. Green, and M. Pasquali, "Carbon nanotube-based neat fibers," *Nano Today*, vol. 3, no. 5, pp. 24–34, 2008, doi: https://doi.org/10.1016/S1748-0132(08)70062-8.

[53] R. H. Baughman *et al.*, "Carbon Nanotube Actuators," *Science (80-.).*, vol. 284, no. 5418, pp. 1340–1344, 1999, doi: 10.1126/science.284.5418.1340.

[54] I. Krucinska and T. Stypka, "Direct measurement of the axial poisson's ratio of single carbon fibres," *Compos. Sci. Technol.*, vol. 41, no. 1, pp. 1–12, 1991, doi: https://doi.org/10.1016/0266-3538(91)90049-U.

[55] S. Blazewicz, B. Patalita, and P. Touzain, "Study of piezoresistance effect in carbon fibers," *Carbon N. Y.*, vol. 35, no. 10, pp. 1613–1618, 1997, doi: https://doi.org/10.1016/S0008-6223(97)00120-6.

[56] C. N. Owston, "Electrical properties of single carbon fibres," *J. Phys. D. Appl. Phys.*, vol. 3, no. 11, pp. 1615–1626, Nov. 1970, doi: 10.1088/0022-3727/3/11/309.

[57] A. Horoschenkoff, T. Mueller, and A. Kroell, "On the characterization of the piezoresistivity of embedded carbon fibres," *ICCM 17th*, 2009.

[58] A. Horoschenkoff, M. Derks, T. Mueller, H. Rapp, and S. Schwarz, "Konzeptstudie zum einsatz von elektrisch kontaktierten carbonfasern als sensor für leichtbaustrukturen aus faserverbundwerkstoff Vorträge. 14," in *Nationales Symp. Sampe Deutschland eV (Garching, 7--28 February)*, 2008.

[59] P. C. CONOR and C. N. OWSTON, "Electrical Resistance of Single Carbon Fibres," *Nature*,

vol. 223, no. 5211, pp. 1146–1147, 1969, doi: 10.1038/2231146b0.

[60] J. Wen, Z. Xia, and F. Choy, “Damage detection of carbon fiber reinforced polymer composites via electrical resistance measurement,” *Compos. Part B Eng.*, vol. 42, no. 1, pp. 77–86, 2011, doi: https://doi.org/10.1016/j.compositesb.2010.08.005.

[61] C. Luan, X. Yao, H. Shen, and J. Fu, “Self-Sensing of Position-Related Loads in Continuous Carbon Fibers-Embedded 3D-Printed Polymer Structures Using Electrical Resistance Measurement,” *Sensors (Basel).*, vol. 18, no. 4, p. 994, Mar. 2018, doi: 10.3390/s18040994.

[62] X. Yao, C. Luan, D. Zhang, L. Lan, and J. Fu, “Evaluation of carbon fiber-embedded 3D printed structures for strengthening and structural-health monitoring,” *Mater. Des.*, vol. 114, pp. 424–432, 2017, doi: https://doi.org/10.1016/j.matdes.2016.10.078.

[63] Y. Goldfeld, S. Ben-Aarosh, O. Rabinovitch, T. Quadflieg, and T. Gries, “Integrated self-monitoring of carbon based textile reinforced concrete beams under repeated loading in the un-cracked region,” *Carbon N. Y.*, vol. 98, pp. 238–249, 2016, doi: https://doi.org/10.1016/j.carbon.2015.10.056.

[64] F.-Y. Yeh, K.-C. Chang, and W.-C. Liao, “Experimental Investigation of Self-Sensing Carbon Fiber Reinforced Cementitious Composite for Strain Measurement of an RC Portal Frame,” *Int. J. Distrib. Sens. Networks*, vol. 11, no. 11, p. 531069, 2015, doi: 10.1155/2015/531069.

[65] A. Todoroki, Y. Samejima, Y. Hirano, and R. Matsuzaki, “Piezoresistivity of unidirectional carbon/epoxy composites for multiaxial loading,” *Compos. Sci. Technol.*, vol. 69, no. 11, pp. 1841–1846, 2009, doi: https://doi.org/10.1016/j.compscitech.2009.03.023.

[66] N. Angelidis, C. Y. Wei, and P. E. Irving, “The electrical resistance response of continuous carbon fibre composite laminates to mechanical strain,” *Compos. Part A Appl. Sci. Manuf.*, vol. 35, no. 10, pp. 1135–1147, 2004, doi: https://doi.org/10.1016/j.compositesa.2004.03.020.

[67] S. Sassi, M. Tarfaoui, and H. Ben Yahia., “In-situ heat dissipation monitoring in adhesively bonded composite joints under dynamic compression loading using SHPB,” *Compos. Part B Eng.*, vol. 54, pp. 64–76, 2018.

[68] R. Damerchely, M. Yazdanshenas, A. Rashidi, and R. Khajavi, “Morphology and mechanical properties of antibacterial nylon 6/nano-silver nano-composite multifilament yarns,” *Text. Res. J.*, vol. 81, pp. 1694–1701, 2011, doi: 10.1177/0040517511410104.

[69] B. M. Latta, “Improved Tactile and Sorption Properties of Polyester Fabrics Through Caustic Treatment,” *Text. Res. J.*, vol. 54, no. 11, pp. 766–775, 1984, doi: 10.1177/004051758405401110.

[70] M. Montazer, F. Alimohammadi, A. Shamei, and M. K. Rahimi, “In situ synthesis of nano silver on cotton using Tollens’ reagent,” *Carbohydr. Polym.*, vol. 87, no. 2, pp. 1706–1712, 2012, doi: https://doi.org/10.1016/j.carbpol.2011.09.079.

[71] L. D. Socaciu, J. Hagen, U. Heiz, T. M. Bernhardt, T. Leisner, and L. Wöste, “Reaction mechanism for the oxidation of free silver dimers,” *Chem. Phys. Lett.*, vol. 340, no. 3, pp. 282–288, 2001, doi: https://doi.org/10.1016/S0009-2614(01)00447-X.

[72] M. Popa, T. Pradell, D. Crespo, and J. M. Calderón-Moreno, “Stable silver colloidal dispersions using short chain polyethylene glycol,” *Colloids Surfaces A Physicochem. Eng. Asp.*, vol. 303, no. 3, pp. 184–190, 2007, doi: https://doi.org/10.1016/j.colsurfa.2007.03.050.

[73] K. Bertuleit., “Silver Coated Polyamide: A Conductive Fabric,” *J. Coat. Fabr.*, vol. 20, no. 3, pp. 211–215, 1991.

[74] S. N. Song, X. K. Wang, R. P. H. Chang, and J. B. Ketterson, “Electronic properties of graphite nanotubules from galvanomagnetic effects,” *Phys. Rev. Lett.*, vol. 72, no. 5, pp. 697–700, Jan. 1994, doi: 10.1103/PhysRevLett.72.697.

[75] W. A. deHeer *et al.*, “Aligned Carbon Nanotube Films: Production and Optical and Electronic Properties,” *Science (80-.).*, vol. 268, no. 5212, pp. 845–847, 1995, doi: 10.1126/science.268.5212.845.

[76] A. Di Bartolomeo *et al.*, “Multiwalled carbon nanotube films as small-sized temperature sensors,” *J. Appl. Phys.*, vol. 105, no. 6, p. 64518, 2009, doi: 10.1063/1.3093680.

[77] J. E. Fischer *et al.*, “Metallic resistivity in crystalline ropes of single-wall carbon nanotubes,” *Phys. Rev. B*, vol. 55, no. 8, pp. R4921--R4924, Feb. 1997, doi: 10.1103/PhysRevB.55.R4921.

[78] L. Langer *et al.*, “Quantum Transport in a Multiwalled Carbon Nanotube,” *Phys. Rev. Lett.*, vol. 76, no. 3, pp. 479–482, Jan. 1996, doi: 10.1103/PhysRevLett.76.479.

[79] N. F. Mott, “Electrons in disordered structures,” *Adv. Phys.*, vol. 16, no. 61, pp. 49–144, 1967, doi: 10.1080/00018736700101265.

[80] P. Sheng, “Fluctuation-induced tunneling conduction in disordered materials,” *Phys. Rev. B*, vol. 21, no. 6, pp. 2180–2195, Mar. 1980, doi: 10.1103/PhysRevB.21.2180.

[81] H. Khayyam *et al.*, “PAN precursor fabrication, applications and thermal stabilization process in carbon fiber production: Experimental and mathematical modelling,” *Prog. Mater. Sci.*, vol. 107, p. 100575, 2020, doi: https://doi.org/10.1016/j.pmatsci.2019.100575.

[82] D.-J. Kwon, P.-S. Shin, J.-H. Kim, Z.-J. Wang, K. L. DeVries, and J.-M. Park, “Detection of damage in cylindrical parts of carbon fiber/epoxy composites using electrical resistance (ER)

measurements," *Compos. Part B Eng.*, vol. 99, pp. 528–532, 2016, doi: https://doi.org/10.1016/j.compositesb.2016.06.050.

[83] D.-J. Kwon, Z.-J. Wang, J.-Y. Choi, P.-S. Shin, K. L. Devries, and J. M. Park, "Interfacial evaluation of carbon fiber/epoxy composites using electrical resistance measurements at room and a cryogenic temperature," *Compos. Part A Appl. Sci. Manuf.*, vol. 72, 2015, doi: 10.1016/j.compositesa.2015.02.007.

[84] Z. Wang, L. Ye, and Y. Liu, "Electro-thermal damage of carbon fiber/epoxy composite laminate," *J. Reinf. Plast. Compos.*, vol. 37, no. 3, pp. 166–180, 2018, doi: 10.1177/0731684417738334.

[85] H. Yu, D. Heider, and S. Advani, "Prediction of effective through-thickness thermal conductivity of woven fabric reinforced composites with embedded particles," *Compos. Struct.*, vol. 127, pp. 132–140, 2015, doi: https://doi.org/10.1016/j.compstruct.2015.03.015.

CHAPTER 3 : REAL-TIME MONITORING OF STRAIN DEFORMATION IN COMPOSITES UNDER QUASI-STATIC LOADINGS

In this chapter, the objective is to monitor the deformation behavior of composites subjected to different cyclic quasi-static loadings in real-time using different sensor systems. each sensor system was integrated at different direction i.e. 0°, +45°, 90°, -45° gradually between each ply of their respective composite specimens which were then machined in star shape where each leg signified the direction of the sensor. These composite samples are then tested under tensile and flexural cyclic loading. There is a good reproducibility in the results and the mechanical response of composite correlated perfectly with the electrical resistance of each sensor system respectively. However, all sensor systems in each sample showed distinct change because of their respective positions and direction in each loading condition. The results established that each sensor system exhibited good potential as a flexible strain sensor for in-situ monitoring of composites and can provide detection over a large section and unapproachable locations. The increase or decrease in the resistance of the fiber sensor signified the presence of tensile or compressive strain respectively and the intensity of the signal quantified the amount of deformation. The results confirmed that in comparison, Nylon/Ag fiber sensor showed good potential as flexible sensor reinforcement in composites for in-situ monitoring, identification, and quantification of the deformation.

3.1. Introduction

Numerous studies examined the strain deformation and failure sensing of the composites using different SHM methods under tensile elongation and flexural deflection, however, very little or no information was available about the influence of the location of the sensor on their sensitivity and damage detection[1]. Currently used SHM techniques include fiber optic sensors, piezoelectric or piezoresistive sensors, strain gauges and accelerometers to monitor the mechanical deformation, vibrations, or other parameters of the structure during the operation [2]–[12]. However, most of these techniques can detect damage near its location therefore they must be placed near the critical zones on the structure. To counter this, sensors network systems had also been used to triangulate the location of the damage using lamb wave propagation, but the cost, size, and weight of such a system limit their use not to mention the complex data processing required [13]. Moreover, SHM systems attached to the surface of the composites such as optical fibers and strain gauges had a drawback of being exposed to the environmental conditions, for example, chemical, thermal, humidity, and external mechanical effect [14], [15]. That is why researchers are more focused on integrable monitoring sensors to not only monitor the overall deformation of the structure but to also monitor the internal behavior between the laminates of the composites. However, the insertion of the monitoring sensor entity in the composites is still underdeveloped and the prime focus is that it would not affect the performance of the composite structures. In previous studies, various sensors were developed and inserted inside the composites such as fiber bragg grating, carbon nanotubes, carbon black or carbon fibers[16]–[21] . However, use of optical sensors methods is limited because of high cost to produce an optical fiber with fiber bragg grating.

The change in electrical resistance measurement (ER) in which resistance change of the material is measured during the operation was one in-situ SHM technique used for monitoring the performance of composites during operation [21–25]. It was often used for carbon fiber reinforced polymer composites (CFRP) because carbon fibers have good electrical conductance and worked based on contact change and rearrangement of carbon fibers within composites during deformation [26,27]. The response signal of resistance change in this technique was in direct correlation to the applied strain in case of unidirectional (UD) fiber composites but the signal response was more complexed for composites with randomly dispersed fibers specifically in applications where large deformation was involved [28–31]. Besides, this technique was considered unfavorable for composites with high resistivity, for example, cementitious composites or glass fiber reinforced polymer (GFRP) composites which required

the addition of nanofillers to reduce their resistivity and improve their self-sensing performance [32,33]. However, increasing the conductivity of the composites structures with low conductivity with the addition of nanofillers did not apply on large-scaled structures because it would require a huge percentage of nanofillers to achieve good conductance behavior that could result in dispersion problems and high cost [32,33].

Flexible smart textiles were then considered to be a favorable alternative for the SHM of structural composites because, after insertion, they could not only monitor the deformation of the structure but also act as reinforcement [34–37]. The working principle of these flexible conductive sensors consisting of textiles, fabrics, and yarns is similar to that of traditional strain gauges [37].

In this experimental investigation, all three sensor systems were positioned in 0°, +45°, 90°, -45° directions through the plies gradually in their respective glass fiber reinforced polymer (GFRP) composite sample and the composite specimens were tested under tensile and flexural cyclic loadings. The results showed interesting behavior and presented that each sensor system showed distinct behavior in the detection of strain deformation of the composite sample under each cyclic loading. Each sensor system not only detected the strain under both loadings but also identified the type of deformation and the intensity of the signal measured the amount of deformation. Moreover, the results demonstrated that the position and direction of the sensor play a vital role in the detection of strain by the sensor.

3.2. Fabrication Procedure

Each sensor system was cut into specific lengths and was inserted between the plies of chopped glass fibers in their respective position and direction during the fabrication of their respective composite specimen. Five plies of chopped glass fiber were used for reinforcement and to separate the fiber sensor from each other. Also, the chopped fiber mat ensured isotropic mechanical behavior with poor conductivity and electrical isolation for each sensor system. Each sensor system in their respective composite samples were inserted in the specimen in their particular direction such that sensor A was in 0° between plies 1 and 2, sensor B was in 45° between plies 2 and 3, sensor C was in 90° between plies 3 and 4 and sensor D was in -45° between plies 4 and 5 from bottom to top. Afterward, the mixture of resin and hardener was added into the mold, full insertion of the sensor systems was achieved in each specimen. After the curation process of 48 hours at room temperature, the specimens were machined using CNC (Computer numerical control) machine in a star shape in which each leg represented the

direction and placement of the sensors, Figure 3-1 (a). The sample consisted of 5 mm of thickness and each leg of the star shape was 25 mm in width and approximately 200 mm in length, Figure 3-1 (b). Furthermore, the geometrical illustration of the star sample explained the location and direction of the fiber sensors in each lag and within the plies (through-thickness), Figure 3-1 (c)-(d).

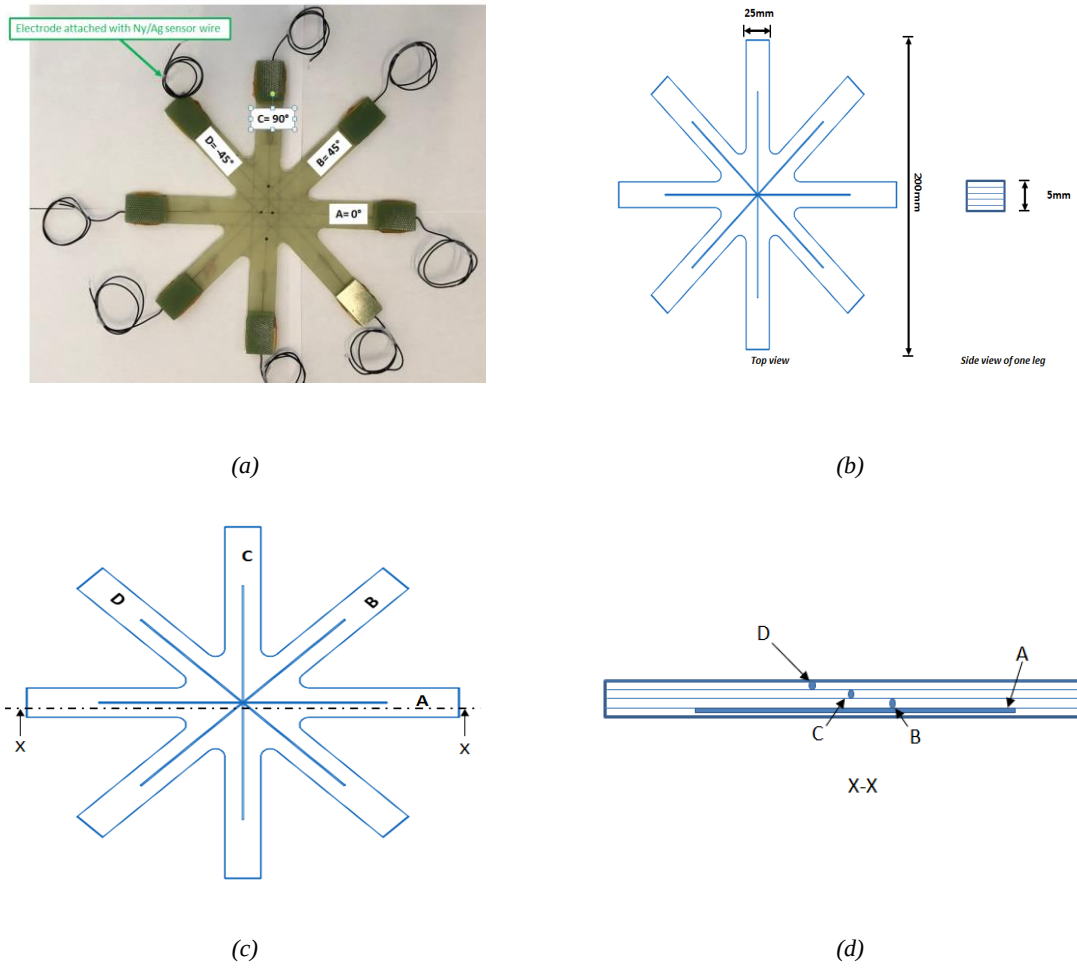

Figure 3-1: Star Specimen with (a) An example of a composite sample embedded with a sensor system of Nylon/Ag fiber sensors which were visible in each leg. (b) Geometric parameters of the star samples. (c)-(d) Geometrical illustration of the placement of sensor systems in their individual sample i.e. in individual leg and through-thickness (section view) correspondingly.

3.3. Experimental Procedure

The star specimens were tested using INSTRON-50 and the data acquisition system was attached to each sensor using electrodes for real-time monitoring of strain deformation. INSTRON-50 recorded the mechanical performance of the composite sample and the data

acquisition system simultaneously recorded the response of the respective sensor system. Two sets of tests were performed, first set of tests included the study of three composite specimens under tensile cyclic loading and the second test was included the testing of three-star specimens under cyclic bending for each sensor system to comprehend their real-time monitoring behavior in detail, Figure 3-2. In both tests, it was important to place the samples properly among the fixtures and isolate the electrical connections as discussed in the previous chapter. Moreover, the shape of the specimen made it easier to place it between the fixtures during the tensile cyclic loading but the placement of the specimen between the rollers of the flexural cyclic test was a bit difficult. That is why the strain rate for the tensile test was kept 5 mm/min applied up to 15 kN and for the flexural test, it was kept 2 mm/min applied up to 2kN to ensure no permanent deformation in the samples. All tests were performed for 10 cycles and it must be noted that the range of strain rate in quasi-static tests is so low that it does not affect the mechanical behavior of the sample or the electrical response of the sensor [39]. Each test presented that all three sensor systems in each position and direction showed a distinct resistance profile in both sets of tests which will be discussed in detail in the next section.

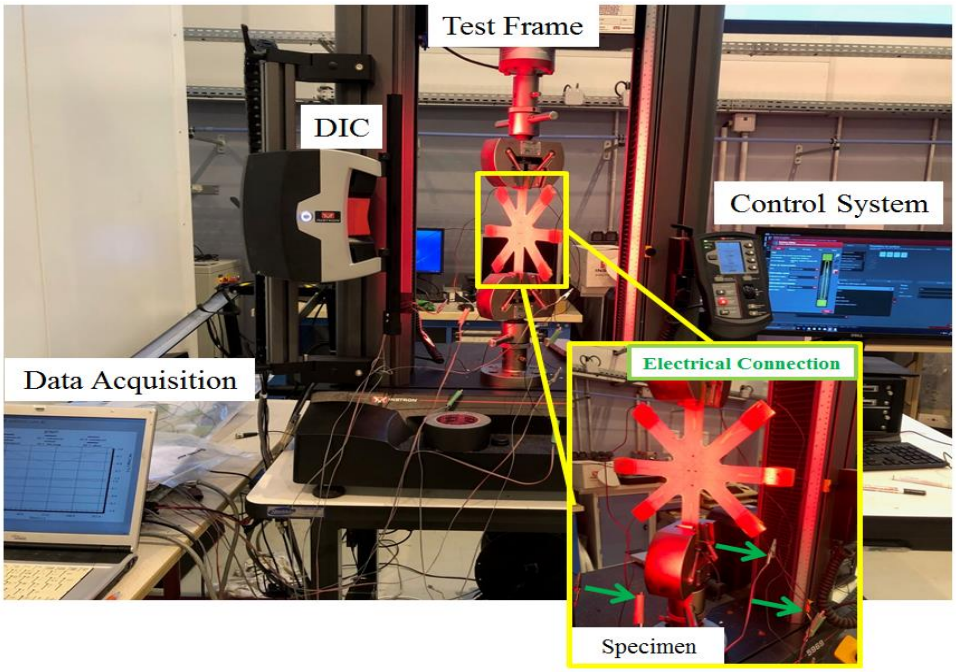

(a) Tensile test setup

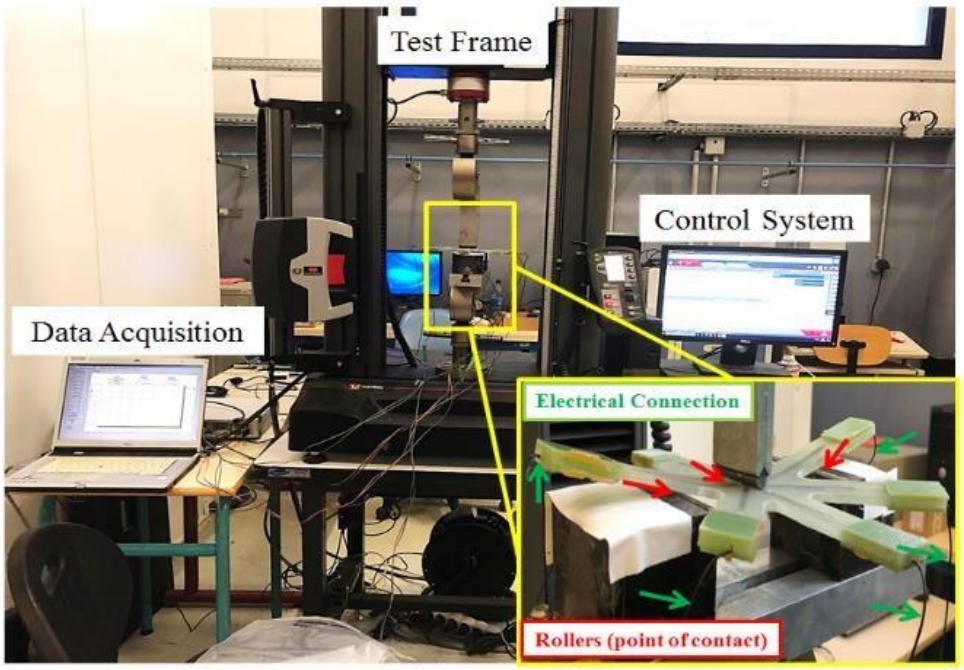

(b) Three-point bend test setup

Figure 3-2: Experimental arrangement to examine the real-time strain monitoring response of each sensor system in composites.

3.4. Results and discussions

3.4.1. Strain monitoring in composites during cyclic tensile loading

First, it is important to understand the strain deformation of the composite under cyclic tensile loading to apprehend the strain detection by all three sensor systems, Figure 3-3. One leg of the

star specimen was fixed between the fixtures of the machine and the other legs were free. The loading axis was considered as the reference and sensor place in this direction was at 0° and labeled as sensor A. When the specimen was loaded, tensile stresses were produced in 0° and compression strains were produced in 90° i.e. transverse direction. In addition, it was understood that the combined effect of tensile and compression strains is generated in oblique direction i.e. ±45°. However, in test 1 and 2, samples were placed between the fixtures in such manner that the leg of the star sample consisting of sensor A was along the loading axis i.e. in 0° and in test 3, the sample was placed in a way that the leg of the composite sample consisting of sensor C was along the loading axis i.e. in 0°, sensor A in 90° and sensor B & D interchanged their position for all three sensor systems, Figure 3-4. The step to interchange the positions of the sensor in test 3 was conducted to examine the load sensitivity of each sensor system and it didn't affect the comparison of the mechanical performance of the composite samples. Three composite specimens were tested for each sensor system successfully, and mechanical behavior was plotted as elastic modulus and overall initial stress-strain curve which showed good repeatability in the behavior. Figure 3-5 shows a comparison of three samples and results confirmed that the mechanical behavior of all composite samples was similar irrespective of the choice of the loaded leg or the sensor system and was isotropic because of the use of the chopped glass fiber mat. The presence of any sensor system in different directions and positions did not affect the structure's integrity.

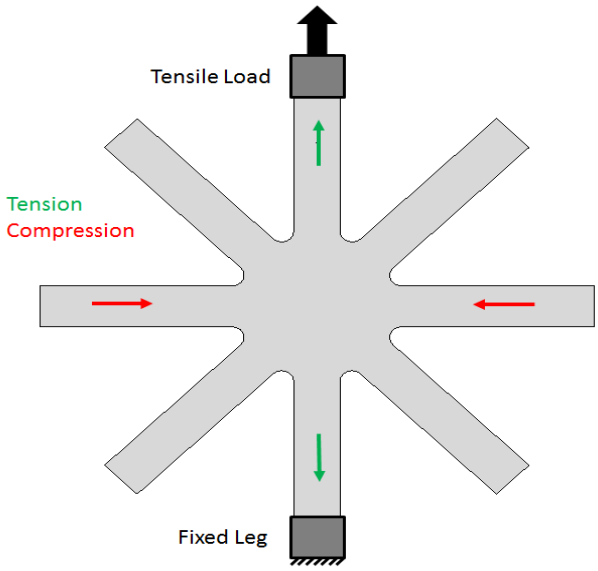

Figure 3-3: Deformation mechanism of the specimen during the applied tensile strain.

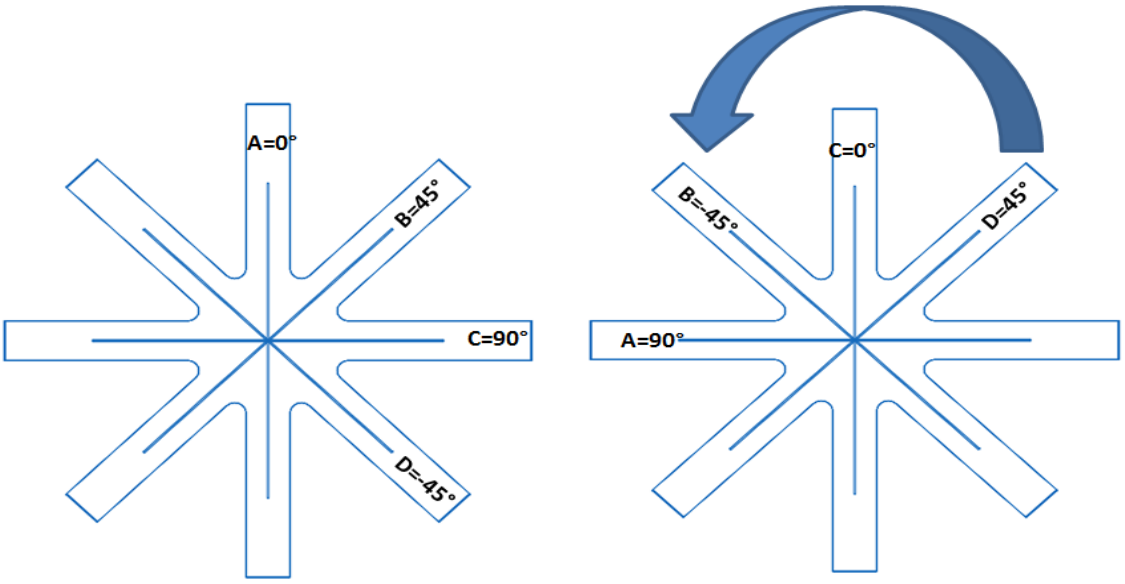

(a) Samples position in test 1 and 2 *(b) Sample position in test 3*

Figure 3-4: Placement of the composite sample between the fixture of the tensile machine

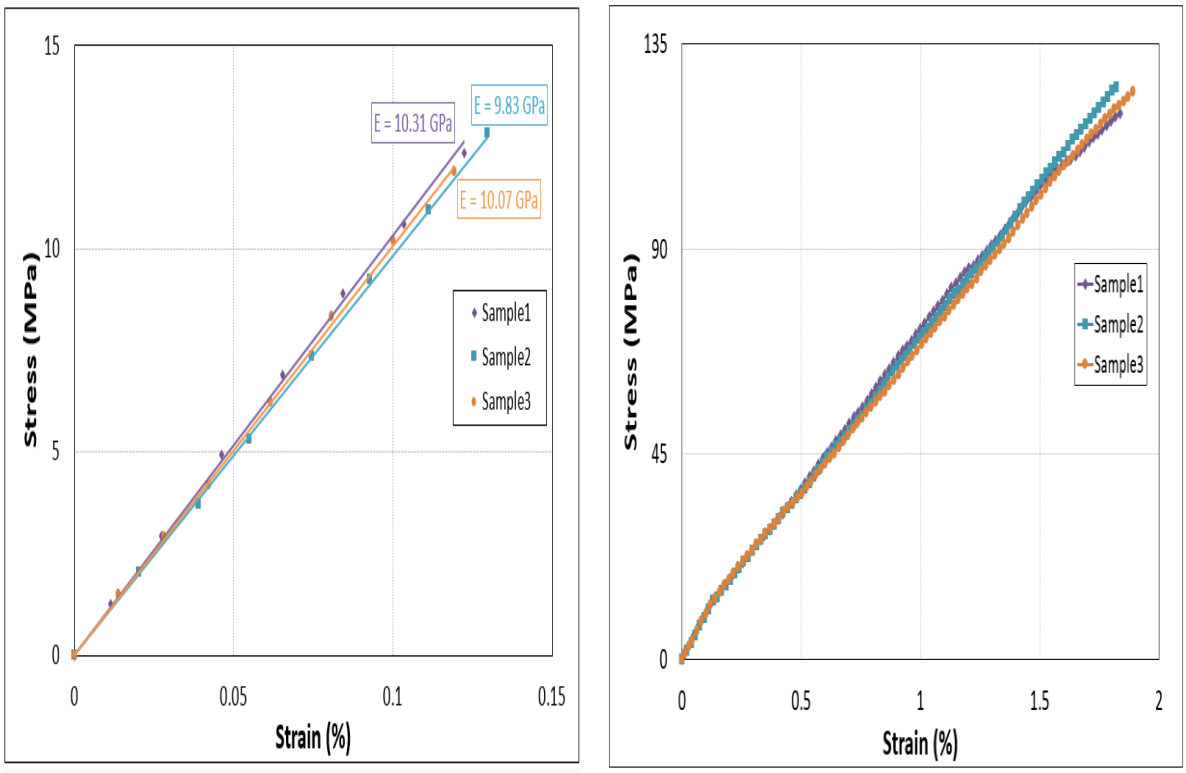

(a) Young's modulus (b) Overall initial stress-strain behavior

Figure 3-5: Mechanical performance of the composite star sample.

A. Sensor I: Nylon/Ag fiber sensor

Nylon/Ag fiber sensor showed good electrical signal response during all three mechanical tests of the composite star specimen. The resistance was changing in each case with the gradual

increase of the load and the fiber sensor showed a similar response in all 4 directions i.e. 0°, +45°, and 90°. The electrical response of each Nylon/Ag fiber sensor showed a change of resistance with an increase of strain in the specimen, however, during deformation the Nylon/Ag fiber sensor within the specimen showed different behavior because of its position and direction regarding the loading axis. This showed that it not only monitored the deformation but, also identified it as to whether it was compressive, tensile, or both. Test 1 and test 2 were performed by placing the specimen in such a way that sensor A was in the loading direction and sensor C was in the transverse direction while in test 3, the specimen was placed in such a way that sensor C was in the loading direction and sensor A was in the transverse direction. The cyclic tensile test further confirmed the reproducibility of electrical response and the real-time strain monitoring behavior of the Nylon/Ag fiber sensor under the 10 cycles of tensile load. This showed that the Nylon/Ag fiber sensor also had stability in the detection response and long-term response cycle. This also verified that this fiber sensor can be reused unless it is fractured even then; the divided part of the fiber sensor could be used as a sensor for damage detection. During the applied cyclic strain as high as between 1-2% and for 10 cycles, the Nylon/Ag fiber sensor perfectly correlated with the applied strain in each cycle. This confirmed the durability and stability of the sensor.

- Test 1 and Test 2 confirmed the reproducibility of electrical response and the real-time strain monitoring behavior of the Nylon/Ag fiber sensor. All sensors A, B, C, and D showed changed in resistance during the deformation and correlated perfectly in both tests, Figure 3-6. Moreover, it was observed that the maximum increase in resistance was recorded by sensor A which confirmed maximum tensile deformation occurred in the loading direction. However, sensor C showed a decrease in resistance and this negative behavior confirmed the presence of compressive strain and deformation which established the Poisson's effect during the deformation of the structure. The minimum change in resistance was recorded by sensors B and D and both sensors showed identical responses. This identical response of sensors B and D was because in isotropic material, these two directions are a mirror of each other regarding the loading axis. However, slight diminution with less than 1 % was recorded for the sensor A in comparison with the sensor B, C, and D. This reduction was negligible in comparison to the overall behavior during the cyclic loading. Nevertheless, the reason behind this behavior of sensor A was because sensor A was placed in the loading direction and was experiencing the maximum effect of the applied strain. Moreover, the applied cyclic strain was

applied between 1-2% which is within the plastic deformation regime. Sensor A might experience minute permanent deformation during cyclic tensile and compressive strain because of the Poisson's effect during the loading and unloading of the cyclic load.

- Test 3 was performed and compared with Test 1 to check the sensitivity of the Nylon/Ag fiber sensor with respect to the loading axis, Figure 3-7. This comparison was carried out to not only confirm the strain detection response of the Nylon/Ag fiber sensor but also showed its sensitivity to the applied load or loading direction. Sensor C recorded the maximum increase in resistance in test 3 because it was placed in the loading direction while sensor A showed a decrease in resistance because it was in a transverse direction regarding the loading axis. However, sensors B and D showed similar behavior in both tests because of their identical response in both directions i.e. +45°. Moreover, it was observed that the change in resistance was the same in each direction in both tests irrespective of the sensor. For example, sensor A in test 1 and sensor C in test 3 showed a similar change in resistance because both placed along the loading axis. This confirmed that the sensitivity of the sensor was dependent on its position and direction of the applied load otherwise the response of each sensor A, B, C, and D can be similar, and, in every case, the strongest signal was recorded along the loading direction, Figure 3-8.

In each specimen, the sensor did not only detect the deformation but also distinguished between the type of deformation whether it was tensile or compression.

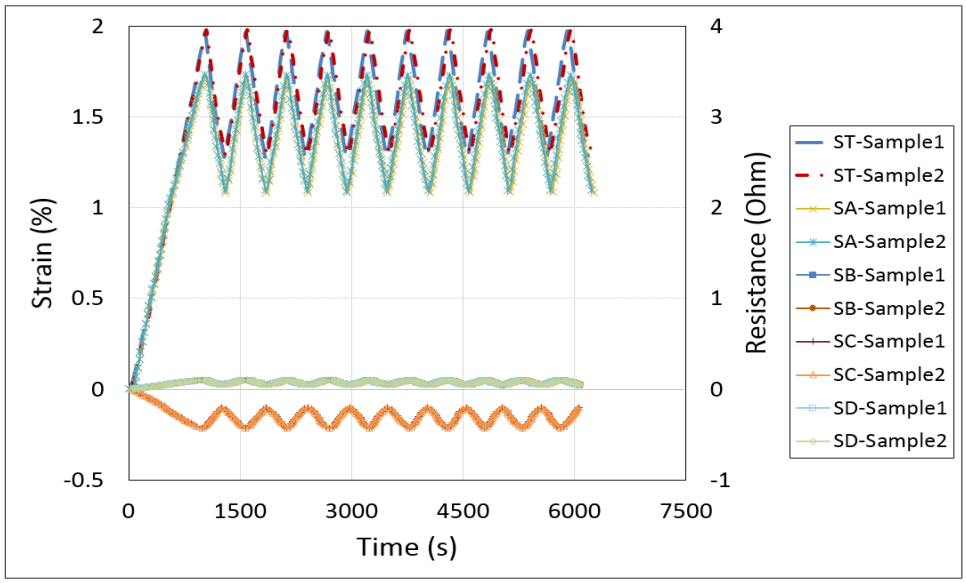

Figure 3-6: Real-time strain monitoring by Nylon/Ag fiber sensor in the composite star specimen during cyclic tensile

loading

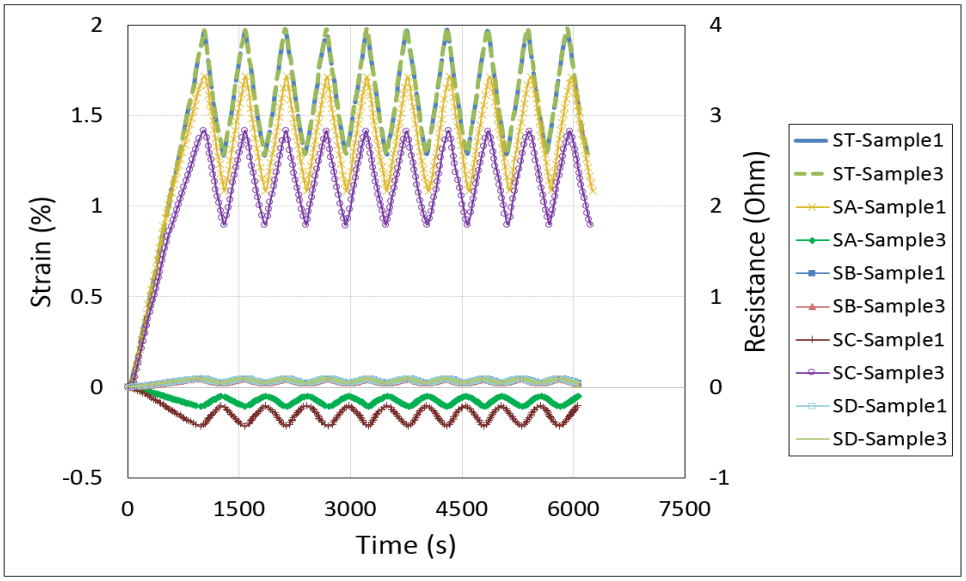

Figure 3-7: Real-time strain monitoring by Nylon/Ag fiber sensor during cyclic tensile strain. In test-1, sensor A was along the loading axis, sensor B at 45, sensor C at 90° and sensor D in -45° while in test-3 the specimen was placed transversely with respect to the specimen 1 and sensor C was along the loading axis, sensor D at 45, sensor A at 90° and sensor B in -45°.

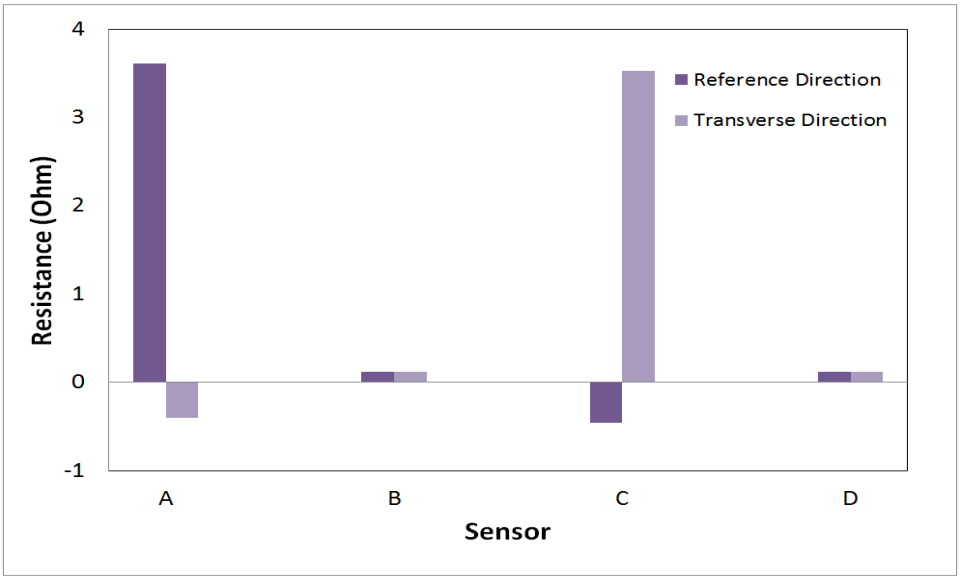

Figure 3-8: Sensitivity of the Nylon/Ag fiber sensor with respect to the loading axis

B. Sensor II: CM sensor

Flexible CM sensor displayed good electrical variation during the strain deformation of the composite specimen in all three experimental tests. The resistance of CM sensor in each composite sample showed gradual change during each cycle of applied strain and showed

similar behavior in each direction. However, the electrical resistance of CM sensor within a single specimen showed difference intensity in the change of the signal with the applied strain because of their specific direction i.e. 0°, ±45°, 90° with respect to the loading axis. This showed that the CM sensor did not only monitor the strain but also showed the amount of strain-induced in each direction with respect to the applied load. Moreover, consistency of the recorded signal during all 10 cycles showed the stability, durability, and integrity of the CM sensor.

- Tests 1 and 2 were performed to further confirmed the repeatability in the behavior of the CM sensor when produced in different batch. All the sensors A, B, C, and D presented variation in resistance according to the intensity of the deformation in their direction and correlated perfectly in both tests and each cycle, Figure 3-9. Furthermore, sensor A demonstrated the maximum change in its resistance when subjected to the cyclic loading that established the presence of maximum deformation of the sample in the loading direction because of the tensile elongation. Then, sensor B and D presented less variation in their resistance during the cyclic strain in comparison with sensor A because of their direction. Moreover, sensor place in B and D direction displayed an identical change in resistance which is because these two positions were the mirror of each other regarding the loading axis and they confirmed the isotropic nature of the material. CM sensor in position C showed minimum variation in the resistance due to its transverse direction with respect to the loading axis. This change was positive however, negative change was expected because of the compressive strains, to justify the Poisson's effect under tensile loading. This positive change could be because of the complex interaction between the laminar stresses and the conduction behavior of the CNTs in the conductive membrane. One reason could be the fact that the curing process densified the arrangement of the CNT network in the layers of conductive membrane and additional compression could not cause a further reduction in the resistance of the CM sensor [39].
- Sample 3 was tested and compared with the results of Sample 1 to test the load sensitivity of the CM sensor, Figure 3-10. In test 3, sensor C recorded the maximum change in the resistance during the cyclic tensile load because of its position along the loaded axis and sensor A showed detection of minimum strain deformation because of its transverse position with respect to the loading axis. However, CM sensors placed in B and D showed an identical change in the signal because of their similar direction according to the loading axis in both tests 1 and 3 i.e. $\pm$45°. Moreover, it was observed

that the intensity of the change in signal of the CM sensor in a particular position was similar in both cases i.e. test 1 and 3 regardless of sensor label. For instance, sensor A in test 1 and sensor C in test 3 showed the almost equal intensity of the increase in resistance with the applied strain because of a similar position. Similar behavior was observed for the rest of the position which confirmed that the position of the sensor plays a key part in not only detecting the deformation but also identify the amount of strain produced in the respective direction. Thus, this confirms the sensitivity of the sensor is dependent on their location according to the loading direction, Figure 3-11.

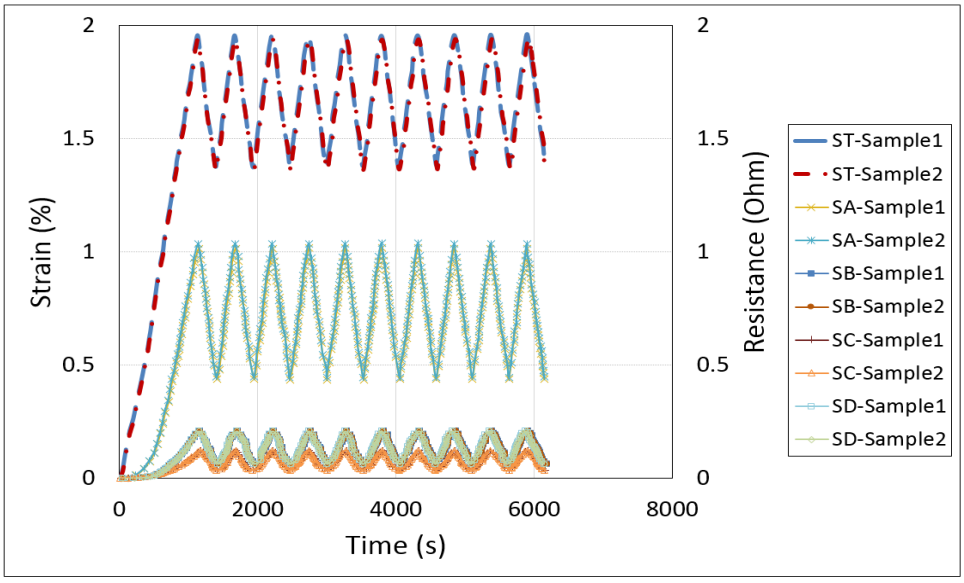

Figure 3-9: Real-time tensile strain monitoring in the composite by CM sensor and verification of the reproducibility of the test

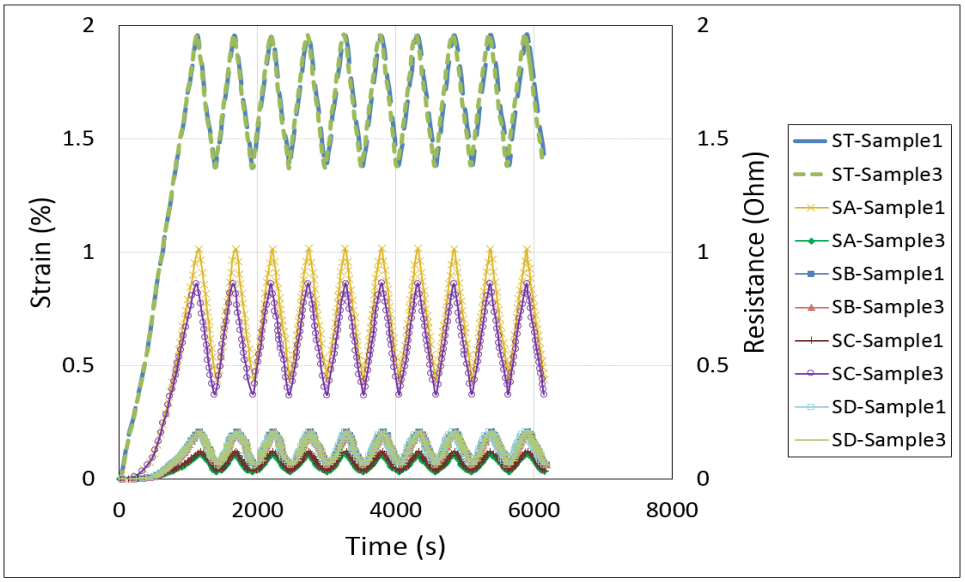

Figure 3-10: Comparison of real-time strain monitoring of composite star specimen by CM sensor during test 1 (when sensor A is placed in loading direction) and test 3 (when sensor C is placed in loading direction).

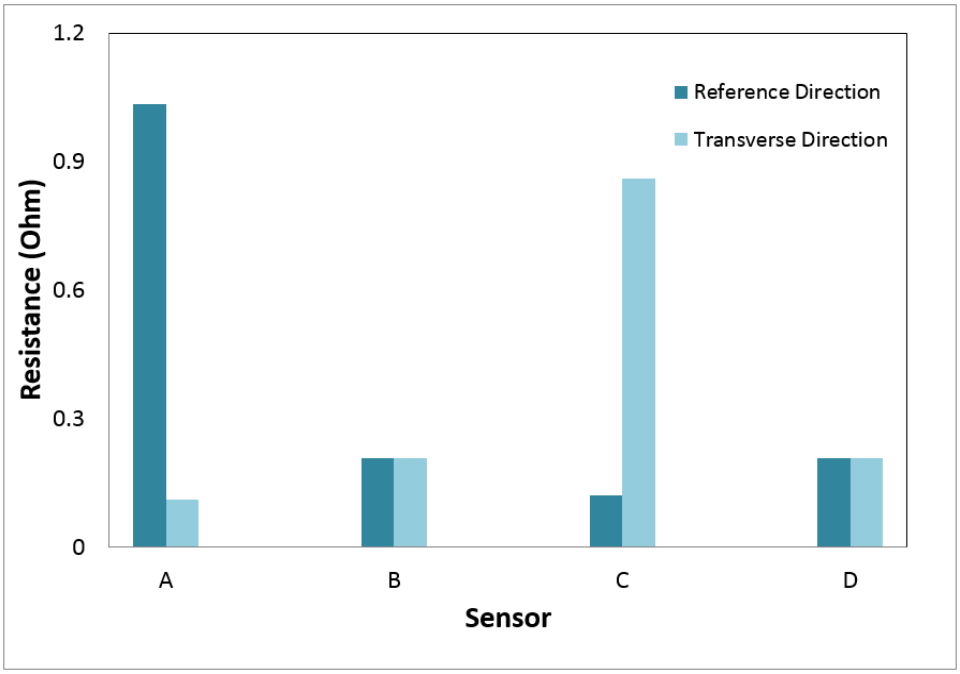

Figure 3-11: Effect of position and direction on the sensitivity of the CM sensor with respect to the applied load.

C. Sensor III: CF sensor

Flexible CF sensor displayed good electrical variation during the strain deformation of composite specimens in all three experimental tests. The resistance of CF sensor in each composite sample showed gradual change during each cycle of applied strain and showed

similar behavior in each direction. However, the electrical resistance of CF sensor within a single specimen showed difference intensity in the change of the signal with the applied strain because of their specific direction i.e. 0°, ±45°, 90° with respect to the loading axis. This showed that the CF sensor did not only monitor the strain but also showed the amount of strain-induced in each direction with respect to the applied load. Moreover, consistency of the recorded signal during all 10 cycles showed the stability, durability, and integrity of the CF sensor.

- Tests 1 and 2 were performed to further confirmed the repeatability in the behavior of the CF sensor when produced in different batch. All the sensors A, B, C, and D presented variation in resistance according to the intensity of the deformation in their direction and correlated perfectly in both tests and each cycle, Figure 3-12. Furthermore, sensor A demonstrated the maximum change in its resistance when subjected to the cyclic loading that established the presence of maximum deformation of the sample in the loading direction because of the tensile elongation. Then, sensor B and D presented less variation in their resistance during the cyclic strain in comparison with sensor A because of their direction. Moreover, sensor place in B and D direction displayed an identical change in resistance which is because these two positions were the mirror of each other regarding the loading axis and they confirmed the isotropic nature of the material. CF sensor in position C showed minimum variation in the resistance due to its transverse direction with respect to the loading axis. This change was positive, however, negative change was expected because of the compressive strains, to justify the Poisson's effect under tensile loading. This positive change could be because of the complex interaction between the laminar stresses and the conduction behavior of the carbon filaments in the CF. As discussed before, the filaments are loosely aligned together in one direction and were only attached in the ends in the CF sensor. The compression strain in the transverse direction could indeed cause the decrease in length of the sensor which would result in the decrease in its resistance but, this compression might cause the increase in the contact distance between the loosely aligned filaments of CF sensors and this could be further facilitated by the tensile elongation in the middle of the specimen where all sensors are passing through the center. That is why the sensor in the transverse direction showed minimum but positive change in the resistance.
- Sample 3 was tested and compared with the results of Sample 1 to test the load sensitivity of the CF sensor, Figure 3-13. In test 3, sensor C recorded the maximum change in the resistance during the cyclic tensile load because of its position along the

loaded axis and sensor A showed detection of minimum strain deformation because of its transverse position regarding the loading axis. However, CF sensors placed in B and D showed the identical change in the signal because of their similar direction according to the loading axis in both tests 1 and 3 i.e. ±45°. Moreover, it was observed that the intensity of the change in signal of the CF sensor in a particular position was similar in both cases i.e. test 1 and 3 regardless of sensor label. For instance, sensor A in test 1 and sensor C in test 3 showed the almost equal intensity of the increase in resistance with the applied strain because of a similar position with minor variation. Similar behavior was observed for the rest of the position which confirmed that the position of the sensor plays a key part in not only detecting the deformation but also identify the amount of strain produced in the respective direction. Thus, this confirms the sensitivity of the sensor is dependent on their location according to the loading direction, Figure 3-14.

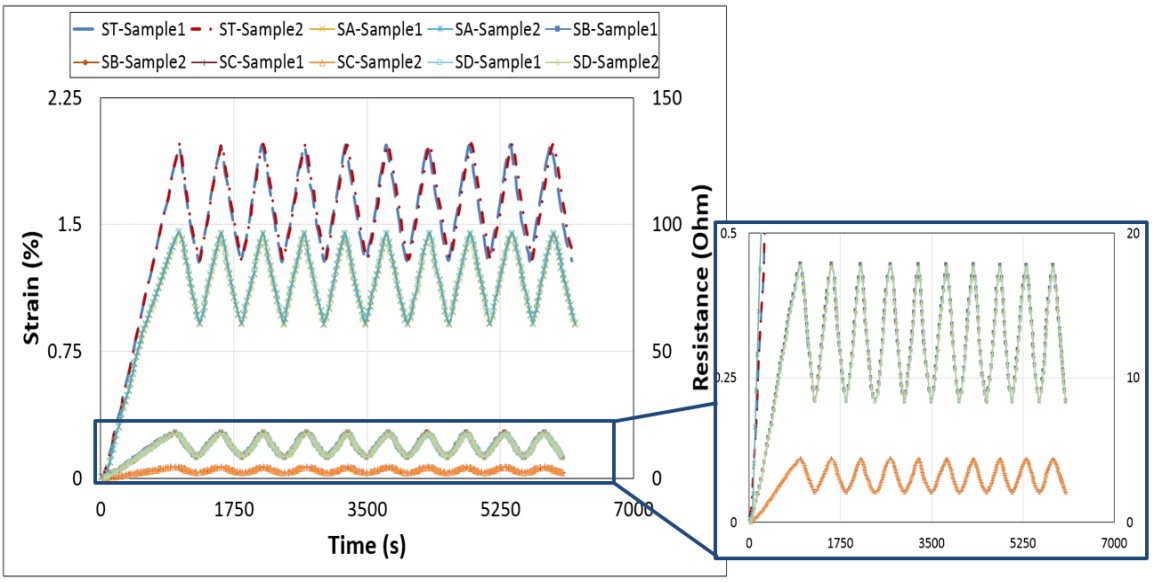

Figure 3-12: Real-time tensile strain monitoring in the composite specimen by CF sensor and verification of the test reproducibility.

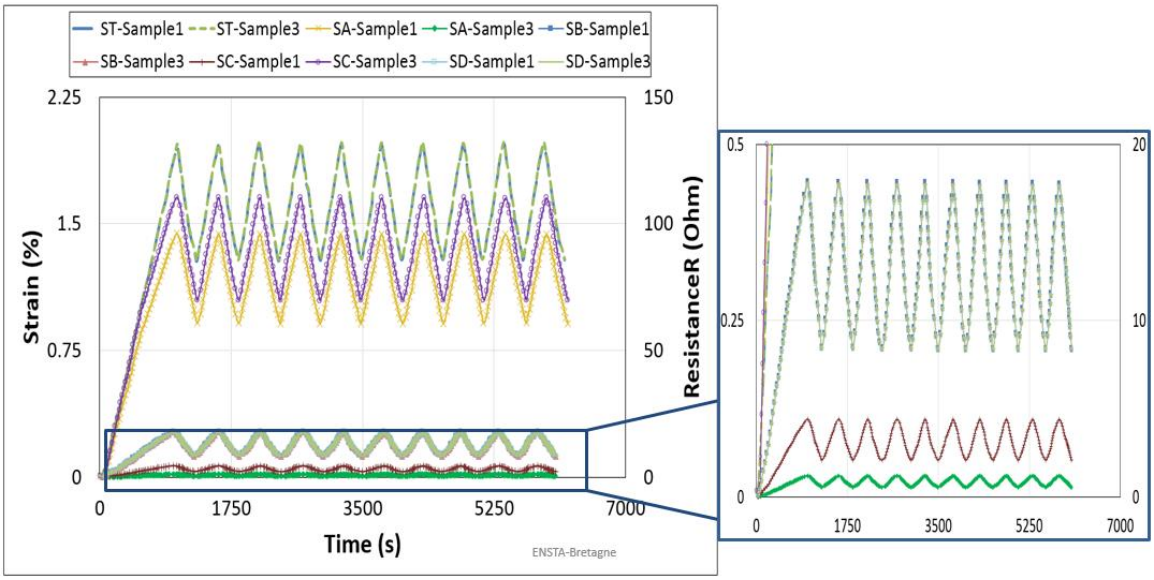

Figure 3-13: Comparison of real-time strain monitoring of composite star specimen by CF sensor during test 1 (when sensor A is placed in loading direction) and test 3 (when sensor C is placed in loading direction).

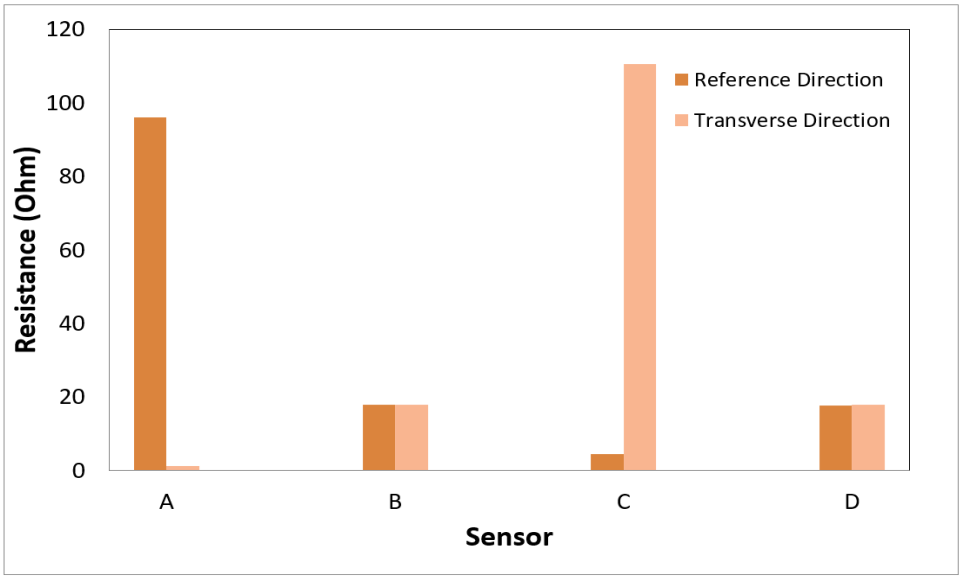

Figure 3-14: Effect of position and direction on the sensitivity of the CF sensor with respect to the applied load.

3.4.2. Strain monitoring in composites during cyclic flexural loading

It was important to evaluate the flexural behavior of the composite sample to understand the signal of each sensor system. Star specimens were placed in the machine as a simply supported beam with one leg of the specimen placed on the bottom rollers and flexural deflection and force was applied by the third roller at the center of the span length of the respective leg of the star sample, Figure 3-15 (a). Moreover, each test sample was placed in the machine in such a

way that sensor A was along the roller axis and the leg of the star sample with sensor C was between the three rollers i.e. along the span length. When the star samples were applied with the flexural deflection, the sample strained inside the span length and this deformation resulted in compression strain at the top surface (shown by green) because of the compressive forces applied by the roller whereas, this deformation caused tensile strain near the bottom surface because of the elongation (shown by red arrows), Figure 3-15 (b). Then these compressive and tensile deformations progressed through each ply from the top and bottom surface and could result in macro damage such as fiber fracture, matrix cracking, and/or interlaminar shear failure.

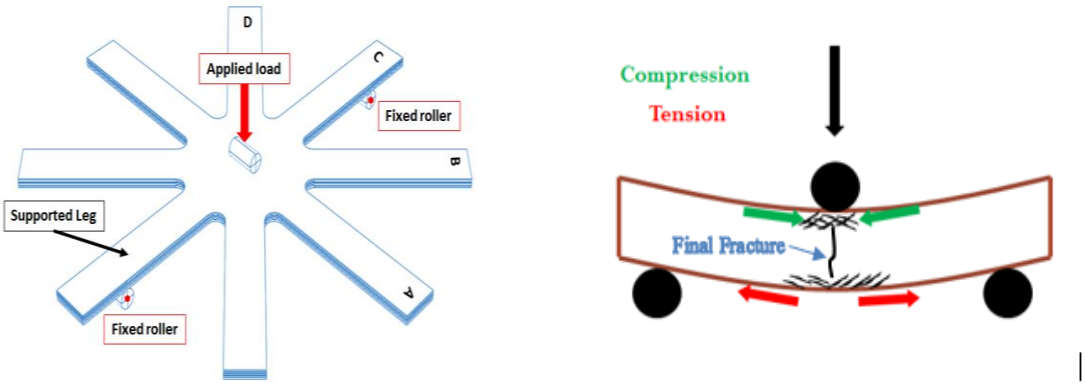

(a) Placement specimen in the machine (b) Deformation behavior of the specimen

Figure 3-15: Deformation behavior of star specimen during a three-point bend test.

Three flexural tests were performed successfully. Sample 1 & 2 were placed in the machine in such a manner that sensor A was in the bottom position along the roller axis (case I) and the leg with sensor C was between the rollers. However, sample 3 was placed in the machine in such a manner that sensor A was in the top position, sensor D was in the bottom position (case II) while keeping the leg with sensor C between the rollers, Figure 3-16. This step was performed to test the sensitivity of the fiber sensor and its ability to detect and identify the type of deformation within the plies of the composite under flexural deformation and results showed that it did not affect the mechanical performance of the specimens with good repeatability in results, Figure 3-17. Moreover, experimental mechanical properties consisting of flexural strength, strain, and modulus were calculated using equations (3-1) - (3-3)

$$\sigma_f = \frac{3FL}{2bd^2} \tag{3-1}$$

$$\varepsilon_f = \frac{6Dd}{L^2} \tag{3-2}$$

$$E_f = \frac{L^3 m}{4bd^3} \tag{3-3}$$

Where, σ_f is flexural stress, ε_f is flexural strain, $E_{f\,is}$ flexural modulus of elasticity, *F* is the load at a given point on the load-deflection curve, *L* is span length, *b* is the width of the specimen, *d* is thickness, *D* is deflection, and *m* is the gradient of the initial straight-line portion of the load-deflection curve.

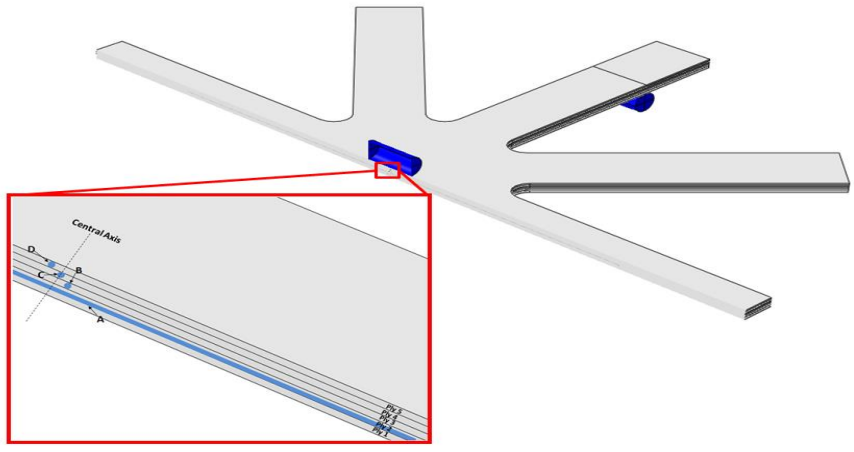

(a) Case I

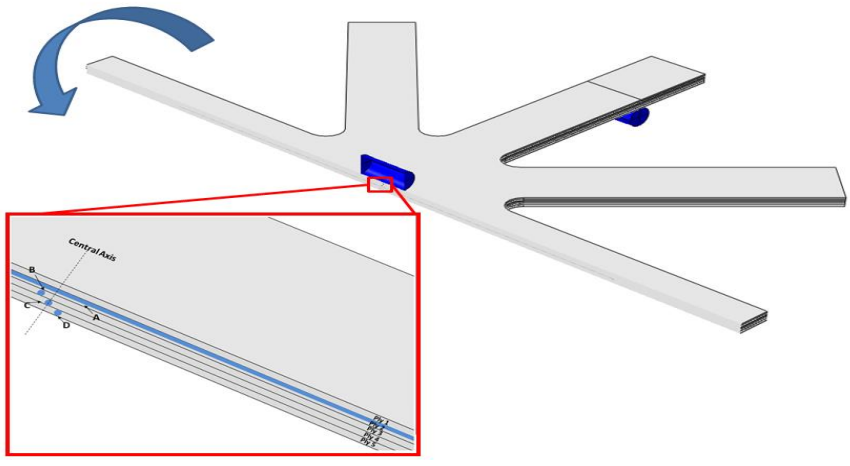

(b) Case II

Figure 3-16: Position of the composite star samples with Nylon/Ag fiber sensor as an example between the three rollers for flexural bending (a) Sample placement in test 1 and 2 and (b) Sample placement in test 3.

Moreover, the mechanical behavior of all the three star-samples was similar to each other regardless of the placement of the specimen. This further confirmed that the placement of fiber

sensors at different positions [40] and directions did not influence the mechanical behavior and integrity of the composite sample and its isotropic nature. Although, it should be kept in mind that the objective of this study was to examine the sensitivity and in-situ monitoring response of each sensor system incorporated into the composite specimens subjected to cyclic flexural loading.

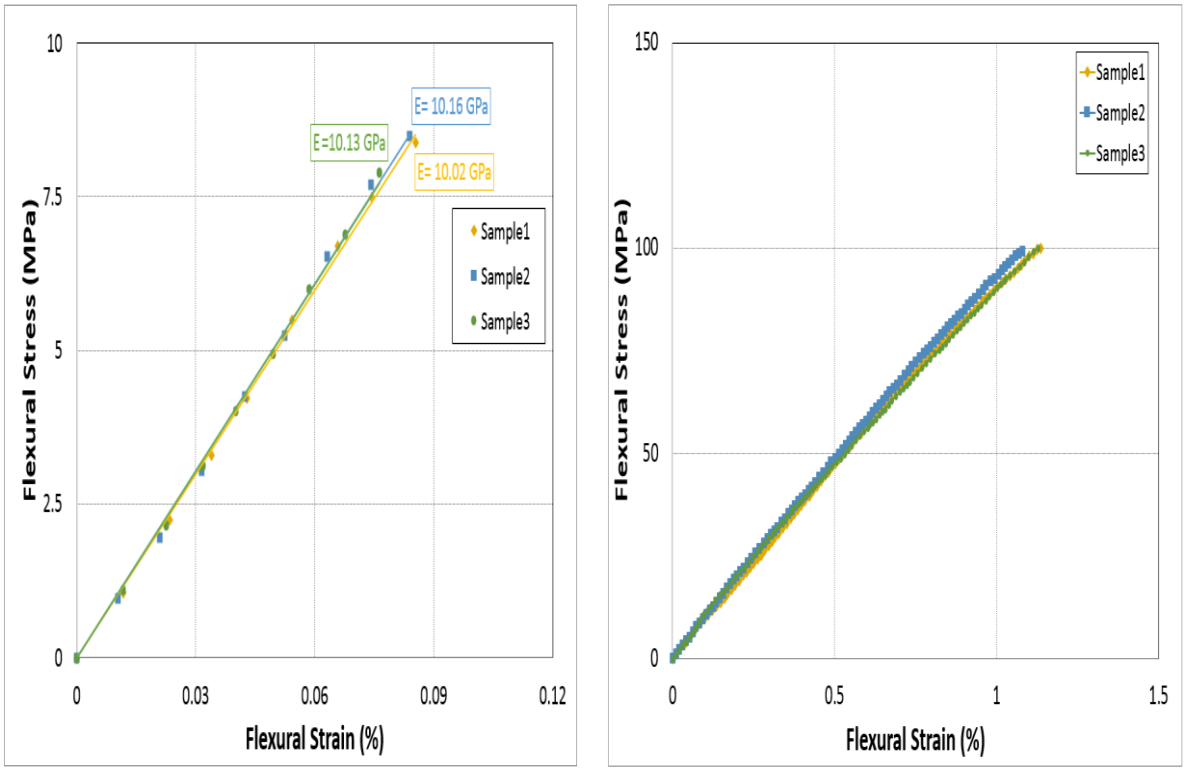

(a) Young's modulus *(b) Overall initial flexural stress-strain behavior*

Figure 3-17: Mechanical behavior of all three star-samples during flexural deflection.

A. Sensor I: Nylon/Ag fiber sensor

The resistance of the Nylon/Ag fiber sensor changed gradually in each case with the strain applied and demonstrated good signal response but, when samples were deforming each fiber sensor inside the sample demonstrated unique signal response because of their specific position regarding the roller axis and position through the thickness. Test 1 and test 2 were conducted by performed by positioning the specimens in such manner that sensor A along the roller axis and was on the bottom position regarding the thickness or loading axis while the specimen of test 3 was positioned in such manner that sensor A was along the roller axis but was on the top position regarding the thickness or loading axis. The position of the other sensors i.e. B, C, and

D was changed accordingly (as discussed previously) however, the leg of the star specimen with sensor C remained the loaded leg in all two cases. Test 1 and Test 2 validated the repeatability in electrical response and in-situ monitoring behavior of the fiber sensor. All four fiber sensors showed changed in resistance and correlated perfectly during the mechanical deformation of the composite specimen in both tests, Figure 3-18. Also, it was detected that all fiber sensors were showing a decrease in resistance with an increase in strain and vice versa. The magnitude of change in resistance of sensor C was maximum in comparison with sensors A, B, and D. Test 3 was conducted and related with test 1 to understand the sensitivity of the fiber sensor regarding the loading axis and placement through the thickness of the specimen, Figure 3-19. Sensor C which was place within the loaded leg in both cases showed opposite behavior and demonstrated the maximum increase in resistance in test 3 while the other three sensors again showed a decrease in resistance however, change in the magnitude of each signal was recorded. In both cases all 4 sensors showed interesting behavior and it was necessary to compare and discuss in detail the response of each fiber sensor sequentially to understand the deformation behavior of the composite star specimen.

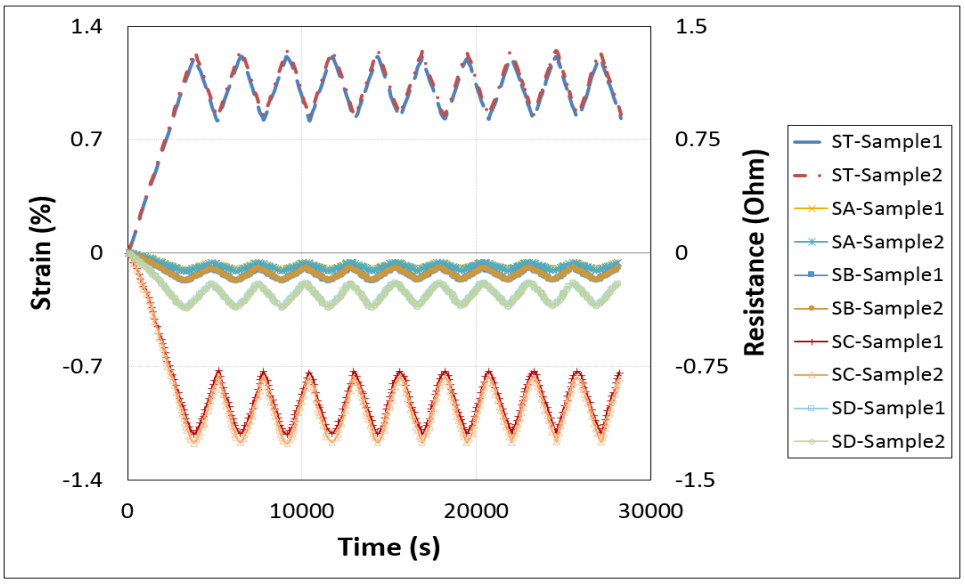

Figure 3-18: In-situ flexural strain monitoring in composite star sample by Nylon/Ag fiber sensor and validation of electrical response of each fiber sensor.

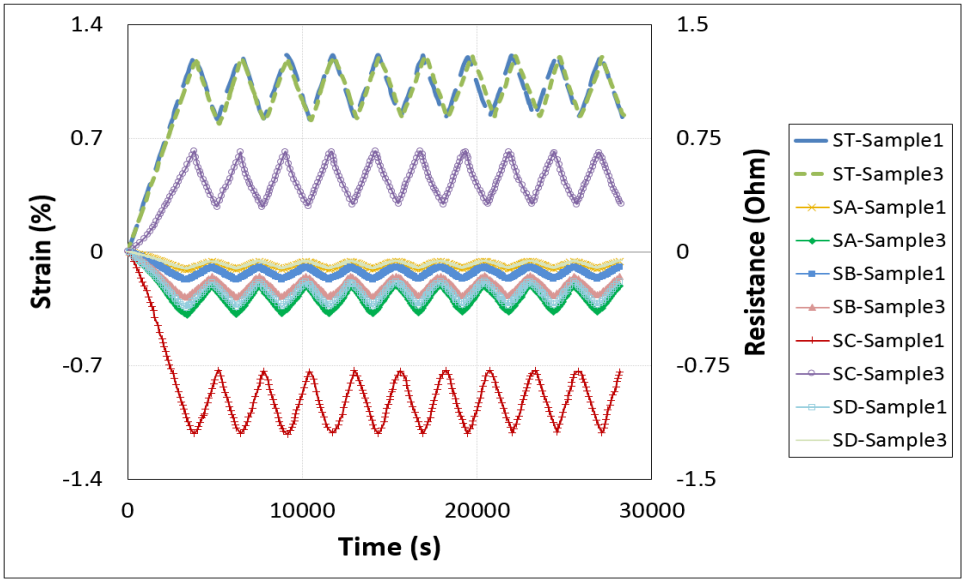

Figure 3-19: In-situ flexural strain monitoring by Nylon/Ag fiber sensor and study of strain sensitivity of each fiber sensor with respect to its position. In test-1, sensor A was on the bottom position with respect to the loading axis, while in test-2 the specimen was rotated with respect to the roller axis and placed in such a manner that sensor A was on the top position with respect to the loading axis.

- Sensor A: as described earlier, it was placed in 0° direction with respect to the roller axis in both cases however, in case I it was positioned on the bottom while in case II it was positioned on the top. It should be kept in mind that this leg of the star specimen was not supported by the rollers and was not under the direct flexural load whether it was the case I or II. This leg of the star specimen was only under the localized effect of the central roller which was applying the load and displacement to the specimen. This localized effect resulted in the detection of compression strains that could be generated in the surface beneath the central roller. In addition, the increase in the magnitude of the signal justified the position of the sensor A with respect to the loading axis/through-thickness i.e. in case I it was at the bottom position where minimum compression strain was generated while in Case II it was on the top position where the effect of the compression strain is maximum Figure 3-18 & 3-19.

- Sensor B: as described earlier, sensor B was placed in 45° direction with respect to the roller axis in both cases, however, in case I it was positioned second from the bottom while in case II it was positioned second from the top surface i.e. between the plies 2 and 3. This leg of the star specimen was also not supported by the rollers and was not under the direct flexural load whether it was case I or II. It was also only under the localized effect of the central roller which was applying the load and displacement to

the specimen. This localized effect resulted in the detection of compression strains that could be generated in the surface beneath the central roller. However, the magnitude of change in resistance of sensor B in comparison with sensor A in case I was more because it was closer to the effect of central roller than sensor A, Figure 3-18. In addition, when the position of the specimen was changed in case II, sensor B showed an increase in the magnitude of the signal in comparison with the signal of the sensor B in case I because of more effect of applied compression load by the central roller, Figure 3-19. But this increase in magnitude was less than the increase in the magnitude of the signal of sensor A in case II because when the position of the specimen was changed sensor A was more in contact with the central roller than sensor B where the effect of compression strain was higher, Figure 3-20.

- Sensor C: as described earlier, sensor C was placed in 90° direction with respect to the roller axis in both cases, however, in case I it was positioned third from the bottom while in case II it was positioned third from the top surface i.e. between the plies 3 and 4. This leg of the star specimen was the only segment of the star specimen supported by the rollers and was under the direct flexural load whether it was the case I or II. The whole leg experienced the bending effect during the experiment and showed the most interesting behavior. This sensor did not only show a change in the magnitude of the signal but also showed different deformation detection. In case I, sensor C showed a decrease in resistance with the increase in the applied strain and the magnitude of the signal was maximum in comparison with sensors A, B, and D, Figure 12. This maximum magnitude of the signal in case I of sensor C was not only because it was closer to the effect of the applied compression load by the roller but also because of the reason that this whole leg of the star specimen was deforming, and the sensor detected the overall deformation in the leg instead of localized deformation, Figure 3-18. Also, when the position of the specimen was changed in case II, sensor C was the only sensor showed an increase in resistance with the increase in the applied strain in addition to the maximum magnitude of the signal in comparison with the other fiber sensors, Figure 3-19. The increase in resistance confirmed the detection of tensile deformation near the bottom surface of the composite star specimen and justified the deformation mechanism of the specimen which is subjected to flexural loading, Figure 3-20. However, the magnitude of the signal of the sensor C during the detection of tensile deformation was less than the magnitude of the signal during the detection of compression strain because

of its position through the thickness of the specimen.

- Sensor D: as described earlier, it was placed in -45° direction with respect to the roller axis in both cases. However, in case I, it was positioned on the top while in case II it was positioned on the bottom, Figure 3-18 & 3-19. It should be kept in mind that this leg of the star specimen was not supported by the rollers and was not under the direct flexural load whether it was the case I or II. This leg of the star specimen was only under the localized effect of the central roller which resulted in the detection of compression strains that could be generated in the surface beneath the central roller. In addition, the decrease in the magnitude of the signal justified the position of the sensor D with respect to the loading axis/through-thickness i.e. in case I it was at the top position where maximum compression strain was generated while in case II it was on the bottom position where the effect of the compression strain is minimum. It was also observed sensor A in case I and sensor D showed similar behavior and vice versa because in case I and II sensor A and D interchanged their position from top to bottom with respect to the thickness, Figure 3-20.

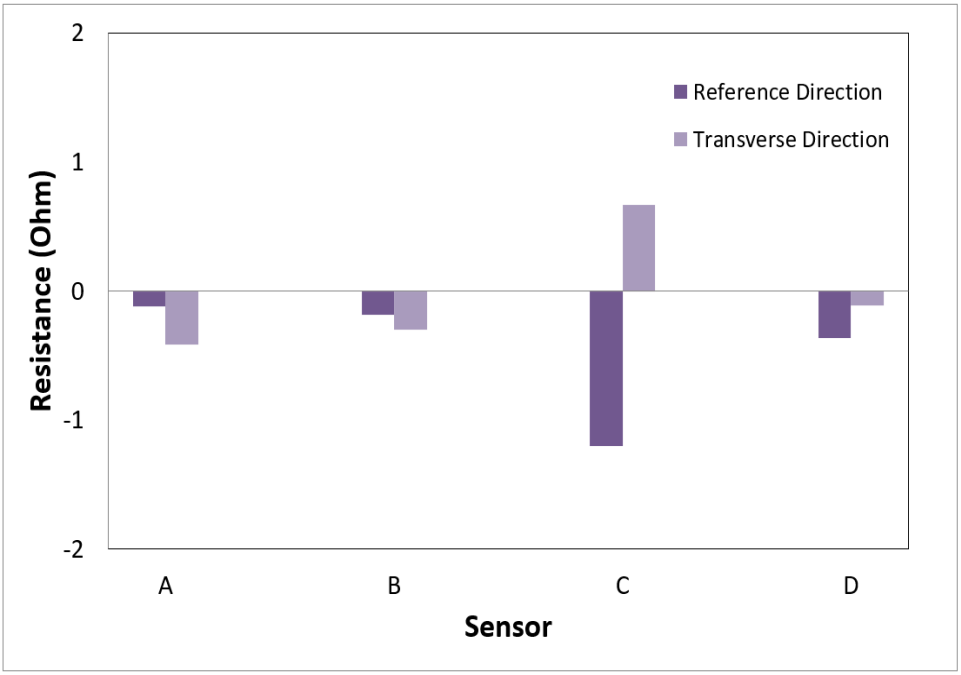

Figure 3-20: Effect of position and direction on the sensitivity of the Nylon/Ag fiber sensor with respect to the loading axis and position through-thickness.

B. Sensor II: CM sensor

The change in electrical resistance of CM sensor was gradual with the applied strain during the flexural deflection with good repeatability in results during each cycle, however, CM sensor in each position showed a distinct change in behavior according to their respective direction according to the roller axis and location between each plie (through-thickness). As discussed before, Sample 1 and 2 were tested with sensor A in the top location and aligned with the roller axis to demonstrate the repeatability in the response and real-time strain monitoring of the CM sensor when prepared in different batch. CM sensor in all four positions showed a gradual change in their resistance and correlated perfectly with the applied strain, Figure 3-21. Moreover, it was observed that CM sensor in all four positions showed a positive change in the resistance with different intensities of the signal. Test 3 was performed to test the position sensitivity of the CM sensor with the loading axis (perpendicular to the specimen) in which sensor A was in the bottom position and position of the other sensors was changed accordingly, Figure 3-22. Even in test 3, CM sensor in all four positions showed a positive change in resistance during the cyclic flexural load with a change in the intensity of the signal with the change of the position. However, it was expected to see a negative change in resistance in the place of compressive strain and positive change is resistance in place of tensile strain [41], but this was not seen in the results because of the same reason discussed in previous section 3.4.1 i.e. real-time strain monitoring during tensile deformation.

In both cases, the CM sensor in all four positions showed distinct performance which was required to be discussed in detail consecutively to understand the detection of deformation during the flexural bending by CM sensor in each position.

- Sensor A: was in 0° direction regarding the roller axis and was positioned on top in case I and in the bottom in case II. It must be noticed that this leg of the star sample wasn't loaded directly but was under the indirect influence of the flexural load applied by the top roller in both cases. This leg of the star sample was solitary under the localized compression of the center roller. Sensor A detected minimum strain deformation in case I while in case II it detected maximum strain deformation when it was in the bottom position, Figure 3-22. This confirmed that the CM sensor was able to detect the tensile elongation in case II but instead of showing the negative change in resistance when placed on the top position in case I to detect the compressive strains it showed a minimum positive change in the resistance which could be because of the densification of the CNT network in the conductive membrane during the curing process of the composite sample. However, changing the position of the

CM sensor in both cases showed the change in the sensitivity of the sensor with respect to the position and applied load axis, Figure 3-23.

- Sensor B: was in +45° in case I and in -45° in case II regarding the roller axis while it was situated second from the top in former and second from the bottom in latter case i.e. between ply 2 and 3. This leg of the star sample was not under the direct impact of the flexural load as well but only under the localized influence of the central roller. In tests 1 and 2 sensor B showed good reproducibility in results and correlated perfectly with the applied strain in each cycle, Figure 3-21. But, the intensity of the change in the detection signal of sensor B in comparison to sensor A was increased because sensor B was closer to the center of the specimen where there is a combined effect tensile and compression exists not just the localized compression because of the roller. In comparison between test 1 and test 3, it was observed that the intensity of the signal of CM sensor change because of the change in the position, Figure 3-22. As discussed earlier the CM sensor shows good detection of a tensile strain than the compression because the network of CNTs already shows excellent conductance that further compression does not affect its resistance change. That is why in test 3, when sensor B was in position near the bottom surface of the composite sample, it experiences elongation when the said region was under the effect of tensile strain and showed an increase in the intensity of the detection signal, Figure 3-23.

- Sensor C: was in 90° direction regarding the roller axis in both cases I and II and in the leg of the star specimens placed between the rollers, along the span length and between the 3rd and 4th ply. This leg of the star sample was the one section in addition to the center of the specimen which was fully under the effect of bending deflection in both cases. During test 1 and test 2, CM sensor as sensor C showed maximum intensity in the detection signal in comparison with all the other sensor positions and correlated perfectly in each cycle of the applied strain, Figure 3-21. This is because of the two reasons, first, it was placed within the loaded leg of the star sample and was under the maximum influence of the flexural deflection and second in case I (test1 and test 2) it was positioned below the neutral axis of the specimen where the specimen experienced tensile strain and elongation. CM sensor detected the tensile strain by showing the increase in resistance with an applied deflection in each cycle and this detection was not localized but along the whole span length. However, in case II when the position of sensor C was change and was above the neutral axis, the intensity of the detection signal of sensor C was dropped because of the more effect of compression strain than the tensile deformation, Figure 3-22. So, even though sensor C was along the span length and

under the direct influence of the bending still its intensity of the signal was less then sensor A and sensor B according to its position, Figure 3-23.

- Sensor D: was in -45° direction in case I and 45° direction in case II regarding the roller axis and was in the bottom position in the former case and the top position in the latter case. This leg of the composite star sample was also not under the direct effect of flexural deflection but only under the localized influence of the central roller. During test 1 and test 2 (case I) in both star specimens, sensor D showed repeatability in detection signal and correlated with the applied strain in a good manner, Figure 3-21. In case I, sensor D showed the second-largest intensity in the detection signal after sensor C because of its position in the bottom of the specimen where it experienced tensile elongation during the deflection of the specimen between the rollers. It should be kept in mind that the change in resistance of sensor D was lower than sensor C even though it was in the bottom of the surface where maximum strain should be present because sensor C was along the span length in the loaded leg and under the direct influence of flexural bending as discussed before. In the comparison of the case, I and case II, the change in resistance of sensor D was decreased remarkably when its position was changed and it was placed in the top surface of the specimen in case II, Figure 3-22 & 3-23.

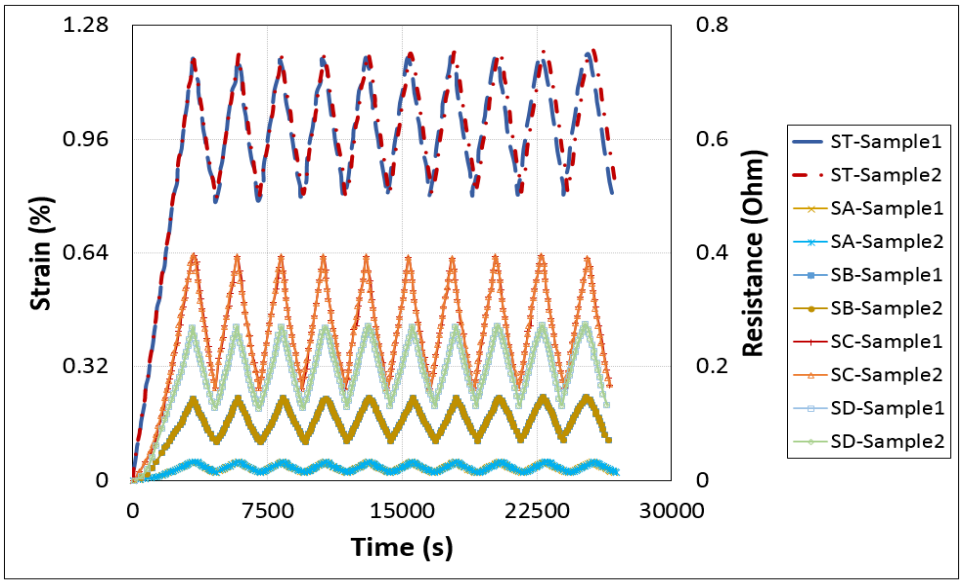

Figure 3-21: Real-time strain monitoring in composite star specimen during cycle flexural bending using CM sensor

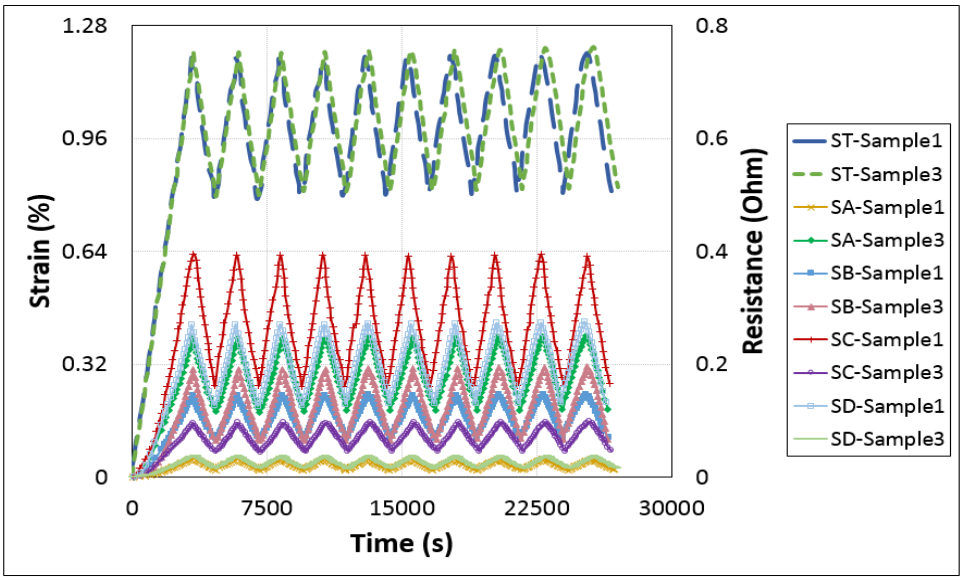

Figure 3-22: Comparison of real-time strain monitoring in composite star specimen during cycle flexural bending during test 1 (when sensor A is placed in top position according to the loading axis) and test 3 (when sensor A is placed in bottom position according to the loading axis).

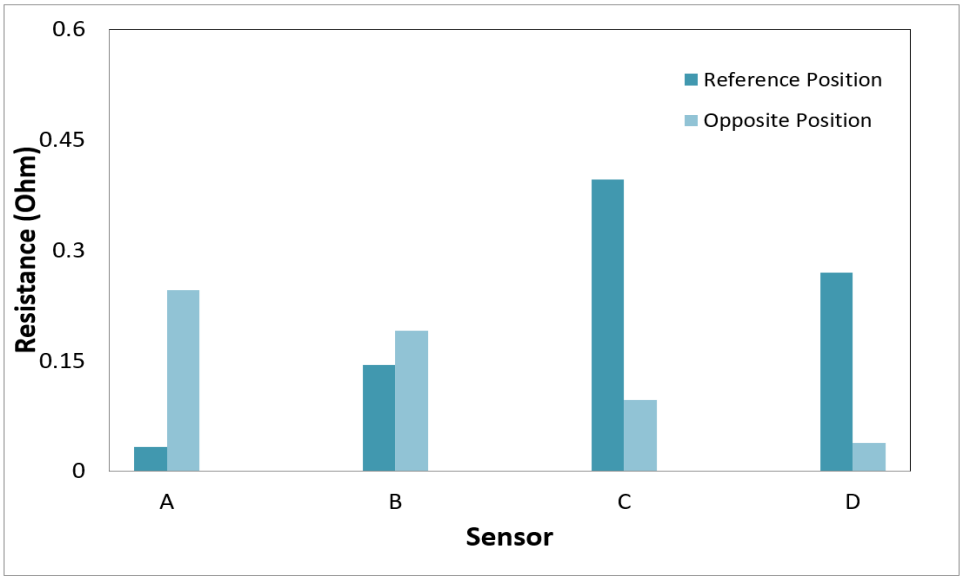

Figure 3-23: Effect of position and direction on the sensitivity of the CM sensor with respect to the loading axis and position through-thickness.

C. Sensor III: CF sensor

The change in electrical resistance of CF sensor was gradual with the applied strain during the flexural deflection with good repeatability in results during each cycle, however, CF sensor in each position showed a distinct change in behavior according to their respective direction according to the roller axis and location between each plie (through-thickness). As discussed

before, Sample 1 and 2 were tested with sensor A in the top location and aligned with the roller axis to demonstrate the repeatability in the response and real-time strain monitoring of the CF sensor when prepared in different batch. CF sensors in all four positions showed a gradual change in their resistance and correlated perfectly with the applied strain, Figure 3-24. Moreover, it was observed that CF sensors showed a positive change in resistance placed below the neutral axis and negative change in resistance placed above the neutral axis of the specimen during the bending. Test 3 was performed to test the position sensitivity of the CM sensor with the loading axis (perpendicular to the specimen) in which sensor A was in the bottom position and positions of the other sensors were changed accordingly, Figure 3-25. Even in test 3, CF sensors i.e. sensor C and D in two positions above the neutral axis showed a decrease in resistance and sensor A, B in two positions below the neutral axis showed an increase in resistance during the cyclic flexural load. Moreover, each sensor showed the different intensity of variation in resistance whether positive or negative thus, quantified the amount of damage induced in each direction and position.

In both cases, the CF sensor in all four positions showed distinct performance which was required to be discussed in detail consecutively to comprehend the in-situ detection of deformation during the flexural bending by CF sensor in each position.

- Sensor A: was in 0° direction regarding the roller axis and was positioned on top in case I and in the bottom in case II. It must be noticed that this leg of the star sample wasn't loaded directly but was solitary under the indirect influence of the flexural load applied by the top roller in both cases. Sensor A detected a maximum decrease in resistance in case I while in case II, when it was in the bottom position, it detected a maximum increase in resistance with maximum strain deformation, Figure 3-24. This confirmed that the CF sensor was able to detect the compression strain induced by the roller which was in direct contact with the upper surface. The localized direct contact between the upper and surface of the composite and roller resulted in the generation of maximum compression strain thus, sensor A showed a maximum decrease in resistance. This behavior was different from the strain detection during the tensile test because during flexural the load is applied perpendicular to the sensor arrangement and it could decrease the contact distance of the loosely aligned carbon filaments of the sensor CF. In case II, sensor A was placed near the bottom surface where the sample experienced tensile elongation and it showed a maximum increase in resistance in comparison to the other sensor in other positions. This showed that it was able to detect the strain in the bottom case and to identify it as the tensile elongation. Moreover, the

intensity of the signal showed the amount of damage induced, Figure 3-25.

- Sensor B: was in +45° in case I and in -45° in case II regarding the roller axis while it was situated second from the top in former and second from the bottom in latter case i.e. between ply 2 and 3 and near the neutral axis of the specimen. This leg of the star sample was not under the direct impact of the flexural load as well but only under the localized influence of the central roller. In tests 1 and 2 sensor B showed good reproducibility in results and correlated perfectly with the applied strain in each cycle, Figure 3-24. The behavior of the signal of sensor B was similar to the sensor A but, the intensity of the change in the detection signal of sensor B in comparison to sensor A was decreased in both cases as it was closer to the neutral axis. In comparison between test 1 and test 3, it was observed that the intensity of the signal of CF sensor change because of the change in the position, Figure 3-25. Sensor B shows good detection of minimum compression strain in case I and minimum tensile strain in case II because it was not only near the neutral axis of the specimen but also under the indirect influence of the bending load as it was not in the loaded leg of the star sample, Figure 3-26.

- Sensor C: was in 90° direction regarding the roller axis in both cases I and II and in the leg of the star specimens placed between the rollers, along the span length and between the 3rd and 4th ply. This leg of the star sample was the one section in addition to the center of the specimen which was fully under the effect of bending deflection in both cases. During test 1 and test 2, the CF sensor as sensor C showed maximum intensity in the detection signal in comparison with all the other sensor positions and correlated perfectly in each cycle of the applied strain, Figure 3-24. This is because it was placed within the loaded leg of the star sample and was under the maximum influence of the flexural deflection and even though it was close to the neutral axis it showed maximum increase in resistance in comparison with sensor D which was placed near the bottom. Moreover, sensor C detected the tensile strain by showing the increase in resistance with an applied deflection in each cycle, and this detection was not localized but along the whole span length. However, in case II when the position of sensor C was change and was above the neutral axis, it showed a maximum decrease in the resistance because of the presence of compression strain and the detection was along the whole span length, Figure 3-25. So, this showed that even though the position of sensor C was near the neutral axis of the sample like sensor B but, it showed the maximum intensity of the signal in both cases in comparison with sensor D because of its presence along the span length of the sample and covering the larger area for detection of deformation,

Figure 3-26.

- Sensor D: was in -45° direction in case I and 45° direction in case II regarding the roller axis and was in the bottom position in the former case and the top position in the latter case. This leg of the composite star sample was also not under the direct effect of flexural deflection but only under the localized influence of the central roller. During test 1 and test 2 (case I) in both star specimens, sensor D showed repeatability in detection signal and correlated with the applied strain in a good manner, Figure 3-24. In case I, sensor D showed the minimum increase in resistance of the signal in comparison with sensor C and other sensors even though it was placed near the bottom of the specimen where it detected only localized tensile elongation during the deflection of the specimen between the rollers and sensor C was along the span length in the loaded leg and under the direct influence of flexural bending as discussed before. In case II, sensor D showed a decrease in the resistance because of the localized compression strain produced by the upper roller however, it was less than the sensor C because of the position along the span length, Figure 3-25 & 3-26.

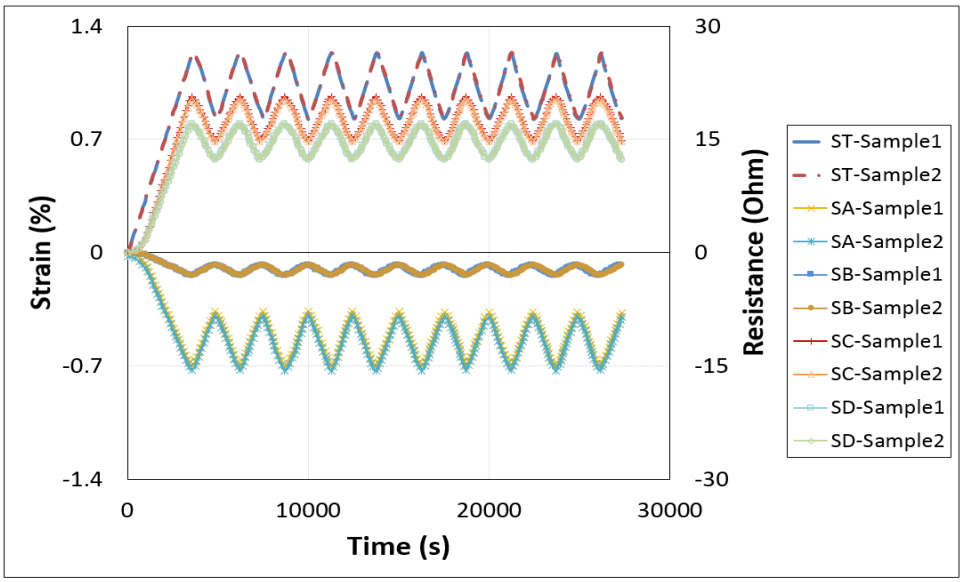

Figure 3-24: Real-time strain monitoring in composite star specimen during cycle flexural bending using CF sensor.

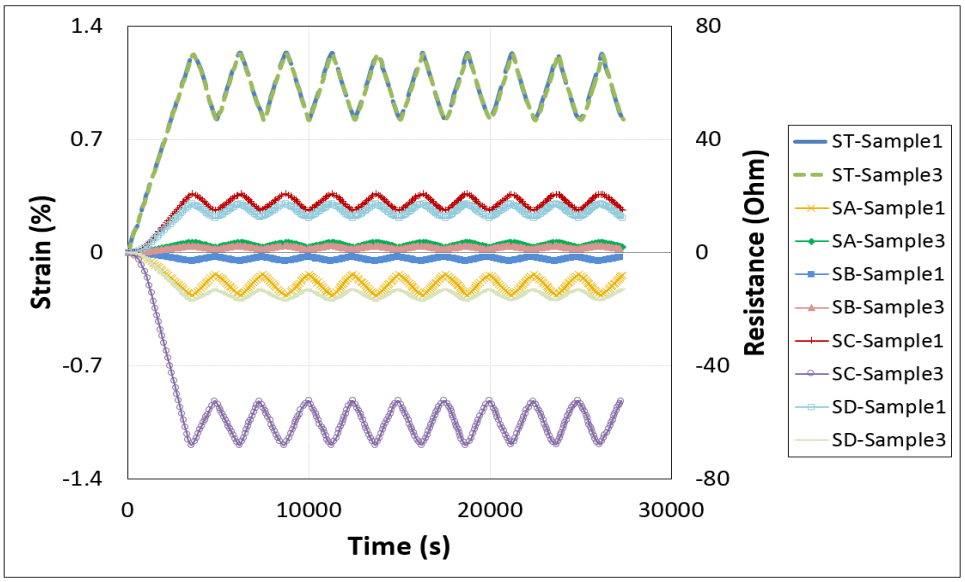

Figure 3-25: Comparison of real-time strain monitoring behavior of CF sensor in composite star specimen during cycle flexural bending during test 1 (when sensor A is placed in top position according to the loading axis) and test 3 (when sensor A is placed in bottom position according to the loading axis).

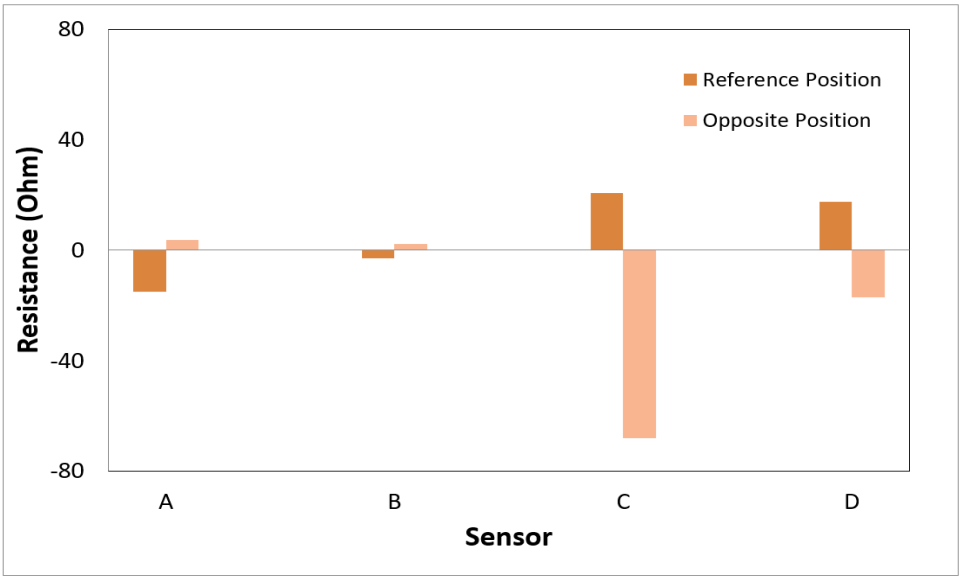

Figure 3-26: Effect of position and direction on the sensitivity of the CF sensor with respect to the loading axis and position through-thickness.

3.5. Comparison of real-time strain monitoring behavior of all three sensor systems

In this section, the real-time multimode strain monitoring of all three sensor systems is compared to understand their detection mechanism for the deformation in composite structures. All three sensor systems i.e. Nylon/Ag fiber sensor, CM sensor, and CF sensor showed distinct

behavior during the deformation of composite samples under tensile and flexural loadings. For example, during tensile deformation, all three sensor systems in position A in both sets of tests showed different detection behavior, Figure 3-27. Nylon/Ag fiber sensor showed a positive change in resistance when position A was along the loading axis and decrease in resistance when position A was in transverse direction during tensile loading. However, CM and CF sensors showed a positive response in both directions with different intensities of the signal. whereas all three sensor systems showed a positive change in resistance in both positions B and D and both positions were mirrored. This comparison showed that among all three sensor systems, Nylon/Ag fiber sensor did not only detect and monitor the strain deformation in different directions within composites but also distinguish between the type of deformation i.e. tensile, compression or both. This is because of the reason that Nylon/Ag fiber sensor exhibited metallic behavior because of the Ag coating, however, CM sensor and CF sensor shoed non-metallic performance because of their microstructure as discussed in detail in the previous section.

Similarly, a comparison of the detection behavior of all three sensor systems during the flexural deformation of composite samples showed interesting results, Figure 3-28. Nylon/Ag fiber sensor once again distinguished between the tensile and compressive strain during the flexural loading according to its position along the loading axis or through-thickness of the specimen. However, CM sensor showed a positive increase in resistance in each position with different intensity of the signal with respect to their placement along the thickness of the composite sample. the dense network of CNTs could not detect the compressive strains during the bending of the composite sample. Whereas, the CF sensor unlike the tensile test, showed a positive change in resistance below the neutral axis and negative change in resistance in positions above the neutral axis of the composite specimen. CF sensor was able to detect and identify the type of strain under flexural loading when the load was applied perpendicular to the sensor arrangement but during tensile loading, it was unable to show a decrease in resistance in the transverse direction because of increase in contact distance between the loosely aligned carbon filaments when the load is applied along the plane of the sensor arrangement.

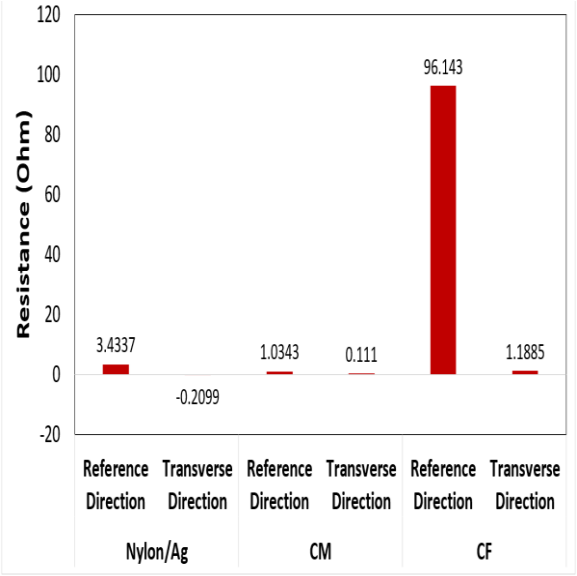

(a) Position A

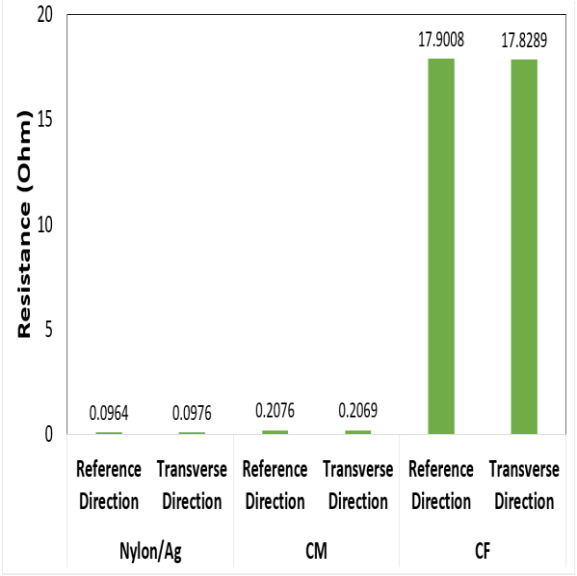

(b) Position B

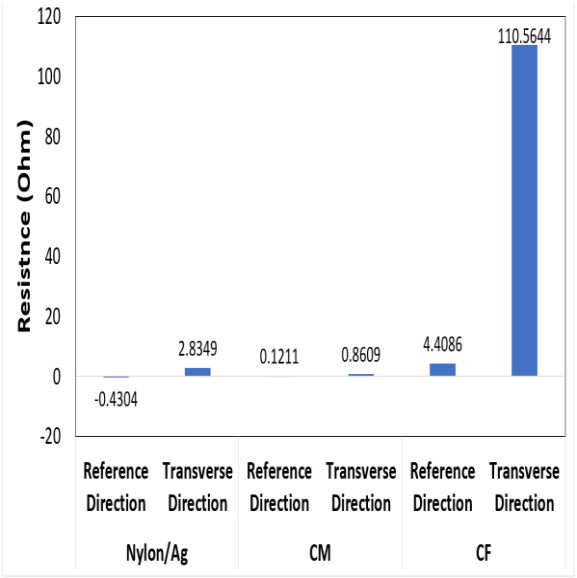

(c) Position C

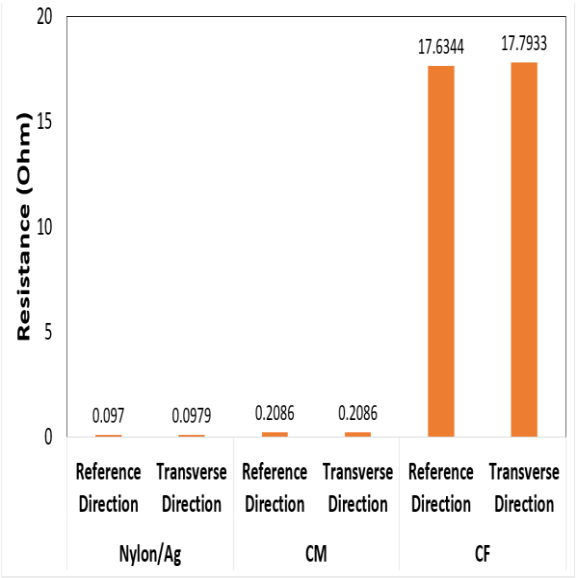

(d) Position D

Figure 3-27: Comparison of real-time detection behavior of all three sensor systems in each position in their respective composite sample during tensile loading.

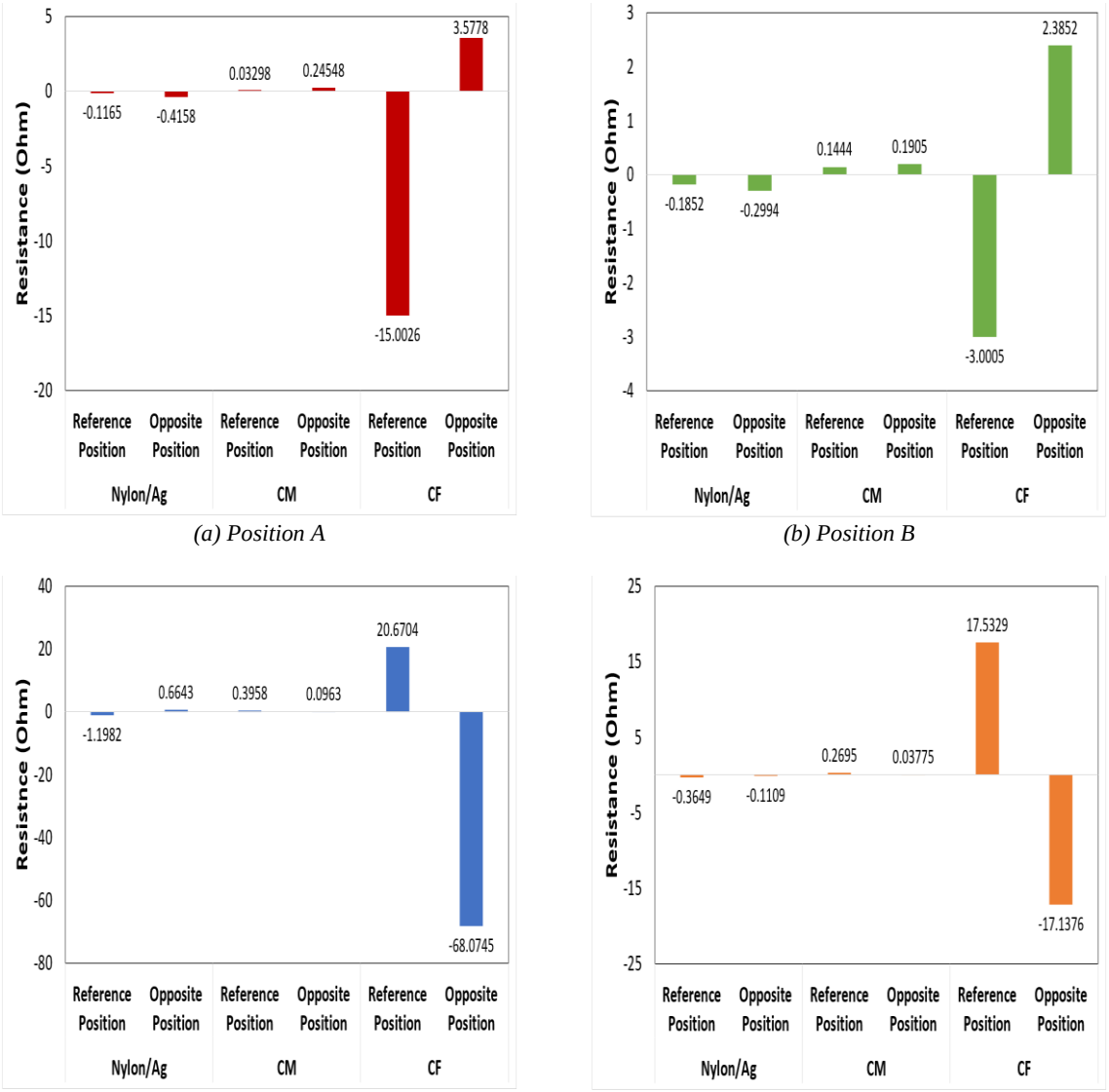

Figure 3-28: Comparison of real-time detection behavior of all three sensor systems in each position in their respective composite sample during flexural loading.

By this comparative study, one can observe that Nylon/Ag fiber sensor showed better real-time monitoring behavior during different quasi-static loadings in comparison with CM sensor and CF sensor. Nylon/Ag fiber sensor showed consistent detection behavior during both loadings and detected, identified and quantified the strain deformation in composite samples.

3.6. Conclusion

In this chapter, an experimental study was performed to examine and understand the application of each sensor system in real-time and in-situ monitoring and identification of strain deformation in composites under cyclic tensile and flexural loadings. Each sensor system was integrated within their respective composite specimens at specific direction and position to

demonstrate their strain detection behavior and identification of different types of deformation which occurred during tensile elongation and flexural deflection. The experimental results showed good repeatability in the mechanical performance of the composite structures and response of each sensor system in the monitoring of the deformation. Monitoring of deformation under tensile strain showed the influence of the direction of the sensor with respect to the loading axis on the change in resistance while monitoring of deformation of the composite specimen showed the influence of the position of the sensor within the plies on the detection signal of the sensor in each case when load is applied perpendicular to the arrangement of the sensors. Moreover, the method of placing these sensors in different directions and positions showed that these sensors can detect deformation over large areas and sections of complex structures and in locations that are not normally accessible to conventional methods.

Four Nylon/Ag fiber sensors, embedded in 0°, ±45°, and 90° direction with respect to the loading axis in each star specimen subjected to tensile loading, showed reproducibility in the electrical signal in the monitoring of the deformation. Nylon/Ag fiber sensor in all four positions in each specimen showed variation in the resistance response because of its different position and direction according to the loading axis and maximum increase in resistance was recording along the loading axis which not only confirmed the detection of tensile load but also predicted that the specimen will most likely fail in this direction. The decrease in resistance in transverse direction confirmed the presence of compressive strains because of the Poisson's effect during the tensile deformation and this behavior was similar in each test. Moreover, Sensor B and D showed that identical response because of their mirror position with respect to the loading axis, however, their minute change in resistance showed detection of less deformation in the oblique direction during the tensile test because of the combined effect of tensile and compressive strains. Moreover, Nylon/Ag fiber sensor in each position and direction showed individual response signals during the deformation of the composite specimen during flexural loading. This distinct behavior of the Nylon/Ag fiber sensor in each position confirmed the detection of different types of damage i.e. tensile or compression during the deflection and different intensity or magnitude of the signals quantified the amount of damage induced. Thus, Nylon/Ag fiber sensor not only showed the detection of different types of deformation but also indicated whether the deformation was overall or localized during flexural bending. The Nylon/Ag fiber sensor demonstrated good potential as a flexible reinforcement in composite materials for in-situ monitoring of strain because the applied strain was up to 1-2% for 10 cycles in each set of tests and the Nylon/Ag fiber showed a perfect correlation of its signal with the

applied strain in each cycle. This verified the stability and durability of this fiber sensor.

Similarly, the study of real-time monitoring of strain by CM sensor under tensile and flexural cyclic loads demonstrated the behavior of detection signals in detail. Results confirmed that CM sensors in both tests reacted to the applied stimuli in every direction and showed a distinct change in their change in resistance thus, not only monitoring the deformation but also detecting the amount of damage induced in each position and direction within the composite sample. However, further study is required to understand the precise mechanism responsible for changing the resistance of the sensors to apprehend its response in the transverse direction or under compression strain. This could be because the tunneling effect between the network of CNTs and compression causes additional stresses on the conductive network thus resulting in an increase of resistance with the applied strain. The response of the CM sensor in each position and direction is the net response of these two reasons and because of the further densification of CNT networks during the curing process of star specimens. Further understanding of these effects on the behavior of CNTs network in the CM sensor could make it possible to tailor the fabrication process of the conductive membrane so that the behavior of the sensor is predictable under both strain deformations i.e. tensile and compression.

Likewise, the Study of real-time monitoring of strain by CF sensor under tensile and flexural cyclic loads demonstrated the behavior of detection signals in detail. Results confirmed that CF sensors in both tests reacted to the applied stimuli in every direction and showed a distinct change in their change in resistance. CF sensor was able to detect and identify the type of strain under flexural loading when the load was applied perpendicular to the sensor arrangement but during tensile loading, it was unable to show a decrease in resistance in the transverse direction because of increase in contact distance between the loosely aligned carbon filaments when the load is applied along the plane of the sensor arrangement. So, in general, it not only monitoring the deformation but also detecting the type of deformation whether tensile or compressive, and quantified the amount of damage induced in each position and direction within the composite sample. However, further study is required to understand the precise mechanism responsible for changing the resistance of the CM and CF sensors to apprehend their response in the transverse direction or under compression strain during tensile loading. Additional understanding could make it possible to tailor the arrangement of filaments in the CF sensor so that the behavior of the sensor is predictable under both loading i.e. tensile and compression. This sensor technology can further advance itself in the real-time sensing applications within composite structures including thermal degradation and detection of dynamic failure. The

sensitivity of this sensor can be further tailored and amplified as desired parameters by modifying the arrangement or alignment of carbon filaments and by modifying the deposition of CNTs network respectively, without any significant requirements.

All three sensor systems showed unique behavior during the detection of deformation in composites. However, the comparative study of all three sensor systems showed that Nylon/Ag fiber sensor showed better real-time strain monitoring behavior under both quasi-static loadings by detection, monitoring, identifying, and quantifying the strain induced in the composite sample during deformation. Now, it is import to study the detection of the behavior of the composite sample during fractur or failure. That is why in the next chapter we will monitor the damage of the composite under different quasi-static loading using the Nylon/Ag fiber sensor.

References

[1] F. Azhari and N. Banthia, “Cement-based sensors with carbon fibers and carbon nanotubes for piezoresistive sensing,” *Cem. Concr. Compos.*, vol. 34, no. 7, pp. 866–873, 2012, doi: https://doi.org/10.1016/j.cemconcomp.2012.04.007.

[2] A. C. Raghavan and C. Cesnik, “Review of Guided-Wave Structural Health Monitoring,” *Shock Vib. Dig.*, vol. 39, pp. 91–114, 2007, doi: 10.1177/0583102406075428.

[3] C. Bois, P. Herzog, and C. Hochard, “Monitoring a delamination in a laminated composite beam using in-situ measurements and parametric identification,” *J. Sound Vib.*, vol. 299, no. 4, pp. 786–805, 2007, doi: https://doi.org/10.1016/j.jsv.2006.07.026.

[4] G. Park, H. H. Cudney, and D. J. Inman, “An Integrated Health Monitoring Technique Using Structural Impedance Sensors,” *J. Intell. Mater. Syst. Struct.*, vol. 11, no. 6, pp. 448–455, 2000, doi: 10.1106/QXMV-R3GC-VXXG-W3AQ.

[5] V. Giurgiutiu, A. Zagrai, and J. J. Bao, “Piezoelectric Wafer Embedded Active Sensors for Aging Aircraft Structural Health Monitoring,” *Struct. Heal. Monit.*, vol. 1, no. 1, pp. 41–61, 2002, doi: 10.1177/147592170200100104.

[6] C. C. Ciang, J.-R. Lee, and H.-J. Bang, “Structural health monitoring for a wind turbine system: a review of damage detection methods,” *Meas. Sci. Technol.*, vol. 19, no. 12, p. 122001, Oct. 2008, doi: 10.1088/0957-0233/19/12/122001.

[7] T. G. Gerardi, “Health Monitoring Aircraft,” *J. Intell. Mater. Syst. Struct.*, vol. 1, no. 3, pp. 375–385, 1990, doi: 10.1177/1045389X9000100307.

[8] C. R. Farrar and K. Worden, “An introduction to structural health monitoring,” *Philos. Trans. R. Soc. A Math. Phys. Eng. Sci.*, vol. 365, no. 1851, pp. 303–315, 2007, doi: 10.1098/rsta.2006.1928.

[9] J. Leng and A. Asundi, “Structural health monitoring of smart composite materials by using EFPI and FBG sensors,” *Sensors Actuators A Phys.*, vol. 103, no. 3, pp. 330–340, 2003, doi: https://doi.org/10.1016/S0924-4247(02)00429-6.

[10] W. Staszewski, C. Boller, and G. R. Tomlinson, *Health monitoring of aerospace structures: smart sensor technologies and signal processing*. John Wiley & Sons, 2004.

[11] Y. ZOU, L. TONG, and G. P. STEVEN, “VIBRATION-BASED MODEL-DEPENDENT DAMAGE (DELAMINATION) IDENTIFICATION AND HEALTH MONITORING FOR COMPOSITE STRUCTURES — A REVIEW,” *J. Sound Vib.*, vol. 230, no. 2, pp. 357–378, 2000, doi: https://doi.org/10.1006/jsvi.1999.2624.

[12] S. W. Doebling, C. R. Farrar, M. B. Prime, and D. W. Shevitz, “Damage identification

and health monitoring of structural and mechanical systems from changes in their vibration characteristics: A literature review," doi: 10.2172/249299.

[13] J. P. Andrews, A. N. Palazotto, M. P. DeSimio, and S. E. Olson, "Lamb Wave Propagation in Varying Isothermal Environments," *Struct. Heal. Monit.*, vol. 7, no. 3, pp. 265–270, 2008, doi: 10.1177/1475921708090564.

[14] R. Schueler, S. P. Joshi, and K. Schulte, "Damage detection in CFRP by electrical conductivity mapping," *Compos. Sci. Technol.*, vol. 61, no. 6, pp. 921–930, 2001, doi: https://doi.org/10.1016/S0266-3538(00)00178-0.

[15] A. Kunadt, E. Starke, G. Pfeifer, and C. Cherif, "Messtechnische Eigenschaften von Dehnungssensoren aus Kohlenstoff-Filamentgarn in einem VerbundwerkstoffMeasuring Performance of Carbon Filament Yarn Strain Sensors Embedded in a Composite," *tm-Technisches Mess. Plattf. für Methoden, Syst. und Anwendungen der Messtechnik*, vol. 77, no. 2, pp. 113–120, 2010.

[16] H. C. H. Li, I. Herszberg, C. E. Davis, A. P. Mouritz, and S. C. Galea, "Health monitoring of marine composite structural joints using fibre optic sensors," *Compos. Struct.*, vol. 75, no. 1, pp. 321–327, 2006, doi: https://doi.org/10.1016/j.compstruct.2006.04.054.

[17] J. Rausch and E. Mäder, "Health monitoring in continuous glass fibre reinforced thermoplastics: Tailored sensitivity and cyclic loading of CNT-based interphase sensors," *Compos. Sci. Technol.*, vol. 70, no. 13, pp. 2023–2030, 2010, doi: https://doi.org/10.1016/j.compscitech.2010.08.003.

[18] M. M. B. Hasan, A. Matthes, P. Schneider, and C. Cherif, "Application of carbon filament (CF) for structural health monitoring of textile reinforced thermoplastic composites," *Mater. Technol.*, vol. 26, no. 3, pp. 128–134, 2011, doi: 10.1179/175355511X13007211258881.

[19] J. Rausch and E. Mäder, "Health monitoring in continuous glass fibre reinforced thermoplastics: Manufacturing and application of interphase sensors based on carbon nanotubes," *Compos. Sci. Technol.*, vol. 70, no. 11, pp. 1589–1596, 2010, doi: https://doi.org/10.1016/j.compscitech.2010.05.018.

[20] J. Rausch and E. Mäder, "Carbon nanotube coated glass fibres for interphase health monitoring in textile composites," *Mater. Technol.*, vol. 26, no. 3, pp. 153–158, 2011, doi: 10.1179/175355511X13007211259042.

[21] N. Forintos and T. Czigany, "Reinforcing carbon fibers as sensors: The effect of temperature and humidity," *Compos. Part A Appl. Sci. Manuf.*, vol. 131, p. 105819, 2020, doi: https://doi.org/10.1016/j.compositesa.2020.105819.

[22] G. Georgousis *et al.*, “Study of the reinforcing mechanism and strain sensing in a carbon black filled elastomer,” *Compos. Part B Eng.*, vol. 80, pp. 20–26, 2015, doi: https://doi.org/10.1016/j.compositesb.2015.05.021.

[23] J. Hoheneder, I. Flores-Vivian, Z. Lin, P. Zilberman, and K. Sobolev, “The performance of stress-sensing smart fiber reinforced composites in moist and sodium chloride environments,” *Compos. Part B Eng.*, vol. 73, pp. 89–95, 2015, doi: https://doi.org/10.1016/j.compositesb.2014.12.028.

[24] J. M. Park, S.-I. Lee, K.-W. Kim, and D.-J. Yoon, “Interfacial Aspects of Electrodeposited Conductive Fibers/Epoxy Composites using Electro-Micromechanical Technique and Nondestructive Evaluation,” *J. Colloid Interface Sci.*, vol. 237, pp. 80–90, 2001, doi: 10.1006/jcis.2001.7426.

[25] J.-M. Park, S.-I. Lee, and K. L. DeVries, “Nondestructive sensing evaluation of surface modified single-carbon fiber reinforced epoxy composites by electrical resistivity measurement,” *Compos. Part B Eng.*, vol. 37, no. 7, pp. 612–626, 2006, doi: https://doi.org/10.1016/j.compositesb.2006.03.002.

[26] A. Todoroki, K. Yamada, Y. Mizutani, Y. Suzuki, and R. Matsuzaki, “Impact damage detection of a carbon-fibre-reinforced-polymer plate employing self-sensing time-domain reflectometry,” *Compos. Struct.*, vol. 130, pp. 174–179, 2015, doi: https://doi.org/10.1016/j.compstruct.2015.04.020.

[27] J. M. Park, D.-J. Kwon, Z.-J. Wang, J.-J. Kim, K.-W. Jang, and K. L. Devries, “New method for interfacial evaluation of carbon fiber/thermosetting composites by wetting and electrical resistance measurements,” *J. Adhes. Sci. Technol.*, vol. 28, 2014, doi: 10.1080/01694243.2014.911646.

[28] D.-J. Kwon, Z.-J. Wang, J.-Y. Choi, P.-S. Shin, K. L. Devries, and J. M. Park, “Interfacial evaluation of carbon fiber/epoxy composites using electrical resistance measurements at room and a cryogenic temperature,” *Compos. Part A Appl. Sci. Manuf.*, vol. 72, 2015, doi: 10.1016/j.compositesa.2015.02.007.

[29] Z.-J. Wang *et al.*, “Mechanical and interfacial evaluation of CNT/polypropylene composites and monitoring of damage using electrical resistance measurements,” *Compos. Sci. Technol.*, vol. 81, pp. 69–75, 2013, doi: https://doi.org/10.1016/j.compscitech.2013.04.001.

[30] S. A. Grammatikos and A. S. Paipetis, “On the electrical properties of multi scale reinforced composites for damage accumulation monitoring,” *Compos. Part B Eng.*, vol. 43, no. 6, pp. 2687–2696, 2012, doi: https://doi.org/10.1016/j.compositesb.2012.01.077.

[31] J. Cagáň, J. Pelant, M. Kyncl, M. Kadlec, and L. Michalcová, “Damage detection in carbon fiber–reinforced polymer composite via electrical resistance tomography with Gaussian anisotropic regularization,” *Struct. Heal. Monit.*, vol. 0, no. 0, p. 1475921718820013, doi: 10.1177/1475921718820013.

[32] T. M. Johnson, D. T. Fullwood, and G. Hansen, “Strain monitoring of carbon fiber composite via embedded nickel nano-particles,” *Compos. Part B Eng.*, vol. 43, no. 3, pp. 1155–1163, 2012, doi: https://doi.org/10.1016/j.compositesb.2011.09.014.

[33] A. Al-Dahawi, O. Öztürk, F. Emami, G. Yıldırım, and M. Şahmaran, “Effect of mixing methods on the electrical properties of cementitious composites incorporating different carbon-based materials,” *Constr. Build. Mater.*, vol. 104, pp. 160–168, 2016, doi: https://doi.org/10.1016/j.conbuildmat.2015.12.072.

[34] M.-J. Lim, H. K. Lee, I.-W. Nam, and H.-K. Kim, “Carbon nanotube/cement composites for crack monitoring of concrete structures,” *Compos. Struct.*, vol. 180, pp. 741–750, 2017, doi: https://doi.org/10.1016/j.compstruct.2017.08.042.

[35] B. Christian, “Next generation structural health monitoring and its integration into aircraft design.,” *Int. J. Syst. Sci.*, vol. 31, no. 11, pp. 1333–1349, 2000.

[36] V. K. Varadan and V. Varadan., “Microsensors, microelectromechanical systems (mems), and electronics for smart structures and systems.,” *Smart Mater. Struct.*, vol. 9, no. 6, pp. 953–972, 2000.

[37] N. Trifigny, F. M. Kelly, C. Cochrane, F. Boussu, V. Koncar, and D. Soulat, “PEDOT: PSS-based piezo-resistive sensors applied to reinforcement glass fibres for in situ measurement during the composite material weaving process.,” *Sensors*, vol. 13, no. 8, pp. 10749–10764, 2013.

[38] O. Atalay and W. R. Kennon, “Knitted Strain Sensors: Impact of Design Parameters on Sensing Properties,” in *Sensors*, 2014.

[39] J. Sebastian *et al.*, “Health monitoring of structural composites with embedded carbon nanotube coated glass fiber sensors,” *Carbon N. Y.*, vol. 66, pp. 191–200, 2014, doi: https://doi.org/10.1016/j.carbon.2013.08.058.

[40] Y. Qureshi, M. Tarfaoui, K. K. Lafdi, and K. Lafdi, “Development of microscale flexible nylon/Ag strain sensor wire for real-time monitoring and damage detection in composite structures subjected to three-point bend test,” *Compos. Sci. Technol.*, vol. 181, p. 107693, 2019, doi: https://doi.org/10.1016/j.compscitech.2019.107693.

[41] Y. Qureshi, M. Tarfaoui, K. K. Lafdi, and K. Lafdi, “In-situ Monitoring, Identification and Quantification of Strain Deformation in Composites under Cyclic Flexural Loading

using Nylon/Ag Fiber Sensor," *IEEE Sens. J.*, p. 1, 2020, doi: 10.1109/JSEN.2020.2969329.

CHAPTER 4 : REAL-TIME MONITORING OF FRACTURE IN COMPOSITE SPECIMENS UNDER DIFFERENT LOADINGS USING NYLON/AG FIBER SENSOR

As per a comparative study conducted in the previous chapters, Nylon/Ag fiber sensor showed better performance in all aspects during the real-time strain monitoring of composite samples under different quasi-static loadings. Therefore, in this chapter, the objective is to monitor the fracture of composites subjected to different loadings in real-time using a Nylon/Ag fiber sensor. Nylon/Ag fiber sensor was placed in two directions i.e. along the loading axis and in the transverse direction in composite samples for tensile loading. While for the flexural test, Nylon/Ag fiber sensors were inserted in different positions through the thickness individually in each sample to demonstrate strain deformation in composites during bending. Also, Nylon/Ag fiber sensors were integrated at different directions and positions gradually between each ply of composite samples for low-velocity impact. Composite samples were then tested under low-velocity impact on the Taylor cannon gun apparatus. This step was carried out to understand the fracture mechanism of the composites sample under these loading conditions in different positions and directions. Under quasi-static loadings, the specimens were subjected to tensile elongation and flexural deflection at the strain rate of 2mm/min. However, under low-dynamic loading, composite samples were tested under low-velocity impact on the Taylor cannon gun apparatus at 2.5m/s, 3m/s, and 6.5m/s respectively. Overall mechanical response of composite specimens and electrical response signal of the Nylon/Ag fiber sensor showed good reproducibility in results however, it showed a specific change in resistance in each specimen because of their respective position. The results established that each sensor system exhibited good potential as a flexible strain sensor for in-situ monitoring of composites and can provide detection over a large section and unapproachable locations. The increase or decrease in the resistance of the fiber sensor signified the presence of tensile or compressive strain respectively and the intensity of the signal quantified the amount of deformation. The results confirmed Nylon/Ag fiber sensor showed good potential as flexible sensor reinforcement in composites for in-situ monitoring the change in the mechanical behavior of the specimen during overall fracture and identified the type of damage during quasi-static loadings. Moreover, it detected the deformation, damage initiation, damage propagation, type of damage, and quantification of the amount of damage induced during dynamic loading as well.

4.1. Introduction

Composites had replaced traditional materials nearly in every industrial application because of their superior mechanical performance, structural durability, low density, cost-effectiveness, and resistance to environmental factors [1,2]. However, even they were not exempt from limitations and their deformation and damage mechanisms were well established [3,4]. Therefore, it was essential to examine and control the performance of the structure during operation to avoid unexpected failure which could be initiated either because of the extreme loading conditions or by extreme environmental conditions such as creep, moisture, etc. Macroscopic damage was usually visible externally in composites, but microscopic damage or internal cracks were extremely challenging to detect and usually required inspection techniques [5–7]. Moreover, impact loading was one of the most common causes of the failure of structure and it was often very difficult to detect failure because damage occurs very fast and generally not visually visible [8]–[11]. The impact such as hailstone, bird strike, and other mechanical collisions were some of the frequent dynamic loadings for structures such as wind turbines, aircraft and bridges which could affect the integrity of the structure and induce fiber breakage, delamination, matrix cracking or interfacial failure [5]–[7].

Structural health monitoring (SHM) is a renowned and extensively used procedure to study and control the performance of composites to ensure more reliable and safer structures [12]. SHM sensors were developed gradually over time form nondestructive testing methods to real-time monitoring of structures [9–12]. In-situ SHM had been often used for sensing different kinds of damages in materials such as thermal degradation, deformation, corrosion, fiber cracking, intralaminar cracking, debonding/delamination, etc. to confirm save and durable service life of the structures [13–18]. Likewise, many studies were available which investigated the strain and damage sensing of the composites structures using different SHM techniques but limited information was available in the literature regarding the effect of sensitivity and location of the sensor on damage detection [19,20]. In addition, detection of impact damage was usually conducted after the impact with non-destructive testing techniques (NDT) such as ultrasonic [25], acoustic emission [26]–[29], fiber Bragg grating (FBG) [30][31], optical fiber [32]. However, these techniques were expensive, difficult to install, prone to external noise, and required complex installation procedure [33][34]. The studies conducted to detect the damage during impact dynamic loading were mostly focused on the damage detection and did not

include the study of detection signal to elaborate the monitoring of deformation, damage initiation, damage propagation, damage quantification, and identification of the type of damage.

So, in this context, an experimental study is conducted to investigate the in-situ/real-time strain and damage sensing capabilities of the Nylon/Ag fiber sensor within composite structures under different quasi-static loadings. The second objective was to study the ability of the sensor to distinguish between the tensile and compressive damage of the composite specimen during the tests. The third objective was to examine the in-situ monitoring capability of the Nylon/Ag fiber sensor within composite material under dynamic impact and the ability of the fiber sensor to distinguish between different types of failures and quantification of induced damage by placing the fiber sensor in different positions. The fabrication process of the specimen was carried out by inserting the Nylon/Ag fiber sensor within the glass fiber plies of the GFRP composites and molds were used for this purpose. Nylon/Ag fiber sensors were placed between the plies in their respective directions depending upon the mode of failure to detect during the tensile test. However, Nylon/Ag fiber sensors were intentionally placed near the top, the middle and bottom surface of the individual specimen rather than in the middle of the thickness of all specimens depending upon the mode of failure to detect during the flexural test. Also, Nylon/Ag fiber sensor was inserted into the composite specimens at their respective position and direction in the specimens for the impact test. Then each specimen was tested and the mechanical performance of samples in each set of tests was correlated with the electrical signal response of the Nylon/Ag fiber sensor. The results showed that the sensor not only detected the strain and damage under different quasi-static and dynamic loadings with good sensitivity but was also able to differentiate between different types of damages. Moreover, the Nylon/Ag fiber sensor showed good potential to monitor damage in dynamic failure and to detect damage propagation phenomenon throughout the sample.

4.2. Fabrication Process

4.2.1. Sample preparation for tensile test

Standard specimens of the composite were prepared using similar materials that were used for the star specimen however, three plies were used for electrical isolation and Nylon/Ag fiber sensors were inserted in two directions intentionally. Then, resin mixed with a hardener with a ratio of 1:4 was poured into the mold and full integration of the sensor in each specimen of the composite was achieved. Once the molds were filled the samples were completely transparent and the chopped glass fiber fabric was not visible, Figure 4-1 (a). Now, Nylon/Ag fiber sensors

in longitudinal and transverse directions were visible in both samples, and afterward, specimens were cured at room temperature for 48 hours. The specimen was characterized as 25 mm in width, 80 mm in length and 3 mm in thickness, Figure 4-1 (b). Schematic representation of the composite star specimen with the demonstrated placement of embedded Nylon/Ag fiber sensors according to the loading axis.

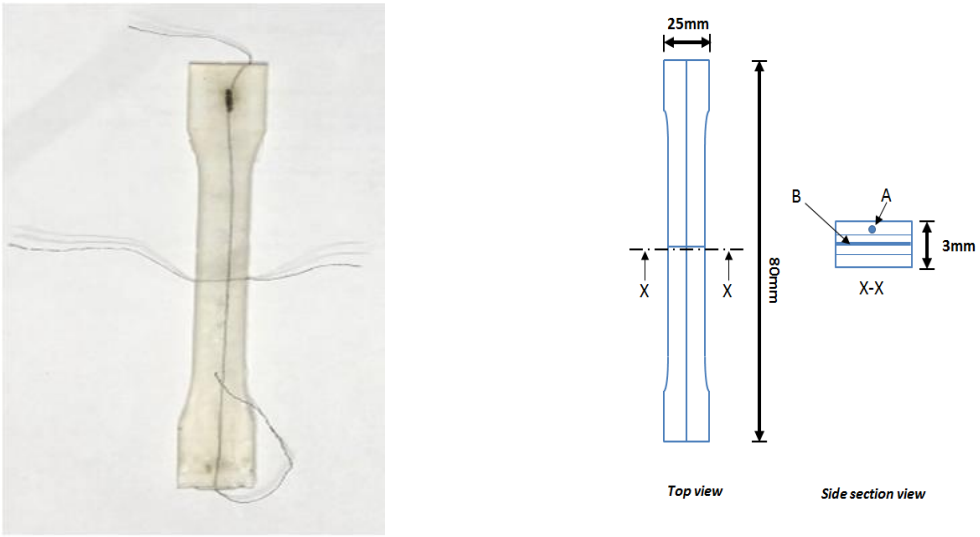

(a) *(b)*

Figure 4-1: (a) Example of a standard composite specimen embedded with Nylon/Ag fiber sensors after the fabrication process. (b) Geometric characteristics of the specimen and schematic representation of the position of Nylon/Ag fiber sensor in 0° and 90° direction.

4.2.2. Sample preparation for the three-point bend test

Specimens of composite with standard dimensions for the flexural test were prepared using silicon molds and the fabric of chopped glass fibers was cut into sections and placed inside the mold gradually. Five plies were used and Nylon/Ag fiber sensor were intentionally placed near the top, middle, and bottom of the respective specimens through-thickness depending upon the in-situ detection of the specific mode of failure. Figure 4-2. Then, resin mixed with a hardener with a ratio of 1:4 was poured into the mold and full integration of sensor in each specimen of the composite was achieved, Figure 4-3. Once the molds were filled, the samples were completely transparent and the chopped glass fiber fabric was not visible, Figure 4-4. Now, Nylon/Ag fiber sensor was visible in all specimens, and afterward, specimens were cured at room temperature for 48 hours.

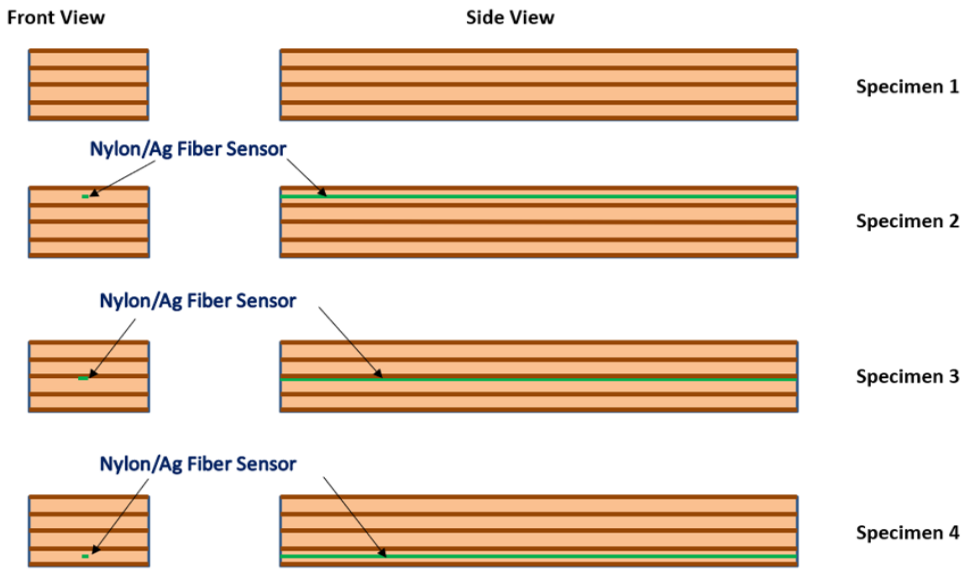

Figure 4-2: Schematic representation of the position of the Nylon/Ag fiber sensor in each composite specimen.

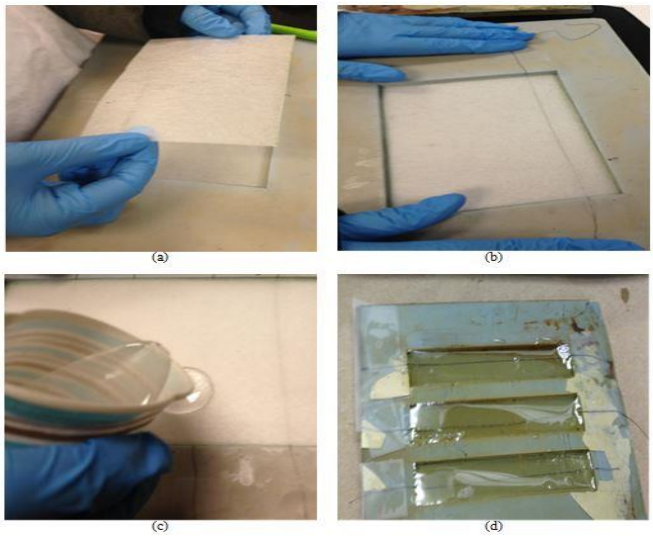

Figure 4-3: Fabrication process of composite specimens with incorporation of Nylon/Ag fiber sensor

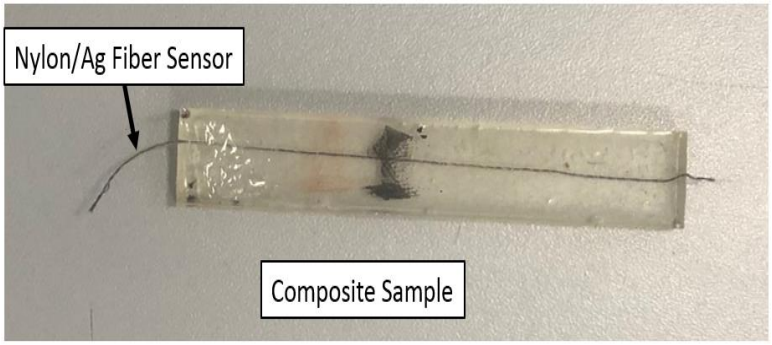

Figure 4-4: Example of a composite specimen after the fabrication process. The specimen became transparent after the curing process and fiber sensor is visible.

4.2.3. Sample Preparation for the dynamic test

Nylon/Ag fiber sensors were cut into the specific length and was inserted between the plies of chopped glass fibers in their respective position and direction during the fabrication of the composite specimen. Three plies of chopped glass fiber matt were used for reinforcement and to separate the fiber sensor from each other, Figure 4-5 (a). Also, the chopped fiber mat ensured isotropic mechanical behavior with poor conductivity and electrical isolation for each fiber sensor. One fiber sensor was inserted between the ply 1 and ply 2 along the width of the sample in the center i.e. W and four nylon/Ag fiber sensors were inserted along the length of the sample at the almost same distance from each other between ply 2 and 3 at position L_1, L_2, L_3 and L_4, Figure 4-5 (b). After a mixture of resin and hardener was added into the mold, composite samples were cured for 48 hr at room temperature and full insertion of fiber sensors was achieved in each specimen, Figure 4-5 (c). Each sample was of 5 mm in thickness, 80 mm in width and 150 mm in length, Figure 4-5 (d)-(e). Furthermore, the geometrical illustration of the sample explained the location and direction of the fiber sensors within the plies.

4.3. Experimental Procedure

4.3.1. Experimental procedure for tensile test

Standard composited specimen consisting of fiber sensors in two directions i.e. 0° and 90° was also tested using INSTRON-50 and data acquisition system (Spider 8 manufactured by HBM) like star specimens, Figure 4-6. INSTRON-50 demonstrated the overall mechanical behavior of the composite specimen while the electrical recorded the signal from the sensors until fracture. It was ensured again that the specimen was placed properly between the fixtures and none of the electrical connections were not in contact with any metallic part of the machine. The test was performed at a low strain rate i.e. 2 mm/min up to final fracture and the mechanical behavior of composite specimen with the resistance profile of each Nylon/Ag fiber sensor was obtained. All tests showed that Nylon/Ag fiber detected the damage and final fracture in each direction according to their position.

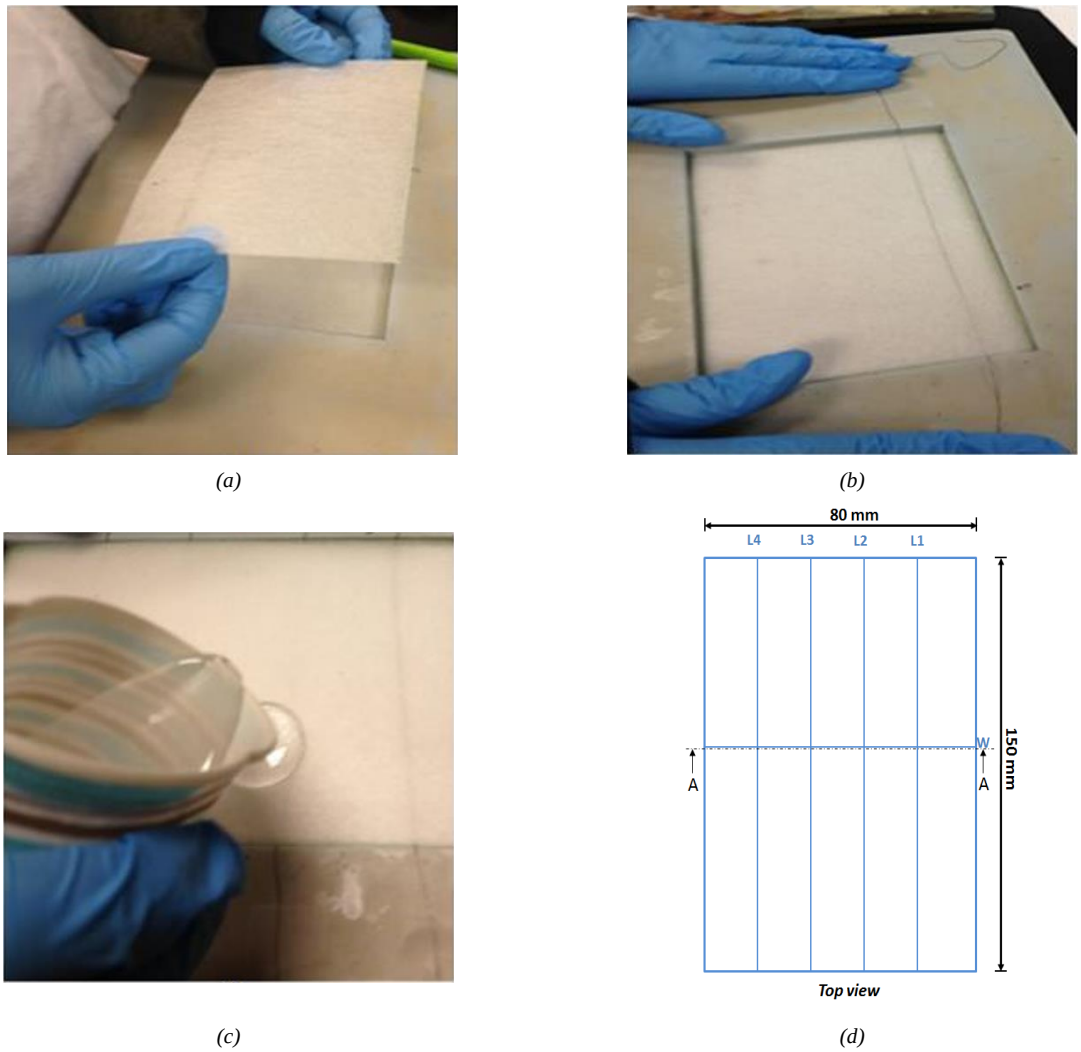

Figure 4-5: (a)-(c) Composite sample preparation process with integration of Nylon/Ag fiber sensors (d)-(e) Geometric parameters of the samples and illustration of the placement of Nylon/Ag fiber sensor in each position correspondingly.

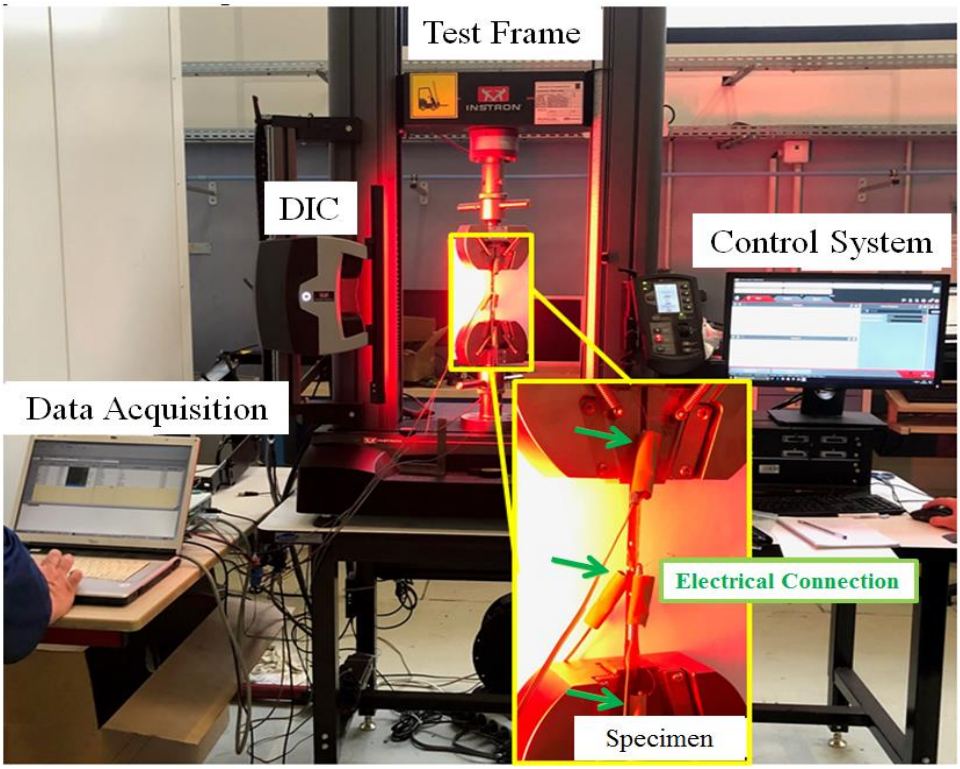

Figure 4-6: Experimental setup to test the overall real-time damage detection of the Nylon/Ag fiber sensor in the standard composite specimen. Electrical connections are highlighted with green arrows.

4.3.2. Experimental procedure for three-point bent test

A cured composite specimen consisting of a Nylon/Ag fiber sensor was tested using the ADEMEL test machine and HBM Spider 8 system with a Lab-view program was connected to the fiber sensor for real-time monitoring damage monitoring of composite sample, Figure 4-7. ADEMEL was used to study the mechanical behavior of the composite specimen and the electrical system was used to record the signal from the fiber sensor simultaneously. It was important not only to ensure that the specimen was placed properly between the 3-point bend fixtures rollers but also that the fiber sensor was not in contact with any metallic part of the machine because it could have influenced the electrical response of the sensor. Then, the specimen was placed in the ADEMEL machine, and the test was performed at a low strain rate i.e. 2mm/min. All specimens were the same in dimensions except for the placement of the fiber sensor inside each specimen and as a result, the mechanical behavior of composite specimen with resistance profile of the Nylon/Ag fiber sensor was obtained. Three specimens contained fiber sensor at different positions respectively and one specimen was used as a reference to ensure the reproducibility of results and to show that the presence of the fiber sensor did not affect the mechanical performance of the composite specimen. Furthermore, each test showed

the sensor detected specific mode of deformation in real-time whether it was tensile, compressive, or both according to the placement of the sensor in addition to the detection of final fracture.

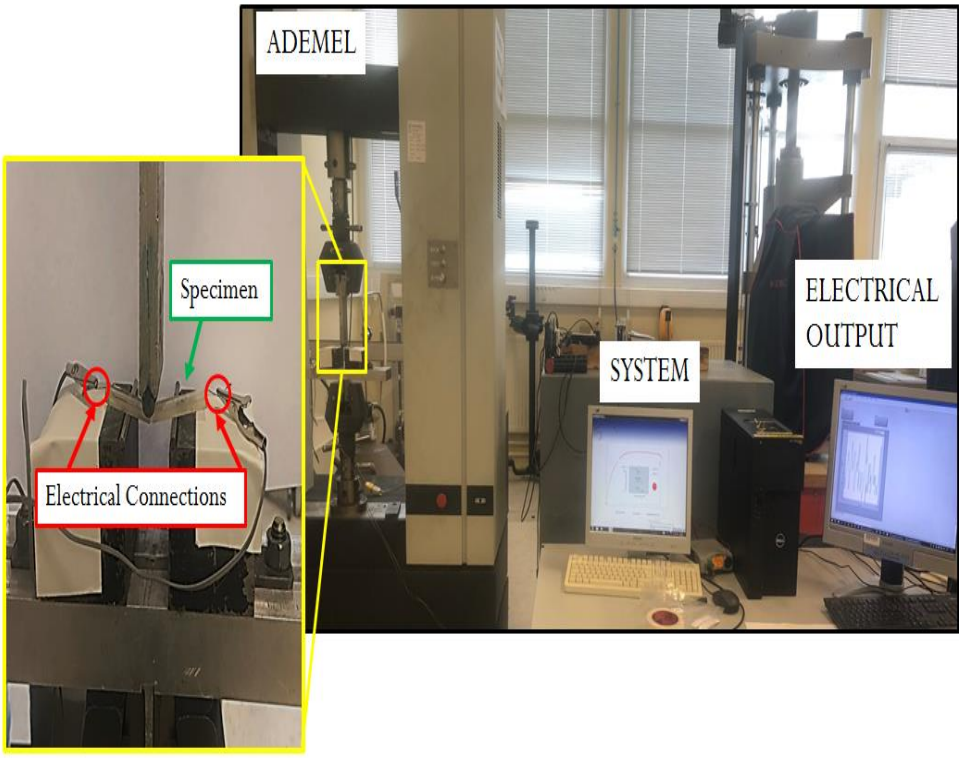

Figure 4-7: Experimental setup to test the real-time damage detection of the Nylon/Ag fiber sensor in the composite specimen under a three-point bend test.

4.3.3. Experimental procedure for dynamic test

A cured composite specimen consisting of fiber sensors was tested using TAYLOR GUN and the data acquisition system (manufactured by HBM) was connected to the electrodes attached with the Nylon/Ag fiber sensors for real-time monitoring of specimen deformation, Figure 4-8 (a). TAYLOR GUN was used to study the mechanical behavior of the composite specimen during dynamic impact and the electrical system was used to record the signal from the fiber sensor simultaneously. It was important to ensure that the sample was attached properly on the holder and the electrical connections were not in contact with any metallic part of the machine because it could have influenced the electrical response of the fiber sensor. Then, the specimens were tested at a low-velocity impact range with an impactor of 1.6 kg, and diodes were used to record the velocity of the impactor, Figure 4-8 (b). Three sets of tests were conducted to study the detection behavior of the fiber sensors. The first test was performed at 2.5 m/s and while the second test was performed at 3 m/s and in each set of tests sample was impacted at the

position shown in Figure 4-9. This position was selected to ensure the maximum possibility of distinct behavior of the Nylon/Ag fiber sensor in each position to demonstrate the complex failure mechanism of the composite sample under dynamic loading. The first two tests were performed to observe examine the sensitivity and real-time damage detection response of the designed Nylon/Ag fiber sensor where there is elastic deformation or some localized permanent deformation at the microscale and the position of impact was selected to demonstrate the detection of damage propagation. The third set of tests was performed at 6.5 m/s to ensure overall damage and final fracture of the samples and samples were impacted in the same position as the first two tests. It should be kept in mind that this study was conducted to understand the real-time damage detection behavior of Nylon/Ag fiber sensors when incorporated into the composite specimens under dynamic loading that could be subjected to variable damage behavior. However, three tests were conducted for overall damage and fracture of the specimen to show the repeatability of the mechanical response of the composite specimen. Two specimens were tested without fiber sensors and one was tested with the integrated fiber sensors at different locations.

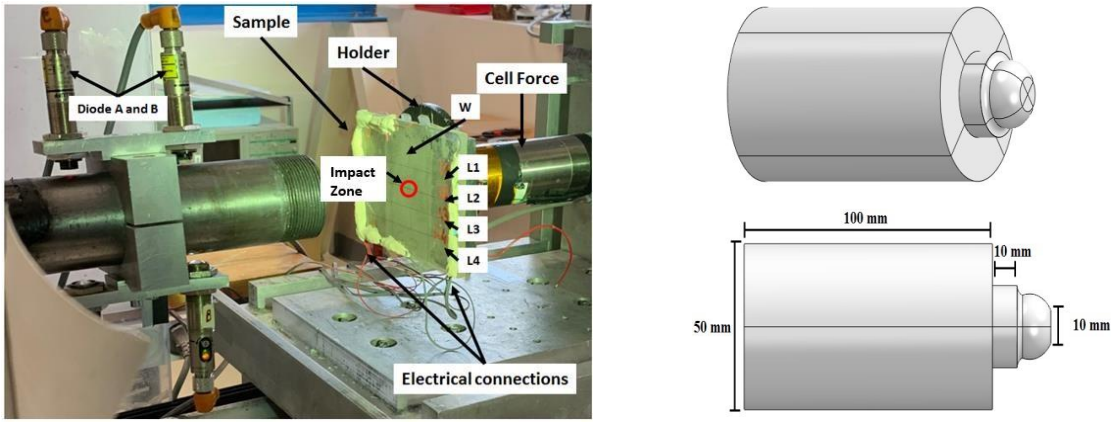

(a) *(b)*

Figure 4-8: Experimental setup to examine the in-situ strain monitoring behavior of the Nylon/Ag fiber sensor within the composite under dynamic impact.

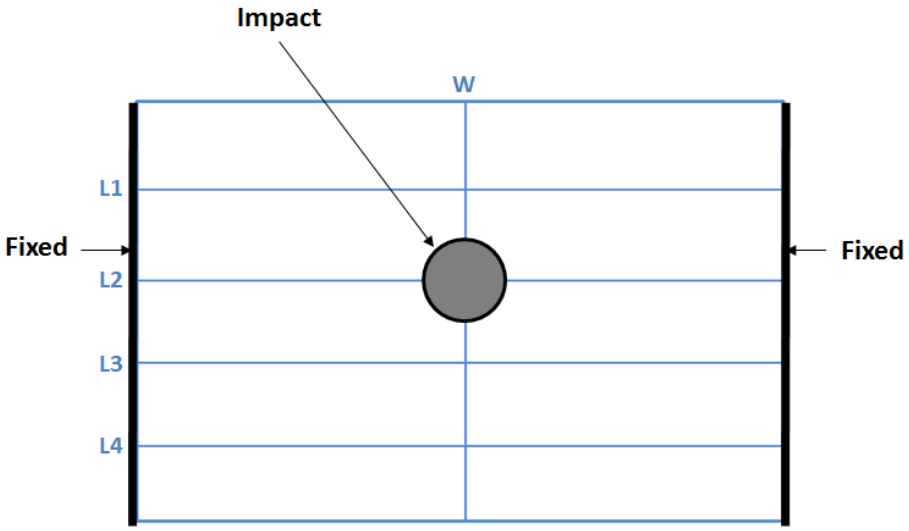

Figure 4-9: Experimental boundary conditions and position of impact.

4.4. Results and Discussion

4.4.1. Real-time monitoring of composite sample under tensile load

The deformation behavior of the standard composite specimen was identical to the star specimen because it was also subjected to the tensile loading, however; the only difference was that these specimens were studied up to final fracture, Figure 4-10 (a). Two composite specimens with fiber sensor in 0° and 90° direction in each specimen were studied for overall deformation behavior. Fiber sensors in each specimen were placed in the middle of both directions however in sample 2; a defect was intentionally introduced near the fixture, Figure 4-10 (b). This step was carried out to observe the difference in the damage detection behavior of the Nylon/Ag fiber sensors especially the sensors placed in the transverse direction in both specimens. This step was vital to understand the deformation detection response of the Nylon/Ag fiber sensor whether the damage occurs near or far from its position. When specimens were subjected to tensile load, the deformation caused tensile stress along the loading axis i.e. 0° because of the elongation and compression strains in the transverse direction of the loading axis i.e. 90°.

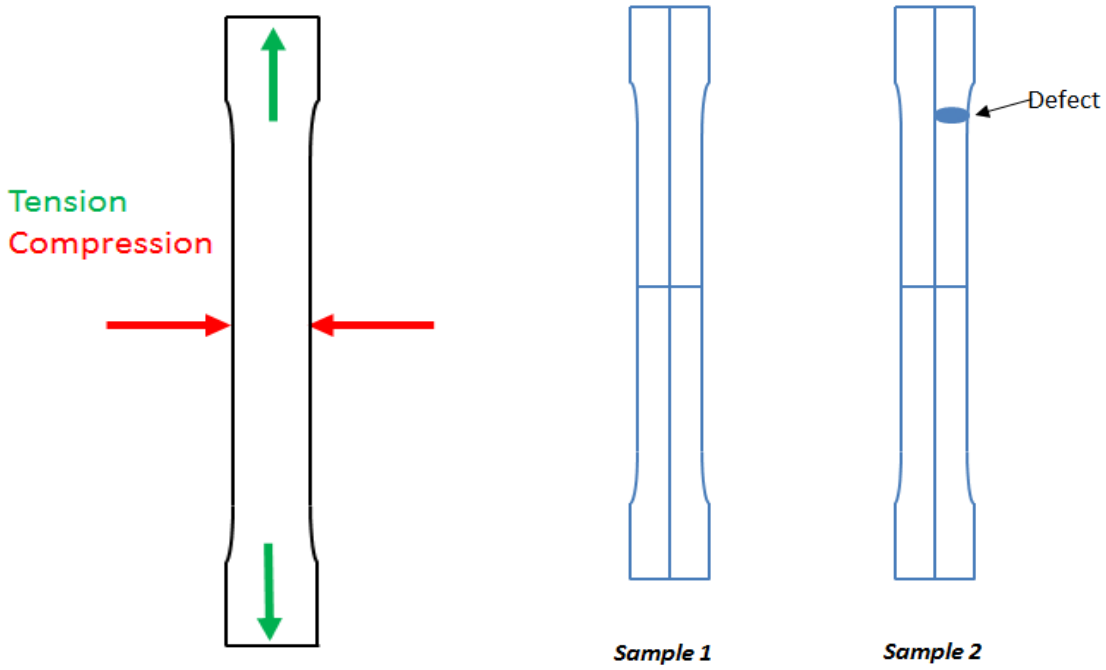

(a) *(b)*

Figure 4-10: (a) Deformation behavior of star specimen during tensile loading. (b) Schematic representation of Sample 1 with no initial defect and Sample 2 with initial defect.

The mechanical response of both samples showed good reproducibility during the elastic deformation and elastic modulus was found out to be in the range of 3.7-3.95 GPa, Figure 4-11 (a). Overall mechanical behavior of both specimens showed good reproducibility during elastic deformation, however, the difference observed in the damage and final fracture was because of irregular stress distribution and damage propagation because of the introduction of an intentional defect in sample 2, Figure 4-11 (b). The objective of this study was to examine the sensitivity and real-time damage detection response of the designed sensor system incorporated into the composite specimens that could be subjected to variable damage behavior.

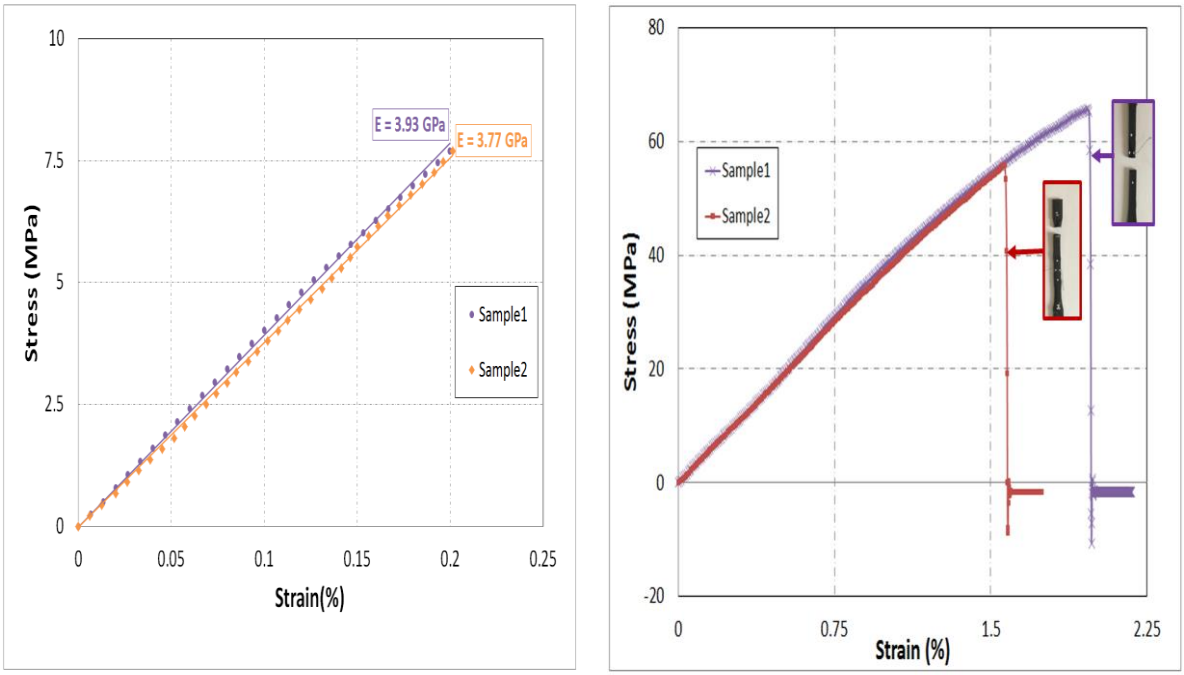

(a) Calculation of Elastic Modulus of each specimen during elastic deformation which showed reproducible behavior.

(b) Overall mechanical behavior of both specimens.

Figure 4-11: Experimental stress-strain behavior of standard composite specimen with and without initial defect.

Furthermore, SEM of the fractured surface of each specimen not only showed fractured fibers and matrix but also indicated the position of the Nylon/Ag fiber sensor (broken), Figure 4-12 (a). Then, on further zoom, fractured Nylon/Ag fiber sensor was also studied and two distinct morphologies were observed. Almost every filament of the Nylon/Ag fiber sensor showed a clean ductile fracture with both coating and core material, Figure 4-12 (b)-(c).

In addition, some filaments also showed a pullout or breakage of the coating during the tensile strain. This breakage of the coating was because of the strain deformation of the core material during elongation and it was more prominent near the ductile failure of the filaments. The breaking of coating could result in the change of resistance of the fiber sensor which would be discussed in detail next section. SEM characterization further confirmed that Nylon/Ag fiber sensor was completely integrated within the matrix and between the random orientation of the fibers as a reinforcement with good contact.

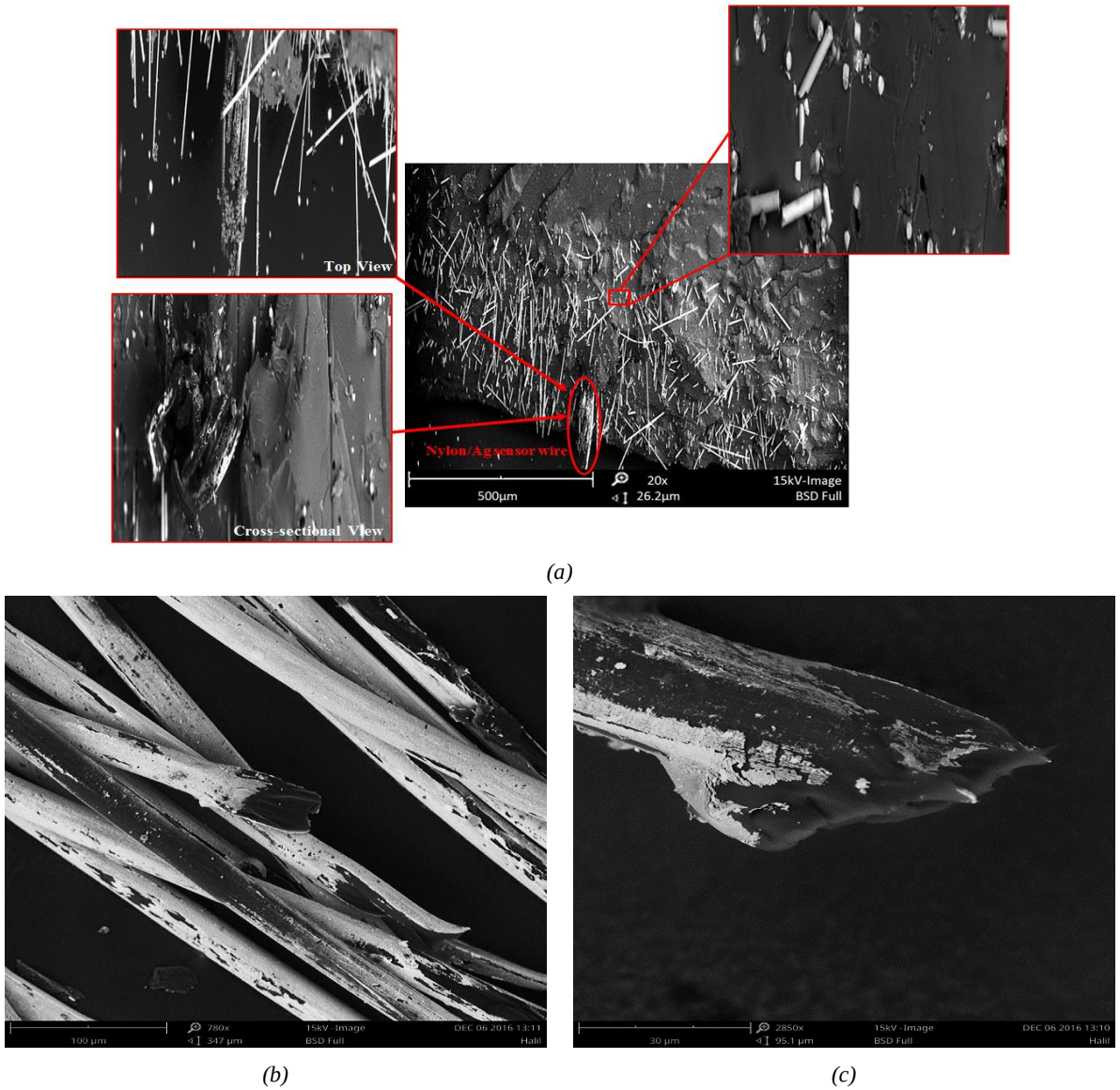

Figure 4-12: SEM characterization of the fractured composite specimen integrated with Nylon/Ag fiber sensor. (a) Random orientation of fibers in the epoxy matrix. It also showed the placement of a Nylon/Ag fiber sensor (after fracture) from both the top and cross-sectional views. (b) Fracture of the Nylon/Ag fiber sensor after the failure of the composite specimen at 100 µm and 786x zoom (c) Single fractured filament of the coated yarn at 30 µm and 2850x zoom.

Both standard specimens with fiber sensors in longitudinal and transverse direction showed good electrical signal response during the mechanical loading. The resistance of fiber sensor along loading (0°) was changing in each case with the gradual increase of the load, however, the response of fiber sensors placed in the transverse direction in both specimens showed a dissimilar response, Figure 4-13 & 4-14. Global electrical response of the sensor system in each specimen showed a change of resistance with the increase of strain in the specimen and resistance reached maximum value during the crack propagation and final fracture. Each position detected different response and it not only monitored the deformation but also identified it as to whether it was compressive or tensile.

In both specimens, the detection of deformation and final fracture by sensor A placed at 0° was identical. The resistance of the sensor A increased gradually in both cases with the increase of strain and reached maximum resistance upon fracture. Moreover, the increase of resistance of sensor A confirmed the presence of tensile stresses along the loading axis in both specimens.

However, sensor B placed in 90° direction in both specimens showed a different overall electrical response. Sensor B in specimen 1 showed a decrease in resistance with the gradual increase of the applied strain which indicated the presence of compressive strains because of the Poisson's effect during the tensile loading and then, resistance reached maximum value upon the damage initiation and final fracture because of breakage, Figure 4-13 & 4-14. Sensor B in specimen 2 showed no prominent change in electrical response during the deformation and even upon fracture, a slight increase in the resistance was observed with good sensitivity, Figure 4-13 & 4-14. This change of behavior of sensor B in specimen 2 was because the damage did not occur in the middle of the specimen where sensor B was placed but occurred near the position of the defect which was introduced during the fabrication. This showed that the placement of the sensor plays a vital role in the monitoring of damage detection. Moreover, the slight increase in the resistance of the sensor B indicated the presence of tensile deformation which confirmed the occurrence of Poisson's effect near the area of the initial defect before final damage. This also verified that even though sensor B did not detect the damage initiation in transverse direction during deformation of the composite specimen but, it indicated the presence of tensile stresses near its position which could be used as a signal to predict that the sample would not fracture ideally because of the presence of imperfection or defect during the fabrication process.

Moreover, it was observed that the resistance increased progressively during the large plastic deformation or damage initiation and propagation just before the final failure of the specimen which was caused by the breaking off of the conductive layer of Ag during the strain deformation of Nylon yarn (as discussed in the previous section). This phenomenon was the actual concept behind the real-time strain monitoring and damage detection performance of the Nylon/Ag fiber sensor. In addition, the SEM images shard in the previous section showed that Nylon/Ag fiber sensor was completely inserted within the fibers and matrix of the composite specimen with good contact and it was deforming simultaneously with the composite specimen that is why there was no loss of contact between the fiber sensor and the mechanical response of the sensor.

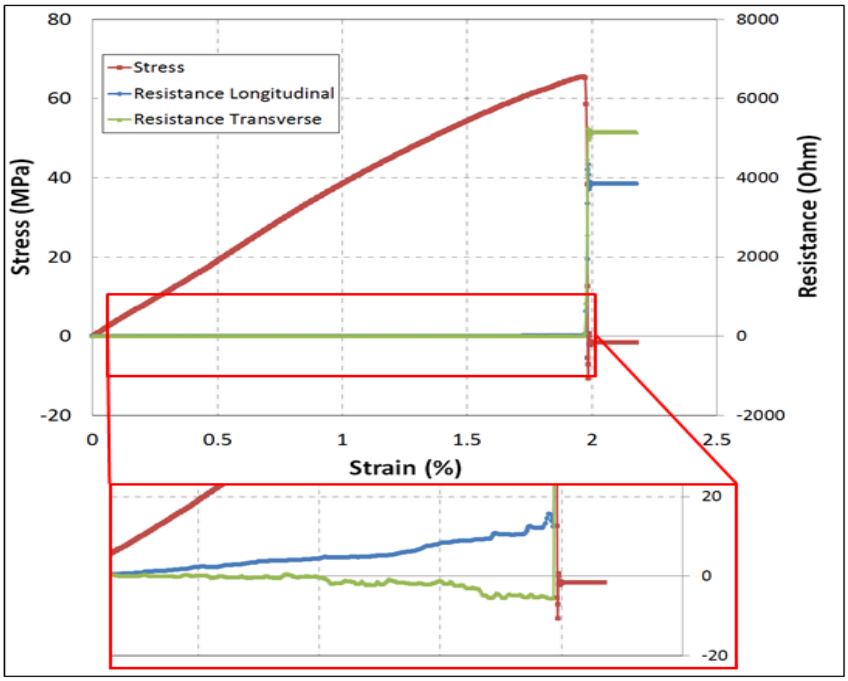

Figure 4-13: Real-time strain monitoring and damage detection by Ny/Ag fiber sensor in standard composite, specimen 1.

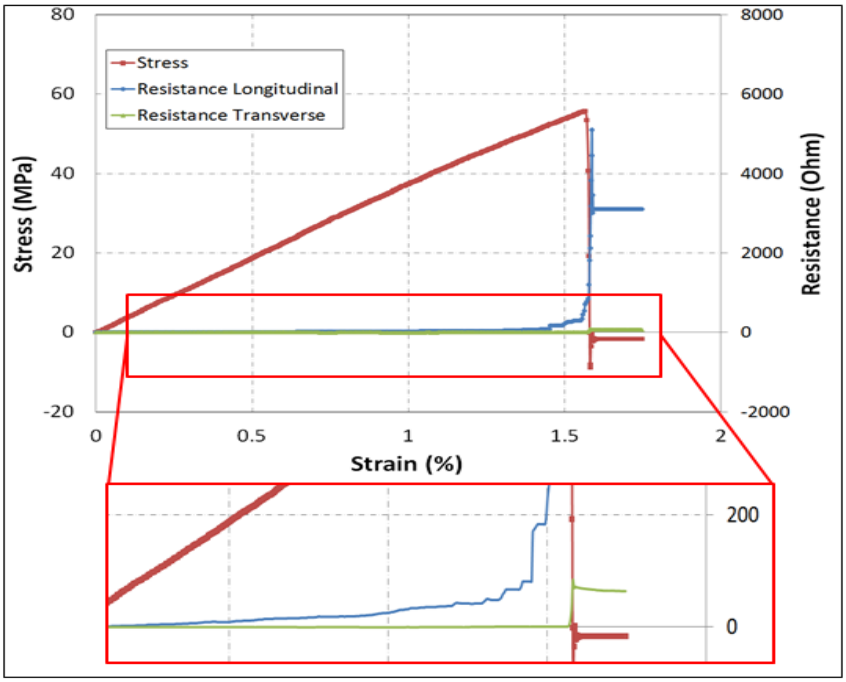

Figure 4-14: Real-time strain monitoring and damage detection by Ny/Ag fiber sensor in standard composite, specimen 2.

Thus, in each specimen, the sensor did not only detect and identify the failure but it also demonstrated the importance of the damage initiation with respect to the position of the fiber sensor in damage detection and prediction. This study can be further continued in the future to study the behavior of the fiber sensor during the fabrication process of composites and to detect any imperfection or defect in the sample before the structural performance.

4.4.2. Real-time monitoring of composite sample under flexural load.

Four successful flexural tests were performed, and data were plotted as stress-strain behavior, Figure 4-15. Both sets of curves presented that all the specimens showed good reproducibility in mechanical response especially in the elastic region which confirmed that the presence of this flexible microscale fiber sensor did not affect the integrity of the composite structure and even their different location in each specimen through the thickness did not act as a defect or inclusion. In addition, mechanical properties consisting of flexural strength, flexural modulus, and fracture strain are given in table 4-1 and were calculated using equations (4-1) - (4-3)

$$\boldsymbol{\sigma_f = \frac{3FL}{2bd^2}} \tag{4-1}$$

$$\boldsymbol{\varepsilon_f = \frac{6Dd}{L^2}} \tag{4-2}$$

$$\boldsymbol{E_f = \frac{L^3 m}{4bd^3}} \tag{4-3}$$

Where, σ_f is flexural stress, ε_f is the flexural strain, E_f is the flexural modulus of elasticity, F is the load at a given point on the load-deflection curve, L is span length, b is the width of the specimen, d is thickness, D is deflection, and m is the gradient of the initial straight-line portion of the load-deflection curve.

The slight difference between at large strain and final fracture observed was because of the reason that stress distribution and damage propagation were complex and slightly unpredictable phenomena in composites because of their complex hybrid structure. This difference in behavior is common in composites and that was the reason why minimum 3-4 tests were conducted to see the reproducibility in results. However, it should be kept in mind that the objective of this study was to examine the sensitivity and real-time damage detection response of the designed fiber sensor incorporated into the composite specimens that could be subjected to flexural failure.

Table 4-1: Mechanical characteristics of the composite specimens subjected to flexural loading

Properties	Unit	Sample 1	Sample2	Sample3	Sample4	Average	St.D.
Flexural Modulus	GPa	11.42	11.52	11.42	11.45	11.4525	0.047
Fracture Strain	%	1.21	1.10	1.40	1.26	1.25	0.124
Flexural Strength	MPa	102.42	106.76	104.83	105.57	105.72	1.831

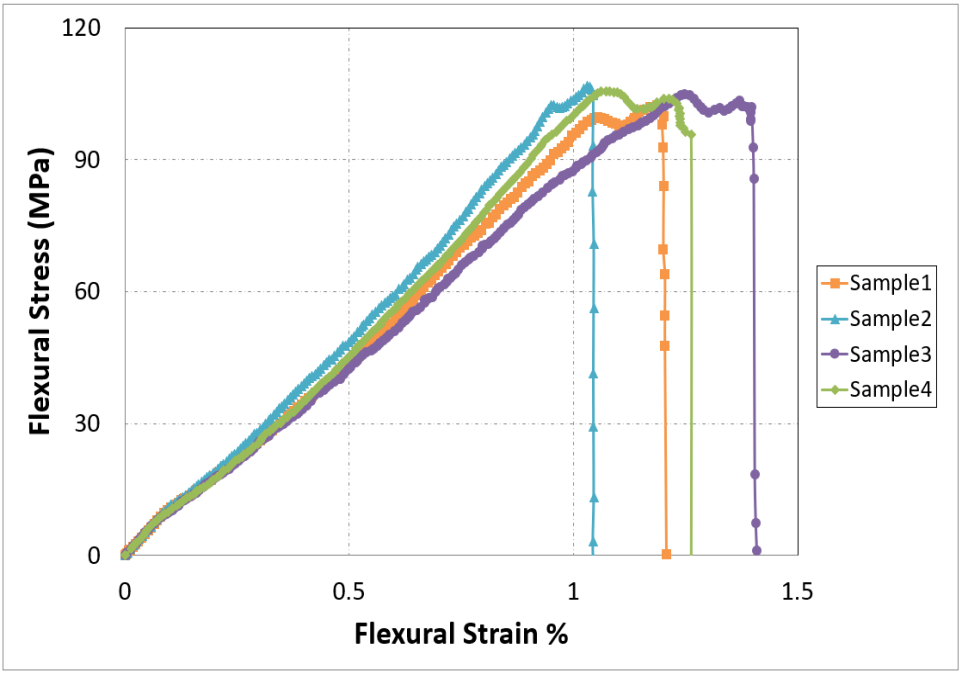

Figure 4-15: Comparison of the experimental flexural stress-strain behavior of all specimens.

The specimen was placed as a simply supported bean on the two bottom rollers while bending force and displacement were applied by the upper third roller at the exact center of the span length. When specimens were subjected to flexural load and the combined effect of both tensile and compressive strains resulted in the generation of macro crack and then final fracture, Figure 4-16 (a). However, in composites, the final fracture was not only dependent on the fiber fracture but was also affected by the interlaminar shear failure and matrix cracking. All four specimens were fractured at the center where there was maximum displacement, Figure 4-16 (b). The optical microscopy (OM) of the fractured surface of each specimen not showed fractured fibers but also indicated the position of the Nylon/Ag fiber sensor (broken), Figure 4-16 (c).

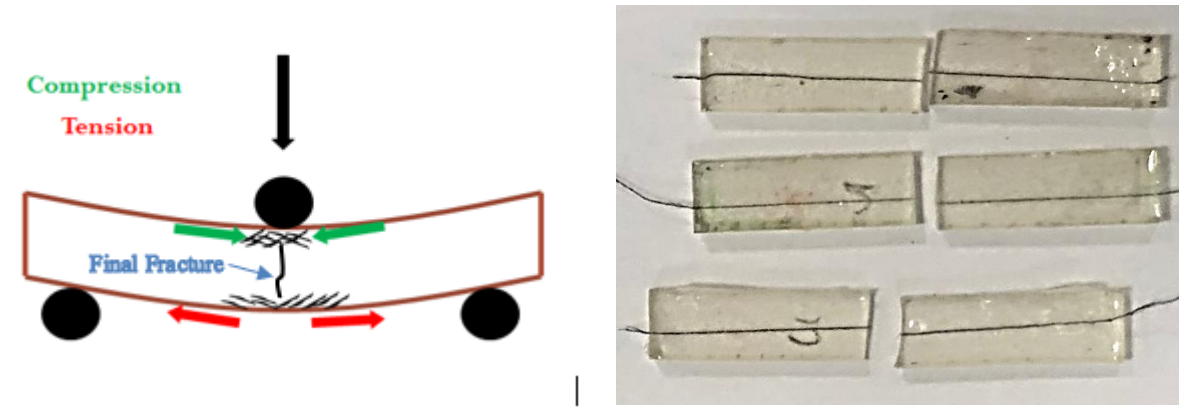

(a) Damage mechanism of the specimen

(b) Fractured specimens

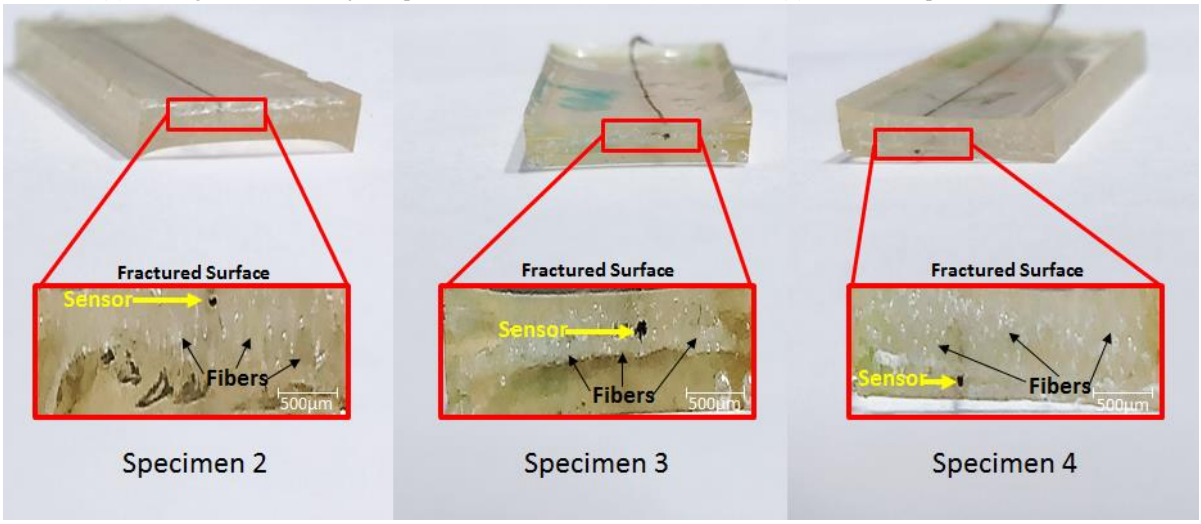

(c) Fractured surface of the all three specimen and position of Nylon/Ag fiber sensor in each specimen.

Figure 4-16: Fracture of composite samples subjected to flexural deflection during a three-point bend test.

Specimen 2, 3, 4 with fiber sensors at the top, middle and bottom respectively showed good electrical signal response during the mechanical loading of the specimen. The resistance was changing in each case with the gradual increase of the load and the Nylon/Ag fiber sensor in all three samples showed similar overall behavior. Global electrical response of the sensor system in each specimen showed a change of resistance with the increase of strain in the specimen and resistance reached maximum value during the crack propagation and final fracture. The maximum value of resistance is achieved at failure, which is identical in all three samples however, during deformation fiber sensor in each specimen showed different behavior because of its position through the thickness. Each position detected different response and it not only monitored the deformation but also identified it as whether it was compressive, tensile, or both.

- Specimen 2 has the fiber sensor beneath the top layer, at the upper surface and showed a decrease in resistance during the deflection just before final failure during the flexural

deflection. This showed that the compression failure was dominant at the upper surface of the specimen just under the roller of the 3-point bend test because the flexural load applied, compressed the upper surface during the deflection, Figure 4-17.

- Specimen 3 has the fiber sensor in the middle and showed a decrease and then a gradual increase in resistance with some variation during the flexural deformation just before the final fracture. This mixed behavior confirmed the presence of tension and compression strains near the center of the composite specimen, Figure 4-18.
- Specimen 4 had the fiber sensor above the bottom layer and showed a gradual increase in resistance during the deformation up to the final failure which showed detection of tensile stresses at the bottom of the specimen because of the localized elongation or stretching of the specimen, Figure 4-19

However, in all three samples, the resistance at the final fracture increased to the maximum value because of the breakage of the sensor system. In each specimen, the sensor did not only detect the failure but it can also differentiate the behavior of failure.

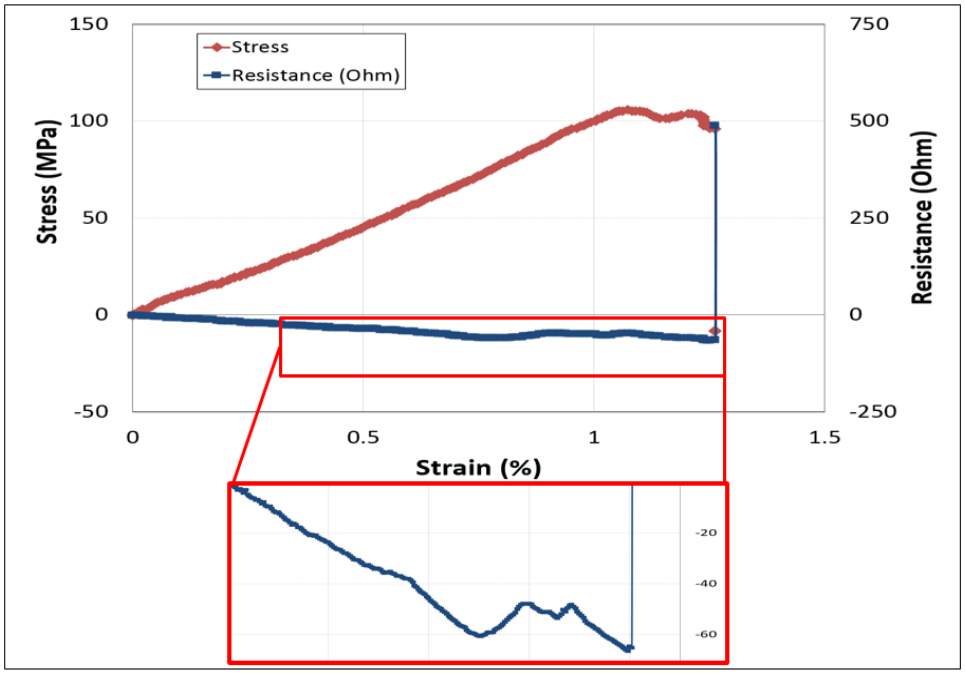

Figure 4-17: Real-time monitoring and damage detection by Nylon/Ag fiber sensor in specimen 2.

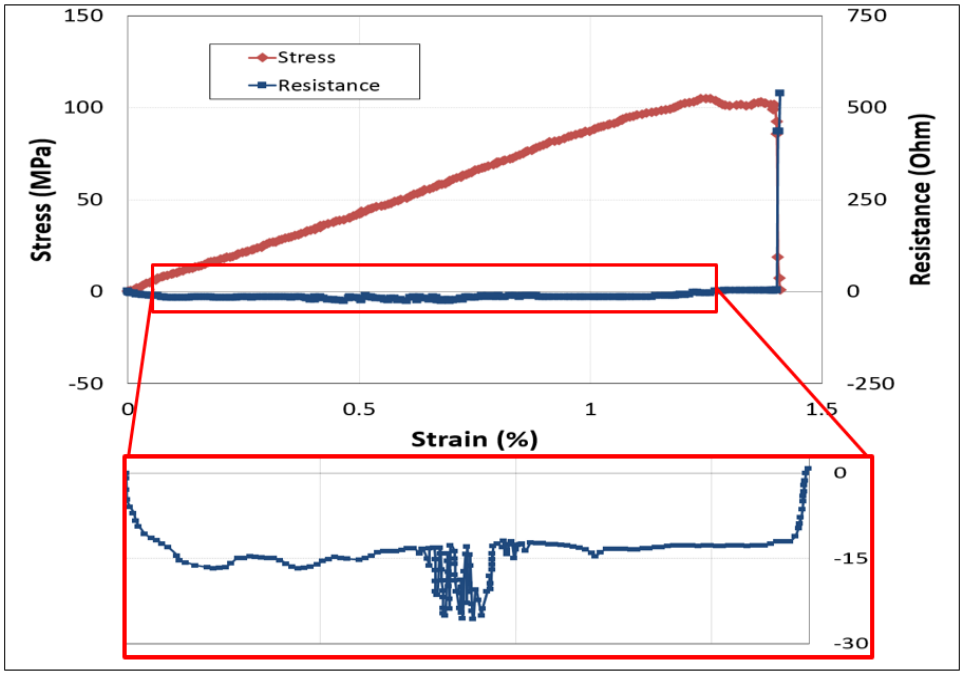

Figure 4-18: Real-time monitoring and damage detection by Nylon/Ag fiber sensor in specimen 3.

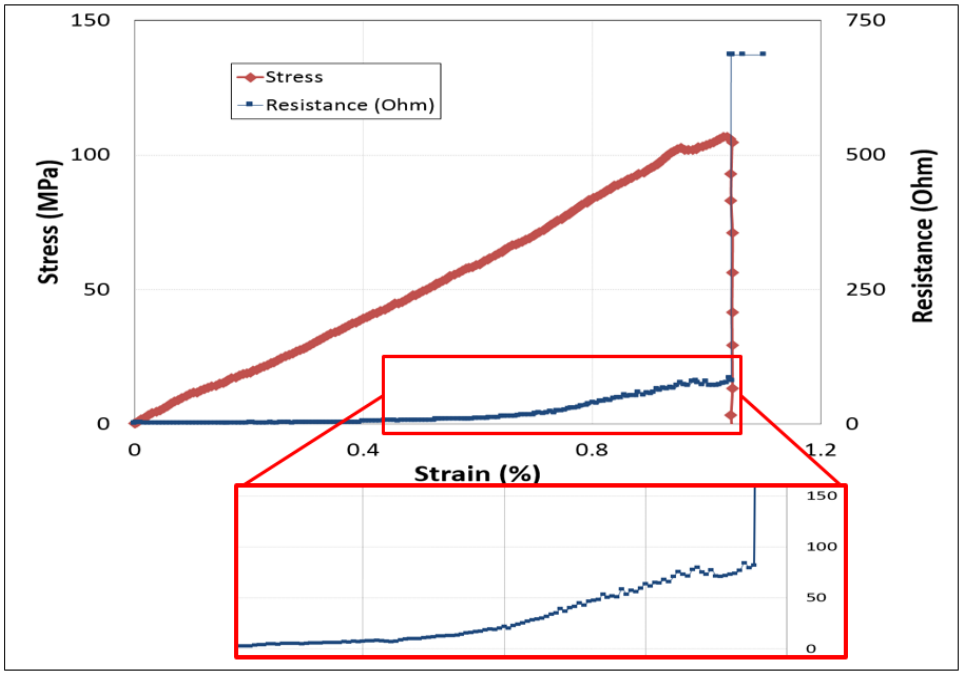

Figure 4-19: Real-time monitoring and damage detection by Nylon/Ag fiber sensor in specimen 4

4.4.3. Real-time monitoring of composite sample under dynamic load

It was necessary to understand the deformation behavior of the composite sample under dynamic impact to apprehend the detection behavior of the Nylon/Ag fiber sensor. The sample was fixed on the two opposite sides and was impacted in the center. The tests performed at 2.5 m/s and 3 m/s respectively showed similar overall mechanical response with a slight increase in the overall force because of the increase in the impact velocity, Figure 4-20. The maximum force at 2.5 m/s and 3 m/s are respectively 12.089 kN and 14.678 kN respectively. During the impact, the sample experienced compression deformation at the upper surface which was in direct contact with the impactor while lower surface experienced tensile stress in response to the compression strain similar to the failure mechanism of the sample subjected to flexural bending [21], Figure 4-21. Then, three tests were performed at 6.5 m/s and they showed good repeatability in the mechanical behavior of the composite samples. The presence of fiber sensors at different locations did not influence the behavior of the composite samples and did not act as inclusion or defect [21]. In addition, the samples were completely fractured at this impact velocity, Figure 4-22. Moreover, there was a significant increase in the mechanical behavior of the sample in comparison to the previous two tests, Figure 4-23.

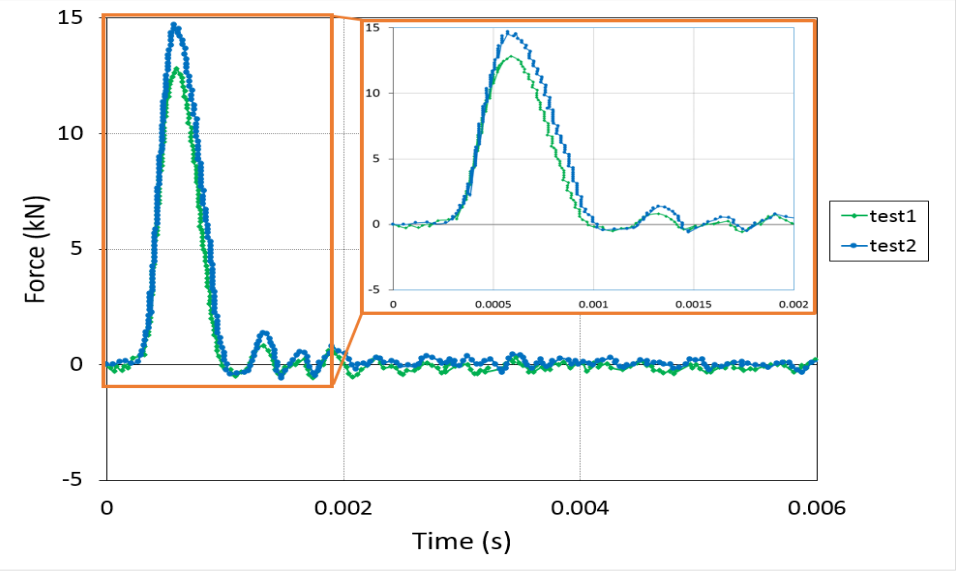

Figure 4-20: Comparison of experimental behavior of the first two tests which were without any visible macro damage.

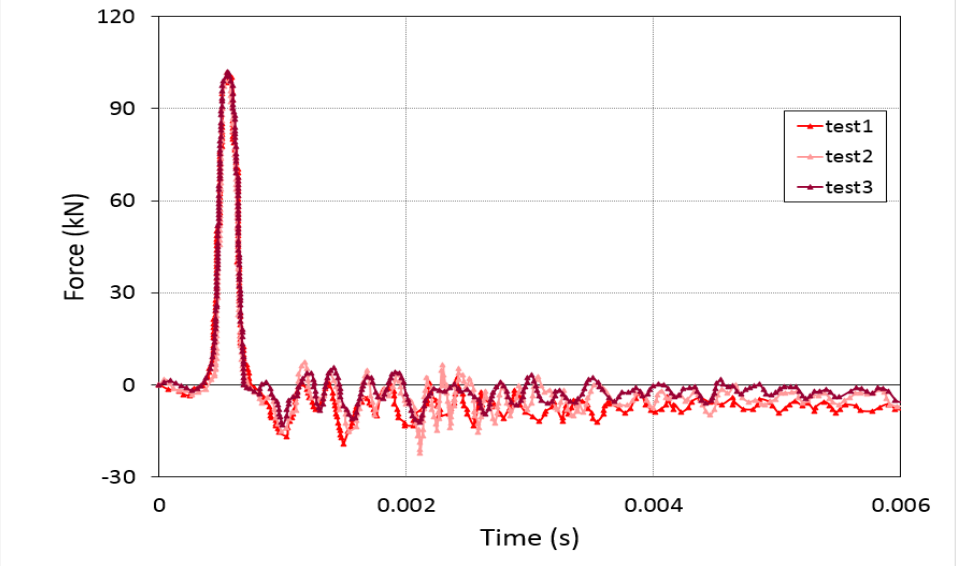

Figure 4-21: Mechanical behavior of fractured composite sample and repeatability of mechanical results. Test 1 was performed on the sample integrated with fiber sensors and test 2 and test 3 were performed on sample without fiber sensors.

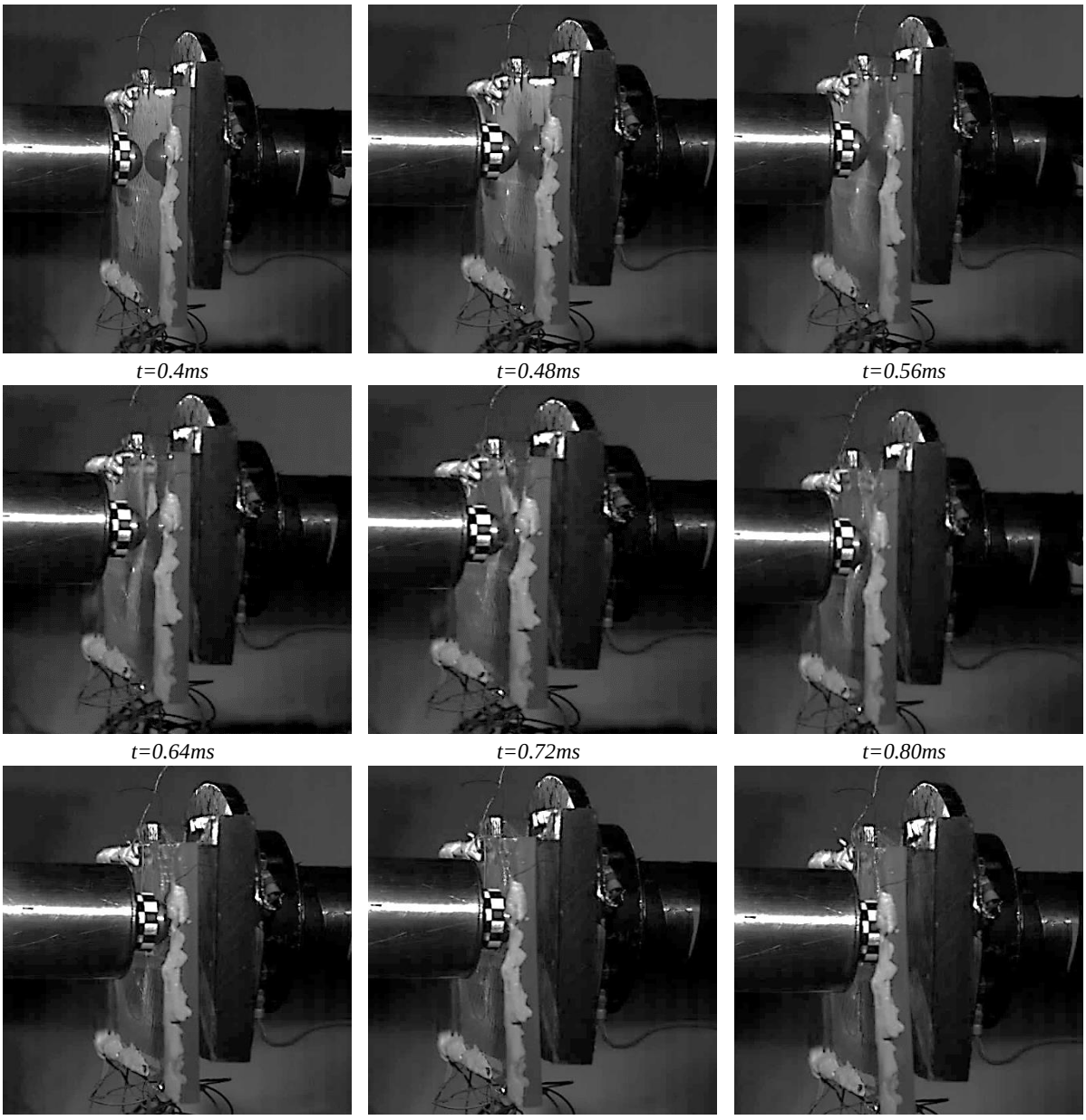

Figure 4-22: Real-time high-speed photographs of dynamic impact test performed at v=6.5 m/s on the composite sample.

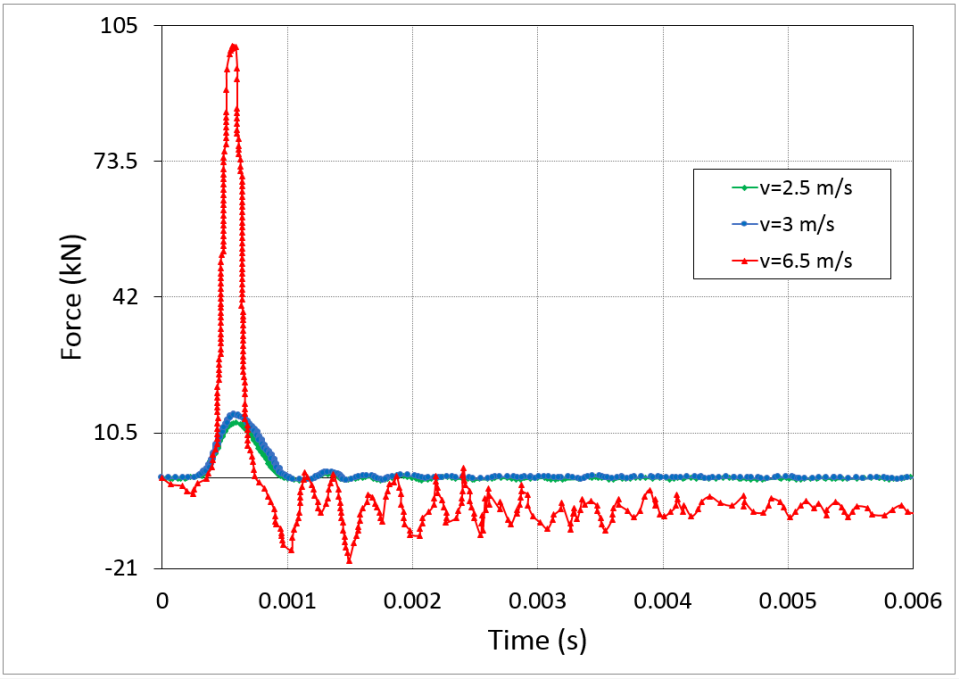

Figure 4-23: Mechanical behavior of all three sets of tests performed at an impact velocity of 2.5 m/s, 3 m/s, and 6.5 m/s respectively.

SEM (Scanning Electron Microscopy) was also carried out of the fractured sample to understand the damage and fracture behavior of the sample and to identify the position of the respective fiber sensors. It was visible in the SEM image that the sample consisted of three plies, figure. It also identified the randomly oriented chopped fibers and epoxy in each ply Figure 4-24 (a)-(b). Moreover, cracks and damage propagation were also visible in the SEM images and one of the interesting things observed was that none of the crack initiation and damage propagation was found near the region of integration of the Nylon/Ag fiber sensor, Figure 4-24 (c)-(d). This concluded that this fiber sensor did not only monitored the sample in real-time but also act as reinforcement and not as a defect [21]. In addition, SEM images also showed the placement of fiber sensors in different positions. For example, two fiber sensors are perpendicular to each other and in different plies were seen in this respective image, Figure 4-24 (e). One of the fiber sensors was in position W and the other one could be anyone from the fiber sensors placed in L_1, L_2, L_3, and L_4. Coated filaments of Nylon/Ag fiber sensors were visible when SEM characterization was carried out at higher magnification, Figure 4-24 (f). Some of the filaments of the broken fiber sensor (during the fracture) also showed removal of coating in some regions and one can distinguish the nylon core from the Ag coating, Figure 4-24 (f).

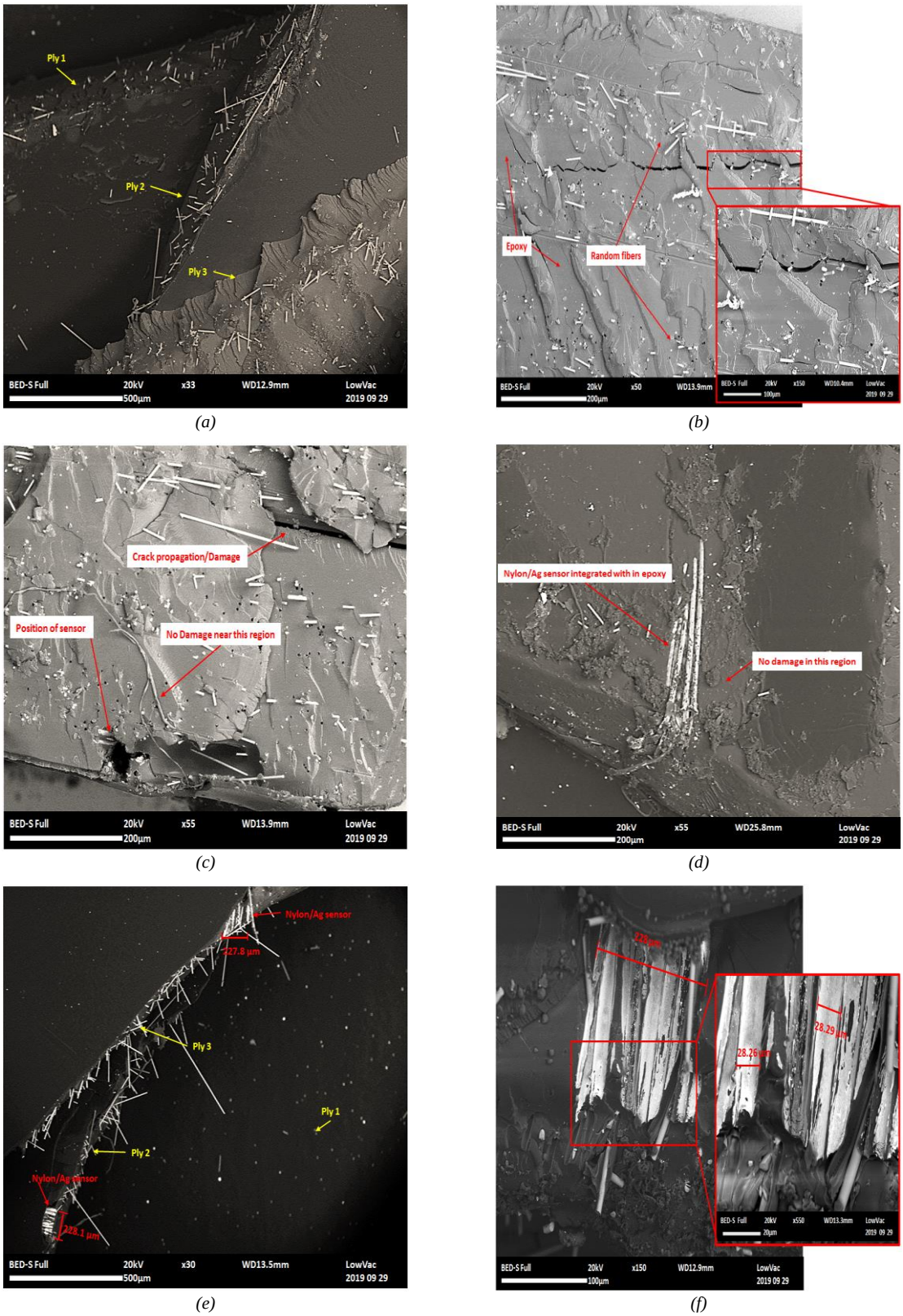

Figure 4-24: SEM characterization of a fractured sample. (a) three plies of the composite specimen with randomly oriented chopped fibers (b) higher magnification to show the presence of a crack (c)-(d) show the positions where Nylon/Ag fibers were placed. These two images were taken at two different coordinates (e) demonstrate two Nylon/Ag fiber sensors placed perpendicular to each other and within different plies (f) shows Nylon /Ag fiber sensor at higher magnification.

The first sample tested at an impact velocity of 2.5 m/s, was to demonstrate the deformation detection by the Nylon/Ag fiber sensor. The electrical response of the sensor correlated

perfectly with the mechanical behavior of the composite. The sample was impacted at the position described in section 4.3 and three very interesting phenomena were observed during the dynamic deformation. The result showed that when the sample was impacted and there was a sudden and quick decrease in the resistance of the sensor placed in L_2 and then it returned to the original behavior, Figure 4-25. The first phenomenon showed that the damage was local and was only detected by the sensor beneath or closer to the impacted region i.e. L_2 and fiber sensor placed in all the other positions did not show any change of behavior. The second phenomenon was that the fiber sensor showed a decrease in resistance which confirmed the presence of compressive strain during the impact which was logical because the surface of the material in direct contact of the impactor experienced compression deformation. The third phenomenon was the return of the electrical resistance to the original signal which showed that there was no permanent damage or damage propagation and the material recovered all the compressive strain induced by the impactor. Furthermore, this test confirmed the ability of the Nylon/Ag fiber sensor to detect the deformation during dynamic deformation or damage in real-time with good accuracy.

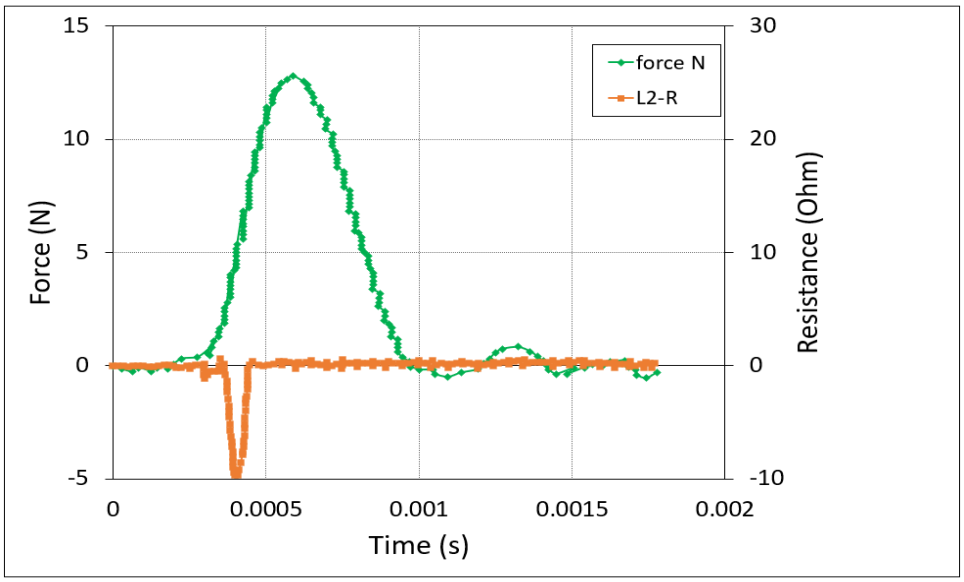

Figure 4-25: In-situ monitoring in the composite sample by Nylon/Ag fiber sensor subjected to dynamic impact at velocity 2.5m/s.

The second sample was tested at the sample position but with slightly higher velocity to induce certain permanent damage in the sample without breakage to understand the behavior of the Nylon/Ag fiber sensor when there is permanent damage and damage propagation. The results showed that sensors in position L_2, L_3, and W showed a change in resistance while fiber sensors in L_1 and L_4 positions did not show any change in the signal, Figure 4-26 (a). This confirmed

that the damage was local and did not propagate on a larger scale. The signal of fiber sensor in positions of L_2, L_3, and W confirmed that the damage propagation was not only in-plane but also through the thickness which confirmed the presence of internal permanent damage whether it was micro or macro in scale. The results of this test showed another important phenomenon, the delay in the change of resistance of each sensor which demonstrated the time taken by the damage to propagate and reach to the region where there was another fiber sensor and this delay was recorded in milliseconds. Furthermore, the distinct behavior each fiber sensor showed the detection of different type of damage, for example, decrease in the resistance of fiber sensor in L_2 and L_3 positions showed the presence of compressive damage in the area which was in direct contact or closer to the impact, however, increase in the resistance of the fiber sensor in W position showed the presence of tensile damage in the lower surface of the specimen.

Another interesting behavior revealed by the signal of these fiber sensors during the deformation was that the fiber sensors in all the three positions showed the different intensity of signal change and all of them did not return to the original signal. The permanent change in the signal of the sensor confirmed the presence of permanent damage or deformation which the difference in the intensity of the signal quantified the amount of damage in the respective regions. For example, fiber sensor in L_2 position showed more increase in resistance than in L_3 position because the L_2 position was closer to the impacted region and experienced maximum effect of the damage while the fiber sensor in W position experienced the minimum effect because damage propagation was more favorable within the ply and travelled faster in comparison to propagating through-thickness.

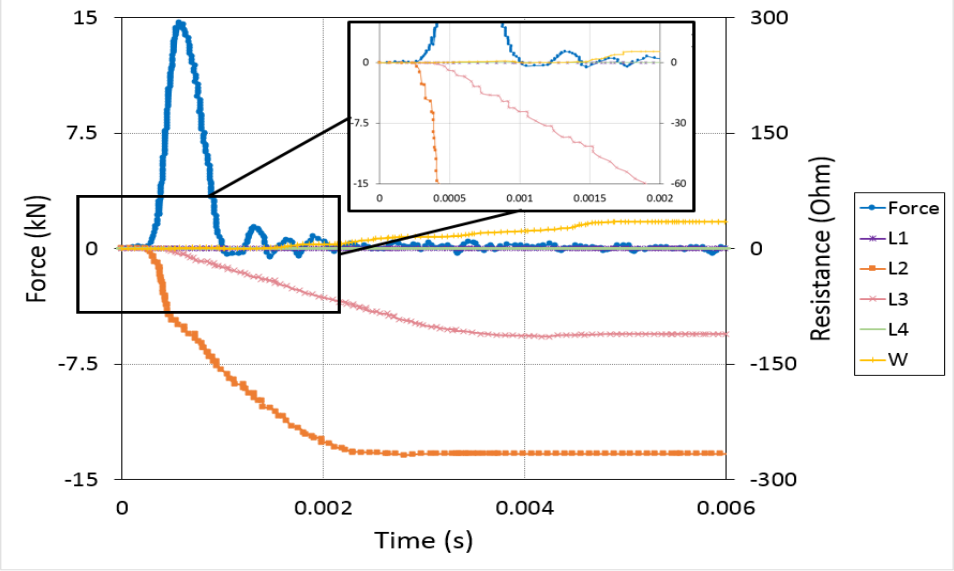

(a)

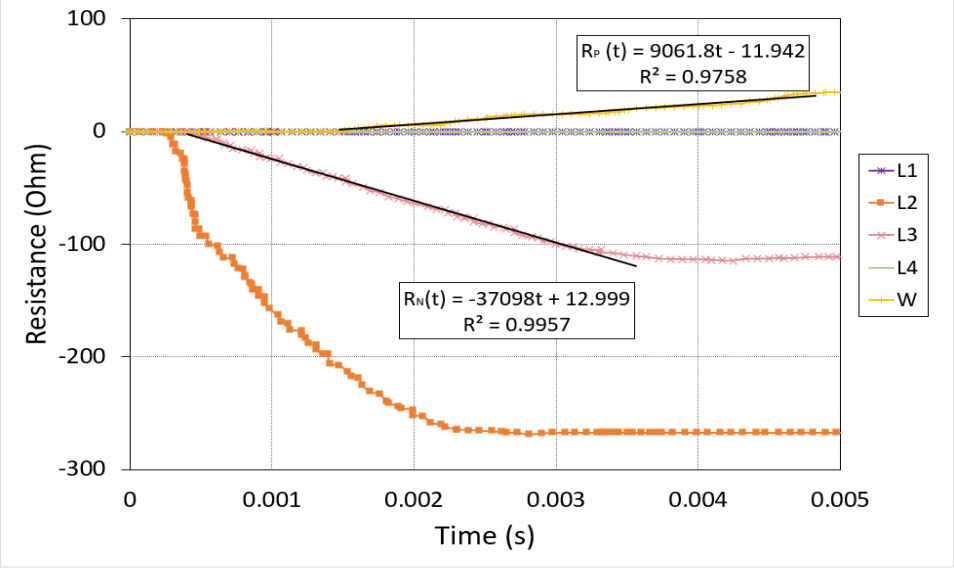

(b)

Figure 4-26: (a) In-situ monitoring in the composite sample by Nylon/Ag fiber sensor subjected to dynamic impact at velocity 3 m/s. (b) Calculation of empirical relations to describe the nonlinear change in resistance with respect to time.

This test confirmed the ability of the said monitoring system to not only detect the damage evolution in the specimen. To further explain the quantification of damage, empirical relations were found to accurately describe the relation of the change in resistance with the damage rate within the composite sample. These empirical relations were derived from the curves in Figure 4-26 (b) and showed a linear change in the resistance (Ohm) with respect to the time (s). Two equations were derived, one for the positive change in resistance (R_P) and one for the negative change in resistance (R_N) of the sensor with respect to the time. These equations are presented as follow:

$$R_P(t) = 9061.8t - 11.942 \quad (4\text{-}4)$$

$$R^2 = 0.9758$$

$$R_N(t) = 37098t + 12.999 \quad (4\text{-}5)$$

$$R^2 = 0.9957$$

Both equations represented similar empirical relations with an accuracy of 97.5-99.5% which further verified the behavior of sensors for the quantification of damage. The relation of resistance with time could be generalized as follow:

$$R(t) = at + b \quad (4\text{-}6)$$

where *a and b* are empirical constants.

Now, to quantify the damage rate within the composite sample, we will use the following relation:

$$GF = \frac{\Delta R/R}{\varepsilon} \quad (4\text{-}7)$$

With $R' = \frac{\Delta R}{R}$

$$\varepsilon = R' * (\frac{1}{GF}) \quad (4\text{-}8)$$

where *GF* is the gauge factor constant of the sensor, *R* is the original resistance of the sensor, and ΔR is the change in the resistance of the sensor with the applied strain ε.

By substituting the equation (4-6) in equation (4-8), the change of resistance with respect to time can give us change in strain with respect to time i.e. damage rate during dynamic deformation of the composite specimen.

$$\varepsilon(t) = R'(t) * (\frac{1}{GF}) \quad (4\text{-}9)$$

Where $\varepsilon(t) = \frac{d\varepsilon}{dt}$

And $$\boldsymbol{R'(t) = \frac{dR'}{dt}}$$

This equation quantifies the strain rate or damage rate in the composite specimen under dynamic loading using the change in resistance of the signal of the Nylon/Ag fiber sensor in real-time.

Furthermore, the Nylon/Ag fiber sensors inserted in the specimens tested at a velocity of 6.5 m/s for the overall fracture and breakage showed a change in resistance in all positions. They further confirmed the phenomena discussed in the previous two sets of tests in addition, the fiber sensor in all the positions reached their maximum resistance to show the final damage depending upon the amount of damage detected. As usual, the fiber sensor in the L_2 position showed a change in resistance before all the other positions and showed a maximum decrease in resistance during fracture of the specimen which confirmed the presence of maximum cracks and damage near and in the impact zone, Figure 4-27. Fiber sensor in position L_1 also showed a decrease in resistance with less intensity than the fiber sensor in position L_2 and with a slight delay in the signal which was less than 1 millisecond. This confirmed the damage propagation form position L_2 to L_1 however, the amount of damage in position L_1 was less than L_2 before final failure. The Nylon/Ag fiber sensors placed in the position L_3 and L_4 showed similar response like position L_1 but their intensity of the signal of lower depending upon their distance from the impact zone. The fiber sensor in position W showed the maximum increase in the resistance before the final fracture indicating the tensile damage but the intensity of the signal confirmed the presence of localized damage. Moreover, it was seen in the results that the delay in the change of signal was maximum for fiber sensor in position L_4 because of the longer distance and it would have taken more time for the damage to propagate there. Damage propagated first to L_1 than to W than to L_3 and L_4 position because the distance through-thickness was less than the position L_3 and L_4. Furthermore, this test helped in understanding the complex damage initiation and propagation behavior in the isotropic composite plate before the final overall fracture.

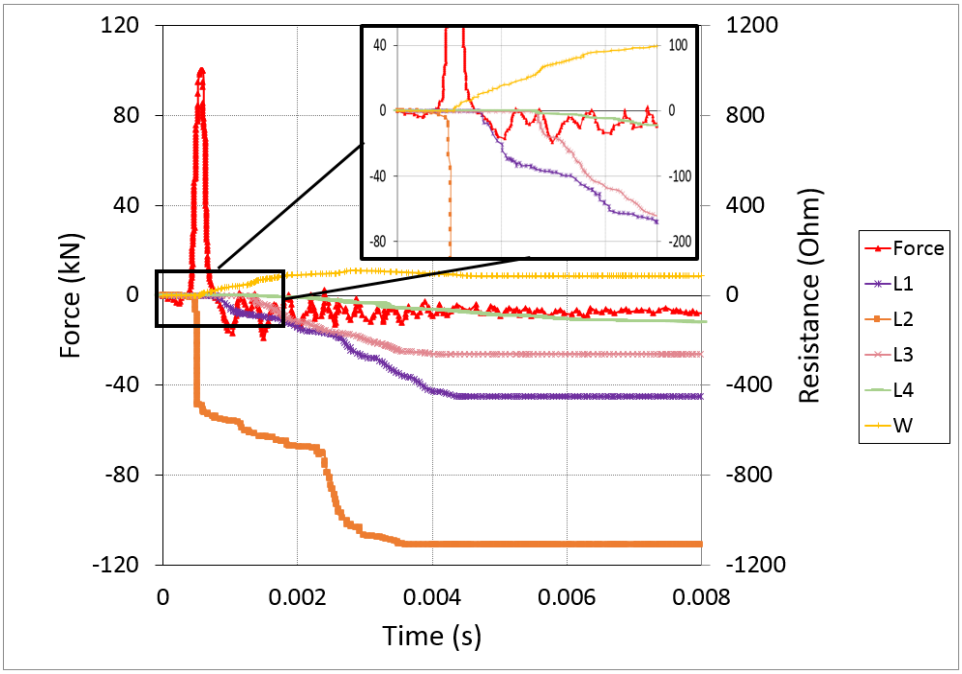

Figure 4-27: In-situ monitoring in the composite sample by Nylon/Ag fiber sensor subjected to dynamic impact at velocity 6.5 m/s.

4.5. Conclusion

In this chapter, an experimental investigation was carried out to examine the application of a Nylon/Ag fiber sensor in real-time monitoring and identification of deformation in composites subjected to tensile and flexural load.

In tensile specimens, the sensor system was inserted in the individual composite specimens at different positions and directions with respect to the loading axis intentionally depending upon the type of damage to be detected. The overall in-situ damage detection of the Nylon/Ag fiber sensor in standard composite specimens showed that the placement of the sensor also plays a vital role in the monitoring of damage and final fracture. Moreover, this study also verified that even though sensor did not detect the damage initiation in the transverse direction of the specimen with initial defect during deformation but its signal indicated the presence of tensile stresses near its position which could be used to predict the presence of imperfection or defect during the fabrication process which led to the imperfect fracture. Moreover, the strain fiber sensor designed did not only monitor the change in the mechanical behavior of the specimen during tensile deformation but, also identified the type of damage whether it was tensile or compressive. Nylon/Ag fiber sensor did not only detect and identify the failure but it also demonstrated the importance of the damage initiation with respect to the position of the fiber sensor in damage detection and prediction.

Similarly, in flexural specimens, Nylon/Ag fiber sensor was inserted in the individual composite specimens at three different locations intentionally depending upon the type of damage to be detected. The experimental results showed good reproducibility in the overall mechanical response of the composite structures and global response of the fiber sensor in the monitoring of the deformation and final fracture. Mechanical response of the composite specimens subjected to flexural loading, not only showed reproducibility of results but also showed that the presence of the strain fiber sensor did not behave like an intrusion or defect even when placed at different positions through the thickness. Overall electrical response of the Nylon/Ag fiber sensor in each specimen also showed reproducibility in results in monitoring of the deformation during the deflection and detecting of final fracture. However, the variation in the resistance response of the Nylon/Ag fiber sensor during the deflection was because of the difference in the placement of fiber sensor in each specimen. It is understood that under flexural deflection the specimen experienced compressive and tensile stresses at the upper and lower surface respectively so the behavior of each fiber sensor showed detection of different types of damage. The sensor system not only monitors the change in the mechanical behavior of the specimen during the deflection and detected the presence of damage until final fracture but also identified the type of damage whether it was tensile, compressive, or both.

In dynamic tests, an experimental study was performed to examine and understand the application of the Nylon/Ag fiber sensor in in-situ monitoring and identification of damage under low-velocity impact. The experimental results showed good repeatability in the mechanical performance of the composite structures and response of the fiber sensor in the monitoring of the deformation correlated perfectly with their dynamic behavior. Each fiber sensor showed individual response signals during the deformation of the composite specimen because of their specific position. This distinct behavior of each fiber sensor confirmed the detection of different types of damage i.e. tensile or compression during the impact and different intensity or magnitude of the signals quantified the amount of damage induced. Moreover, delay in the change of resistance of the Nylon/Ag fiber sensor according to its respective position demonstrated the damage propagation phenomenon for dynamic loading and this detection was in milliseconds. Thus, each fiber sensor showed the detection of different types of deformation, quantified them, indicated whether the deformation was overall or localized, and demonstrated damage propagation throughout the sample.

This Nylon/Ag fiber sensor showed good potential as a flexible reinforcement in composite materials for real-time monitoring, detection, and identification of damage. Moreover, this

study also showed that it is possible to detect the damage whether it is within the direction of applied load or not by studying the response of the Nylon/Ag fiber sensor. Moreover, the Nylon/Ag fiber sensor demonstrated good potential for in-situ monitoring under dynamic loading by demonstrating a perfect correlation of its signal with the dynamic failure mechanism of the composite specimen. This verified the stability and durability of this fiber sensor and this study can be further continued with different types of composite specimens such as unidirectional (UD) composites or under other dynamic configurations.

References

[1] C. F. Campbell, *Structural Composite Materials*. Ohio: ASM International, 2010.

[2] D. Cai, J.; Qiu, L.; Yuan, S.; Shi, L.; Liu, P.; Liang, "No Title," in *Composites and Their Applications*, Ning Hu, Ed. InTech Open, 2012.

[3] Z. K. Awad, T. Aravinthan, Y. Zhug, and F. Gonzalez., "A review of optimization techniques used in the design of fibre composite structures for civil engineering applications.," *Mater. Des.*, vol. 33, pp. 534–544, 2012.

[4] *ASM Handbook Volume 21: Composites,*. ASM International, 2001.

[5] J. W. C. Pang and I. P. Bond, "A hollow fibre reinforced polymer composite encompassing self-healing and enhanced damage visibility," *Compos. Sci. Technol.*, vol. 65, no. 11, pp. 1791–1799, 2005, doi: https://doi.org/10.1016/j.compscitech.2005.03.008.

[6] C. Dry, "Procedures developed for self-repair of polymer matrix composite materials," *Compos. Struct.*, vol. 35, no. 3, pp. 263–269, 1996, doi: https://doi.org/10.1016/0263-8223(96)00033-5.

[7] C. Dry and W. McMillan, "A novel method to detect crack location and volume in opaque and semi-opaque brittle materials," *Smart Mater. Struct.*, vol. 6, no. 1, pp. 35–39, Feb. 1997, doi: 10.1088/0964-1726/6/1/004.

[8] H. Benyahia, M. Tarfaoui, A. El Moumen, D. Ouinas, and O. H. Hassoon, "Mechanical properties of offshoring polymer composite pipes at various temperatures," *Compos. Part B Eng.*, vol. 152, pp. 231–240, 2018, doi: https://doi.org/10.1016/j.compositesb.2018.07.014.

[9] S. Sassi, M. Tarfaoui, and H. B. Yahia, "Thermomechanical behavior of adhesively bonded joints under out-of-plane dynamic compression loading at high strain rate," *J. Compos. Mater.*, vol. 52, no. 30, pp. 4171–4184, 2018, doi: 10.1177/0021998318777048.

[10] A. El Moumen, M. Tarfaoui, H. Benyahia, and K. Lafdi, "Mechanical behavior of carbon nanotubes-based polymer composites under impact tests," *J. Compos. Mater.*, vol. 53,

no. 7, pp. 925–940, 2019, doi: 10.1177/0021998318793502.

[11] O. H. Hassoon, M. Tarfaoui, and A. E. M. Alaoui, “An experimental investigation on dynamic response of composite panels subjected to hydroelastic impact loading at constant velocities,” *Eng. Struct.*, vol. 153, pp. 180–190, 2017, doi: https://doi.org/10.1016/j.engstruct.2017.10.029.

[12] J.-B. Ihn and F.-K. Chang, “Pitch-catch active sensing methods in structural health monitoring for aircraft structures,” *Struct. Heal. Monit.*, vol. 7, no. 1, pp. 5–9, 2008.

[13] B. Lin and V. Giurgiutiu, “Modeling and testing of PZT and PVDF piezoelectric wafer active sensors,” *Smart Mater. Struct.*, vol. 15, p. 1085, 2006, doi: 10.1088/0964-1726/15/4/022.

[14] A. C. Raghavan and C. Cesnik, “Review of Guided-Wave Structural Health Monitoring,” *Shock Vib. Dig.*, vol. 39, pp. 91–114, 2007, doi: 10.1177/0583102406075428.

[15] V. Zilberstein *et al.*, “MWM eddy-current arrays for crack initiation and growth monitoring.,” *Int. J. Fatigue.*, vol. 25, no. 9–11, pp. 1147–1155, 2003.

[16] A. Loayssa, “Optical Fiber Sensors for Structural Health Monitoring,” in *New Developments in Sensing Technology for Structural Health Monitoring*, S. C. Mukhopadhyay, Ed. Berlin, Heidelberg: Springer Berlin Heidelberg, 2011, pp. 335–358.

[17] J. P. Lynch, K. H. Law, A. S. Kiremidjian, T. W. Kenny, E. Carryer, and A. Partridge, “The Design of a Wireless Sensing Unit for Structural Health Monitoring,” in *3rd International Workshop on Structural Health Monitoring*, 2001.

[18] F.-G. Yuan, *Structural Health Monitoring (SHM) in Aerospace Structures*. Oxford, UK: Elsevier, 2016.

[19] J. E. Michaels, “Detection, localization and characterization of damage in plates with an in situ array of spatially distributed ultrasonic sensors.,” *Smart Mater. Struct.*, vol. 17, no. 3, 2008.

[20] X. P. Zhu, P. Rizzo, A. Marzani, and J. Bruck, “Ultrasonic guided waves for nondestructive evaluation/structural health monitoring of trusses.,” *Meas. Sci. Technol.*,

vol. 21, no. 4, 2010.

[21] S. Sassi, M. Tarfaoui, and H. Ben Yahia., “In-situ heat dissipation monitoring in adhesively bonded composite joints under dynamic compression loading using SHPB,” *Compos. Part B Eng.*, vol. 54, pp. 64–76, 2018.

[22] M. Tarfaoui, A. El Moumen, and H. Ben Yahia., “Damage detection versus Heat dissipation in E-Glass/Epoxy laminated composites under dynamic compression at high strain rate.,” *Compos. Struct.*, vol. 186, pp. 50–61, 2018.

[23] M. Saafi, “Wireless and embedded carbon nanotube networks for damage detection in concrete structures,” *Nanotechnology*, vol. 20, no. 39, p. 395502, 2009, doi: 10.1088/0957-4484/20/39/395502.

[24] F. Azhari and N. Banthia, “Cement-based sensors with carbon fibers and carbon nanotubes for piezoresistive sensing,” *Cem. Concr. Compos.*, vol. 34, no. 7, pp. 866–873, 2012, doi: https://doi.org/10.1016/j.cemconcomp.2012.04.007.

[25] H. Cho and C. J. Lissenden, “Structural health monitoring of fatigue crack growth in plate structures with ultrasonic guided waves,” *Struct. Heal. Monit.*, vol. 11, no. 4, pp. 393–404, 2012, doi: 10.1177/1475921711430439.

[26] M. Saeedifar, M. A. Najafabadi, J. Yousefi, R. Mohammadi, H. H. Toudeshky, and G. Minak, “Delamination analysis in composite laminates by means of Acoustic Emission and bi-linear/tri-linear Cohesive Zone Modeling,” *Compos. Struct.*, vol. 161, pp. 505–512, 2017, doi: https://doi.org/10.1016/j.compstruct.2016.11.020.

[27] D. Crivelli *et al.*, “Localisation and identification of fatigue matrix cracking and delamination in a carbon fibre panel by acoustic emission,” *Compos. Part B Eng.*, vol. 74, pp. 1–12, 2015, doi: https://doi.org/10.1016/j.compositesb.2014.12.032.

[28] S. Wang, D. D. L. Chung, and J. H. Chung, “Impact damage of carbon fiber polymer–matrix composites, studied by electrical resistance measurement,” *Compos. Part A Appl. Sci. Manuf.*, vol. 36, no. 12, pp. 1707–1715, 2005, doi: https://doi.org/10.1016/j.compositesa.2005.03.005.

[29] S.-C. Woo and T.-W. Kim, “High-strain-rate impact in Kevlar-woven composites and fracture analysis using acoustic emission,” *Compos. Part B Eng.*, vol. 60, pp. 125–136,

2014, doi: https://doi.org/10.1016/j.compositesb.2013.12.054.

[30] E. Vorathin, Z. M. Hafizi, S. A. C. Ghani, and K. S. Lim, “Real-time monitoring system of composite aircraft wings utilizing Fibre Bragg Grating sensor,” 2016.

[31] H. Liu, Z. Zhang, H. Jia, D. Zhang, Y. Liu, and J. Leng, “Real-time monitoring system for multi-MW scale wind blades using FBG sensors,” in *Health Monitoring of Structural and Biological Systems XIII*, 2019, vol. 10972, pp. 353–360, doi: 10.1117/12.2514675.

[32] B.-W. Jang and C.-G. Kim, “Impact localization of composite stiffened panel with triangulation method using normalized magnitudes of fiber optic sensor signals,” *Compos. Struct.*, vol. 211, pp. 522–529, 2019, doi: https://doi.org/10.1016/j.compstruct.2019.01.028.

[33] C. R. Farrar and K. Worden, “An introduction to structural health monitoring,” *Philos. Trans. R. Soc. A Math. Phys. Eng. Sci.*, vol. 365, no. 1851, pp. 303–315, 2007, doi: 10.1098/rsta.2006.1928.

[34] X. Wang and D. D. L. Chung, “Real-time monitoring of fatigue damage and dynamic strain in carbon fiber polymer-matrix composite by electrical resistance measurement,” 1997.

CHAPTER 5 : FINITE ELEMENT MODELING AND NUMERICAL INVESTIGATION

In this chapter, numerical simulations are performed using finite element modeling (FEM) in ABAQUS to develop a model in which the electrical and mechanical behavior of the respective specimen can be correlated. The objective of this study is to correlate the electrical signal of the sensor with the mechanical deformation of the composite sample using numerical modeling. In addition, this model is used to verify the experimental results of detecting deformation in different directions and positions of the composite sample under different loading conditions. However, it should be kept in mind that the purpose of this study is to develop a simple macroscale model to demonstrate the electromechanical correlation between two different geometries and materials. Micromechanics and interfacial interaction of the molecular level are not in the scope of this study though, it will be considered in the future. First, the experimental electromechanical response of the selected sensor system Nylon/Ag fiber sensor is sensor wire was t verified numerically with good agreement in results. Then, the simplified model of single fiber with electrical behavior of Ag and mechanical response of Nylon was inserted into a composite specimen to demonstrate the detection of strain deformation under different quasi-static loadings similar to experimental studies. The results were very encouraging and the signal from the sensor was correlated perfectly with the mechanical behavior of the specimen. In addition, the numerical results of not only the composite sample but also the detection signal of the sensor system correlated with the experimental results according to its specific position and direction. Afterward, an attempt was carried out to correlate the strain deformation rate during dynamic impact using empirical correlations because the study of electrical response in dynamic explicit of ABAQUS is still not developed yet.

5.1. Introduction

In addition to experimental investigation, numerical and analytical approaches had also been used to model the real-time behavior of different sensing techniques. They include advanced in-situ SHM techniques such as Piezo-electric sensors, ultrasonic transducers to in-situ SHM with nanomaterials. However, the FE modeling of SHM with nanotechnology is still under development.

Numerous analytical approaches were developed in the past to study the electromechanical response of nanomaterials reinforced adhesives and composites [1], [2]. Besides this, various numerical models were also established in recent years to overcome restrictions of analytical approaches [3]–[7]. However, these numerical approaches were more focused on electromechanical response of nanocomposites developed by inserting the smart nanoparticles in the parent structure but no or very limited research had been conducted in developing finite element modeling in which real-time sensor wires or thin films created by nanomaterials such as CNTs, graphene or metal nanoparticles is attached or inserted in the structure and to correlate the electromechanical response of the sensor with the mechanical behavior of the specimen. This area is still to be discovered.

It is also important to understand the concept of computational modeling of these flexible yarns to model and analyze their behavior numerically. However, very little research has been conducted to use the concept of coated yarn as a flexible piezo-resistive strain sensor for structural health monitoring without jeopardizing the mechanical behavior of core material especially numerically. Different researchers had worked on numerical models and had used finite element analysis (FEA) to predict the mechanical behavior of yarn [8]–[10]. With the advancement of computer-aided design (CAD) and computer-aided engineering (CAE), it is possible to investigate the mechanical behavior of yarn using finite element modeling (FEM) [11]. Many CAD models of filaments, yarns, and fabrics have been developed by researchers with most of them related to geometrical modeling of yarns based on single lined yarn path also known as pitch length [12]–[15]. Some researchers have attempted to overcome difficulties like small and large scale deformation, complex material properties, and 3D modeling [16]. Several analytical models had been established for the estimation of the mechanical tensile performance of yarns. The tensile behavior of yarn, using force method, was first studies 90 years ago which were then extended to examine the mechanical behavior of continuous filament yarns [17], [18]. Other than the force method, the energy method was used to study the continuous filament and

to predict the whole stress-strain behavior in Tenasco yarn which was first proposed by Treloar and Riding [19]. Then, Riding and Wilson [20] extended this study and predicted the stress-strain relations for materials such as low tenacity Terylene, Super Tenasco, and Nylon 6-6. Moreover, the energy method was also used to study the tensile and torsional behavior of bulky wool single yarn [21]. Cartraud and Messager [22] studied the model of 1+6 (six cylindrical filaments were wrapped around a straight filament at the core) stranded fibrous structure in tensile behavior. Vassiliadis et al. [16] suggested a computational method to study the mechanical behavior of multifilament twisted yarn from 2 to 1200 filaments based on FEM. However, up to this date and to the best knowledge of the author, very limited or no research has been conducted to experimentally and/or numerically analyze a coated yarn and to study the electromechanical response of coated yarn-based wires models.

In this chapter, we will discuss the modeling of the electromechanical response of a standalone sensor and correlation of electrical response of a sensor embedded within a composite specimen with the mechanical deformation of the sample under different loading conditions including quasi-static and dynamic loading. These finite element models will be used to correlate the experimental results of the selected sensor system i.e. Nylon/Ag fiber sensor. Therefore, this chapter is divided into three sections:

- Section I: 3D modeling and numerical investigation of standalone Nylon/Ag sensor fiber
- Section II: 3D modeling and numerical investigation of Nylon/Ag fiber sensor within the composite sample in different positions and directions to monitor strain deformation under cyclic quasi-static loadings i.e. tensile and flexural
- Section III: 3D modeling and numerical investigation of Nylon/Ag fiber sensor within the composite sample under dynamic impact to monitor elastic deformation.

All these numerical results were correlated with the experimental results of the respective sensor system. The purpose of this numerical investigation was to develop a finite element model which can duplicate experimental results and has the ability of present the detection strain deformation in the composite sample with a 3D sensor embedded in it, however, this model can be further modified and studied on molecular interaction level to validate the experimental investigation of other two sensor systems which is in the scope of future work.

5.2. Section I: Standalone Sensor-Nylon/Ag fiber sensor

5.2.1. 3D modeling of Nylon/Ag standalone sensor

Coupled field analysis in commercial ABAQUS/standard software was used to model the electromechanical behavior and verification of experimental behavior of standalone Nylon/Ag fiber sensor results. The sample geometry of conductive thin film coated monofilament was developed at the microscale to avoid aspect ratio problems during meshing and reduce the computational time, Figure 5-1 (a). Coating and monofilament fiber was model as three-dimensional isotropic materials because Ag metal and nylon polymer both materials show isotropic deformation behavior under mechanical loading. Both coating and monofilament fiber were assigned their respective mechanical, thermal, and electrical properties which are essential to conduct coupled field analysis even though, thermal behavior is not a concern. The conductive coating was attached with the core of nylon monofilament through surface-node interaction as electro-thermo-mechanical, Figure 5-1 (b). As per experimental results, the standalone sensor was fixed from one end and tensile elongation was applied on the other end in the machine while electrodes were attached at both ends of the sensor system. Similar boundary conditions were applied consisted of both mechanical and electrical loads, Figure 5-1 (c). The model was then discretized into 3D elements and mesh convergence study was conducted to eliminate any dependency upon the mesh size and its effect on the numerical simulation. Figure 5-2 (a) demonstrates that total 5 mesh sizes were studies to achieve the mesh convergence in maximum mechanical stresses of both materials i.e. nylon core and Ag coating, however, to achieve the precision in results without compromising the computational time, mesh size at which convergence of the curve began i.e. m=0.08 was selected. The model was meshed using a Q3D8 8-node brick element with trilinear electric, mechanical and temperature, Figure 5-2 (b).

This 3D model was first used to verify the experimental results of a standalone test performed on untwisted yarn (Annex I). This step was carried out because untwisted yarn had all coated filaments arranged unidirectionally and was resembled more the coated monofilament model. The objective was to simplify the model enough so it can easily be used to monitor the behavior of the composite sample by inserting in different positions and directions.

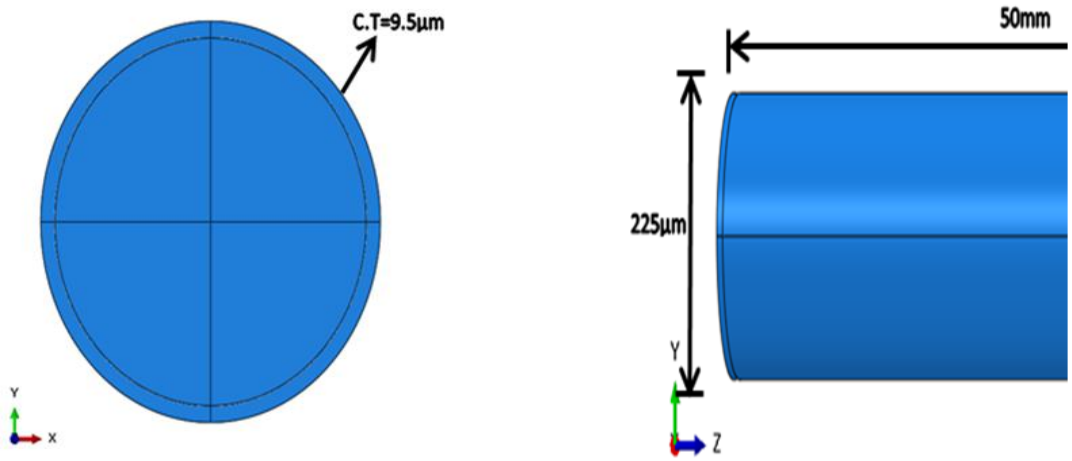

(a) 3D Model of Assembly

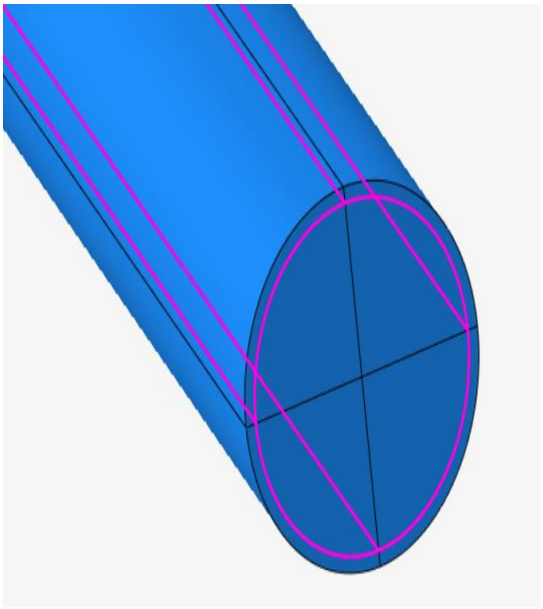

(b) Surface interaction between the Ag coating and Nylon core

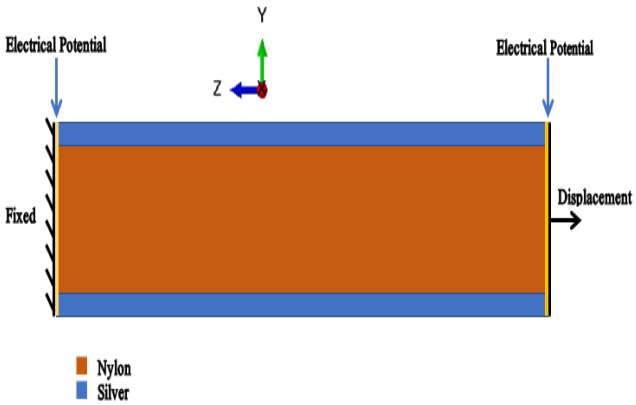

(c) Applied Mechanical and electrical loads

Figure 5-1: 3D model and finite element modeling of the Nylon/Ag fiber sensor.

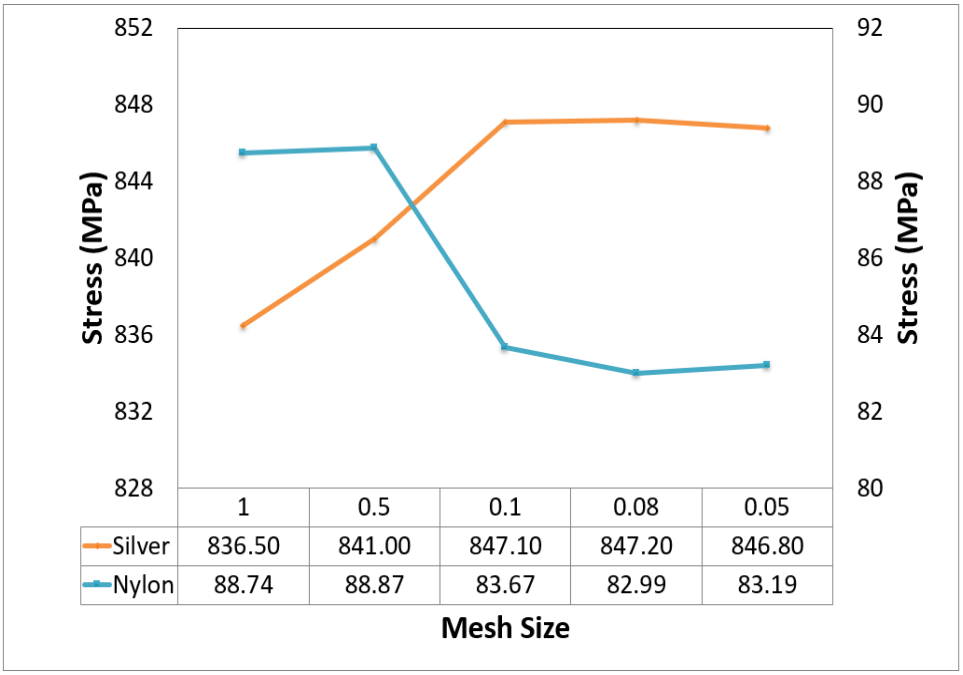

	1	0.5	0.1	0.08	0.05
Silver	836.50	841.00	847.10	847.20	846.80
Nylon	88.74	88.87	83.67	82.99	83.19

(a) Mesh Convergence Study

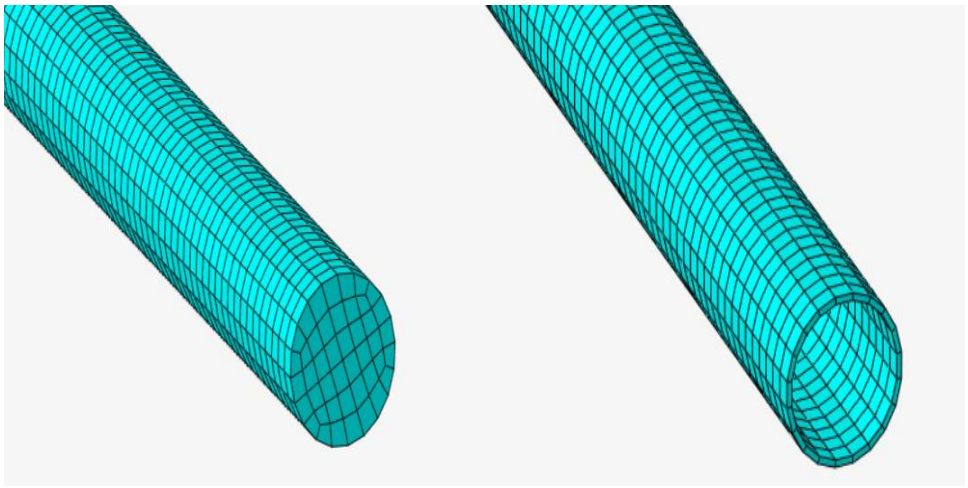

(b) Final Mesh of the whole geometry

Figure 5-2: Discretization of the model of Ag coated monofilament of Nylon/Ag fiber sensor for numerical simulation.

5.2.2. FE analysis and verification of experimental results

The untwisted coated yarn was modeled as a ductile material using the built-in elastic, plastic, and ductile damage criteria of ABAQUS because silver and nylon both are ductile. The electrical conductance of both materials nylon and Ag thin film was defined in ABAQUS to model the electrical response during the mechanical analysis, Table 5-1. For the numerical analysis, the experimental tensile behavior of pure silver thin film was applied [45] in addition to the mechanical response of nylon untwisted yarn, Table 5-1.

Furthermore, the rate-dependent power law was defined using the experimental curves in the plasticity model because it plays a vital role in damage initiation and neck formation during ductile failure. Therefore, strain hardening stress coefficient K and strain hardening index n were calculated using eqs. (5-1) and (5-2).

$$\boldsymbol{n = \frac{log\sigma_2 - log\sigma_1}{log\varepsilon_2 - log\varepsilon_1}} \tag{5-1}$$

$$\boldsymbol{log\, K - log\sigma_1 = n(log\, x - log\varepsilon_1)} \tag{5-2}$$

Where $\sigma_{1,2}$ is stress points in the plastic region, $\varepsilon_{1,2}$ is the corresponding strain points in the plastic region, K is strain hardening stress and n is strain hardening exponent.

Ductile damage criteria built in ABAQUS was used to define the model failure. Damage initiation was dependent on fracture strain, strain rate, and stress triaxiality whereas damage evolution required displacement at failure, Table 5-1. The evolution of the damage defined the material's behavior by illustrating the degradation of material stiffness after damage initiation. Scalar damage approach was used for formulating the rate of damage as given in (5-3). D is the overall damage variable showing the combined effect of all active damage mechanisms and when it reached 1 fracture occurred.

$$\boldsymbol{\sigma = (1\text{-}D)\, \sigma'} \tag{5-3}$$

Where σ is the stress due to damage response, D is the damage variable, σ' is the stress due to undamaged response.

Table 5-1: Experimental elastic, plastic and failure data of nylon and pure Ag-thin film

Material	Electrical Conductance	Young's Modulus	Poisson Ratio	Yield Strength	Fracture Strain	Strain Rate
	S/mm	MPa	-	MPa	-	mm/min(s^{-1})
Nylon	$1x10^{-15}$	1348.5	0.39	20.13	0.12	5
Silver	$63x10^{3}$	47230	0.37	431.1	0.08	$60x10^{-5}$

The nylon monofilament coated with the silver thin film was subjected to tensile elongation until failure. Results showed that it was viable to use one filament to validate the piezo-resistive

behavior of untwisted coated yarn. The true stress-strain behavior showed a good correlation with the experimental results in the elastic-plastic region, Figure 5-3. It can be seen in the results that it was fine to use the coated monofilament model to verify the result because the plane of stress is the same. However, there is a slight difference in the failure initiation and breakage which is understandable because, in experimental results, the failure showed the gradual breakage of all the monofilaments whereas in the numerical model the set of monofilaments is modeled by a single thread. The electrical response was recorded as electrical current density (ECD) in Abaqus which was then converted to resistance response using eqs. (5-4), (5-5) and (5-6) to validate the experimental piezo-resistive behavior of fiber sensor. The electromechanical behavior of the monofilament is shown in Figure 5-4.

$$\boldsymbol{J = \alpha E \ with \ \alpha = \frac{1}{\rho}} \tag{5-4}$$

$$\boldsymbol{J = \frac{E}{\rho} \Rightarrow J \propto \frac{1}{\rho}} \tag{5-5}$$

$$\boldsymbol{R = \frac{\rho L}{A}} \tag{5-6}$$

Where, J is Current density, E is Electric Field, α is Electrical Conductivity, ρ is Resistivity, L is Length, A is Cross-sectional Area, and R is Resistance.

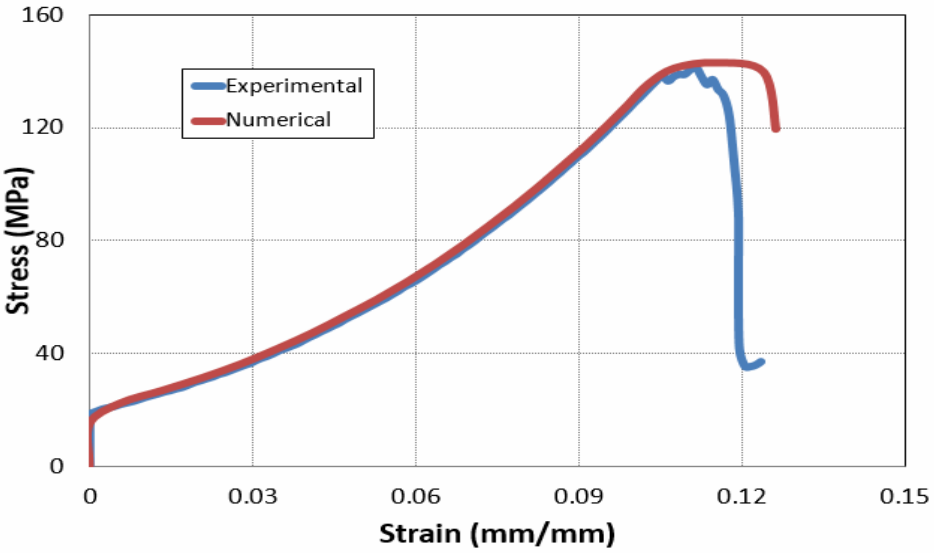

Figure 5-3: Numerical verification of experimental mechanical behavior of Ag coated untwisted nylon yarn

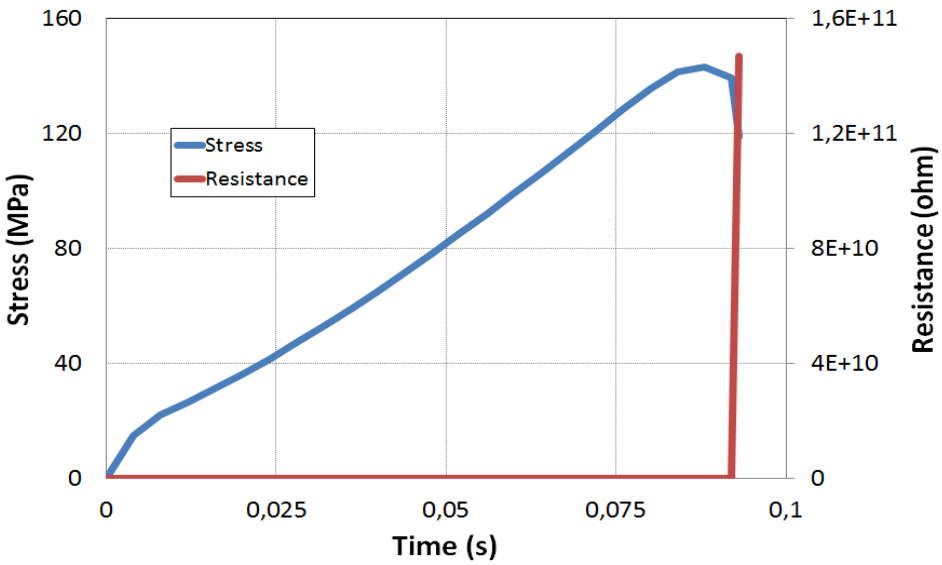

Figure 5-4: FE analysis of the electromechanical response of Ag coated monofilament.

It was observed that till the plastic region, the electrical resistivity of the yarn was changed but this change in resistance was very small as compared to change in resistance on damage when there was complete breakage in current flow. No gradual increase in the resistance was seen in experimental results because of the monofilament model. The 3D discrete model of coated monofilament before and after failure is shown in Figure 5-5.

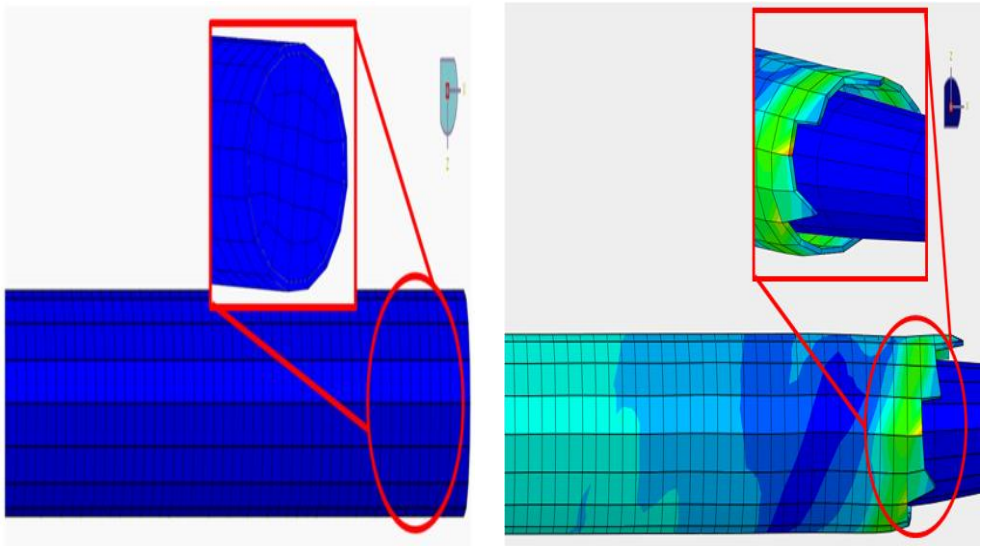

(a) *(b)*

Figure 5-5: 3D discrete model (a) before failure and (b) after failure.

In this numerical investigation, it was found that in the electromechanical behavior of the standalone sensor, the mechanical response of the whole model was dependent on the nylon core and the Ag coating was responsible for the conductive behavior of the sensor. In this context, the model of the standalone sensor was further simplified by using a single geometry of fiber which was assigned with the mechanical behavior of nylon and electrical properties of Ag- metal thin film coating. The results showed that a single fiber model without coating showed a good correlation in mechanical behavior with both experimental results and the previous model, Figure 5-6. Moreover, the deformation of the single fiber showed an increase in electrical resistance, and final fracture showed achievement of maximum value of resistance of the sensor. This showed that the model can be further simplified using a single monofilament with electrical properties of the Ag-metal and mechanical properties of nylon untwisted yarn. This step was justifiable because the sensor was considered as a whole, unified single entity, and the main objective was to achieve correlation between the electro-mechanical response of the 3D model. The effect of twisted yarn, number of filaments, and other geometric parameters will be considered in future studies.

This model was then utilized to correlate the electromechanical behavior of the standalone sensor system of the Nylon/Ag fiber sensor (twisted yarn) mentioned in chapter 2. The mechanical behavior of the Nylon/Ag fiber sensor showed a good correlation between experimental and numerical results thus, proof that it was acceptable to use a simplified model of monofilament with electrical behavior of Ag metal thin film and mechanical behavior of twisted nylon yarn, Figure 5-7 (a). It can be seen in the results that it was fine to use the monofilament model to verify the result because the plane of stress is the same. Moreover, the electromechanical response also replicated the experimental behavior of the standalone sensor of the Nylon/Ag fiber sensor. The electrical resistance was increased gradually with the plastic deformation of the sensor and during fracture initiation, there was a sudden increase in resistance which reached maximum value upon overall failure, Figure 5-7 (b). The 3D discrete model of monofilament after failure is shown in Figure 5-8.

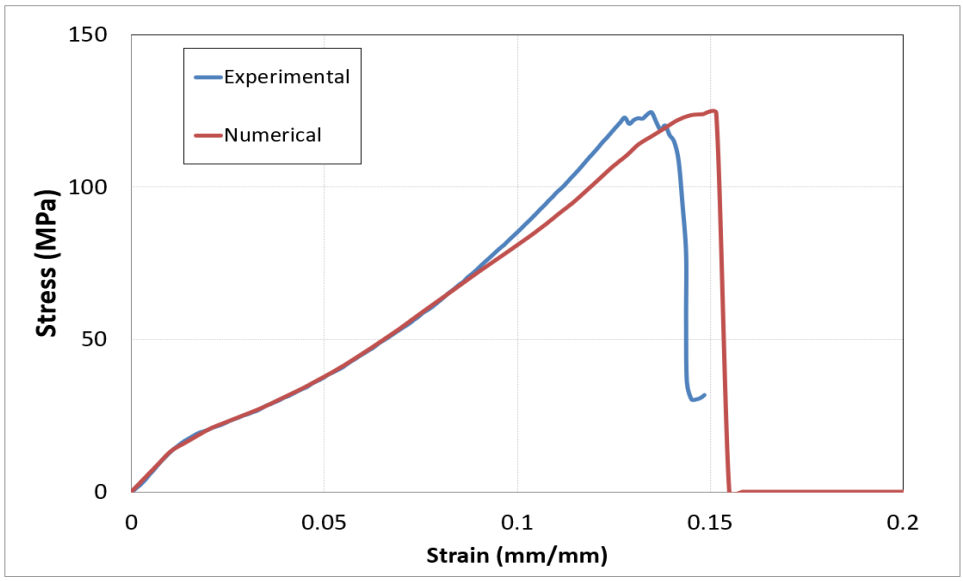

(a)

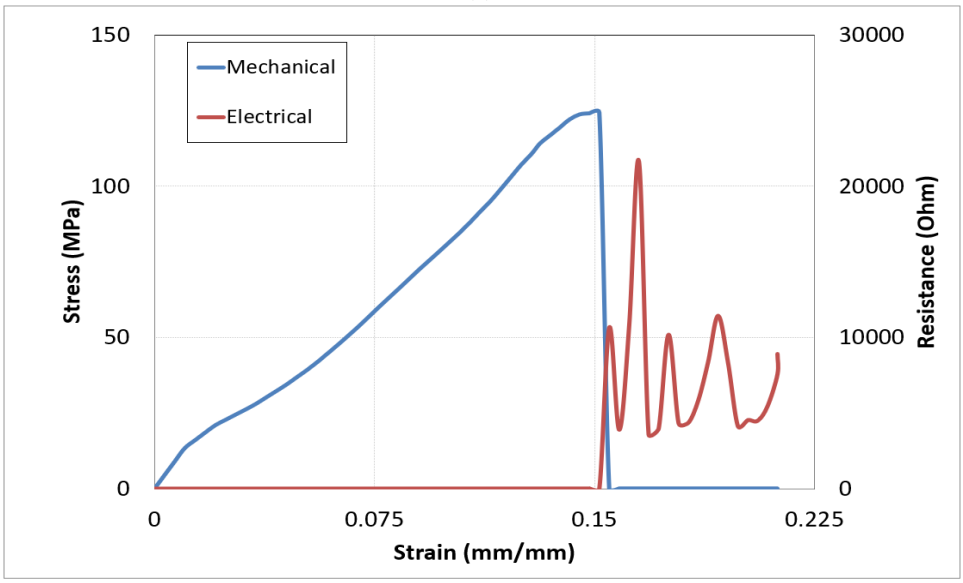

(b)

Figure 5-6: Numerical verification of experimental mechanical behavior of Ag coated untwisted nylon yarn using monofilament geometry

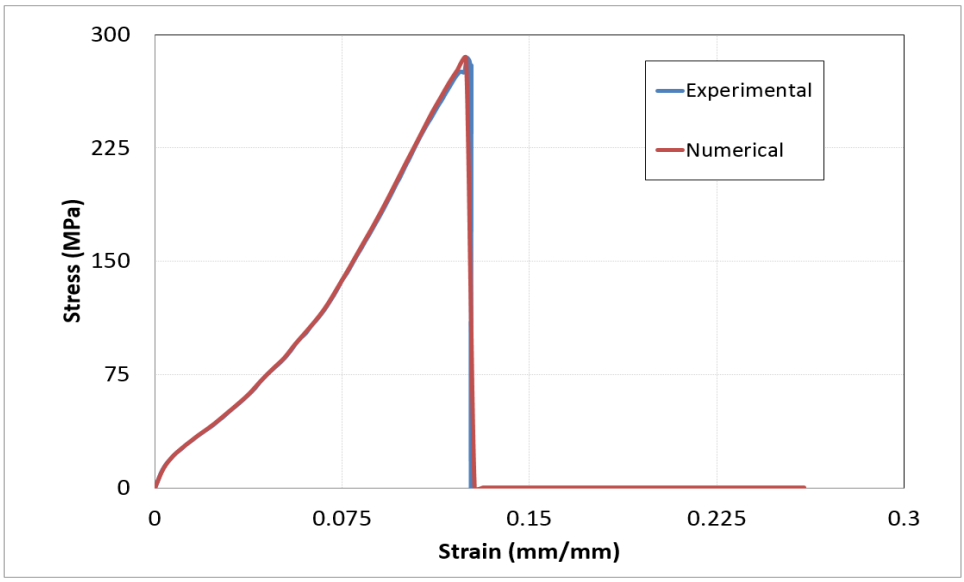

(a)

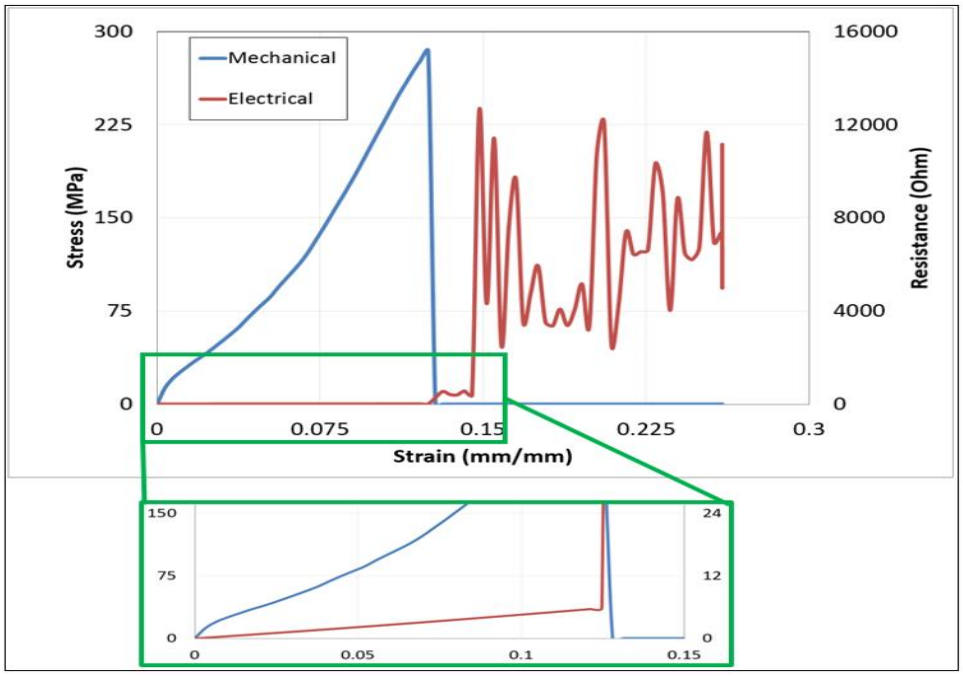

(b)

Figure 5-7: (a) Numerical verification of experimental mechanical behavior of Nylon/Ag fiber sensor (twisted yarn). (b) FE analysis of the electromechanical response of Nylon/Ag fiber sensor (twisted yarn).

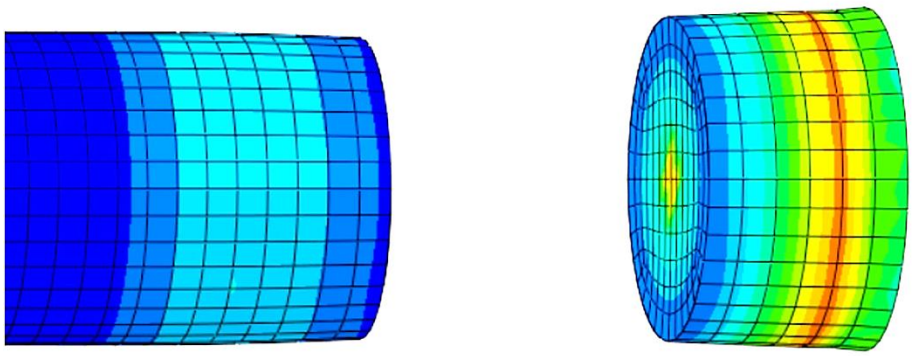

Figure 5-8: 3D discrete model of after failure of Nylon/Ag fiber sensor monofilament

This study confirmed that the 3D finite element model consisting of a simplified monofilament model was viable to use to verify the experimental behavior of the sensor system Nylon/Ag fiber sensor. The numerical results showed a good correlation between the electromechanical response of the numerical model and correlated perfectly with the experimental electromechanical behavior of the sensor. That is why in the next section, this simplified model will be utilized to monitor the strain deformation in the composite specimen in different directions and positions under different quasi-static loadings. this will reduce the computational work and time without compromising the accuracy of results. Moreover, the following sections include strain monitoring within elastic-plastic deformation of the star specimen so the slight difference in the failure between this model and experimental results will not be a problem.

5.3. Section II: Sensor embedded within composite under quasi-static loadings -star specimen

5.3.1. 3D Model of Star specimen embedded with a sensor

In this study, a star-shaped specimen was developed with five plies embedded with four sensors at different directions i.e. 0°, 90°, $+45^{o,}$ and -45°, and each sensor was separated by each ply. The total length of each leg of the star specimen was kept 200 mm with a width of 25 mm and a thickness of 4 mm and the gauge length of each sensor was 150 mm, Figure 5-9. The sensor was assigned the material model based on the experimental results of the sensor system Nylon/Ag fiber sensor while star specimen was assigned the experimental behavior of star specimen studied in chapter 3. The star specimen was considered isotropic 3D model because

star specimen was fabricated chopped glass fiber plies which showed quasi-isotropic behavior. This quasi-isotropic behavior meant that they show isotropic deformation within the plane and applied tensile load generated two-dimensional deformation while deformation through-thickness was negligible. The experimental material properties have been shown in table 5-2.

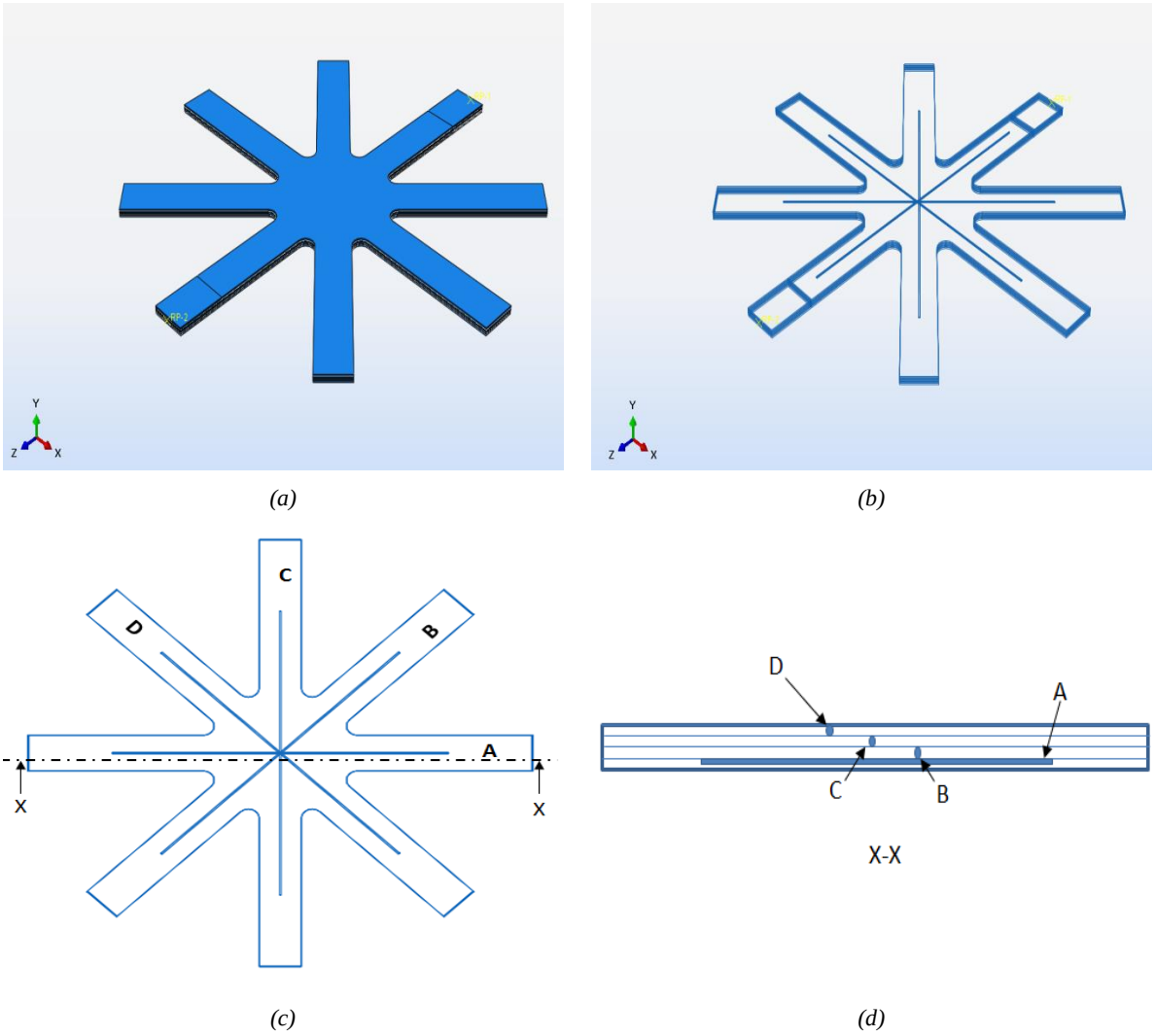

Figure 5-9: 3D model of star specimen embedded with a sensor at different positions and directions.

Table 5-2: Experimental mechanical and electrical behavior of star composite specimen and Nylon/Ag fiber sensor

Material	Electrical Conductance	Young's Modulus	Poisson Ratio
	S/mm	GPa	-
Composite Sample	$1x10^{-15}$	9.924	0.15
Sensor System	$63x10^{3}$	4.269	0.39

The plastic behavior was added using tensile experimental results using the built-in elastic, plastic criteria of ABAQUS as discussed in detail in section 5.2.2. Mesh refinement with structured mesh was performed and mesh size was m=0.5 for the sensors and m=2 for the Star specimen was assigned, Figure 5-10. Moreover, the mesh of star specimen was further refined by localized mesh refinement near the region where sensors were embedded. Moreover, each ply was attached with the sensor and with each other with the surface to node interaction as electro-thermo-mechanical however, the electrical conductance between the plies and between each ply and sensor was negligible because of the non-conductive nature of chopped glass fiber mat, Figure 5-11.

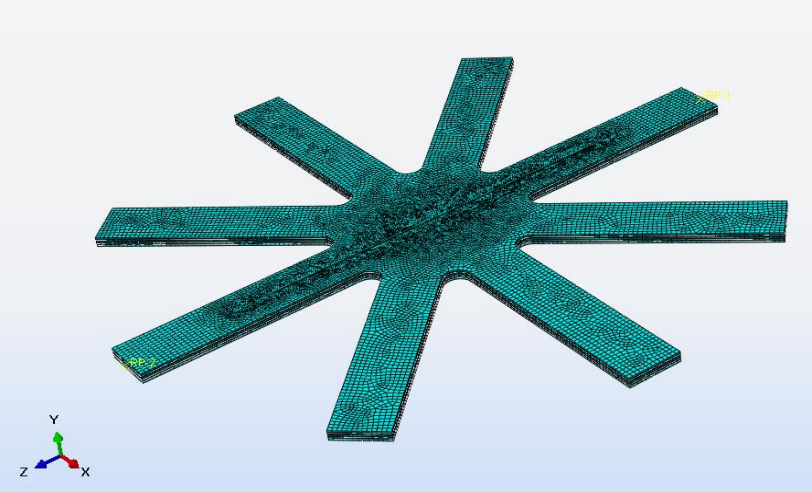

Figure 5-10: Mesh configuration with localized refinement.

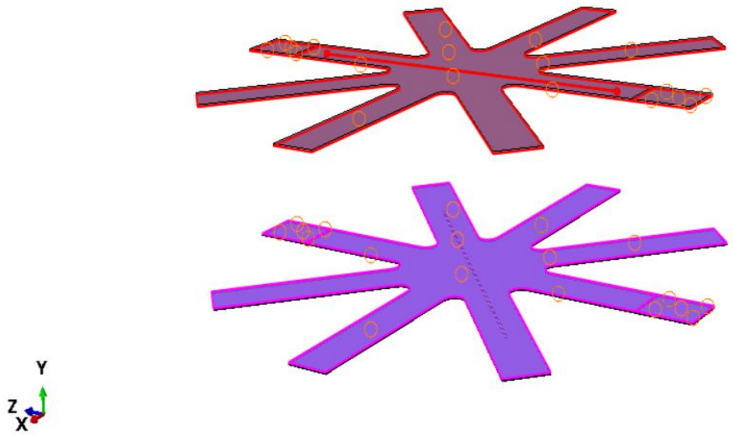

Figure 5-11: An example of surface interaction between the plies of the composite.

5.3.2. FE analysis and verification of experimental results during cyclic tensile loading

During the numerical investigation, the star specimen was loaded with tensile elongation in such a manner that the loading leg was along the z-axis while the transverse leg was along with the x-axis, Figure 5-12. Therefore, it was expected to observe tensile elongation along the z-axis while compression along the x-axis. Tensile loading was applied to the specific leg of the star specimen consisting of sensor A and electrical loads were applied to all the sensors inside the specimen, Figure 5-13. Electrical loads were directly applied on the cross-section surface on both ends of each sensor while reference points were defined for the mechanical loads. Both ends of a leg with sensor A was attached with each reference point through tie interaction as a rigid body. Then, one reference point was kept fixed and displacement was applied to the other reference point according to the experimental tests, Figure 5-13.

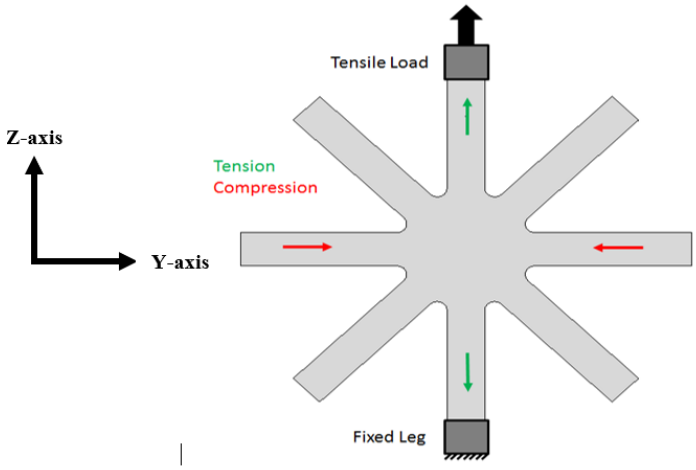

Figure 5-12: Mechanical behavior and loading direction of star specimen during numerical investigation.

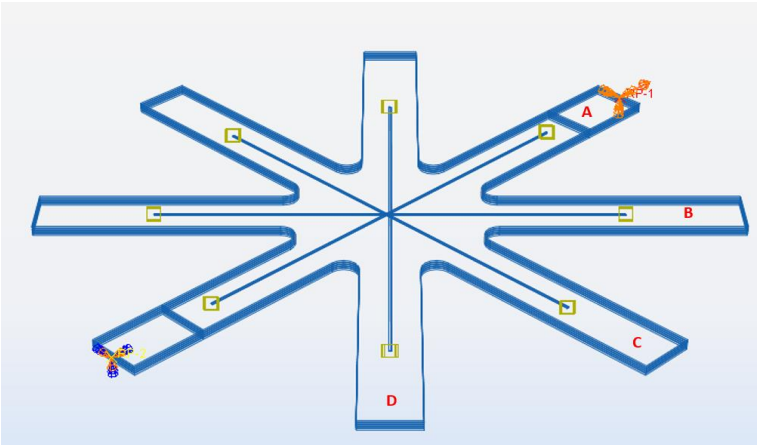

Figure 5-13: Electrical and mechanical boundary conditions applied to the 3D model of sensor embedded within the composite star specimen.

The specimen was loaded with tensile elongation and it was observed that the maximum deformation was mostly active in the loaded leg and the center of the specimen and the other six legs played no vital role in the mechanical behavior of the star specimen, Figure 5-14. The mechanical response showed good agreement between experimental and numerical results, Figure 5-15. The mechanical response of the star specimen was obtained as a force-displacement curve from Abaqus as an overall response. then, this force-displacement curve was converted into stress-strain behavior using geometrical parameters of the 3D model of star specimen and following equations.

$$\boldsymbol{\sigma = \frac{F}{A}} \tag{5-7}$$

$$\boldsymbol{\varepsilon = \frac{\Delta L}{L}} \tag{5-8}$$

where σ is the tensile stress, ε is the applied tensile strain, ΔL is the change in length or elongation of the sample in terms of displacement, L is the original length of a leg of a star specimen and A is the cross-sectional area of a leg of the star specimen.

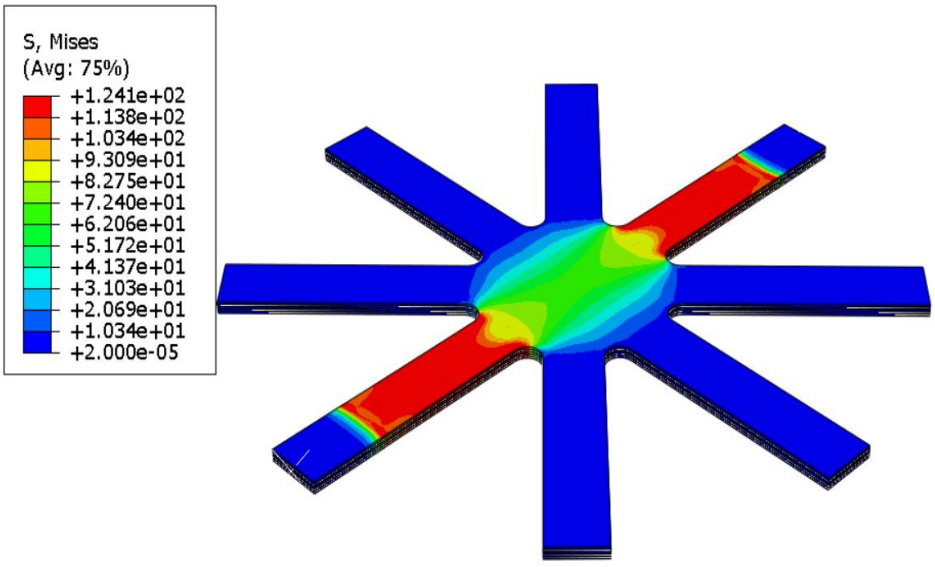

Figure 5-14: Maximum Von Mises stress contour during the tensile loading of star specimen.

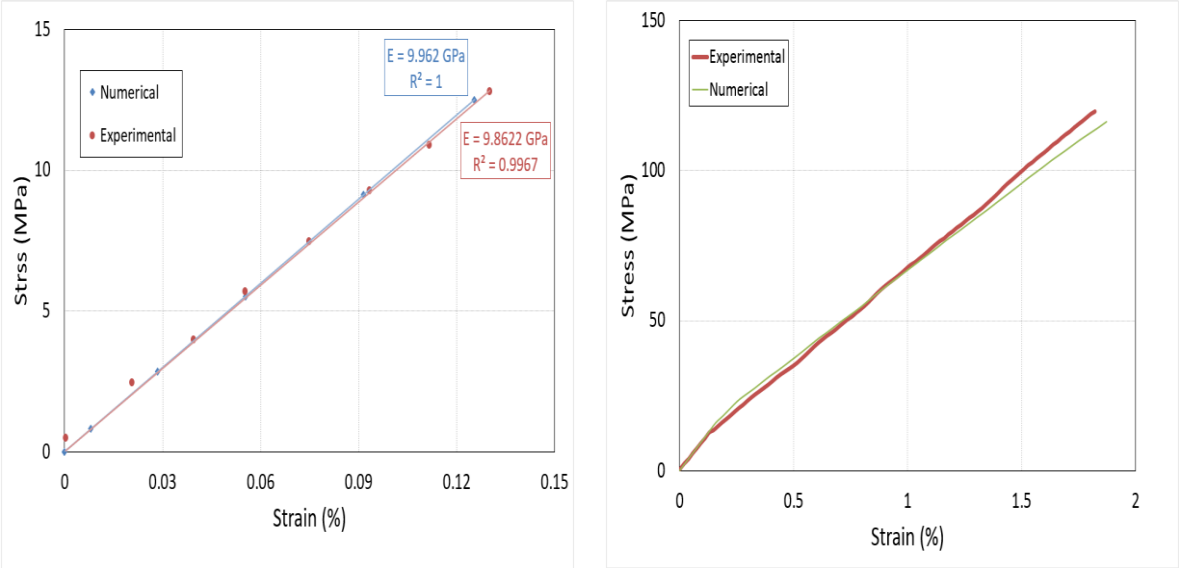

(a) Elastic modulus *(b) Stress-strain behavior*

Figure 5-15: Verification of Experimental mechanical behavior of Star specimen during tensile loading

During tensile loading, the direction of the sensor with respect to the loading axis played an essential role in determining their detection signal. Sensor A was along the loading axis i.e z-axis, sensor C was in the transverse direction i.e. x-axis while sensor B and sensor D were in an oblique direction between xz-plane. The electrical response of each sensor was obtained as electrical current density (ECD) from Abaqus, Figure 6-16. The resistivity of the sensor was calculated using eqs. (5-4) to (5-5) and this resistivity was converted to change in resistance by eq. (5-6) using overall deformation and eq. (5-6) was modified as follow

$$\boldsymbol{R_o = \frac{\rho L_o}{A_o}} \tag{5-7}$$

$$\boldsymbol{R_i = \frac{\rho L_i}{A_i}} \tag{5-8}$$

Where R_o is the original resistance at the original length i.e. L_o and initial cross-sectional area of the sensor i.e. A_o. R_i is the incremental change in resistance because of the change in length L_i and area of the sensor A_i during tensile elongation.

For example, the change in resistance of sensor A was calculated by using the total deformation of the sensor i.e. elongation along z-direction and transverse deformation along the y-direction. Then, implementing the total displacement and change in area in eqs. (5-7) and (5-8). A similar concept was carried out for the calculation of the change in resistance of sensors in the rest of

the positions. Numerical results showed similar behavior of all four sensors in each cycle during the cyclic tensile deformation of composite star specimen, Figure 5-17. Sensor A, in 0° position, showed a maximum increase in resistance because of its position along the loading axis i.e. in the z-direction. Sensor C, in 90° position, showed a decrease in resistance during the applied cyclic tensile strain because of its transverse direction i.e. x-axis. Sensor B in 45° and sensor D in -45° position, showed an identical response because of their mirror position according to the loading axis and showed a minimum increase in resistance. The numerical results correlated with experimental results in good agreement and showed that the model was able to not only able to show the change in resistance of 3D embedded sensor with the strain deformation of the parent model but also replicate the experimental results, Figure 5-18. Slight difference in their correlation could be because of the use of monofilament 3D model of sensor however, this amount of difference between experimental results and numerical simulations is acceptable. The comparison of the maximum value of the first cycle of change in resistance of all four sensors with their experimental results showed perfect correlation with a percentage difference of less than 10% in each direction, Figure 5-19.

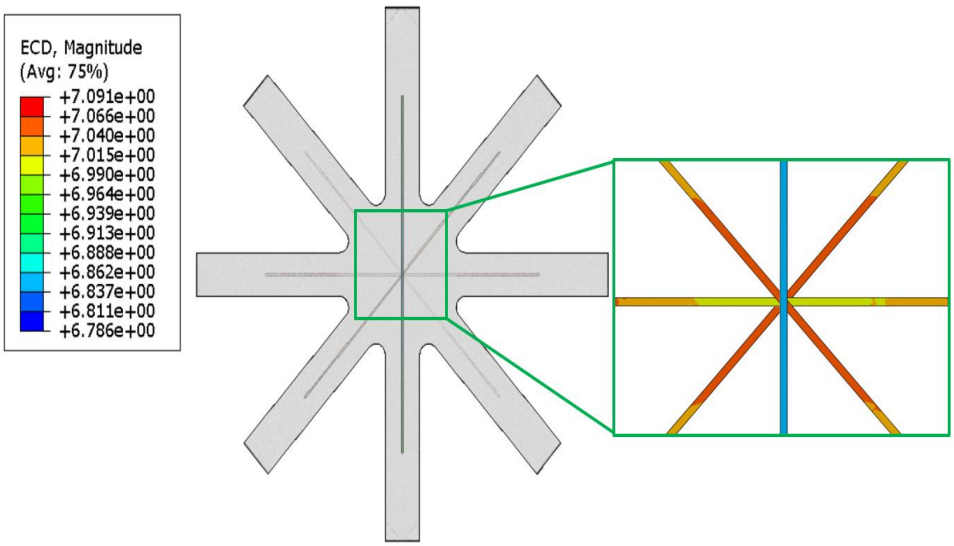

Figure 5-16: Electrical behavior of the 3D model. The change in electrical behavior was visible in each sensor with variation with respect to the deformation in their directions. However, it can be seen that electrical behavior was negligible in the composite star specimen because of their poor conductance.

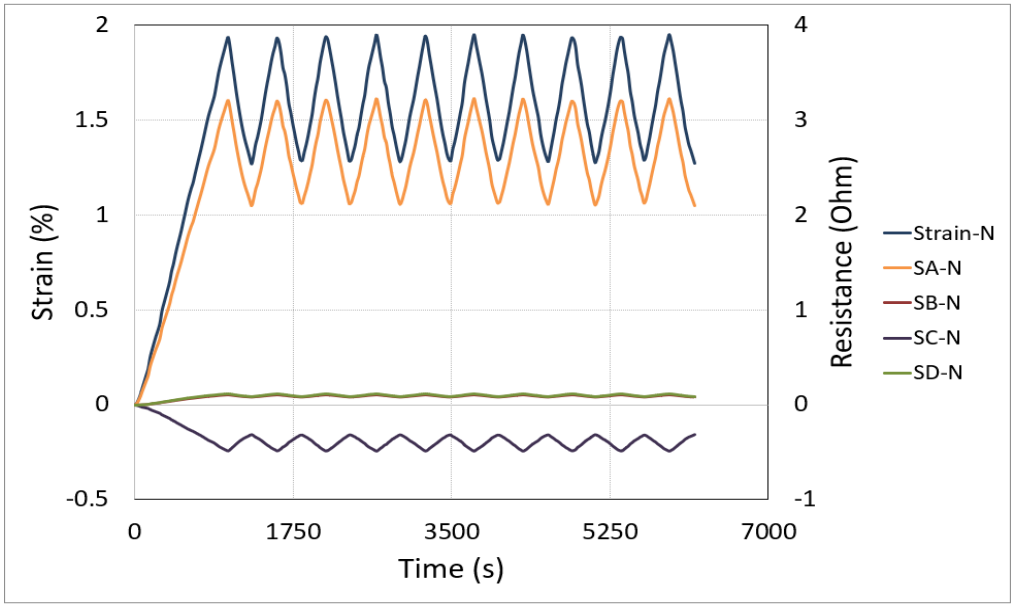

Figure 5-17: Real-time signal of all four sensors with respect to their position and their correlation with the cyclic tensile strain deformation of composite star specimen in numerical (N) investigation.

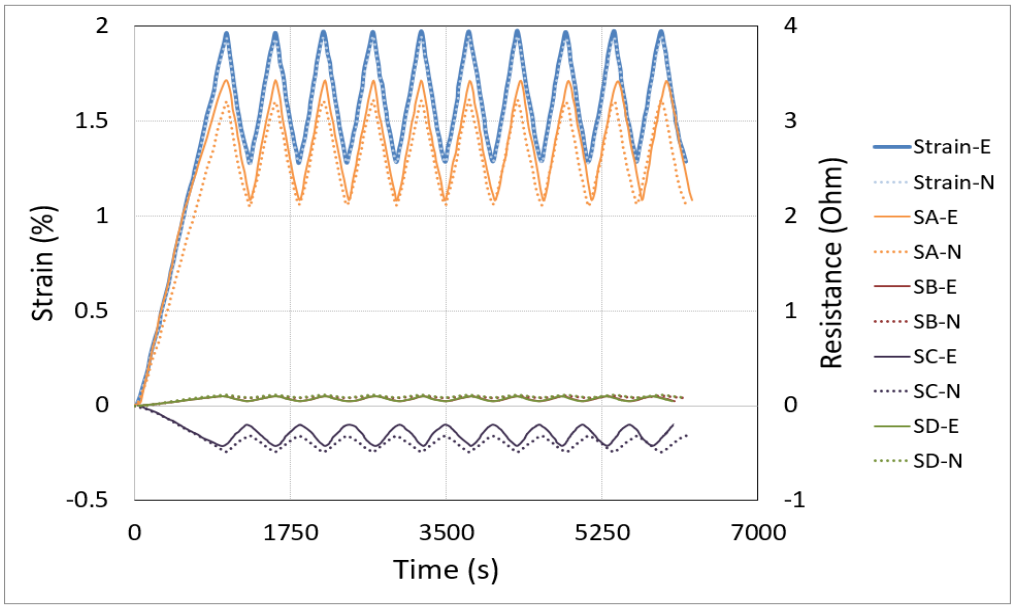

Figure 5-18: Correlation between experimental (E) and numerical (N) results of real-time strain monitoring of strain deformation in composite star specimen subjected to cyclic tensile loading in all four positions i.e. sensor A in 0°, sensor B in 45°, sensor C in 90° and sensor D in -45°.

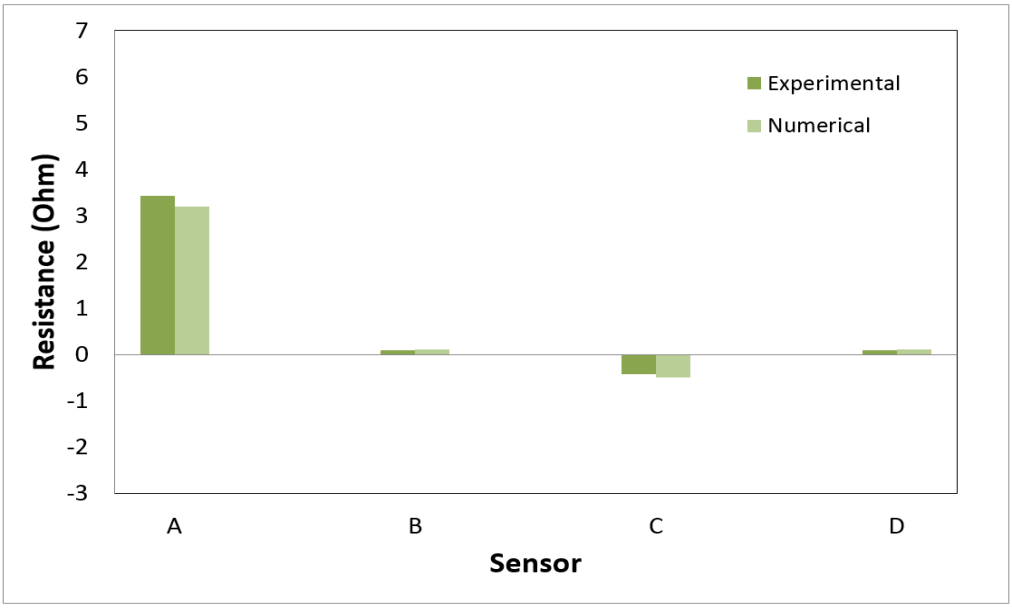

Figure 5-19: Comparison of the maximum value of change in resistance of the first cycle between experimental and numerical results.

5.3.3. FE analysis and verification of experimental results during cyclic flexural loading

In this section, the 3D model of star specimen was studied under a three-point bend test to see if the sensors can detect flexural deformation during the numerical investigation and verify the experimental results. The star specimen was loaded with a flexural deflection in such a manner that bending load was applied along the y-axis and star specimen was placed between the rollers in a way that leg with sensor A was along the roller axis and leg with sensor C was between the three rollers, Figure 5-20. Therefore, it was expected to observe flexural deflection along the y-axis. Three rollers were modeled as rigid bodies and flexural loading was applied to the upper roller which caused the deflection of the star specimen and electrical loads were applied to all the sensors inside the specimen. The span length was kept 160 mm similar to experimental tests and all the other geometric parameters were also kept identical to the experimental setup. Each roller was attached with their respective reference point and deflection through tie interaction as a rigid body. Then, the flexural deflection was applied to the reference point attached to the upper roller while the reference points attached to the bottom rollers were kept fixed according to the experimental tests. General frictional contact was defined between the rollers and the surface of the star specimen. Star specimen was meshed similarly to the previous section with local mesh refinement however, all three rollers were meshed as rigid bodies, Figure 5-21.

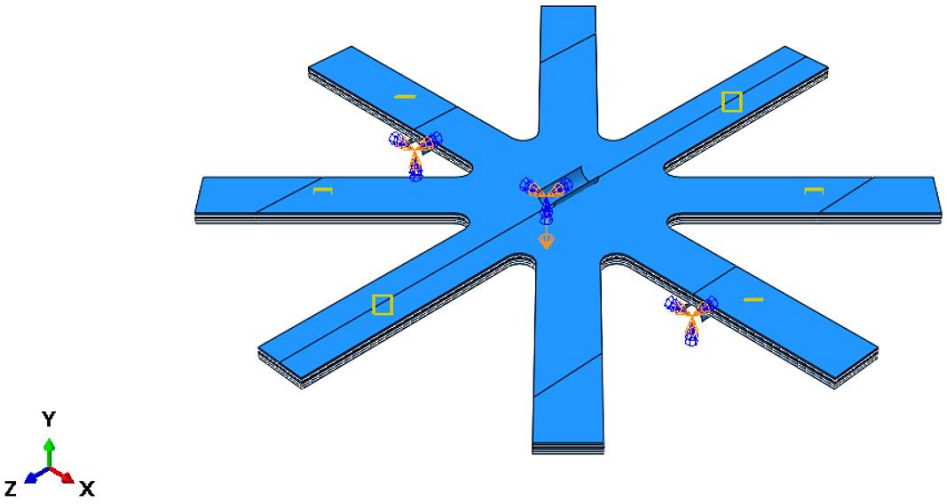

(a)

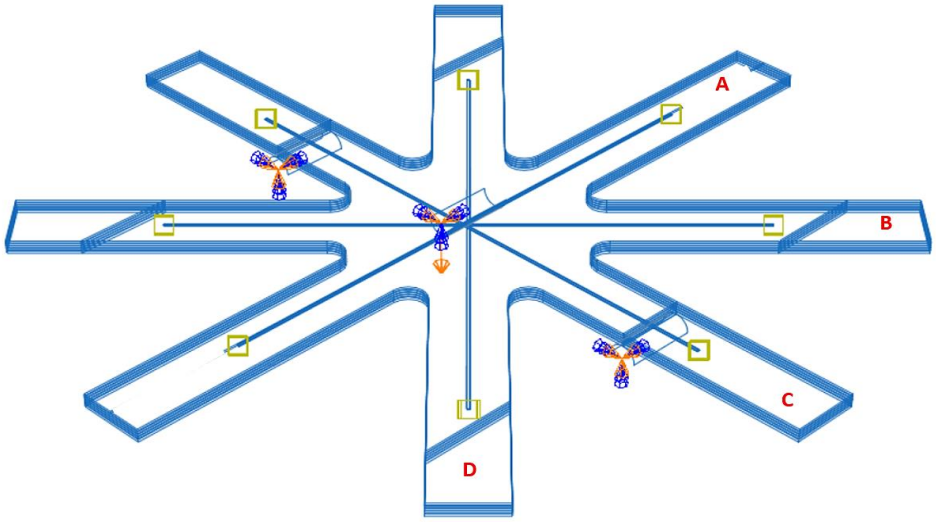

(b)

Figure 5-20: Electrical and mechanical boundary conditions applied on the 3D model of sensor embedded with in composite star specimen

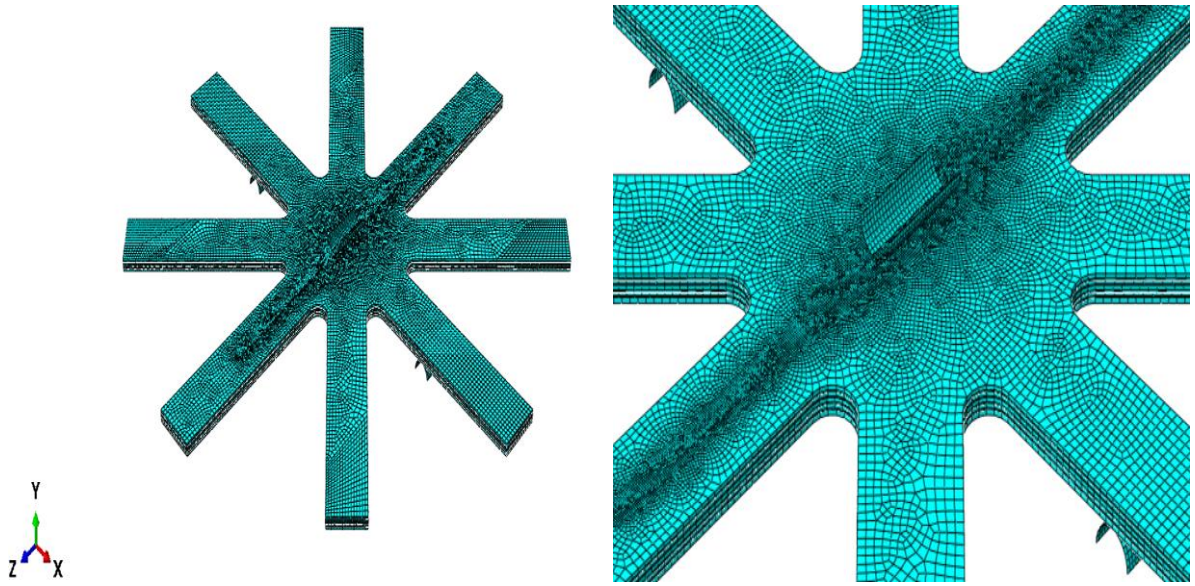

(a) Overall setup *(b) Zoom-in image of span length*

Figure 5-21: Mesh configuration with local refinement for specimen subjected to flexural bending.

The specimen was loaded with flexural deflection and it was observed that the maximum deformation was mostly active in the loaded leg i.e. along the span length and in the center of the specimen and the other six legs played no vital role in the mechanical behavior of the star specimen, Figure 5-22. The mechanical response showed good agreement between experimental and numerical results, Figure 5-23. The elastic behavior of the specimen correlated perfectly however; the minute difference was observed during the large plastic deformation. This difference could be because the experimental specimen was quasi-isotropic while this 3D model was assigned material properties as isotropic deformation behavior. This difference was not observed during tensile loading because tensile deformation was mostly planer and negligible through the thickness of the specimen, however, the flexural deflection was applied perpendicular to the planer surface of the specimen and the deflection was along the thickness of the specimen during bending. This could result in a minute difference in the mechanical response of the star sample during large plastic deformation however, this difference was not greater than 10 %. The mechanical response of the star specimen was obtained as a force-displacement curve from Abaqus as an overall response then, this force-displacement curve was converted into stress-strain behavior using geometrical parameters of the 3D model of star specimen and following equations.

$$\sigma_f = \frac{3FL}{2bd^2} \tag{5-9}$$

$$\varepsilon_f = \frac{6Dd}{L^2} \tag{5-10}$$

$$E_f = \frac{L^3 m}{4bd^3} \tag{5-11}$$

Where, σ_f is flexural stress, ε_f is flexural strain, $E_{f\,is}$flexural modulus of elasticity, *F* is the load at a given point on the load-deflection curve, *L* is span length, *b* is the width of the specimen, *d* is thickness, *D* is deflection, and *m* is the gradient of the initial straight-line portion of the load-deflection curve.

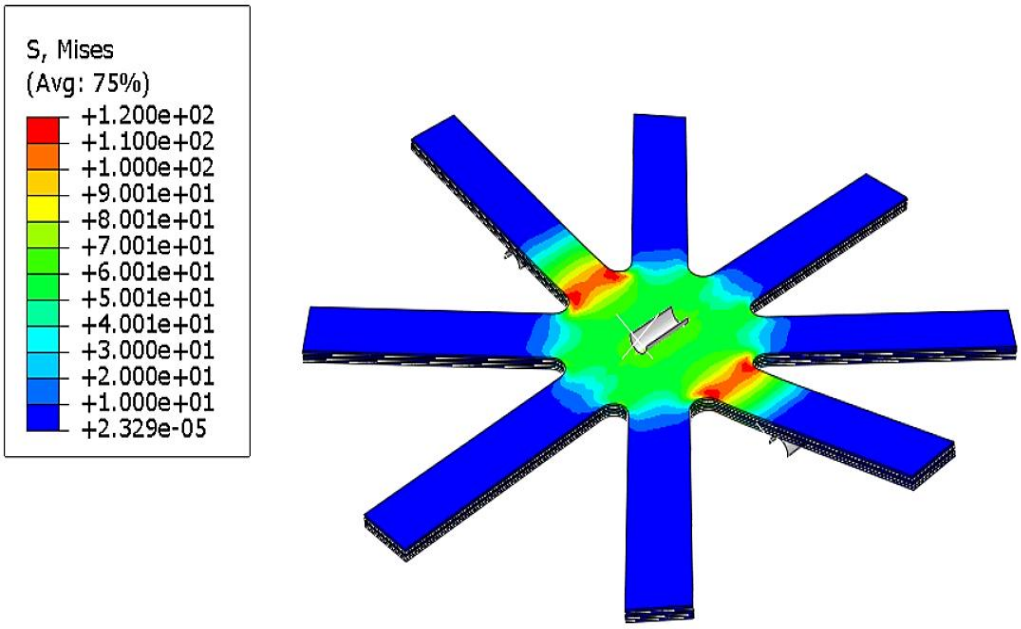

Figure 5-22: Maximum Von Mises stress contour during flexural loading of star specimen.

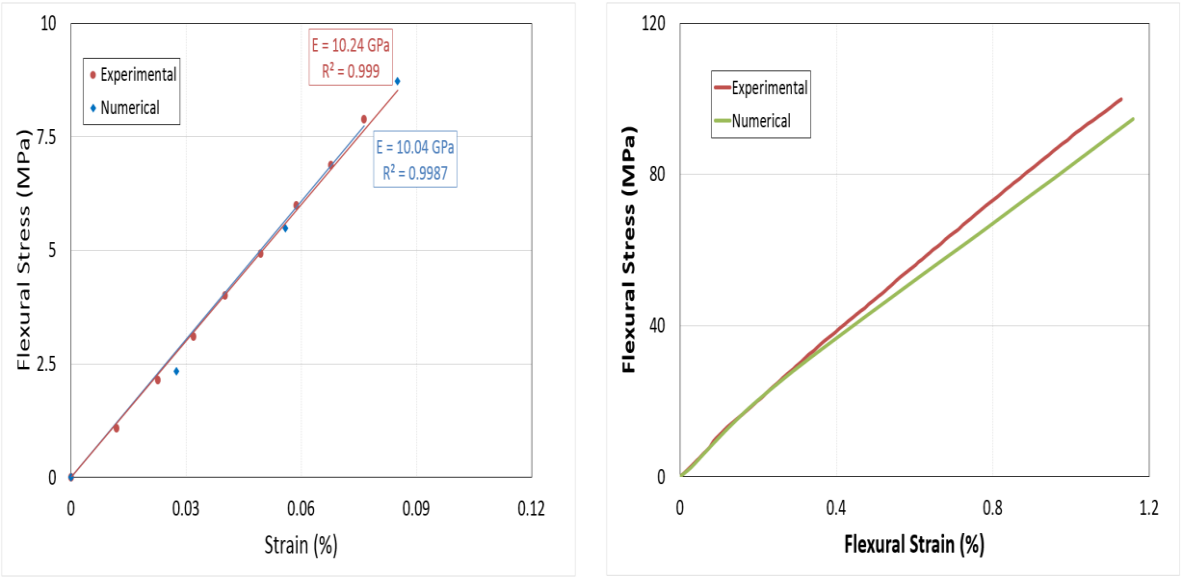

(a) Elastic modulus *(b) Stress-strain behavior*

Figure 5-23: Verification of Experimental mechanical behavior of Star specimen during flexural loading.

During flexural loading, the position of the sensor within the plies of the sample with respect to the loading axis played an essential role in determining their detection signal. Sensor A was along the roller axis i.e. z-axis and near the top surface of the star sample. All the other three sensors were then gradually placed between the plies with sensor D near the bottom surface, Figure 5-24. However, sensor C was along the x-axis, between the rollers, and while sensor B and sensor D were in an oblique direction between xz-plane. The electrical response of each sensor was obtained as electrical current density (ECD) from Abaqus, Figure 5-25. The resistivity of the sensor was calculated using eqs. (5-4) to (5-5) and this resistivity was converted to change in resistance by eqs. (5-7) and (5-8) using overall deformation. For example, the change in resistance of sensor A was calculated by using the total deformation of the sensor i.e. elongation along z-direction and deformation along the y-axis. A similar concept was carried out for the calculation of the change in resistance of sensors in the rest of the positions. Numerical results showed similar behavior of all four sensors in each cycle during the cyclic flexural deformation of composite star specimen, Figure 5-26. Sensor A is in top position with respect to thickness and it showed a maximum decrease in resistance. Sensor C, in 90° and along the span length, showed an increase in resistance during the applied cyclic tensile strain because of its position along the span length. Sensor B and sensor D also correlated with the experimental results with good agreement. This showed that the model was able to not only able to show the change in resistance of 3D embedded sensor with the strain deformation

of the parent model but also replicate the experimental results, Figure 5-27. Slight difference in their correlation could be because of the difference in the plastic deformation of the 3D model because of the use of isotropic material model as discussed previously. However, this amount of difference between experimental results and numerical simulations is acceptable. The comparison of the maximum value of the first cycle of change in resistance of all four sensors with their experimental results showed perfect correlation with percentage difference of less than 10% in each direction, Figure 5-28.

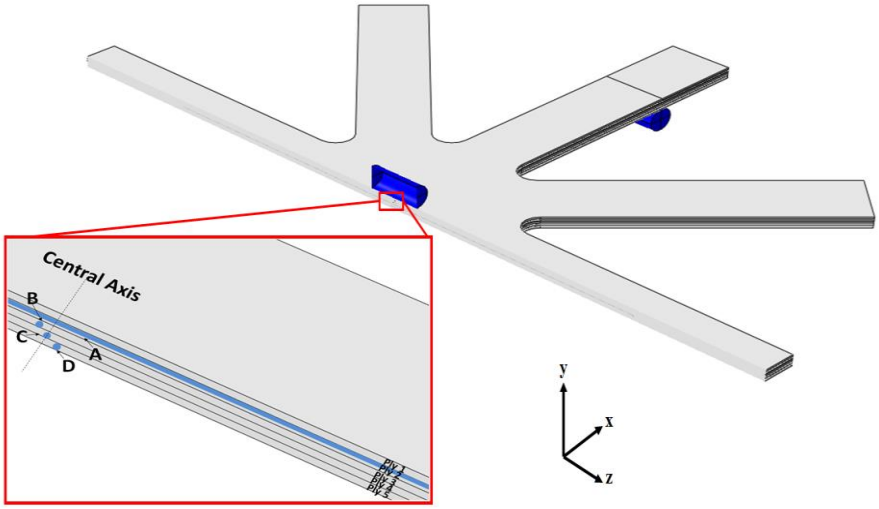

Figure 5-24: Position of sensor embedded within it during the numerical investigation under flexural loading.

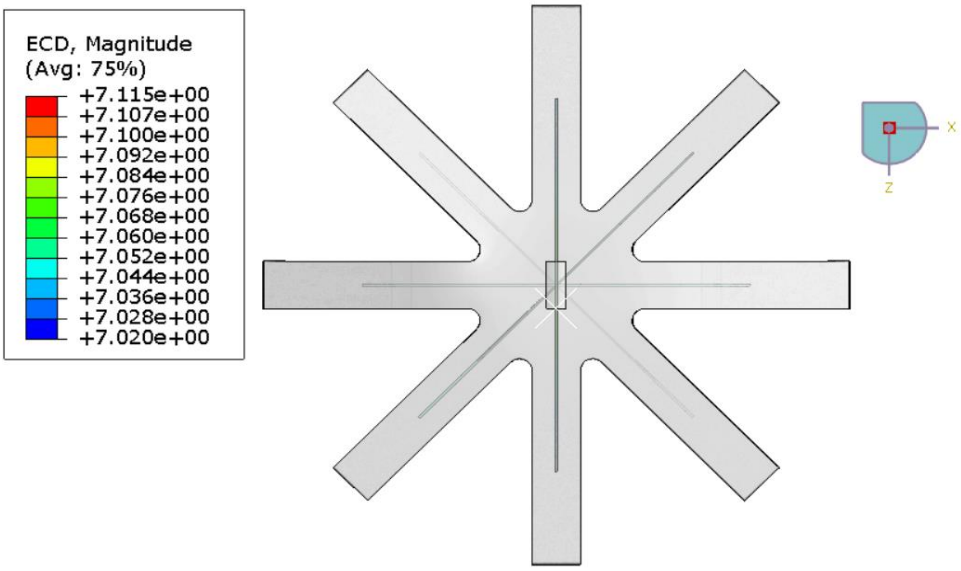

Figure 5-25: Electrical behavior of the 3D model during flexural loading. The change in electrical behavior was visible in each sensor with variation with respect to the deformation in their directions. However, it can be seen that electrical behavior was negligible in the composite star specimen because of their poor conductance.

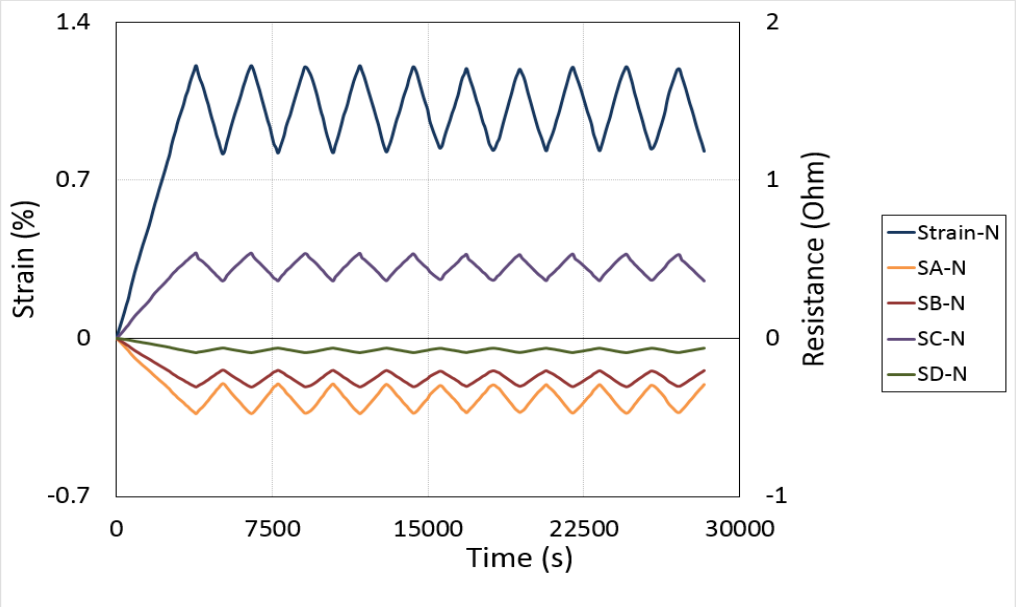

Figure 5-26: Real-time signal of all four sensors with respect to their position and their correlation with the cyclic flexural strain deformation of composite star specimen in numerical (N) investigation.

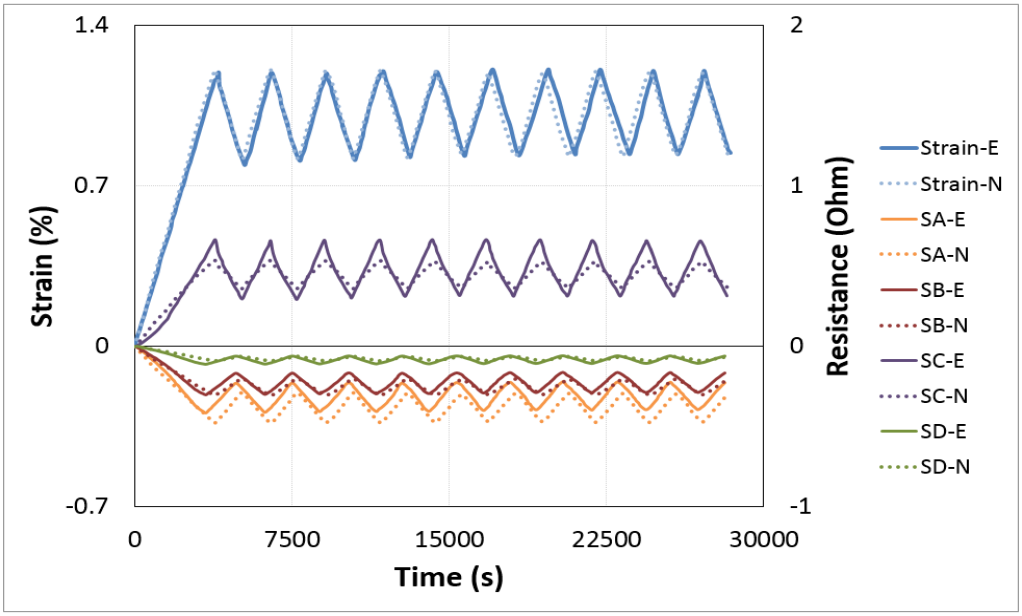

Figure 5-27: Correlation between experimental (E) and numerical (N) results of real-time strain monitoring of strain deformation in composite star specimen subjected to cyclic flexural loading in all four positions i.e. sensor A in 0°, sensor B in 45°, sensor C in 90° and sensor D in -45° with respect to the roller axis.

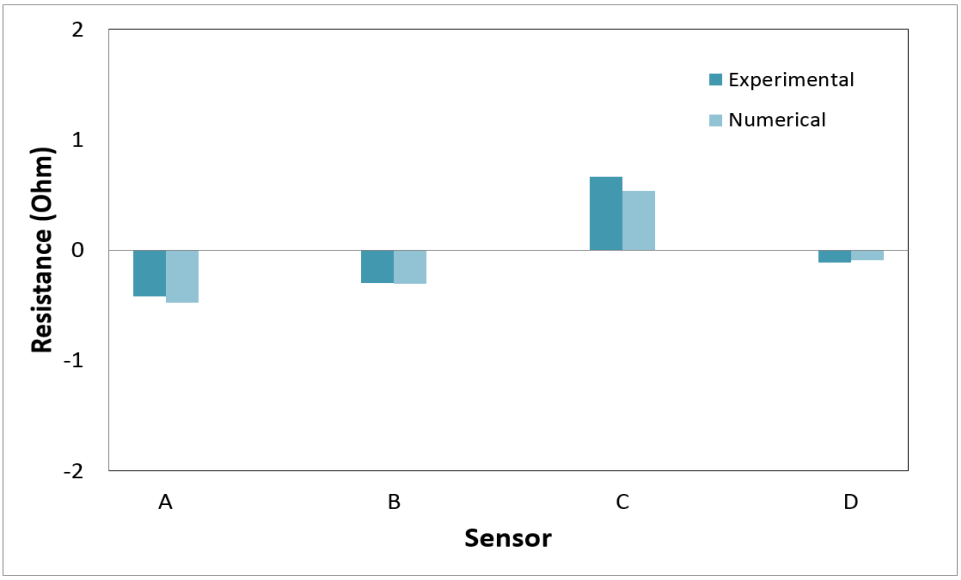

Figure 5-28: Comparison of the maximum value of change in resistance of the first cycle between experimental and numerical results.

This study confirmed that the 3D finite element model consisting of embedded monofilament Nylon/Ag fiber sensor in composite star specimen was viable to use to verify the experimental behavior of strain monitoring in real-time under cyclic tensile and flexural loading. The numerical results showed a good correlation between the electromechanical response of the numerical model and correlated perfectly with the experimental results. This numerical simulation not only showed the detection of strain deformation in composite samples during different cyclic quasi-static loadings using embedded sensors in different directions and positions but, also showed the verification of experimental results.

5.4. Section III: Sensor embedded within composite under dynamic impact

5.4.1. 3D Model of composite plate specimen embedded with a sensor

In this section, the 3D finite element model is developed to verify the damage detection behavior of the Nylon/Ag fiber sensor within the composite plate under the dynamic loading. Unfortunately, the study of electrical behavior during dynamic explicit study in Abaqus is not very well established or developed. Therefore, instead of recording the electrical current density in numerical simulation, the strain deformation rate was recorded using the skin as a sensor with electromechanical properties of Nylon/Ag fiber sensor. Then, this strain deformation rate will be compared with the experimental results by converting the experimental change in resistance of the sensor into a strain deformation rate using the empirical relations and equation defined in section 4.4.3. This attempt was carried out to develop a model in which deformation

in the composite sample could be detected using a sensor under dynamic loading and correlate experimental and numerical studies. However, it should be kept in mind that the main objective is to propose a model for deformation detection under dynamic loading and demonstrate similar behavior.

In this study, a rectangular composite plate embedded with Nylon/Ag fiber sensor was model similar to the experimental setup. Nylon/Ag fiber sensors were inserted between the plies of composite laminate in their respective position and direction. Three laminates were used and one fiber sensor was inserted between the ply 1 and ply 2 along the width of the sample in the center i.e. W and four nylon/Ag fiber sensors were inserted along the length of the sample at almost same distance from each other between ply 2 and 3 at position L_1, L_2, L_3 and L_4, Figure 5-29. Each sensor was assigned with the material model based on the experimental results of the sensor system Nylon/Ag fiber sensor to monitor the strain deformation rate during the dynamic explicit simulation while the composite plate was assigned the experimental behavior of composite sample studied in chapter 4. The composite sample was considered isotropic 3D model because the experimental specimen was fabricated chopped glass fiber plies which showed quasi-isotropic behavior. Initially, the impactor was designed similar to the one used in experimental setup but to improve the computational work and time, the impactor geometry was modified, Figure 5-30. This modification did not affect the impact on the plate because the impactor was modeled as a rigid body and was assigned the 1.6 kg weight similar to the impactor used in experimentation.

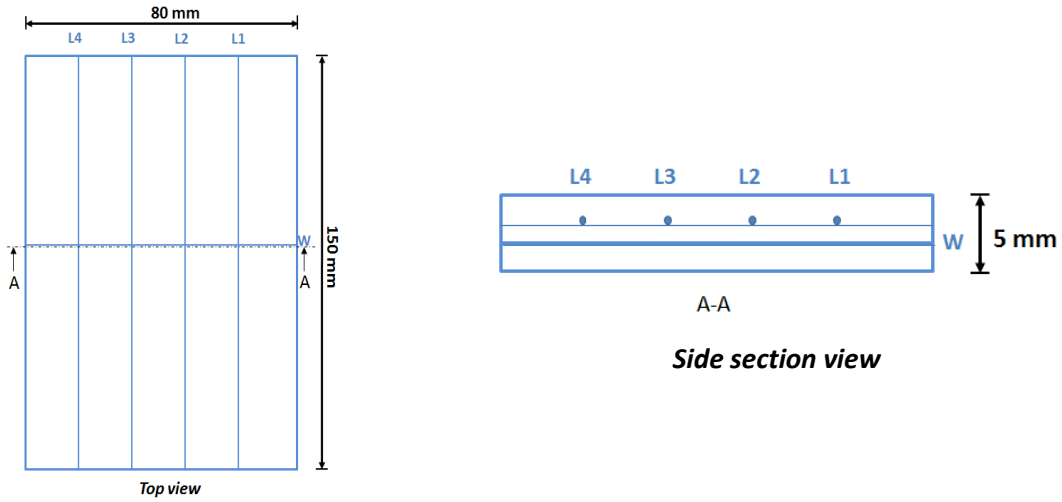

(a) *(b)*

Figure 5-29: (a)-(b) Geometric parameters of the 3D model of composite plate embedded with Nylon/Ag fiber sensor in each position correspondingly.

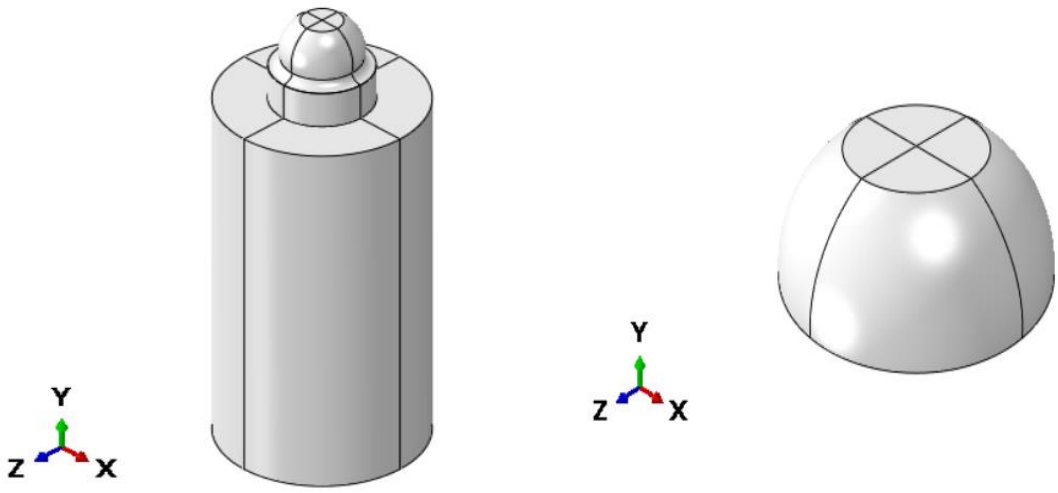

(a) Original Geometry *(b) Modified Geometry*

Figure 5-30: Impactor geometry used in dynamic impact numerical simulation.

The overall assembly of dynamic explicit simulation consisted of a cell force, a holder, the composite plate, and the impactor, Figure 5-31. The holder was attached to the cell force and the composite plate was attached to the holder through general contact defined in Abaqus. Contact between composite plate and the holder is highlighted as an example of a contact in Figure 5-30. The whole geometry was discretized using mesh convergence study and mesh size m=1 for composite plate and m=3 for the rest of the geometry was used, Figure 5-32. The impactor was assigned with the impact velocity and cell force was fixed, Figure 5-33.

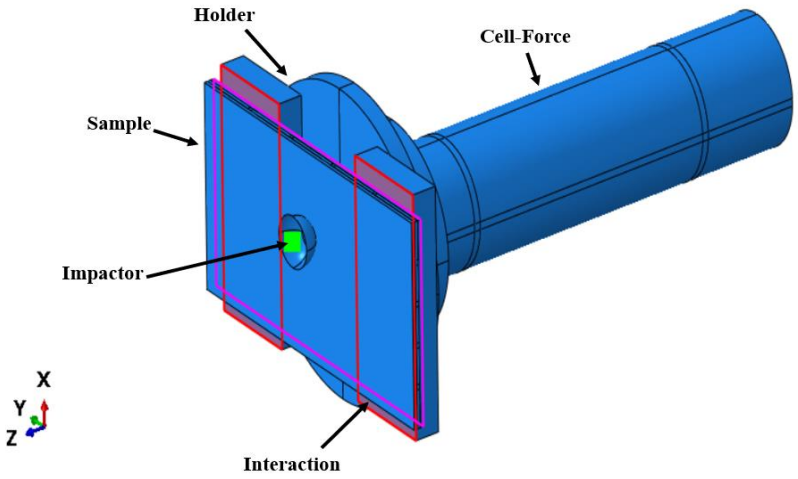

Figure 5-31: 3D model of whole assembly setup for dynamic impact

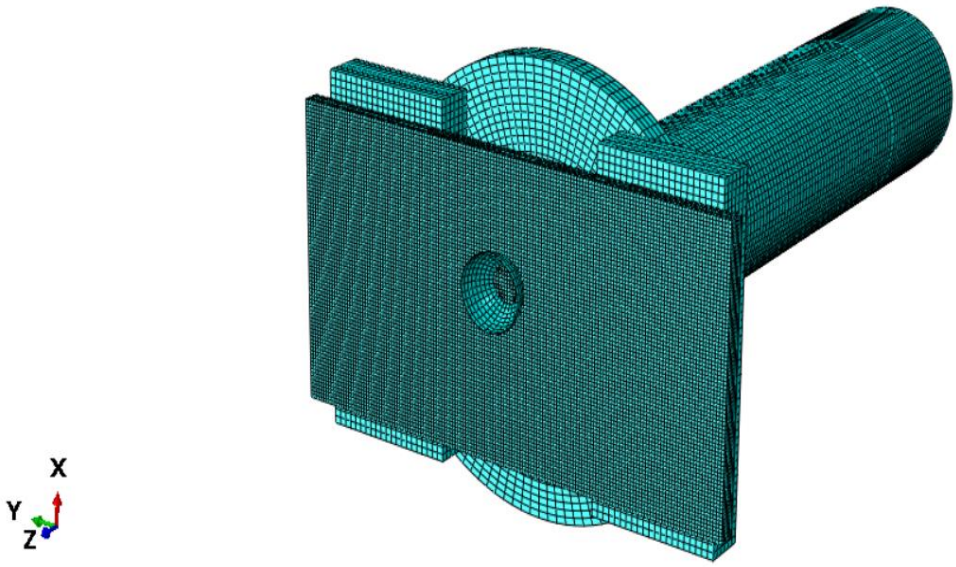

Figure 5-32: Mesh configuration of the whole assembly.

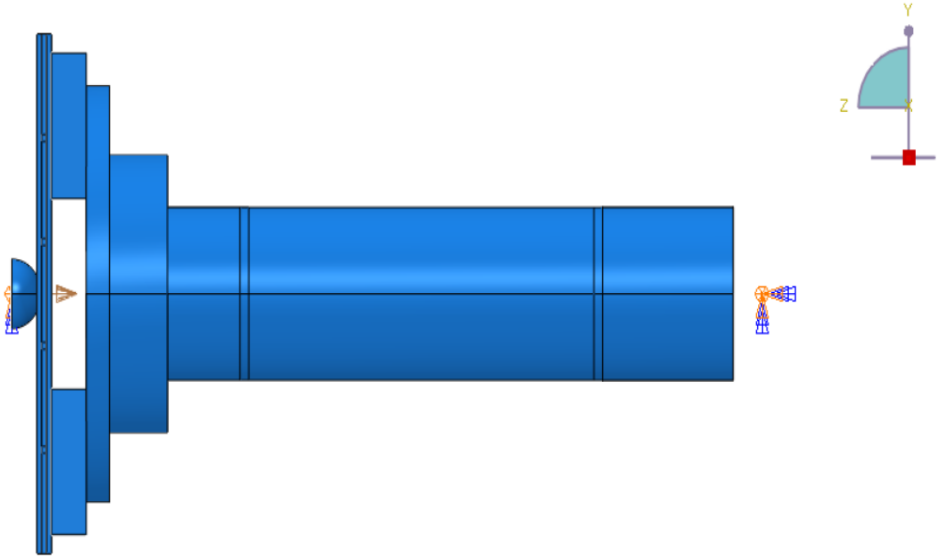

Figure 5-33: Boundary conditions applied to the 3D model assembly for dynamic impact simulation of composite plate embedded with Nylon/Ag fiber sensors.

5.4.2. FE analysis and verification of experimental results during dynamic impact

The specimen was loaded impacted with an impactor of 1.6 kg at a velocity of 2.5 m/s and it was observed that the composite sample showed localized bending, Figure 5-34. This numerical investigation was performed to study the detection behavior of the sensor during elastic deformation of the composite plate subjected to dynamic impact and correlated with the

experimental results. The mechanical response showed good agreement between experimental and numerical results, Figure 5-35. The elastic behavior of the specimen correlated perfectly, and the specimen showed localized deformation however, the deflection was along the thickness of the specimen. The mechanical response of the composite plate was obtained as a force curve from Abaqus as an overall response while Nylon/Ag fiber sensor recorded the strain deformation rate during the impact. Resistance recorded by the Nylon/Ag fiber sensor during the experimental test was converted to strain deformation rate using empirical relations defined in chapter 5. Then, this experimental strain deformation rate was compared with the strain deformation rate recorded by the sensor during the numerical investigation, and results showed good agreement in the experimental and numerical behavior of the sensor in terms of strain rate (s^{-1}), Figure 5-36. This difference in values of experimental and numerical strain rate was because experimental results were obtained by the overall behavior of the whole sensor in that direction while in numerical results skin consisting of single mesh was used to demonstrate the behavior. Moreover, a comparison of numerical mechanical deformation of the composite plate with the recorded signal from the sensor showed similar behavior as experimental results, Figure 5-37. This numerical investigation not only developed a model to monitor damage in a sample during dynamic loading and verified the experimental results but also validated the empirical relations defined in chapter 4 to convert the change in resistance of the sensor into a strain deformation rate detection signal.

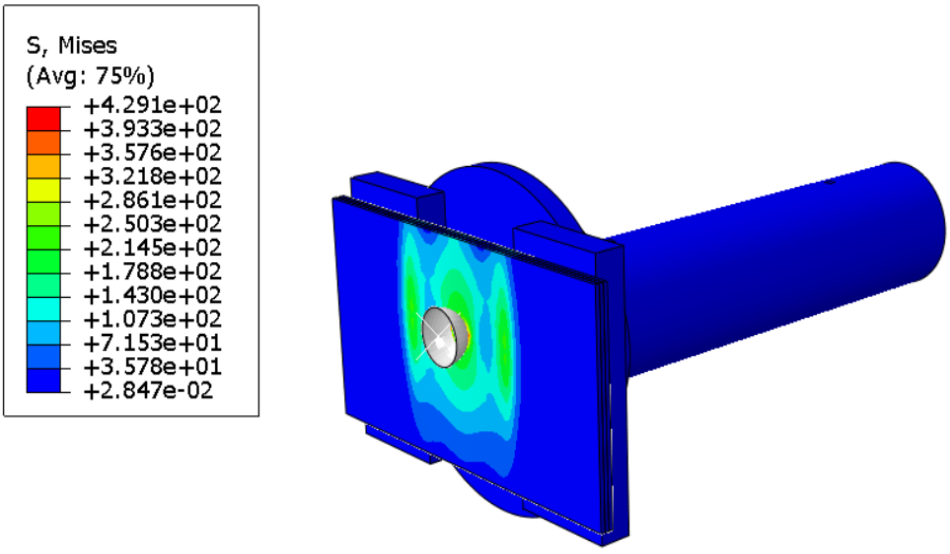

Figure 5-34: Maximum Von Mises stress contour during a dynamic impact at v=2.5 m/s

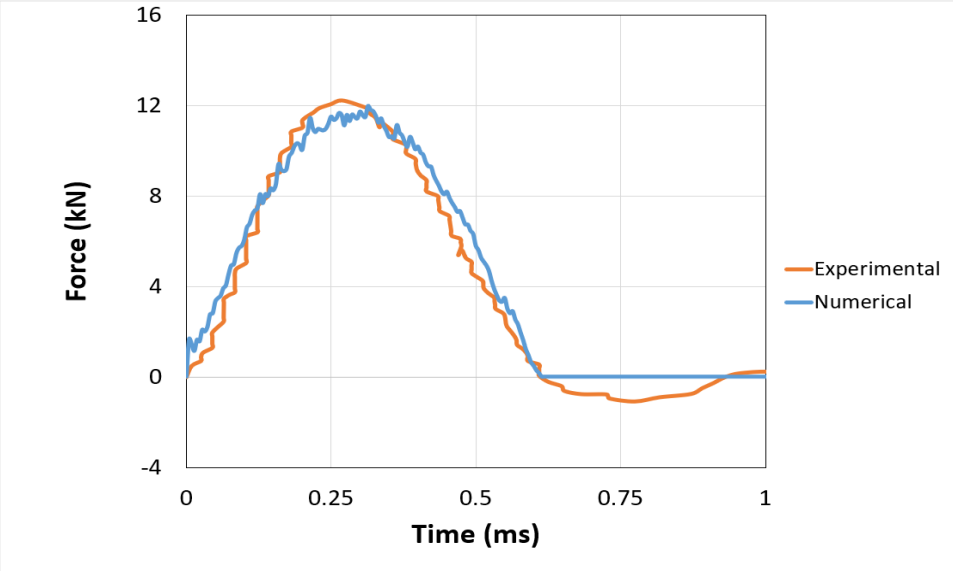

Figure 5-35: Verification of experimental mechanical behavior of composite plate during a dynamic impact.

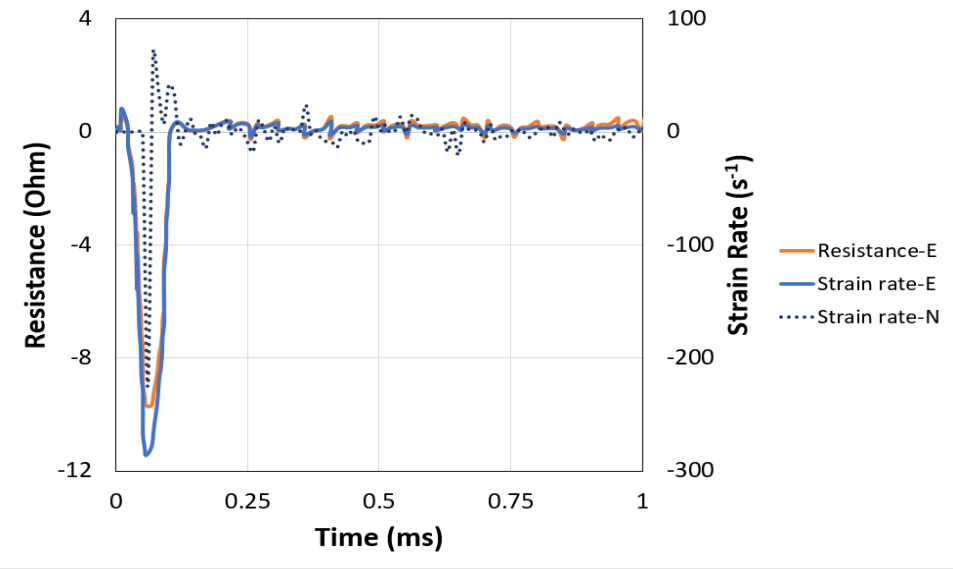

Figure 5-36: Conversion of change in resistance of real-time signal of the sensor in L2 position recorded during the experimental (E) test of dynamic impact and converted signal into strain deformation rate. Comparison of this experimental (E) strain deformation rate with the numerical (N) signal all four sensors with respect to their position and their correlation with the cyclic flexural strain deformation of composite star specimen in numerical (N) investigation.

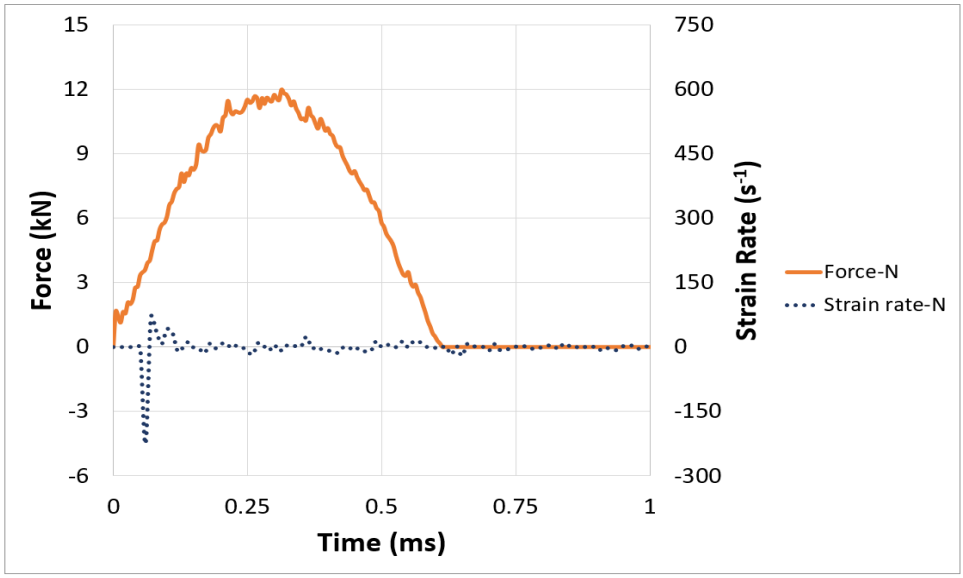

Figure 5-37: Real-time deformation monitoring in a composite plate subjected to dynamic impact during elastic deformation in the numerical investigation.

5.5. Conclusion

In this chapter numerical investigation was carried out to develop different models for studying the detection behavior of sensors in different conditions using electromechanical coupled field analysis in Abaqus. These models were used to verify the experimental results of Nylon/Ag fiber sensors as a standalone sensor and embedded within composite samples at different directions and positions. Moreover, the 3D finite element model of sensor embedded within the composite sample was studied under different loading conditions including quasi-static and dynamic loadings and correlated with the experimental results. All numerical models showed good agreement with their respective experimental results. This showed that these numerical simulations not only showed the development of models to show real-time damage monitoring in the parent model but also verified the experimental results.

The numerical investigation of the standalone sensor showed that it was viable to use monofilament fiber to validate the experimental electromechanical response of the Nylon/Ag fiber sensor. The numerical results showed good agreement with the experimental results. Moreover, the finite element model developed to demonstrate real-time strain monitoring of Nylon/Ag monofilament fiber sensor in composite star specimen at different positions and directions under quasi-static cyclic tensile and flexural loadings also showed good correlation with the experimental results. The detection signal of the fiber sensor showed the influence of the position and direction of the fiber sensor during the numerical simulation similar to

experimental results. Afterward, a 3D model was developed to demonstrate the monitoring behavior of the sensor in a composite plate subjected to dynamic impact. Unfortunately, the study of change of electrical behavior during dynamic explicit analysis in Abaqus is still not developed or very limited. Therefore, the change in resistance of the sensor during experimentation was converted into the strain deformation rate using the empirical relation and was compared with the recorded strain deformation rate by the sensor during the numerical investigation. This model was studied to correlate experimental and numerical results during elastic deformation, and they showed a good correlation in the between the sensor and composite sample during deformation but further investigation is required to improve the model. This also validated the empirical relations defined to correlate resistance change with time to strain deformation detection by the sensor.

These numerical models can be further modified to monitor the damage in composite samples and to validate the experimental results of the other two sensor systems, however, this would require a study of additional parameters that are not in the scope of this research study and are recommended for future studies.

References

[1] Y. Shindo, Y. Kuronuma, T. Takeda, F. Narita, and S.-Y. Fu, "Electrical resistance change and crack behavior in carbon nanotube/polymer composites under tensile loading," *Compos. Part B Eng.*, vol. 43, no. 1, pp. 39–43, 2012, doi: https://doi.org/10.1016/j.compositesb.2011.04.028.

[2] S. Anand and M. D. Roy, "Quasi-static and dynamic strain sensing using carbon nanotube/epoxy nanocomposite thin films," *Smart Mater. Struct.*, vol. 18., 2009.

[3] M. Park, H. Kim, and J. Youngblood, "Strain-dependent electrical resistance of multi-walled carbon nanotube/polymer composite films," *Nanotechnology*, vol. 19, p. 55705, 2008, doi: 10.1088/0957-4484/19/05/055705.

[4] C. Li and T.-W. Chou, "Modeling of damage sensing in fiber composites using carbon nanotube networks," *Compos. Sci. Technol.*, vol. 68, no. 15, pp. 3373–3379, 2008, doi: https://doi.org/10.1016/j.compscitech.2008.09.025.

[5] Alamusi, Y. L. Liu, and N. Hu, "Numerical Simulations on Piezoresistivity of CNT/Polymer Based Nanocomposites," *Comput. Mater. Contin.*, vol. 20, pp. 101–117, 2010.

[6] B. Hu *et al.*, "Multi-scale numerical simulations on piezoresistivity of {CNT}/polymer nanocomposites," *Nanoscale Res. Lett.*, vol. 7, no. 1, 2012.

[7] A. R. Alian and S. A. Meguid, "Multiscale modeling of the coupled electromechanical behavior of multifunctional nanocomposites," *Compos. Struct.*, vol. 208, pp. 826–835, 2019, doi: https://doi.org/10.1016/j.compstruct.2018.10.066.

[8] R. G. Djaja, P. J. Moses, A. J. Carr, G. A. Carnaby, and L. D. Hankoff., "Finite element modeling of an oriented assembly of continuous fibers," *Text. Res. Journal.*, vol. 62, no. 8, pp. 445-457., 1992.

[9] W. A. Munro, G. A. Carnaby, A. J. Carr, and P. J. Moss, "Some textile applications of finite-element analysis part I: finite elements for aligned fibre assemblies," *J. Text. Inst.*, vol. 88, no. 4, pp. 325–338, 1997.

[10] W. A. Munro, G. A. Carnaby, A. J. Carr, and P. J. Moss, "Some textile applications of finite-element analysis part II: finite elements for yarn mechanics," *J. Text. Inst.*, vol. 88, no. 4, pp. 339-351., 1997.

[11] W. He, X. Wang, and S. Zhang., "Mechanical behavior of irregular fibers. part II: nonlinear tensile behavior," *Text. Res. Journal.*, vol. 71, no. 11, pp. 939–942, 2001.

[12] M. Keefe, D. C. Edwards, and J. Yang., "Solid modeling of yarn and fiber assemblies,"

J. Text. Inst., vol. 83, no. 2, pp. 185–196, 1992.

[13] S. Adanur and T. Liao., "3D modeling of textile composite preform," *Compos. Part B Eng.*, vol. 29, no. 6, pp. 787–793, 1998.

[14] Y. Jiang and X. Chen., "Geometric and algebraic algorithms for modelling yarn in woven fabrics," *J. Text. Inst.*, vol. 96, no. 4, pp. 237–245, 2005.

[15] K. Sriprateep and A. Pattiya., "Computer aided geometric modeling of twist fiber," *J. Comput. Sci.*, vol. 5, no. 3, pp. 221–225, 2009.

[16] S. Vassiliadis, A. Kallivretaki, and C. Provatidis, "Mechanical modelling of multifilament twisted yarns," *Fibers Polym.*, vol. 11, no. 1, pp. 89–96, 2010.

[17] F. T. Peirce., "Tensile tests for cotton yarns v.—'The Weakest Link' theorems on the strength of long and of composite specimens," *J. Text. Inst. Trans.*, vol. 17, no. 7, pp. T355-T368., 1925.

[18] J. W. S. Hearle, P. Grosberg, and S. Backer, *Structural mechanics of fibers, yarns, and fabrics*. New York: John Wiley & Sons Inc, 1969.

[19] L. R. G. Treloar and G. Riding, "16—A THEORY OF THE STRESS–STRAIN PROPERTIES OF CONTINUOUS-FILAMENT YARNS," *J. Text. Inst. Trans.*, vol. 54, no. 4, pp. T156–T170, Apr. 1963, doi: 10.1080/19447026308660166.

[20] G. Riding and N. Wilson, "The stress–strain properties of continuous-filament yarns," *J. Text. Inst. Trans.*, vol. 56, no. 4, pp. T205–T214, 1965.

[21] T. Liu, K. F. Choi, and L. Yuan., "Mechanical modeling of singles yarn," *Text. Res. J.*, vol. 77, pp. 123-130., 2007.

[22] P. Cartraud and T. Messager, "Computational homogenization of periodic beam-like structures.," *Int. J. Solids Struct.*, vol. 43, no. 3–4, pp. 686-696., 2006.

CHAPTER 6 : CONCLUSIONS & PROSPECTIVES

In this research work, the development of different sensor systems was carried out to monitor the damage in composites in real-time. Three different sensor systems i.e. Nylon/Ag fiber sensor, CM sensor, and CF sensor were fabricated, and experimental investigation was performed to study their electromechanical response as a standalone sensor and examined their strain sensitivity by calculating their gauge factor. Then, these sensor systems were embedded within their respective composite samples at different directions and positions to monitor their strain deformation in real-time under different quasi-static loadings. In this thesis, new approaches to examine the detection behavior of different sensors, when embedded within the sample, were presented and also showed that how the position and direction of the sensor with respect to the loading axis play a vital role. The comparison of these sensors resulted in the selection of the best sensor system among all for real-time structural health monitoring of composites subjected to fracture under different quasi-static and dynamic loadings.

Moreover, in this Ph.D. work, a new numerical approach to examine the detection behavior of the sensor in real-time was presented whether the sensor was treated as a standalone sensor or embedded within a composite sample. this numerical approach assisted in developing a model in which electrical response and mechanical behavior are studied simultaneously and verified the experimental results for different loading conditions.

Conclusions

An experimental investigation carried out to study the three sensor systems i.e. Nylon/ Ag fiber sensor developed by deposition of Ag nanoparticles on nylon yarn through electroless plating, CM sensor developed using deposition of a dense network of CNTs in form of thin film using chemical vapor deposition and CF sensor consisting of PAN carbon fiber filaments aligned unidirectionally together, as a standalone sensor under both mechanical and thermal loadings. The results were very encouraging and the electromechanical response was reproducible not only in overall behavior but also during plastic strain deformation and fracture for all three sensor systems which showed that they are suitable for high strain applications and real-time sensing applications within composite structures including strain monitoring, thermal degradation and detection of failure and energy release during dynamic loading. However, the

comparison of these sensor systems showed that Nylon/Ag fiber sensor demonstrated better performance than the other two systems in mechanical and strain sensitivity behaviors. However, CM sensor not only detected the change in environmental temperature but also distinguished it whether it was positive or negative but showing an increase in resistance during temperature drop and decrease in resistance during elevation of temperature. Though this comparative study was based on their individual performance and it is important to study their performance within specimen for the selection of a better real-time multimode detection system for composite structures.

Then, the experimental study performed to examine and understand the application of each sensor system in real-time and in-situ monitoring and identification of strain deformation in composites under cyclic tensile and flexural loadings, showed detection of different types of strain deformation. The experimental results showed good repeatability in the mechanical performance of the composite structures and response of each sensor system in the monitoring of the deformation. Monitoring of deformation under tensile strain showed the influence of the direction of the sensor with respect to the loading axis on the change in resistance while monitoring of deformation of the composite specimen under flexural bending showed the influence of the position of the sensor within the plies on the detection signal of the sensor in each case when the load is applied perpendicular to the arrangement of the sensors. Moreover, the method of placing these sensors in different directions and positions showed that these sensors can detect deformation over large areas and sections of complex structures and in locations that are not normally accessible to conventional methods. All three sensor systems showed unique behavior during the detection of deformation in composites however, the comparative study showed that the real-time strain monitoring behavior Nylon/Ag fiber sensor was better than other two sensor systems under both quasi-static loadings by detecting, monitoring, identifying and quantifying the strain induced in the composite sample during deformation.

Moreover, the application of the Nylon/Ag fiber sensor in real-time monitoring and identification of deformation in composites subjected to tensile fracture showed that the placement of the sensor also plays a vital role in the monitoring of damage and final fracture. This study also verified that even though sensor did not detect the damage initiation in the transverse direction of the specimen with initial defect during deformation but its signal indicated the presence of tensile stresses near its position which could be used to predict the presence of imperfection or defect during the fabrication process which led to the imperfect

fracture. Similarly, in flexural specimens, the experimental results showed good reproducibility in the overall mechanical response of the composite structures and demonstrated that the presence of the strain fiber sensor did not behave like an intrusion or defect even when placed at different positions through the thickness. Overall electrical response of the Nylon/Ag fiber sensor in each specimen also showed reproducibility in results however, the variation in its resistance response during the deflection was because of its specific position each specimen. The sensor system not only monitors the change in the mechanical behavior of the specimen during the deflection and detected the presence of damage until final fracture but also identified the type of damage whether it was tensile, compressive, or both. This sensor system showed good potential as a flexible sensor reinforcement in composite materials for real-time monitoring, detection, and identification of damage.

In addition, Nylon/Ag fiber sensor was also used for in-situ monitoring and identification of damage in composites subjected to dynamic impact. The fiber sensor was integrated at specific directions and positions within the composite sample plate. Nylon/Ag fiber sensor monitored the deformation of the composite sample and correlated perfectly with their dynamic behavior. The distinct behavior of each fiber sensor, placed in different directions and position, confirmed the detection of different types of damage i.e. tensile or compression during the impact and different intensity or magnitude of the signals quantified the amount of damage induced. Moreover, delay in the change of resistance of the Nylon/Ag fiber sensor according to its respective position demonstrated the damage propagation phenomenon for dynamic loading. Thus, the Nylon/Ag fiber sensor also demonstrated good potential for in-situ monitoring of the dynamic failure mechanism of the composite specimen.

The numerical approach, developed in this research study, presented a coupled field analysis to examine the real-time monitoring behavior of the sensor whether the sensor was standalone or embedded within a sample. The finite element models not only showed the detection behavior of the sensor whether it was considered as standalone or was embedded within the composite sample during numerical simulations but, also verified the experimental results conducted under different loading conditions.

Perspectives

This research work was conducted to develop sensor systems to study mechanical deformation of composite samples with quasi-isotropic materials behavior and this study can be extended to study the application of these sensor systems in other composite materials especially with anisotropic or orthotopic properties.

Moreover, these sensors systems were studied under selective quasi-static and dynamic loadings and this can be extended to study the real-time monitoring of composites subjected to other types of loadings such as fatigue, ballistic impact, etc. which can include the detection of another type of failures such as shear failure or delamination in the composite sample.

In this study, all three sensor systems were studied to detect environmental temperature as a standalone sensor which showed that they have to ability to demonstrate electrothermal behavior. This can be utilized in the future to detect energy release during the dynamic failure of composites.

The numerical investigation conducted in this study validated the electromechanical response of the selected sensor system i.e. Nylon/Ag fiber sensor which can be extended to verify the experimental behavior of the other two sensor systems. Furthermore, the numerical approach can be modifying to detect the damage in composites as well.

Finally, the ultimate goal of future studies would be the implementation of these real-time damage detection techniques in large scale realistic structures and to ensure industrialization of this knowledge and technology. To reduce this gap, repeatable and reliable results at an industrial scale is necessary for the progress. The implementation of this smart sensing techniques in industrial components for damage detection is a requirement to improve the structural integrity and lifetime estimation of structural components.

Annex I: PUBLICATIONS

Book: Advances in Structural Health Monitoring

Chapter: Nanotechnology and development of Strain Sensor for damage detection

Yumna Qureshi* (1), Mostapha Tarfaoui (1,2), Khalil K. Lafdi, and Khalid Lafdi (2)

(1) ENSTA Bretagne, IRDL - FRE CNRS 3744, F-29200 Brest, France.

(2) University of Dayton, Dayton, OH 45469-0168, United States.

*Corresponding author. E-mail address: yumna.qureshi@ensta-bretagne.org, mostapha.tarfaoui@ensta-bretagne.fr

Abstract :

Composite materials, having better properties than traditional materials, are susceptible to potential damage during operating conditions and this issue is usually not found until it's too late. Thus, it is important to identify when cracks occur within a structure, to avoid catastrophic failure. The objective of this paper is to fabricate a new generation of strain sensors in the form of a wire/thread that can be incorporated into a material to detect damage before they become fatal. This microscale strain sensor consists of flexible, untwisted nylon yarn coated with a thin layer of silver using electroless plating process. The electromechanical response of this fiber sensor was tested experimentally using tensile loading & then verified numerically with good agreement in results. This flexible strain sensor was then incorporated into a composite specimen to demonstrate the detection of damage initiation before the deformation of structure becomes fatal. The specimens were tested mechanically in a standard tensometer machine while the electrical response was recorded. The results were very encouraging and the signal from the sensor was correlated perfectly with the mechanical behavior of the specimen. This showed that these flexible strain sensors can be used for in-situ SHM and real-time damage detection applications.

Keywords: Composites, Structural Health Monitoring, Flexible yarn; Strain sensor; Conductive film Ag-coating; Electromechanical behavior.

Composites Science and Technology

Volume 181, 8 September 2019, 107693

Development of microscale flexible nylon/Ag strain sensor wire for real-time monitoring and damage detection in composite structures subjected to three-point bend test

Yumna Qureshi* (1), Mostapha Tarfaoui (1,2), Khalil K. Lafdi, and Khalid Lafdi (2)

(1) ENSTA Bretagne, IRDL - FRE CNRS 3744, F-29200 Brest, France.

(2) University of Dayton, Dayton, OH 45469-0168, United States.

*Corresponding author. E-mail address: yumna.qureshi@ensta-bretagne.org, mostapha.tarfaoui@ensta-bretagne.fr

Abstract :

Composite are prone to failure during operation and that's why vast research had been carried out to develop in-situ sensors and monitoring systems to avoid their catastrophic failure and repairing cost. The aim of this research was to develop a flexible strain sensor wire for real-time damage detection in the composites. This strain sensor wire was developed by depositing conductive silver (Ag) nanoparticles on the surface of nylon (Ny) yarn by electroless plating to achieve the smallest uniform coating without jeopardizing the integrity of each material. The sensitivity of this Ny/Ag strain sensor wire was calculated experimentally and gauge factor (G.F) was found to be in the range of 21–25. Then, Ny/Ag strain sensor wire was inserted in each composite specimen at different position intentionally through the thickness during their fabrication depending upon the type of damage to detect. The specimens were subjected to flexural deflection using a 3-point bend test at the strain rate of 2 mm/min. Overall mechanical response of composite specimens and electrical response signal of the Ny/Ag strain sensor wire showed good reproducibility in results however, Ny/Ag sensor showed a specific change in resistance in each specimen because of their respective position. The sensor wire designed, did not only monitor the change in the mechanical behavior of the specimen until final fracture but also identified the type of damage whether it was compressive, tensile or both. This sensor wire showed good potential as a flexible reinforcement in composite materials for in-situ SHM applications before it can become fatal.

Keywords: Structural composites; Mechanical properties; Deformation; Non-destructive testing; Strain sensor wire

Structural Health Monitoring

Volume: 19, Issue: 3, page(s): 885-901

Real-time strain monitoring and damage detection of composites in different directions of the applied load using a microscale flexible Nylon/Ag strain sensor

Yumna Qureshi* (1), Mostapha Tarfaoui (1,2), Khalil K. Lafdi, and Khalid Lafdi (2)

(1) ENSTA Bretagne, IRDL - FRE CNRS 3744, F-29200 Brest, France.

(2) University of Dayton, Dayton, OH 45469-0168, United States.

*Corresponding author. E-mail address: yumna.qureshi@ensta-bretagne.org,

Abstract :

Composites are prone to failure during operating conditions and that is why vast research studies have been carried out to develop in situ sensors and monitoring systems to avoid their catastrophic failure and repairing cost. The aim of this research article was to develop a flexible strain sensor wire for real-time monitoring and damage detection in the composites when subjected to operational loads. This flexible strain sensor wire was developed by depositing conductive silver (Ag) nanoparticles on the surface of nylon (Ny) yarn by electroless plating process to achieve smallest uniform coating film without jeopardizing the integrity of each material. The sensitivity of this Nylon/Ag strain sensor wire was calculated experimentally, and gauge factor was found to be in the range of 21–25. Then, the Nylon/Ag strain sensor wire was inserted into each composite specimen at different positions intentionally during fabrication depending upon the type of damage to detect. The specimens were subjected to tensile loading at a strain rate of 2 mm/min. Overall mechanical response of composite specimens and electrical response signal of the Nylon/Ag strain sensor wire showed good reproducibility in results; however, the Nylon/Ag sensor showed a specific change in resistance in each direction because of the respective position. The strain sensor wire designed not only monitored the change in the mechanical behavior of the specimen during the elongation and detected the strain deformation but also identified the type of damage, whether it was compressive or tensile. This sensor wire showed good potential as a flexible reinforcement in composite materials for in situ structural health monitoring applications and detection of damage initiation before it can become fatal.

Keywords: Structural composites; mechanical deformation; nylon/Ag strain sensor wire; real-time monitoring; damage detection

Sensors and Actuators A: Physical

Volume 295, 15 August 2019, Pages 612-622

Real-time strain monitoring performance of flexible Nylon/Ag conductive fiber

Yumna Qureshi* (1), Mostapha Tarfaoui (1,2), Khalil K. Lafdi, and Khalid Lafdi (2)

(1) ENSTA Bretagne, IRDL - FRE CNRS 3744, F-29200 Brest, France.

(2) University of Dayton, Dayton, OH 45469-0168, United States.

*Corresponding author. E-mail address: yumna.qureshi@ensta-bretagne.org,

Abstract :

Smart textiles have generated significant importance because of the advent of portable devices and easy computing, however, they did not replace the conventional electronics on the whole however, this development is now advanced to the fabrication of wearable technologies. The aim of this research paper was to develop a flexible microscale conductive fiber for real-time strain monitoring applications. This conductive fiber was developed by depositing conductive silver (Ag) nanoparticles on the surface of Nylon-6 polymer yarn by electroless plating process to achieve smallest uniform coating film over each filament of the Nylon yarn without jeopardizing the integrity of each material. The sensitivity of this Nylon/Ag conductive fiber was calculated experimentally and gauge factor was found to be in the range of 21–25 which showed that it had high sensitivity to the applied strain. Then, Nylon/Ag conductive fiber was tested up to fracture under tensile loading and a good agreement between mechanical and electrical response was observed with reproducibility of the results. The results demonstrated the way to design a cost-effective microscale smart textile for strain monitoring. This Nylon/Ag conductive fiber can then be used in a wide range of high strain applications such as in-situ structural health monitoring or for medical monitoring because of their high sensitivity, flexibility, and stability.

Keywords: Smart textile; Flexible polymer yarn; Conductive surface coating; Electro-mechanical response; Real-time strain monitoring

IEEE Sensors Journal

Volume 20, Issue 10, pages 5492-5500

In-Situ Monitoring, Identification and Quantification of Strain Deformation in Composites Under Cyclic Flexural Loading Using Nylon/Ag Fiber Sensor

Yumna Qureshi* (1), Mostapha Tarfaoui (1,2), Khalil K. Lafdi, and Khalid Lafdi (2)

(1) ENSTA Bretagne, IRDL - FRE CNRS 3744, F-29200 Brest, France.

(2) University of Dayton, Dayton, OH 45469-0168, United States.

*Corresponding author. E-mail address: yumna.qureshi@ensta-bretagne.org,

Abstract :

Despite having vast structural applications, Composites are not exempt from limitations and are susceptible to deforming during operation. Therefore, it is essential to develop in-situ monitoring systems to avoid their catastrophic failure or high repairing cost. So, the objective of this study was to monitor the deformation behavior of composites subjected to cyclic flexural deformation in real-time using a Nylon/Ag fiber sensor. Nylon/Ag fiber sensor was integrated at different direction i.e. 0°, +45°, 90°, -45° gradually between each ply of the composite specimens which were then machined in star shape where each leg signified the direction of the sensor. These specimens were then tested under cyclic flexural deflection at the strain rate of 2mm/min for 10 cycles. Mechanical results of composite specimens and electrical response of each Nylon/Ag sensor fiber showed excellent repeatability however, each Nylon/Ag fiber sensor showed a specific resistance behavior because of their respective position. The increase or decrease in the resistance of the fiber sensor signified the presence of tensile or compressive strain respectively and the intensity of the signal quantified the amount of deformation. The results confirmed that the fiber sensor showed good potential as flexible sensor reinforcement in composites for in-situ monitoring, identification and quantification of the deformation.

Keywords: Composite structures; mechanical deformations; in-situ strain monitoring; fiber sensory

International Journal of Mechanical and Production Engineering (IJMPE)

Volume-7, Issue-10, pages 18-21

A Flexible Strain Sensor Design based on Ny-6 Yarn Coated with Ag Nanoparticles for Real Time Strain Monitoring Application

Yumna Qureshi* (1), Mostapha Tarfaoui (1,2), Khalil K. Lafdi, and Khalid Lafdi (2)

(1) ENSTA Bretagne, IRDL - FRE CNRS 3744, F-29200 Brest, France.

(2) University of Dayton, Dayton, OH 45469-0168, United States.

*Corresponding author. E-mail address: yumna.qureshi@ensta-bretagne.org,

Abstract :

Composites show better performance than traditional materials however, they are inclined to damage formation, delamination, or fracture. So, it is necessary to detect damage or crack formation with in time in these materials to avoid any catastrophic incident. Therefore, numerous researchers have been developing in-situ sensors and monitoring systems for composite structures. The objective of this study is to create a micro scale, flexible strain sensor wire for real-time sensing applications. This strain sensor wire was developed by depositing conductive silver (Ag) nanoparticles on the surface of Ny-6 untwisted yarn using electroless plating process to achieve uniform conductive coating over each filament of the Ny-6 polymer. The electro-mechanical behavior of this Ny/Ag sensor wire was verified experimentally and gauge factor was found to be in range of 62-69. This flexible Ny/Ag sensor wire was then integrated with in a composite sample to validate the monitoring of deformation and detection of damage initiation. Experimental procedure was performed where the mechanical behavior of the composite sample was tested in a standard tensometer machine, while the electrical signal of the Ny/Ag sensor wire was recorded. The results showed that the electrical response of the sensor was correlated perfectly with the mechanical behavior of the specimen. This indicated that Ny/Ag strain sensor wire can be used for real-time damage detection and structural health monitoring (SHM) applications.

Keywords: Composites; Structural Health Monitoring; Conductive Ag-Metal Coating; Microscale Strain Sensor Wire; Electro-Mechanical Response

SPIE Digital Library

Proceedings Volume 11380, Nondestructive Characterization and Monitoring of Advanced Materials, Aerospace, Civil Infrastructure, and Transportation IX; 113800Y (2020)

https://doi.org/10.1117/12.2558106

Event: SPIE Smart Structures + Nondestructive Evaluation, 2020, California, United States

In-situ Damage Monitoring of Composites under Dynamic Impact using Nylon/Ag Fiber Sensor

Y. Qureshi*[a], M. Tarfaouia, H. Benyahia[a], K. K. Lafdi[b], K. Lafdi[b,c]

[a]ENSTA Bretagne, IRDL - UMR CNRS 6027, F-29200 Brest, France.

[b]University of Dayton, Nanomaterials Laboratory, Dayton, OH 45469-0168, United States.

[c]Department of Mechanical and Construction Engineering, Northumbria University, Newcastle upon Tyne, UK

Abstract :

Despite having a vast structural application, Composites are not exempt from limitations and are also susceptible to deforming during operations. Therefore, it is essential to develop in-situ monitoring systems and sensors to avoid their catastrophic failure, especially for dynamic failure. So, the objective of this study was to investigate and monitor the dynamic behavior of composites in real-time using a Nylon/Ag fiber sensor under the low-velocity impact. Nylon/Ag fiber sensors were integrated at different directions and positions within the composite specimens which were tested under low-velocity impact on the Taylor cannon gun apparatus. Three sets of tests were performed at 2.5m/s, 3m/s and 6.5m/s respectively to demonstrate the detection signal of the fiber sensors when there is no damage, some micro damage and overall breakage of the sample. The results confirmed that each Nylon/Ag fiber sensor showed a specific resistance behavior in all three specimens because of their respective position and direction and detected the deformation, damage initiation, damage propagation, type of damage and quantification of the amount of damage induced.

Keywords: Composites, impact, mechanical deformation, in-situ monitoring, Nylon/Ag fiber sensor

Smart Materials and Structures

(Accepted recently)

Multi-Mode Real-Time Strain Monitoring in Composites using Low Vacuum Carbon Fibers as a Strain Sensor under Different Loading Conditions

Yumna Qureshi* (1), Mostapha Tarfaoui (1) and Khalid Lafdi (2,3)

(1) ENSTA Bretagne, IRDL - FRE CNRS 3744, F-29200 Brest, France.

(2) University of Dayton, Dayton, OH 45469-0168, United States.

(3) Department of Mechanical and Construction Engineering, Northumbria University, Newcastle upon Tyne, UK

*Corresponding author. E-mail address: yumna.qureshi@ensta-bretagne.org,

Abstract:

Structural health monitoring is a vastly growing field consisting of sensors embedded in or attached with the structure which respond to the strain or other stimuli to monitor the deformation in real-time. In this study, a multi-mode strain detection is carried out in composites using nanomaterial-based sensor technology. A Carbon fiber (CF) sensor was developed using unidirectional carbon filaments aligned straightly together and its sensitivity was calculated experimentally, with gauge factor (GF) in 10.2-10.8 range. Then, this CF sensor is embedded gradually at different directions i.e. 0°,+45°,90°,-45° between the plies of composite for real-time/in-situ strain monitoring. The composite specimen was then cut in star profile, each leg demonstrating the direction of the CF sensors. These composite samples are then tested under tensile and flexural cyclic loading. There is a good reproducibility in the results and the mechanical response of composite correlated perfectly with the electrical resistance of the CF sensor. It can also be noted that the sensors, depending on their respective position, manage to faithfully reproduce the mechanical behavior of the specimen tested (traction/compression). The results established that the CF exhibited good potential as flexible reinforcement for in-situ monitoring of composites and can provide detection over large sections and unapproachable locations. This study also showed that direction and position of the sensor plays a vital role in the detection, identification (whether its tensile or compressive) and quantification of the deformation experienced by the structure under different loading conditions.

Keywords: Composites, strain deformation, real-time monitoring system, carbon fiber sensor, multi-mode detection

Smart Materials and Structures

(Accepted recently)

Nylon/Ag Fiber Sensor for Real-Time Damage Monitoring of Composites Subjected to Dynamic Loading

Y. Qureshi*[a], M. Tarfaouia, H. Benyahia[a], K. K. Lafdi[b], K. Lafdi[b,c]

[a]ENSTA Bretagne, IRDL - UMR CNRS 6027, F-29200 Brest, France.

[b]University of Dayton, Nanomaterials Laboratory, Dayton, OH 45469-0168, United States.

[c]Department of Mechanical and Construction Engineering, Northumbria University, Newcastle upon Tyne, UK

*Corresponding author. E-mail address: yumna.qureshi@ensta-bretagne.org,

Abstract:

In this article, the goal is to monitor the deformation and damage behavior of composites in real-time using a Nylon/Ag fiber sensor when subjected to dynamic loading. Composite samples are integrated with Nylon/Ag fiber sensors at distinct locations and directions between the plies. Then, these samples are experimentally impacted with low-velocity impact using the Taylor Cannon Gun apparatus at three different velocities i.e. 2.5 m/s, 3 m/s, and 6.5 m/s, respectively. These three sets of tests are conducted to determine the detection performance of the Nylon/Ag fiber sensor when the composite sample experiences no damage, some microdamage, and overall breakage. Besides, the fiber sensor placed in each position showed distinct electrical behavior in all three tests and detected the deformation, damage initiation, quantification, identification, and damage propagation. The results confirmed the ability of the fiber sensor to monitor and identify the mechanical deformation during dynamic loading and showed that the sensor can be used as a flexible sensor reinforcement in composites for in-situ monitoring as well.

Keywords: Composites; Dynamic loading; Damage behavior; Real-time monitoring; fiber sensor

Materials Science & Engineering B

(Accepted recently)

Electro-thermal-mechanical Performance of a Sensor Based on PAN Carbon Fibers and Real-Time Detection of Change Under Thermal and Mechanical Stimuli

Yumna Qureshi* (1), Mostapha Tarfaoui (1) and Khalid Lafdi (2,3)

(1) ENSTA Bretagne, IRDL - FRE CNRS 3744, F-29200 Brest, France.

(2) University of Dayton, Dayton, OH 45469-0168, United States.

(3) Department of Mechanical and Construction Engineering, Northumbria University, Newcastle upon Tyne, UK

*Corresponding author. E-mail address: yumna.qureshi@ensta-bretagne.org,

Abstract:

Structural health monitoring (SHM) is a vastly growing field consisting of sensors embedded in or attached with the structure which respond to the strain or other stimuli to monitor the deformation in real-time. In this study, a carbon fiber (CF) sensor was developed using unidirectional Polyacrylonitrile (PAN) carbon filaments aligned straightly together and its sensitivity was calculated experimentally, with the gauge factor (GF) in 10.2-10.8 range. The electro-thermal behavior of this CF sensor showed distinct performance and detected the change in the surrounding temperature. There is a good reproducibility in the results in both piezoresistive and electro-thermal behavior of the CF sensor and its electrical performance showed real-time detection of both mechanical and thermal stimuli. The results established that the CF exhibited good potential as a flexible strain sensor for in-situ monitoring of damage or energy release during the failure of composites.

Keywords: Real-time monitoring system, PAN carbon fiber sensor, electromechanical performance, electro-thermal behavior

Titre: Développement d'une nouvelle génération de capteurs pour la surveillance de la santé structurale des composites

Mots clés: Surveillance de la santé structurelle; Systèmes de capteurs; Matériaux composites; Surveillance en temps réel; Détection de dommages

Résumé: Les composites ont remplacé les matériaux traditionnels dans presque toutes les applications d'ingénierie et de structure en raison de leurs performances extraordinaires, mais ils ne sont pas exemptes de limitations et de problèmes. Bien qu'il s'agisse d'un matériau polyphasé, les mécanismes d'initiation et de propagation des dommages conduisant à la rupture est bien établi et le problème est que ces dommages ou défaillances ne sont pas toujours visibles. Ainsi, même lorsque la structure globale est toujours intacte, il est essentiel d'étudier ses performances en conditions opérationnelles en temps réel pour éviter tout incident catastrophique. Ainsi, une surveillance de la santé structurelle in-situ a été développée dans laquelle les données structurelles peuvent être collectées et analysées en temps réel pour identifier la présence de dommages. L'étude menée dans le cadre de ce travail de thèse s'inscrit dans le cadre du développement d'un système de capteurs sensible et robuste qui peut non seulement surveiller la déformation des structures composites en temps réel, mais aussi détecter l'initiation et la propagation des dommages sous différentes conditions de charge. Dans cette étude, trois systèmes de capteurs différents ont été développés en utilisant des matériaux fonctionnels intelligents pour étudier leur efficacité dans le suivi de la déformation des composites dans différentes directions et positions sous différente type de chargement. Un objectif supplémentaire de ce projet est d'étudier les performances de détection de chaque système de capteurs et de démontrer s'ils peuvent identifier le type de déformation en plus de leur détection en temps réel. Les résultats ont établi que chaque système de capteur présentait un bon potentiel en tant que capteur flexible de contrainte pour la surveillance in-situ des composites et leur disposition peut fournir une détection sur une grande section et des emplacements inaccessibles. La comparaison des résultats de la campagne d'essais a permis de sélectionner les meilleurs systèmes de capteur qui sont ensuite utilisés pour la détection des dommages dans les composites sous l'action des charges statiques et dynamiques. Cette étude donne une vision complète concernant le comportement de détection de différents systèmes de capteurs sous différentes charges opérationnelles et montre également que la position et l'orientation du capteur dans l'échantillon jouent un rôle vital. Sur la base de cette comparaison détaillée, le système de capteurs sélectionné surveille non seulement la déformation en temps réel, mais permet également de détecter le déclenchement et la propagation des dommages ainsi que d'identifier et quantifier leur nature sous des chargements statiques et dynamiques. De plus, des modèles numériques robuste ont été développés et corréler avec les résultats expérimentaux. Les résultats numériques ont non seulement validé le comportement mécanique expérimental de l'échantillon composite, mais ont également confirmé le signal de détection du capteur placé dans différentes positions et directions au sein de l'échantillon composite. Ce travail de recherche a donné lieu à plusieurs publications dans des revues de rang A (6 articles), 1 chapitre dans un livre, 1 publication dans la bibliothèque numérique SPIE et 6 présentations orales dans différentes conférences, Annexe I

Title: Development of a new generation of fiber sensors for structural health monitoring in composites

Keywords: Structural Health Monitoring; Sensor Systems; Composites; Real-time Monitoring; Damage detection

Abstract: Composites have substituted traditional materials in almost every engineering and structural application because of their extraordinary performance but still, they are not exempt from limitations and problems. Despite being a multiphase material, their mechanism of damage initiation and propagation leading to failure are well established and the problem is that these damages or failures are not visible always. So, even when the overall structure is still intact, it is essential to study their performance during operational conditions in real-time to avoid any catastrophic incident. Thus, in-situ structural health monitoring was developed in which structural data can be collected and analyzed in real-time to identify the presence of damage. The study conducted in this research is within the framework of development affective and robust sensor system which can monitor not only the deformation in composite structures in real-time but also can detect damage initiation and damage propagation under different loading conditions. In this study, three different sensor systems are developed using smart functional materials to study their effectiveness in monitoring deformation in composites in different directions and positions under different quasi-static loadings. An additional goal of this research was to study the detection behavior of each sensor system and demonstrate whether they can identify the type of deformation besides their detection in real-time. The results established that each sensor system exhibited good potential as a flexible strain sensor for in-situ monitoring of composites and their arrangement can provide detection over a large section and unapproachable locations. The comparison of their results assisted in the selection of better sensor systems which is then utilized to detect damage and final fracture in composites during overall mechanical behavior under quasi-static and dynamic loadings. This study provides a comprehensive understanding regarding the detection behavior of different sensor systems under different operational loads and also shows that the position and direction of the sensor within the sample plays a vital role in it. Based on this detailed comparison, the selected sensor system does not only monitor the deformation in real-time but also, detect damage initiation, identify the type of damage, quantifies them, and also sense damage propagation under both quasi-static and dynamic loadings. Moreover, numerical models are developed to verify the detection behavior of this sensor system to verify the experimental results. Numerical results not only validated the experimental mechanical behavior of the composite sample but also confirmed the detection signal of the sensor placed in different positions and directions within the composite sample. This research study has resulted in several publications in rank A journals (6 articles), 1 chapter in a book, 1 publication in SPIE digital library, and 5 oral presentations in different conferences, Annex I.